NAM

V5 Ground-Motion Model (GMM) for the Groningen Field

Julian J Bommer[1], Benjamin Edwards[1], Pauline P Kruiver[2], Adrian Rodriguez-Marek[1], Peter J Stafford[1], Bernard Dost[3], Michail Ntinalexis[1], Elmer Ruigrok[3] and Jesper Spetzler[3]

1. Independent consultant,
2. Deltares,
3. Royal Netherlands Meteorological Institute (KNMI)

Datum October 2017

Editors Jan van Elk & Dirk Doornhof

General Introduction

The hazard due to induced earthquakes is primarily presented by the ground motion to which buildings and people are subjected. The prediction of ground motion, resulting from the earthquakes in the Groningen area induced by the production of gas, is therefore critical.

This research was started in 2012 and is continuing with ever more ground motion data from Groningen earthquakes being collected. The methodology for Ground Motion Model (GMM) was therefore updated and progress documented regularly. In the Technical Addendum to Winningsplan 2013, a Ground Motion Prediction methodology based on a catalogue of tectonic earthquakes in southern Europe, was presented (Ref. 1). This methodology was inherently conservative, in the sense that it predicted ground motions which in future are in general more likely to be adjusted downwards than upwards.

In the report "Development of GMPEs for Response Spectral Accelerations and for Strong-Motion Durations (Version 1)" the status in May 2015 was documented (Ref. 2). An update of this document was issued in November 2015 and presented version 2 of the of the GMPE methodology (Ref. 3), which was an update of this Ground Motion Prediction methodology tailored to the Groningen situation (Ref. 4 to 7). In general, this update led to downward adjustment of assessed ground motions for larger earthquakes, resulting in a reduction of the assessed hazard. After incorporating some adjustments, this version of the GMM was used for the hazard and risk assessment supporting Winningsplan 2016, issued in April 2016.

Originally, an update of the GMM (version 3) was planned for July 2016, in support of the hazard and risk assessment for Winningsplan 2016. However, when early 2016 the deadline of submission for the Winningsplan was brought forward from July 2016 to April 2016, version 3 of the GMM could not be ready in time to be implemented in the hazard and risk assessment for this winningsplan.

Version 4 of the Ground Motion Model (GMM) was completed mid-2017 and shared with experts for an assurance review (Ref. 8). The current version of the GMM, version 5, has been updated based on the comments from the assurance review and was used in the Hazard, Building Damage and Risk Assessment of November 2017.

References:

1 Technical Addendum to the Winningsplan Groningen 2013; Subsidence, Induced Earthquakes and Seismic Hazard Analysis in the Groningen Field, Nederlandse Aardolie Maatschappij BV (Jan van Elk and Dirk Doornhof, eds), November 2013.

2 Development of Version 1 GMPEs for Response Spectral Accelerations and for Strong-Motion Durations, Julian J Bommer, Peter J Stafford, Benjamin Edwards, Michail Ntinalexis, Bernard Dost and Dirk Kraaijpoel, March 2015.

3 Development of Version 2 GMPEs for Response Spectral Accelerations and Significant Durations for Induced Earthquakes in the Groningen field, Julian J Bommer, Bernard Dost, Benjamin Edwards, Adrian Rodriguez-Marek, Pauline P Kruiver, Piet Meijers, Michail Ntinalexis & Peter J Stafford, October 2015

4 Geological schematisation of the shallow subsurface of Groningen (For site response to earthquakes for the Groningen gas field) – Part I, Deltares, Pauline Kruiver and Ger de Lange.

5 Geological schematisation of the shallow subsurface of Groningen (For site response to earthquakes for the Groningen gas field) – Part II, Deltares, Pauline Kruiver and Ger de Lange.

6 Geological schematisation of the shallow subsurface of Groningen (For site response to earthquakes for the Groningen gas field) – Part III, Deltares, Pauline Kruiver and Ger de Lange.

7 Modifications of the Geological model for Site response at the Groningen field, Deltares, Pauline Kruiver, Ger de Lange, Ane Wiersma, Piet Meijers, Mandy Korff, Jan Peeters, Jan Stafleu, Ronald Harting, Roula Dambrink, Freek Busschers, Jan Gunnink

8 V4 Ground-motion Model (GMM) for Response Spectral Accelerations, Peak Ground Velocity and Significant Duration in the Groningen field, Julian Bommer, Bernard Dost, Benjamin Edwards, Pauline Kruiver, Pier Meijers, Michail Ntinalexis, Adrian Rodriguez-Marek, Elmer Ruigrok, Jesper Spetzler and Peter Stafford, Independent Consultants, Deltares and KNMI, June 2017 with Parameter files - V4 Ground-Motion Model (GMM) for Response Spectral Accelerations, Peak Ground Velocity, and Significant Durations in the Groningen Field, Supplement to V4 GMM, Julian Bommer and Peter Stafford, Independent Consultants, June 2017

These reports are also available at the study reports page of the website www.namplatform.nl.

NAM

Title	**V5 Ground-Motion Model (GMM) for the Groningen Field**		**Date**	October 2017
			Initiator	NAM
Autor(s)	Julian J Bommer[1], Benjamin Edwards[1], Pauline P Kruiver[2], Adrian Rodriguez-Marek[1], Peter J Stafford[1], Bernard Dost[3], Michail Ntinalexis[1], Elmer Ruigrok[3] and Jesper Spetzler[3]	**Editors**	Jan van Elk & Dirk Doornhof	
Organisation	1. Independent consultant, 2. Deltares, 3. Royal Netherlands Meteorological Institute (KNMI)	**Organisation**	NAM	
Place in the Study and Data Acquisition Plan	Study Theme: Ground Motion Prediction Comment: The prediction of Ground Motion is central to the hazard assessment. This report describes an update of the Ground Motion Prediction methodology (version 5) for the Groningen situation.			
Directliy linked research	(1) Hazard Assessment. (2) Fragility assessment of buildings in the Groningen region.			
Used data	Accelerograms from the accelerometers placed in the Groningen field. P- and S-wave velocity model sub-surface Groningen. Description of the shallow geology of Groningen.			
Associated organisation	KNMI			
Assurance	External assurance team has reviewed the report for GMM version 4. Comments from the assurance team on GMM version 4 have been addressed in the GMM version 5 and this report.			

V5 Ground-Motion Model for the Groningen Field

A report prepared for NAM

Julian J Bommer[1], **Benjamin Edwards**[1], **Pauline P Kruiver**[2], **Adrian Rodriguez-Marek**[1], **Peter J Stafford**[1] , **Bernard Dost**[3], **Michail Ntinalexis**[1], **Elmer Ruigrok**[3], **Jesper Spetzler**[3],

1. Independent consultant, 2. Deltares, 3. Royal Netherlands Meteorological Institute (KNMI),

30 October 2017

TABLE of CONTENTS

Acknowledgements

The report on the V4 ground-motion model includes almost three full pages of acknowledgements to the numerous individuals who have contributed in many important ways to the development of this work. Those expressions of gratitude and appreciation remain equally valid with regards to the V5 model.

In view of their critical role in providing detailed feedback on the draft V4 report and offering constructive suggestions that have contributed to important refinements in this latest stage of model development, we reiterate our debt of gratitude to the international GMM review panel, chaired by Jonathan Stewart and comprising Norm Abrahamson, Gail Atkinson, Hilmar Bungum, Fabrice Cotton, John Douglas, Ivan Wong and Bob Youngs.

We also add a note of thanks to the reviewers of the various journal papers that have been published from the work on the Groningen ground-motion model. Their comments and challenges have also been very valuable in assisting with the continued improvement of the GMM.

Renewed thanks are also due to Stephen Bourne, Steve Oates, Pourya Omidi and Tomas Storck for the invaluable feedback and testing of the model through implementation in the Groningen hazard and risk engine, and to Assaf Mar-Or for generating hazard and risk results that have provide very helpful insights into the performance of the model and changes from previous versions. We also thank Helen Crowley and Rui Pinho for keeping us informed of the ground-motion input needs for the derivation of building fragility functions for Groningen.

Finally, we must express our debt to Jan van Elk for continuing to provide the space and conditions to undertake this work and supporting for us in so many ways. The assistance of Dirk Doornhof and Jeroen Uilenreef in supporting Jan is also gratefully acknowledged.

1. Introduction

Following the magnitude M_L 3.6 Huizinge earthquake in August 2012, NAM has engaged in a major endeavour of data acquisition and model development to quantify the risk due to induced earthquakes in the Groningen field. A core component of the model for risk estimation is a ground-motion model (GMM) for the prediction of parameters characterising the shaking at the surface due to each earthquake scenario considered.

The Groningen GMM has been developed in successive stages, with the work beginning in the first half of 2013 when a very preliminary model was produced for the 2013 Winningsplan. Subsequently, over a period of four years, a much more sophisticated model has been developed in five successive and iterative stages, culminating in the V5 model presented in this report. The derivation of the previous four versions of the model were all documented in great detail in reports that collectively have a total length of 1,845 pages, supported by numerous other documents of even greater length presenting the underlying data collection activities to characterise the near-surface soil profiles across the Groningen field and the database of ground-motion recordings that have underpinned the model development. Additionally, several papers on different aspects of the model development process have been published in peer-reviewed journals. In view of the extensive documentation already available, this report presents a more succinct overview of the V5 model, presenting a summary of the model and brief narration of the modifications with respect to the V4 model, referencing earlier reports and published papers to guide the reader who seeks more detailed information.

Chapter 2 presents an overview of the evolution of the GMM for Groningen, including the incremental differences at each stage of development and most specifically the modifications of the V4 model included in the V5 model. The key features of the model are then explained in three sequential chapters: Chapter 3 presents the model for spectral accelerations and peak ground velocity (PGV) at the NS_B reference rock horizon; Chapter 4 presents the site amplification factors that transfer the rock motions to the ground surface; and Chapter 5 presents the model for durations. Chapter 6 summarises the complete guidance for implementing the GMM in terms of the logic-tree structure and the sampling of the variance components; for the user looking for a concise summary of the model without explanation of its derivation, this is fully self-contained in the sixth chapter. The report concludes with a brief discussion of the applicability of the current model and potential future developments. In order to keep the main body of the report to an accessible length, additional information and plots are presented in six appendices.

2. Evolution of GMM Framework

As noted in the Introduction, work on developing a ground-motion model for induced and triggered earthquakes in the Groningen field began more than four years ago and the model has evolved through various stages to reach the current formulation. The purpose of this chapter is to summarise the process both in terms of timelines and reviews of the various versions of the model, and also in terms of the evolution of the framework for the model.

2.1. Timeline of GMM development

In order to develop a probabilistic seismic hazard analysis for the 2013 Winningsplan, a seismological source model was developed that related the induced seismicity to reservoir compaction (Bourne *et al*., 2014) and the hazard calculations realised through Monte Carlo simulations (Bourne *et al*., 2015). A preliminary ground-motion model was developed within a short timeframe using the database available at that time, which included just 40 recordings from eight earthquakes with magnitudes in the range from M_L 2.7 to 3.6. The model was derived only for peak ground acceleration (PGA) and PGV, and was based on the European ground-motion prediction equation (GMPE) of Akkar *et al*. (2014) using hypocentral distance, R_{hyp}. The GMPE was deployed with an assumed V_{S30} of 200 m/s—which has since been found to be a very good estimate of the field average (Kruiver *et al*., 2017)—with various coefficients adjusted with magnitude-dependent alternatives so that below about magnitude 4 the predictions would match the Groningen data. The model consisted of a single equation for each ground-motion parameter and was a deliberately conservative choice in terms of the expected motions from larger earthquakes. The model, described in Bourne *et al.* (2015), was also limited by not being specific to Groningen conditions for larger earthquakes that will generally drive hazard and risk estimates.

In order to develop a model that more closely reflects the specific source, path and site characteristics of Groningen earthquakes and also captures the range of epistemic uncertainty in extrapolations from the existing data to larger magnitudes, a process was initiated in late 2013 that has led to five successive versions of the GMM (Figure 2.1). The short timescales for each stage of model development are immediately apparent. The number of development and reporting stages was dictated by regulatory requirements to provide periodic updates and also the requirement to develop a model to underpin the hazard and risk calculations developed for the 2016 Winningsplan. The process has also included additional reviews by an international panel of ground-motion experts, which has been supplemented by the peer review of the various papers submitted for publication in seismological and earthquake engineering journals.

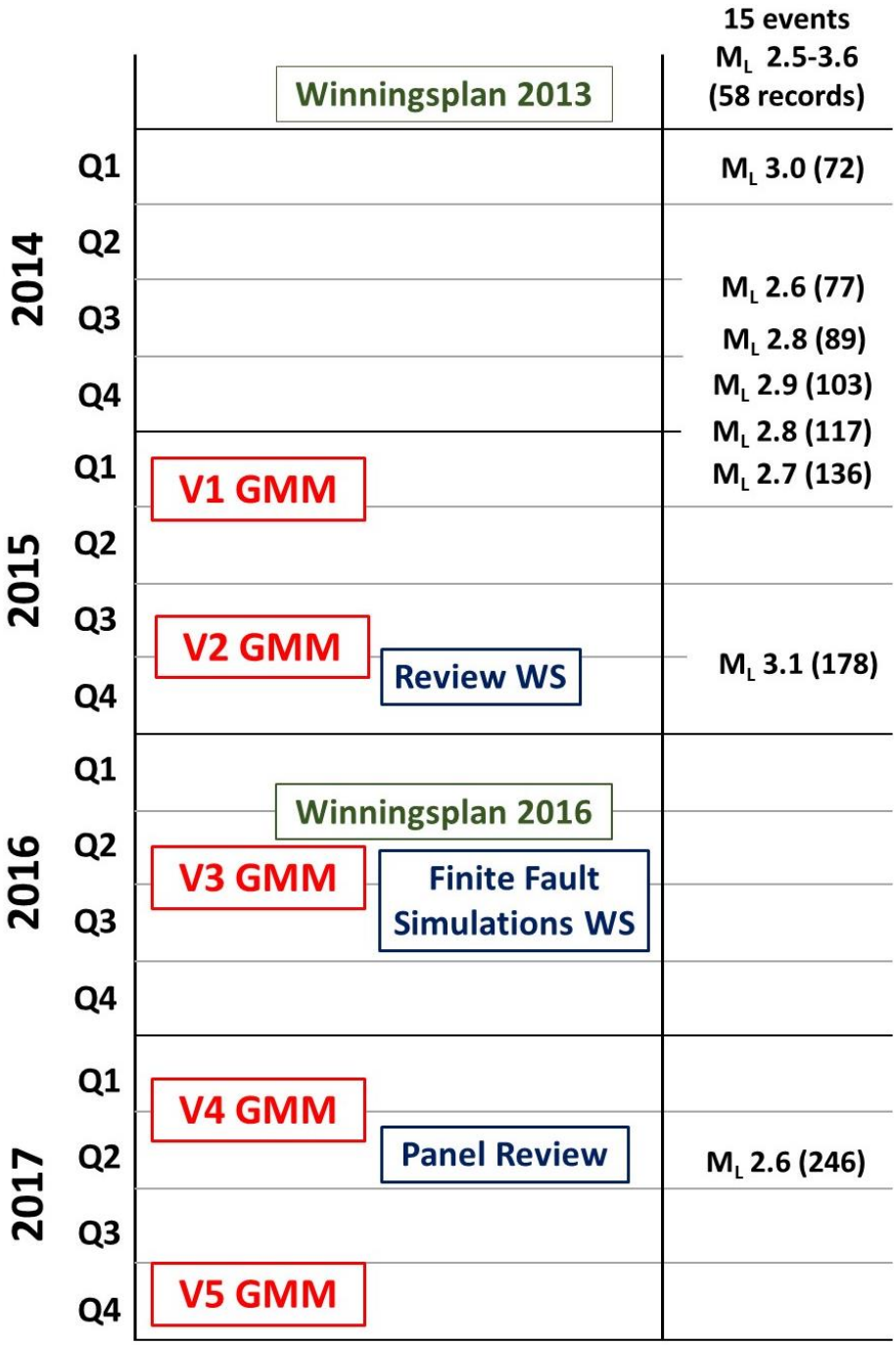

Figure 2.1. Timeline of GMM development for Groningen, with models indicated by date of issue of first report. The right-hand side indicates the growth of the ground-motion database in terms of recordings from events of M_L 2.5 and greater.

The technical advances in each stage of the model development, intended primarily to improve the representation of Groningen-specific conditions, are outlined below in Section 2.2. Externals factors that have influenced the process include the growth of the ground-motion database, aided by the expansion of seismic recording networks in the field (Dost *et al*., 2017a). At the end of 2013, the database contained just 58 records from 15 earthquakes; by the time of the V3 model development, the

database had grown to 178 recordings from 22 earthquakes, thus more than doubling the average number of recordings per event. The database remain unchanged for the V4 model development, but for the V5 database 68 new recordings from the Slochteren earthquake of May 2017 were added; an overview of the recordings from this earthquake is given in Appendix I. Figure 2.2 shows the magnitude-distance distribution of the final V5 database.

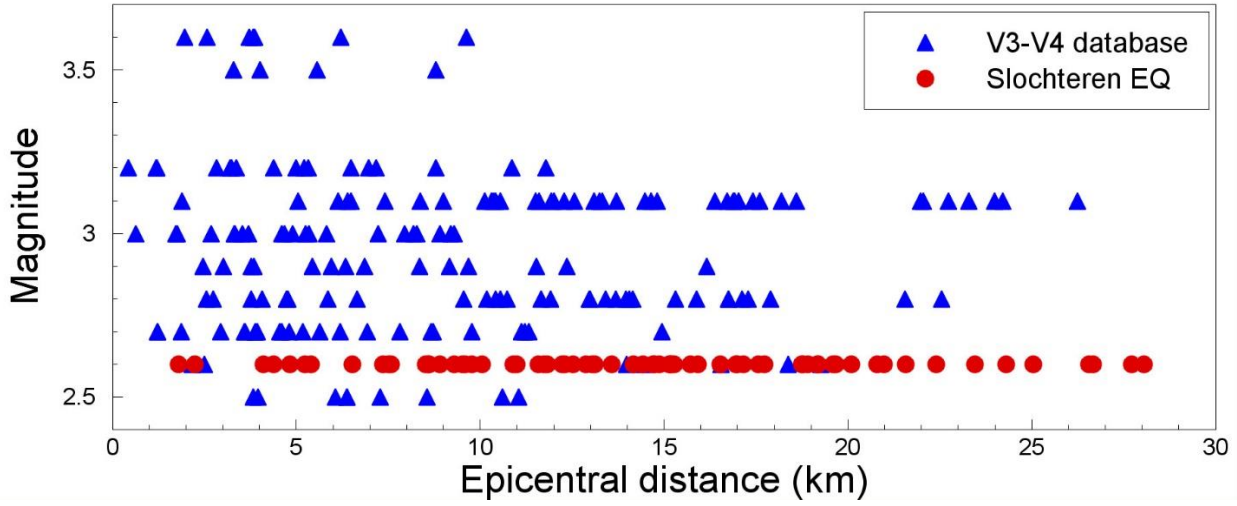

Figure 2.2. Distribution of the V5 Groningen ground-motion database in terms of local magnitude, M_L, and epicentral distance, R_{epi}.

Another important factor in the GMM development has been external review of the model, which has come from various sources including the Dutch State Supervision of Mines (SodM) and their expert advisors Dr William Ellsworth, Dr Art McGarr, and Professor Stefan Wiemer. Additionally, there were numerous review meetings with the Scientific Advisory Committee (SAC) chaired by Lucia van Geuns and some written comments from the SAC were also issued. Several questions and challenges on the GMM were posed to the development team, primarily by SAC members Dr Stefan Baisch and Professor Iunio Iervolino.

The GMM development also sought feedback and critical review from experts whose primary area of expertise is ground-motion modelling and site response analysis. An international panel was assembled consisting of Professor Gail Atkinson, Dr Hilmar Bungum, Professor Fabrice Cotton, Professor John Douglas, Professor Jonathan Stewart, Mr Ivan Wong, and Dr Bob Youngs. A two-day review workshop was conducted with the panel members on 27-28 October 2015, during which the V2 model was presented to the panel. The feedback received during the workshop and subsequently in written comments from most of the panel members were taken into account in the development of the V3 model.

Critical review and suggestions for improvement of the model have also been provided at numerous stages by colleagues from URC at ExxonMobil, particularly with regard to the use of ground-motion simulations using finite rupture models. To discuss these approaches, a second workshop was held in London from 18-20 July 2016. The workshop was attended by several colleagues from URC and some invited external experts: Dr Luis Angel Dalguer, who has worked for many years on finite rupture simulations, and Drs Norm Abrahamson, Christine Goulet and Bob Youngs, who all have experience in the use of ground-motion simulations in GMPE development. The workshop began with a presentation of the V3 model, with comments and feedback from the participants, and then focused primarily on the best options for incorporating finite rupture simulations into the V4 model.

After the V4 model was developed and documented, the report was circulated to the members of the original review panel, plus Dr Abrahamson, and written review comments from all eight panel members were compiled by Professor Stewart who coordinated the review. These comments were taken into account in the issue of revised version of the V4 GMM report but most importantly were considered in the development of the V5 model.

The intervals of time allocated to each stage of model development have been very short, which has meant that the time available for exploratory analyses and iterations within each development stage has been extremely limited. While this schedule has created challenging conditions for the development of a stable and robust model, it has also brought some advantages in terms of the model being fully documented at each staging point and also implemented into the NAM seismic hazard engine, both of which have facilitated review and feedback. From this perspective, the V1, V3 and V4 models can all be viewed as internal checking points along the path of the model development toward each Winningsplan submission (Figure 2.1). The primary targets have been the risk calculations rather than simply generating hazard maps since only the former provide a rational basis for decision making (Bommer *et al*., 2015a). The one exception to this, however, is the NEN-NPR seismic design code that the Dutch authorities have developed for the Groningen region, which adopted hazard estimates based on the V4 GMM for the specification of seismic loading in its current revised issue.

2.2. Evolution of the ground-motion model

Before the Akkar *et al.* (2014) GMPE derived from recordings of tectonic earthquakes in Europe and the Middle East was adjusted to Groningen data in the small-magnitude range for the preliminary seismic hazard model, the original intention had been to adopt the GMPE of Dost *et al*. (2004), which had been derived from recordings of small-to-moderate magnitude induced earthquakes in gas fields in the northern Netherlands. The data were mainly from the Roswinkel gas field rather

than Groningen but were also recorded on soft soil sites from shallow induced earthquakes and therefore seemed a logical choice for application to the Groningen field. However, the Dost *et al.* (2004) equations for PGA and PGV were found to grossly over-predict the recorded amplitudes of motion in the Groningen field. This was interpreted as being mainly due to the fact that in Groningen the high-velocity Zechstein salt layer lies above the gas reservoir—and is known to have a strong effect on the propagation of seismic waves ascending from ruptures initiating within the reservoir (Kraaijpoel & Dost, 2013)—whereas in the Roswinkel field the gas reservoir is above the Zechstein.

The observations prompted us to seek to develop a Groningen-specific model. The basic framework adopted for this was to invert the Fourier amplitude spectra (FAS) of surface motions in the field to estimate source, path and site parameters, and then to use simulations to estimate the motions from larger earthquakes. In order to capture the epistemic uncertainty associated with the extrapolations from small- to large-magnitude earthquakes, a logic-tree framework was adopted with the branches occupied by different versions of the simulation parameters, in effect following the 'backbone' GMPE approach (Atkinson *et al*., 2014).

Figure 2.3 schematically illustrates the approach adopted for the V1 GMM (Bommer *et al*, 2015b; Bommer *et al*., 2016a).

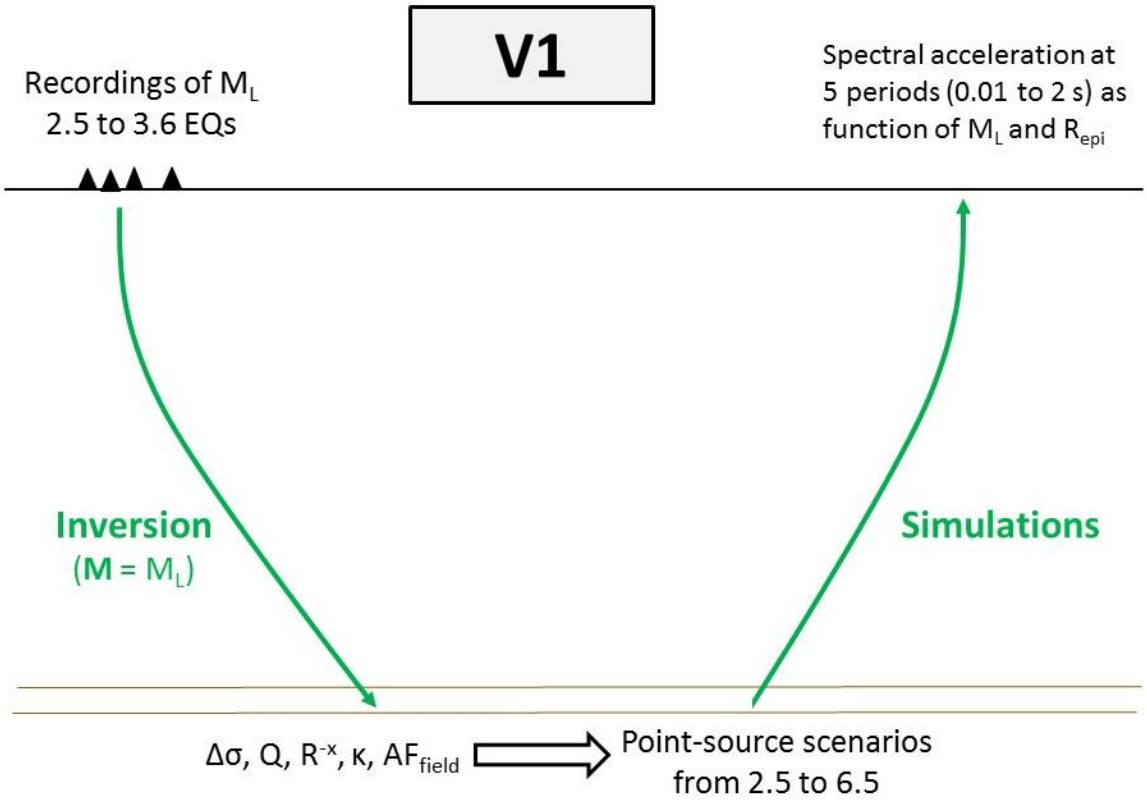

Figure 2.3. Schematic illustration of the development process adopted for the V1 GMM

The inversions identified optimal values of the parameters characterising the source, path and site, but in the forward simulations three different models for the stress parameter were adopted. While the V1 model was calibrated to Groningen conditions, it was considered deficient in terms of site response characteristics for two reasons. Firstly, the model included a field-wide site amplification function—inferred from the average amplification function for the recording network—without any lateral variation. Secondly, the amplification functions were linear and thus did not capture the potential effects of non-linear response of the soft soils under higher levels of acceleration.

The V2 model was the first model to capture local site effects (Bommer *et al*., 2015c). This was done by developing predictive equations for a reference rock horizon and then combining these with non-linear site amplification functions for the overlying soil layers. The starting point was to deconvolve the FAS and the response spectra of the surface recordings using the shear-wave velocity (V_S) profiles developed for the field by Deltares (Kruiver *et al.,* 2017). A key assumption here was that since the recorded motions are weak, it could be assumed that the soil response was linear. For the V2 model, the reference rock horizon was the base of the Upper North Sea formation (NU_B) located at a depth of about 350 m (Figure 2.4). The forward simulations for the rock motions were performed for an increased range of response periods in order to match the definitions of the building fragility functions.

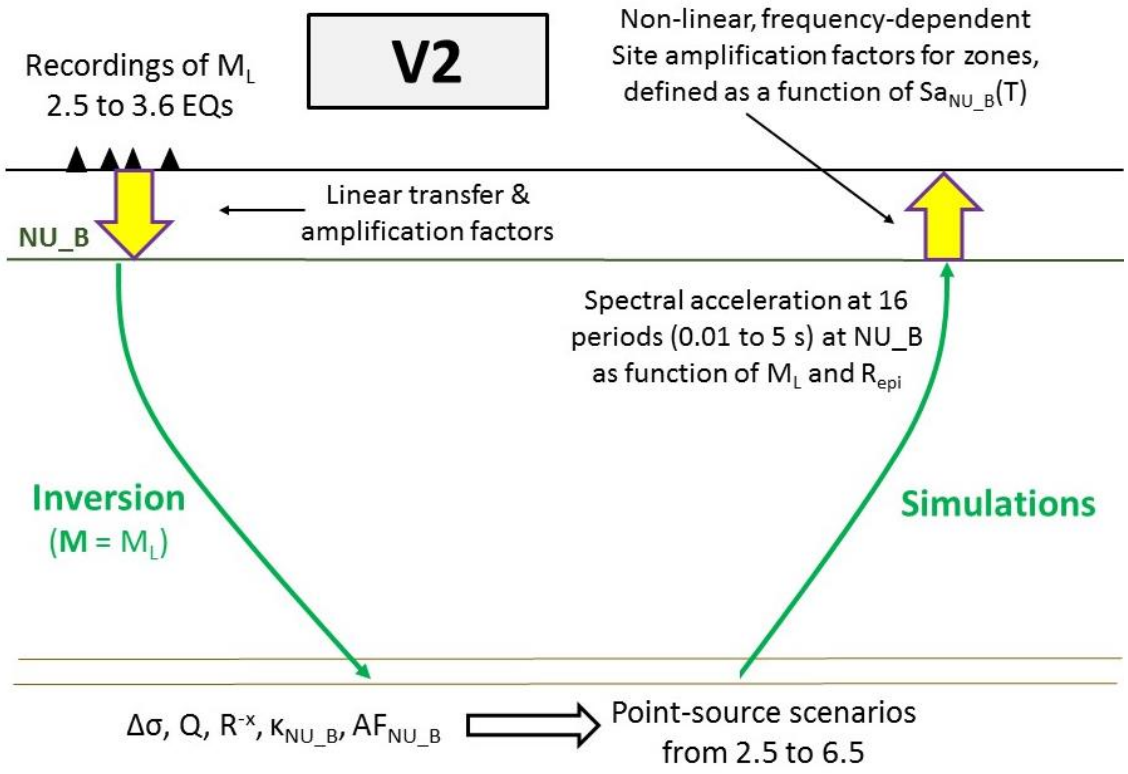

Figure 2.4. Schematic illustration of the development process adopted for the V2 GMM

The simulations were also used to generate FAS for a wide range of magnitude and distance combinations, and these were then used as input to RVT-based site response calculations to estimate amplification factors (AF) for the overlying soil layers. A zonation of the field, modified from a geological zonation, was defined such that within each zone an AF would apply at all locations for each response period.

The V3 model was a modification of the V2 GMM, with the most important change being to move the reference rock horizon to the more pronounced impedance contrast at the base of the North Sea supergroup (NS_B), located at a depth of 800 m (Figure 2.5). In most other regards, the model derivation followed the same procedures, except that seven additional response periods were added in the short-period range to enable more realistic vertical spectra by application of V/H ratios. Both the NS_B reference horizon and the 23 target oscillator periods have remained fixed in subsequent versions of the model. The V3 GMM was documented in a report (Bommer *et al*., 2016b) and also summarised in journal papers on the site response model (Rodriguez-Marek *et al*., 2017) and the overall model (Bommer *et al*., 2017a).

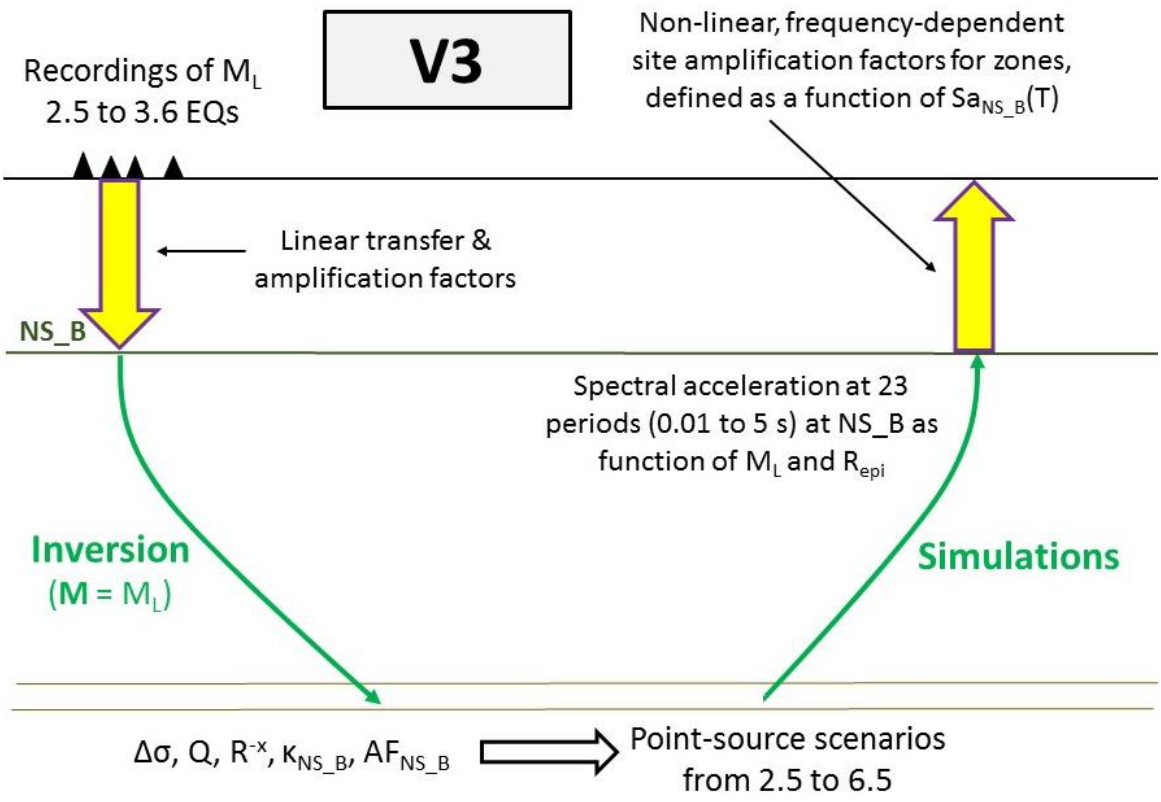

Figure 2.5. Schematic illustration of the development process adopted for the V3 GMM

While the basic framework of the V3 GMM was largely retained for the V4 model, some important innovations were also made, as detailed in the report by Bommer *et*

al. (2017b) and a paper by Bommer *et al*. (2017c). In Figure 2.6 the changes from the V3 to V4 model derivation are highlighted in red, and these include the following:

1. A move from point-source simulations using SMSIM (Boore, 2005a) to using simulations based on extended fault ruptures using EXSIM (Motezadian & Atkinson, 2005); this resulted in a change from epicentral distance (R_{epi}) to rupture distance (R_{rup}).
2. Scenario-dependence was introduced into the linear site amplification factors at short periods, an innovation not only for the Groningen project but in this field in general (Stafford *et al*., 2017).
3. In the inversions, the previous assumption that moment and local magnitudes were equivalent was replaced by a relationship that indicated that for events of magnitude 2.5 and greater, moment magnitudes are on average 0.2 units smaller than M_L values.
4. The simulations included PGV in addition to spectral accelerations at 23 response periods since although not used in the risk model, this parameter is of interest because it is widely used to define tolerable levels of shaking.
5. Following an expert workshop on Mmax for Groningen held in Amsterdam in March 2016, the largest magnitude for which the GMM needs to be applicable increased from 6.5 to greater than 7 (Bommer & van Elk, 2017).

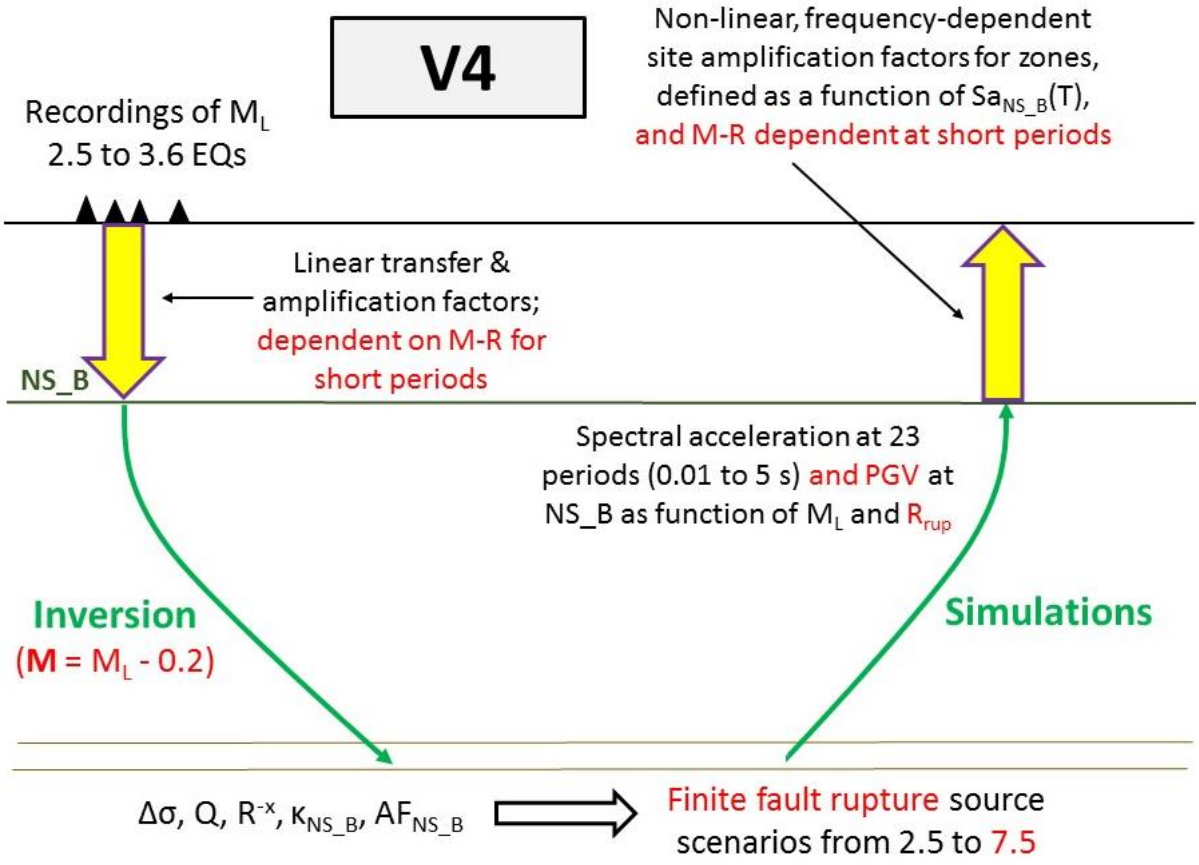

Figure 2.6. Schematic illustration of the development process adopted for the V4 GMM

The V5 GMM was intended to be a refinement of the V4 model, maintaining the same framework as illustrated in Figure 2.6, taking account of comments and suggestions from the review panel. Among the points raised by the reviewers was the calibration of the highest branch on the GMM logic-tree to match predictions from GMPEs derived from recordings of tectonic earthquakes. For the site response component of the model, particular focus was given to refining the magnitude- and distance-dependence of the linear AFs, and to accounting for uncertainty in the modulus reduction and damping (MRD) curves in the site-to-site variability. As has been noted in Section 2.1, an unforeseen modification was to add the recordings from the May 2017 Slochteren earthquake to the database.

However, there was another very important change from V4 to V5, which is the relationship between local and moment magnitudes in Groningen. Extension and refinement of the analyses that had previously suggested a systematic difference of 0.2 magnitude units between the two scales now concluded that for $M_L \geq 2.5$, the scales were in fact equivalent, on average (Dost *et al*., 2017b). Therefore, the V5 inversions were performed assuming **M** = M_L, as indicated in Figure 2.7. Although this is the only major change in the model derivation from V4 to V5, the **M**-M_L relationship exerts a major influence on inversions and consequently on GMM. The issue of the relationship between the magnitude scales is discussed in Appendix II.

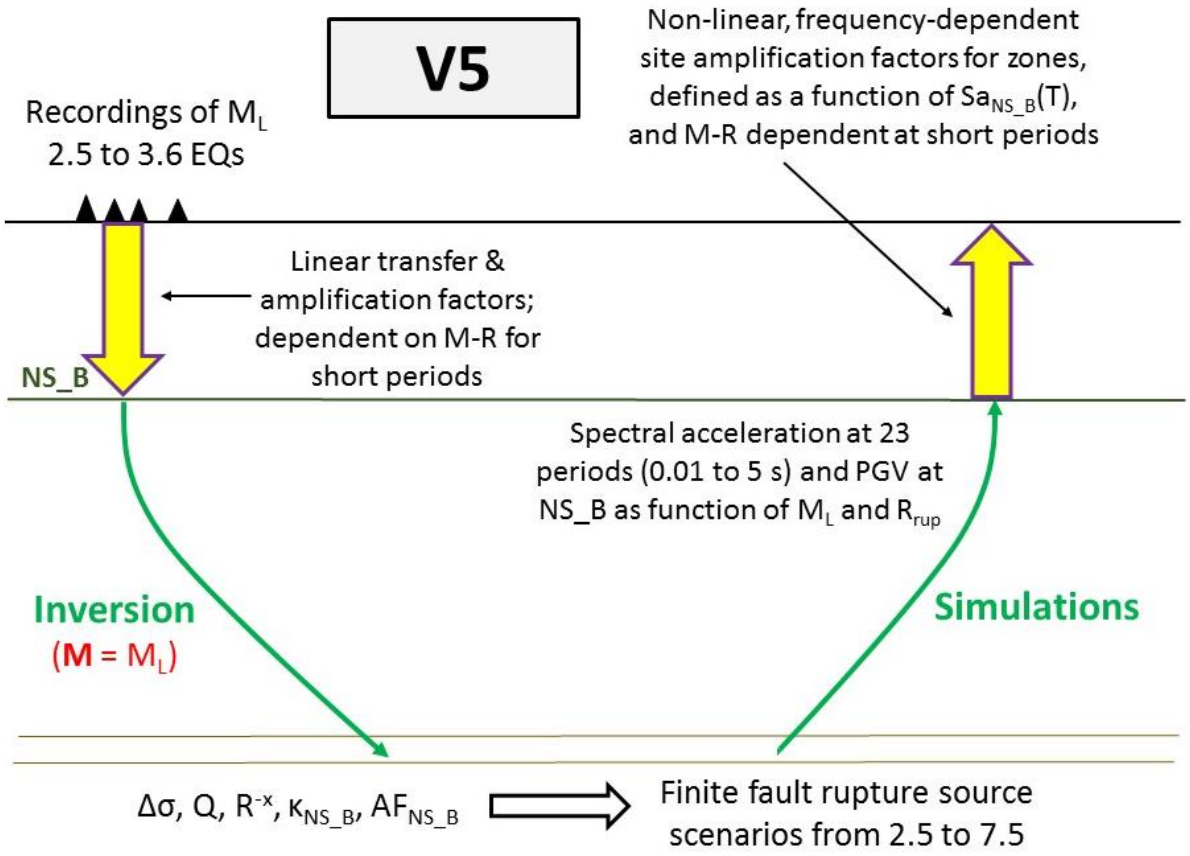

Figure 2.7. Schematic illustration of the development process adopted for the V5 GMM

The **M**-M_L relationship used in the development of the V4 model is now considered to be inappropriate, and its correction now makes the V5 model a stable framework. As is discussed later in the report, the single application of an incorrect relationship between the magnitude scales for one of the five model development stages creates an exaggerated impression of the instability in the process.

The schematic illustrations in Figures 2.3 to 2.7 provide only very high-level illustrations of the processes involved. A more detailed overview is given in Figure 2.8, which highlights several of the additional inputs to the process, including the following:

- FAS and response spectra of recordings from the B-station accelerographs were transformed to the NS_B horizon using the V_S profiles from the field-wide model of Kruiver *et al*. (2017) modified over the uppermost ~30 m using *in situ* measurements (Noorlandt *et al.,* 2017). For the G-stations, where such *in situ* V_S measurements have not yet been made, rather than using surface accelerograms, recordings from geophones at 200 m depth were used to avoid the uncertainty in the highly influential uppermost part of the V_S profiles.

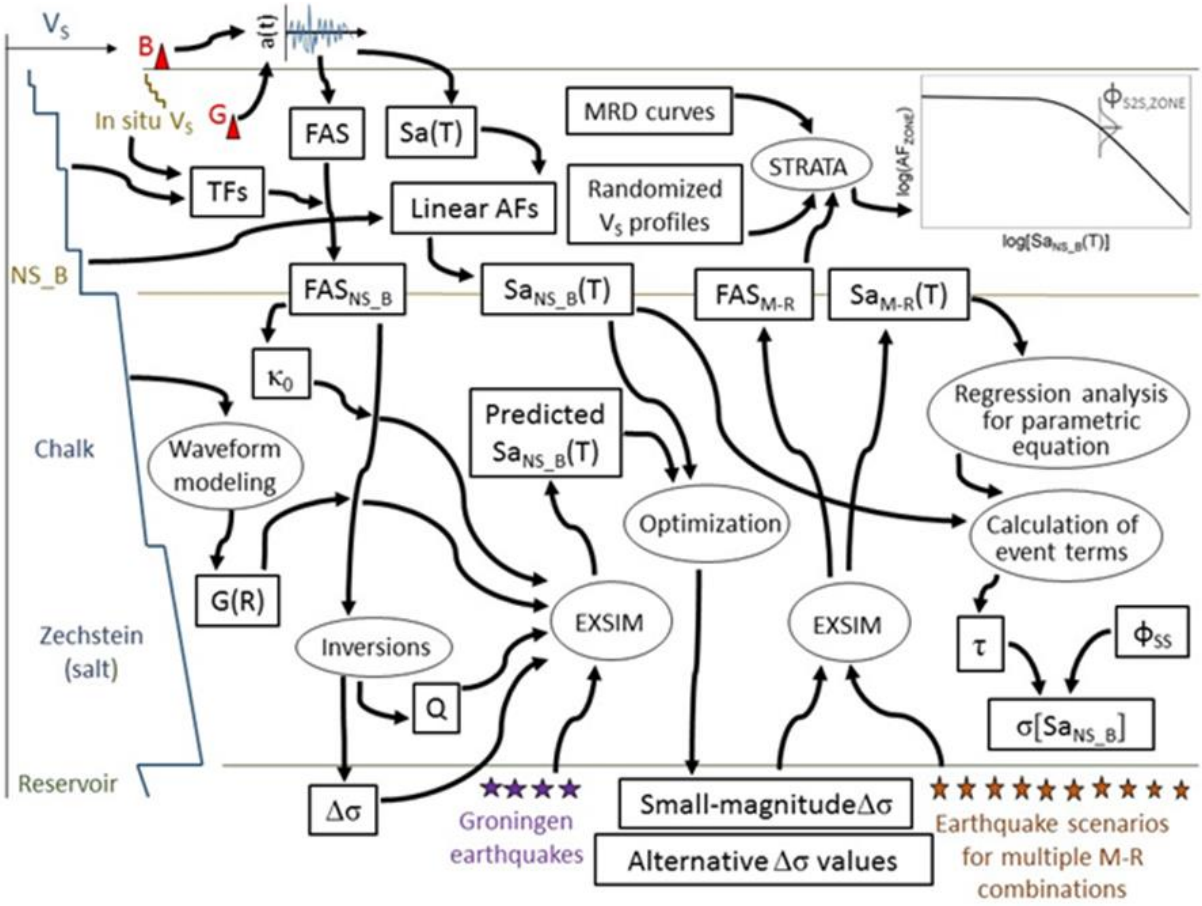

Figure 2.8. Illustration of the process for the derivation of the V4 and V5 GMM, adapted from Bommer *et al*. (2017a)

- In order to reduce the numbers of degrees of freedom in the inversion of the FAS at the NS_B horizon, some of the parameters were constrained independently. The kappa values were estimated directly using the method of Anderson & Hough (1984) and the geometrical spreading patterns were constrained with finite difference waveform simulations using a detailed 3D velocity model of the field.

Since the fragility functions for some building types in Groningen are defined in terms of both spectral accelerations and duration, a model has also been required for the prediction of the latter. In the V1 model, the duration was estimated simply using the Kempton & Stewart (2006) equation for durations with an assumed field-wide V_{S30} value of 200 m/s. In the V2 model, the duration GMPE of Afshari & Stewart (2016) was modified to provide a better fit to the Groningen data, and a similar procedure was followed for the V3 GMM. For the V4 model, a new equation was derived from regression on the durations of simulated motions from EXSIM at the NS_B horizon, and the site amplification factors of Afshari & Stewart (2016) adapted to transfer the rock durations to the ground surface.

In closing this chapter, a brief comment is in order regarding the oscillator periods for which the model provides predictions of spectral accelerations. There are 23 target periods between 0.01 s and 5 s, the spectral acceleration at the former period being equivalent to PGA. This wide range of periods is covered so that the model may address all current and future requirements, but in assessing the model and its performance it is worth considering the response periods that are actually relevant to the risk calculations. Figure 2.9 displays information regarding the periods used to characterise the fragility functions for the 54 building types classified in the Groningen exposure database. For some building types, the spectral acceleration at the fundamental period, T1, is found to be sufficient to define the fragility function; for others, a second period, T2, and/or the duration is also required. The top plot shows the T1-T2 pairs, in which 0.001 s implies that the second period is not needed. There are fewer than 54 points on this plot because several building types have the same two controlling periods. The middle plot shows the distribution of building types with regards to the period T1; note that the first bar represents characterisation by Sa(0.01s), or PGA. The lower plot shows the same information but in terms of the number of buildings in each period range, from which it is clear that apart from a large number of buildings characterised by PGA, the majority of the building stock has dominant periods in the range from 0.25 to 0.6 seconds. If one takes into account that these intermediate periods will often correspond to larger or taller structures, the distribution of exposed population would be even more concentrated in this period range. Periods beyond 1 second are of limited importance currently. The dense sampling of periods from 0.025 to 0.20 seconds has been primarily to allow the application of V/H ratios to lead to appropriate shapes for vertical response spectra; however, there has, to date, been little need for such spectra.

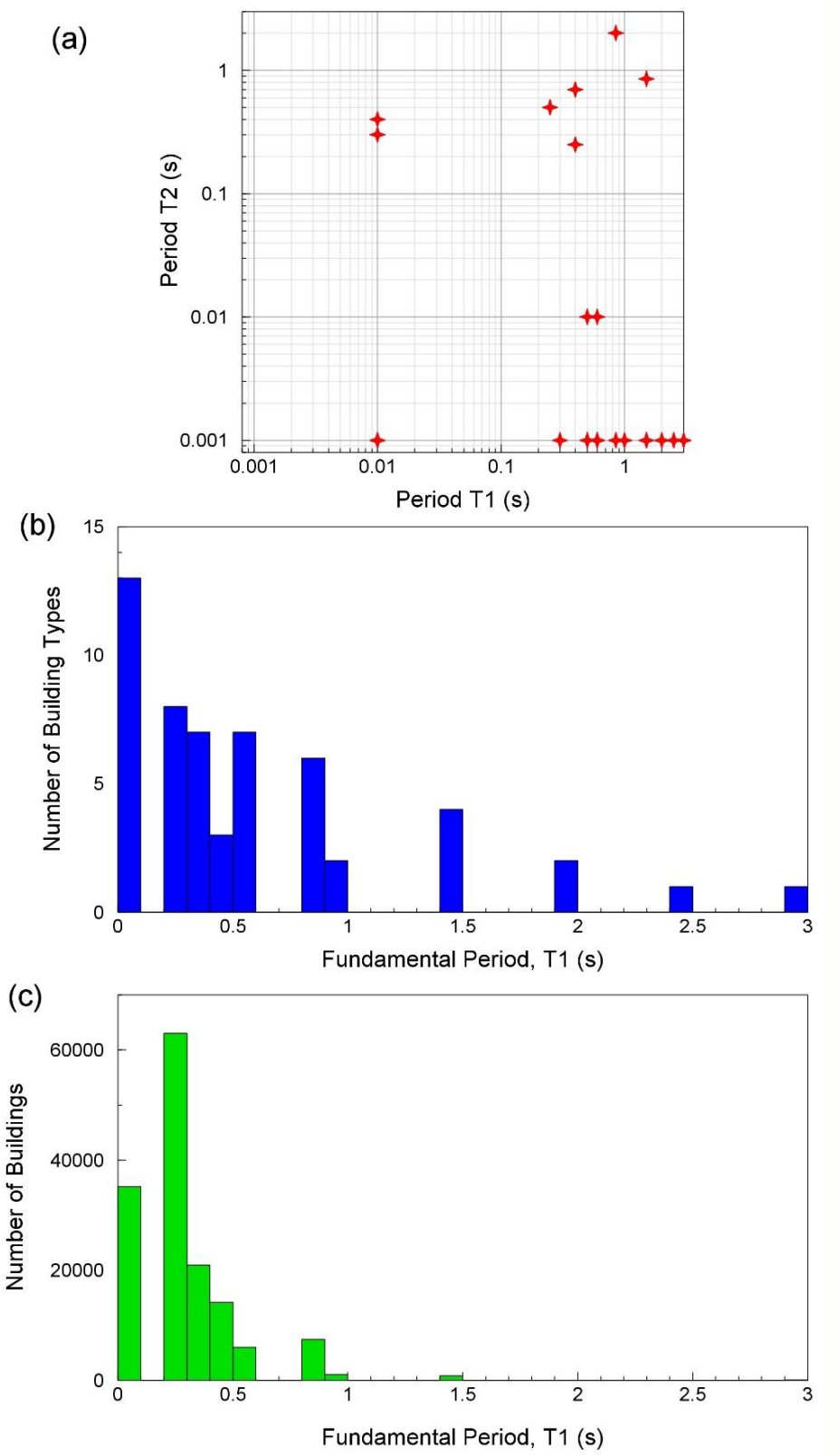

Figure 2.9. Characteristics of the V5 exposure database in terms of periods at which spectral accelerations define the fragility functions: (a) primary and secondary periods, in which a value of 0.001 s implies no secondary period; (b) numbers of building types in each period range; (c) numbers of buildings in each period range. Data provided by Helen Crowley.

3. V5 GMM for Amplitudes at NS_B

The first part of the model for the prediction of Sa(T) and PGV is a suite of ground-motion prediction equations (GMPEs) for the estimation of these parameters at the reference rock horizon (NS_B). The derivation of the V5 model for the motions at the rock horizon followed the same procedures as used in the V4 GMM development. However, three changes influenced the outcomes of this process. The first of these is minor updating of the soil properties tables (see Section 4.1) that led to minor modifications in the transfer functions used to translate the FAS of recordings at or near the surface to the NS_B horizon. The more significant changes were addition of a large number of recordings from the May 2017 Slochteren earthquake (Appendix I) and the update of the relationship between moment and local magnitudes in the Groningen region (Appendix II). This chapter briefly summarises the modifications from the V4 rock model as a result of these changes to the input data and concludes with a comparison of the two models.

3.1. Inversion of NS_B motions

In view of the limited magnitude range of the earthquakes represented in the Groningen ground-motion database—with an upper limit of M_L 3.6—one of the key challenges in developing the GMM for the hazard and risk models has been the extrapolation to the largest magnitude currently considered, **M** 7.25. In order to accomplish this for the V5 Groningen GMM, motions are calculated using finite-fault, stochastic simulations. The method used is based on a discretised rupture model with dynamic corner-frequency (EXSIM: Motazedian & Atkinson, 2005; EXSIM_dmb: Boore, 2009). Each of the distributed sub-faults in this technique is assumed to be a point source (effectively a small magnitude earthquake), and can be characterised using the seismological parameters observed in events recorded in the Groningen gas field. More specifically, the seismological characteristics required for modelling ground motion using EXSIM are estimates of the source, path and site parameters that define the Fourier amplitude spectra (FAS) and duration of the motion. This section presents how the V5 GMM has been updated with respect to the V4 model. In all other aspects the inversion methodology and results remain as per the V4 GMM.

The ground-motion database, comprising recorded surface motions (B-stations) or 200 m borehole motions (G-stations), has been expanded by one event to 23 in the V5 model, and now includes 248 records, each of which has been deconvolved to the base of the North Sea supergroup (NS_B) horizon using the linear anelastic amplification functions corresponding to the velocity profile beneath each site (Figure 3.1). When deconvolving the borehole data within-column motions are used, such that the down-going waves are accounted for.

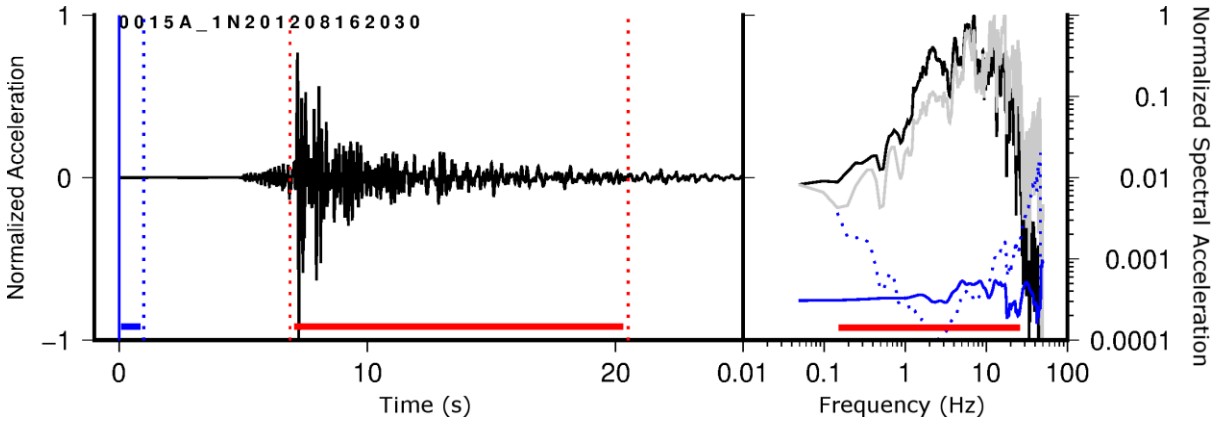

Figure 3.1. *Left*: example acceleration time series of the 2012 M_L3.6 Huizinge earthquake recorded at station 15 (GARST), 14 km from the epicentre. The period highlighted in red indicates the signal and in blue the noise. *Right*: Fourier amplitude spectrum of the acceleration time series. Black: as recorded at the surface; grey: deconvolved to the NS_B; solid blue: recorded noise; dotted blue: noise after deconvolution to the NS_B and low frequency adjustment; the frequency range highlighted in red shows the FAS used in inversions (SNR > 3)

The FAS of recordings, deconvolved to the NS_B horizon, were then used to determine the source, path and NS_B rock parameters for use in subsequent forward simulations. In a refinement to the inversion methodology used in the V4 GMM, a Bayesian-approach was implemented to reduce the strong trade-off between the event stress-parameter (and equivalently, f_{0i}) and κ. A prior distribution for the stress-parameter was produced using a median and log-normal standard-deviation. Standard deviations of 1.0, 1.25 and 1.5 ($\log_{10}$ units) were tested (note that they do not directly relate to the posterior distribution of Δσ). 1.25 was selected as a compromise between the prior having limited influence (1.5, Δσ outliers still present), and too-much (1.0, standard deviation of Δσ < 0.2): the aim being to reduce strong trade-offs, rather than controlling the median. Medians of the prior were 30, 50 and 70 bars (based on results using an initial uniform prior).

In the analyses (using three priors with median Δσ = 30, 50, 70 bar and 1.25 $\log_{10}$-unit standard deviation) Q values of 220-250 were obtained for an average shear-wave velocity of 2.6 km/s. In addition we determine site specific NS_B κ_0 of 0.01 to 0.045 s (5^{th}, 95^{th} percentiles). Figure 3.2 shows typical surface FAS fits using the resulting source (**M**, Δσ) and path (Q) model along with site-specific amplification (including κ_0) computed using the NS_B corrected FAS, and applying the NS_B to surface transfer function. Using the 70, 50 and 30 bar priors resulted in median stress parameters of 40, 35 and 35 bars respectively (using a common Q, with site specific κ_0), indicating that the results are robust regardless of the choice of prior (Figure 3.3).

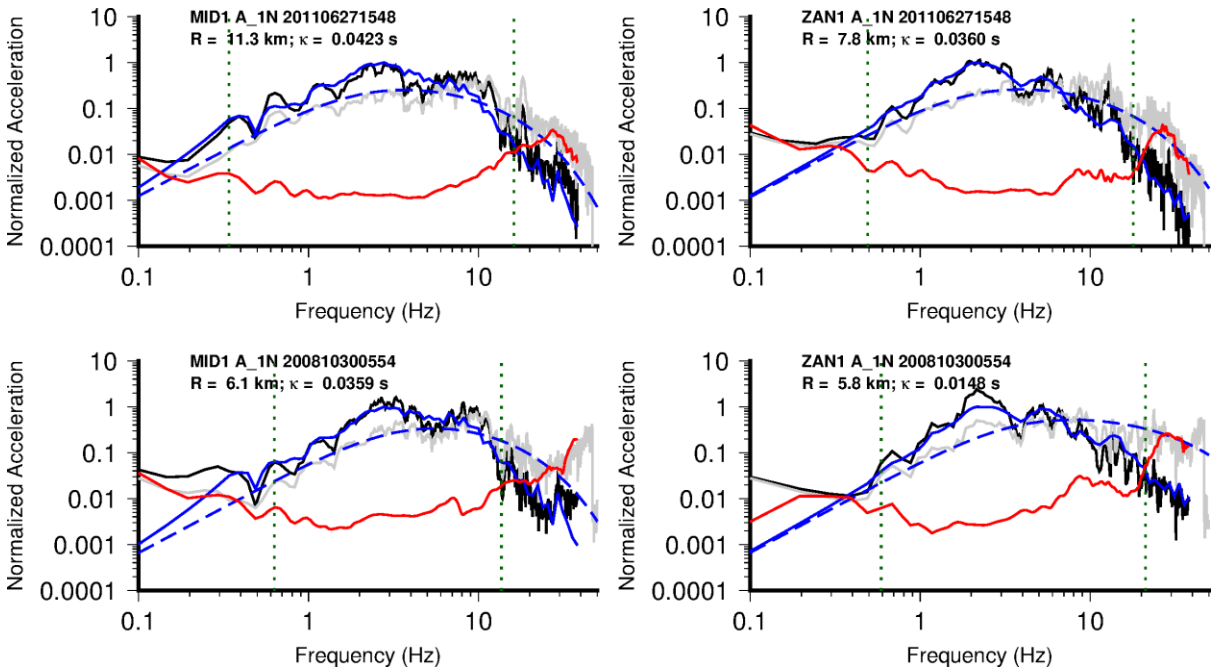

Figure 3.2. Comparison of observed (surface recordings at MID1 and ZAN1 accelerometers) and modelled FAS for two M_L = 3.2 events: top – 2011 Garrelsweer event (f_0 = 2.1 Hz); bottom – 2008 Westeremden event (f_0 = 3.7 Hz). Note absolute amplitudes are normalized such that only spectral shape is fit. Black line: surface acceleration FAS; red: surface noise FAS; grey: FAS deconvolved to NS_B using site transfer function; blue: modelled FAS (dashed: at NS_B; and solid: at surface).

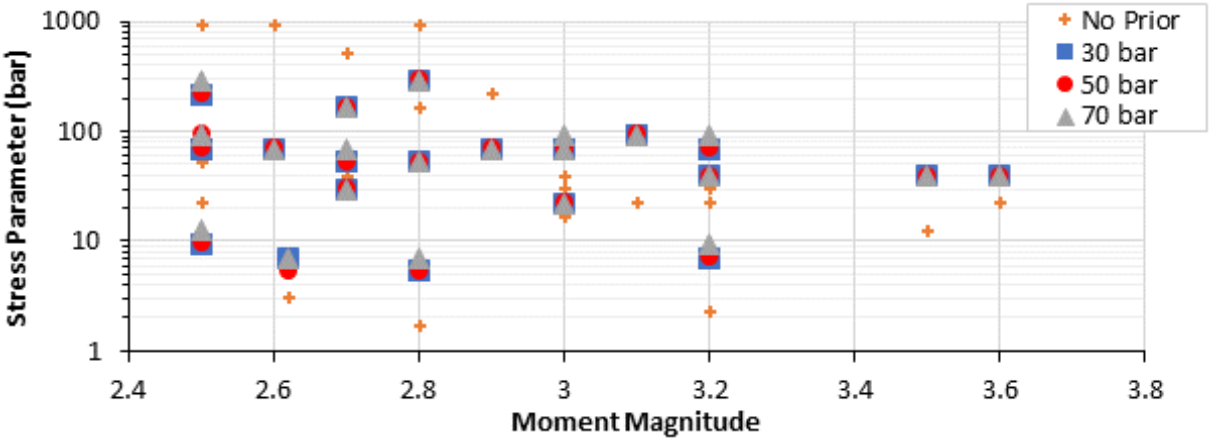

Figure 3.3. Best-fitting stress parameter for Groningen earthquakes using no prior, and 30, 50 and 70 bar priors in the stress-parameter distribution.

Using the long-period displacement plateau of the NS_B-corrected FAS, the geometrical decay function was inverted for along with average site amplification, fixing the moment magnitudes as determined by KNMI. The hinge points of the geometrical spreading function were selected to coincide with the distances observed during the full waveform simulations undertaken at Shell: 7 km and 12 km.

We assume that below 3 km (the minimum observed hypocentral distance), the decay is the same as between 3 to 7 km. The shape of the decay observed is similar (although less pronounced) to that seen during the simulations, indicating that the velocity structure has a strong impact on the recorded amplitudes as a function of distance. The decay rates observed were: $R^{-1.55}$ up to 7 km, $R^{-0.23\pm0.22}$ from 7 to 12 km, and $R^{-1.43\pm0.39}$ from 12 to 25 km. There is no error assigned to the first rate of decay, as it is conditioned on the selected **M** values (and segmentation distances). Although there are no data beyond around 25 km we assume R^{-1}, as indicated by the full waveform analyses. It is noted that the initial rate of decay is strongly dependant on the **M** values used in the inversion. In the previous V4 GMM, we used lower values of **M** (*i.e.*, assuming **M** = M_L - 0.2 rather than **M** = M_L), and therefore with seismic moments ~2 times weaker). This led to a stronger rate of decay in the first 7 km for the V5 model (and similar to the decay seen for the V3 model, which also used **M** = M_L). The reason for this is that the moment magnitude (and therefore seismic moment) sets the initial (source) amplitude, while the first observations occur at ~3-7 km. The difference between source and observations then defines the initial rate of decay.

In order to define a field average amplification at the NS_B level, the (geometric) average amplification (source to NS_B) of all sites was computed. The amplification was found to be broadly frequency-independent between ~1 and 10 Hz and around 0.8-1.0 (albeit with a large standard deviation), suggesting that the effect of the velocity structure between the source (the reservoir) and the NS_B interface results, overall, in no significant resonance (Figure 3.4). The mild de-amplification between 1 and 10 Hz may be indicative of the velocity inversion present between the source and NS_B. At 0.6 Hz a pronounced peak exists which is also clear in the ground-motion residuals from previous GMMs. This feature is therefore retained. At high frequency the amplification increases, and plateaus at ~1.5, consistent with expectations from quarter-wavelength modelling of the velocity profile.

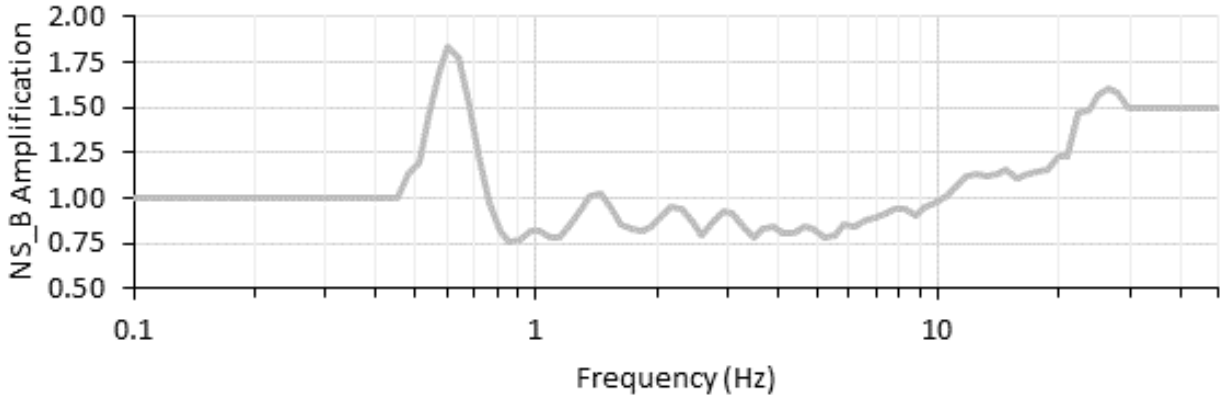

Figure 3.4. Network average source to NS_B amplification.

3.2. Selection of forward simulation parameters

In the Groningen GMM input ground motions are calculated using a finite-fault stochastic simulation methodology (EXSIM_dmb [version date: 17/10/2016]: Boore, 2009, based on EXSIM: Motazedian & Atkinson, 2005). This approach produces full time-histories and corresponding spectral ordinates by specifying a simplified seismological model (earthquake source, propagation and site effects).

The inversions discussed in Section 3.1 yield a range of possible combinations of source, path and site parameters that are consistent with the recorded data. While there is therefore an estimate of the mean value of each of the parameters obtained from the inversion, what is sought is the combination that when used in stochastic simulations yields predicted spectral ordinates that best reproduce the recordings. Based on the initial observations and spanning a broad range of the model space, we defined 72 parameter combinations based on: κ_0 values of 0.001, 0.005, 0.010, 0.015, 0.020 and 0.025 s; Brune stress parameter, $\Delta\sigma$, of 10, 30, 50, 60, 70, 80, 90, 100, 120, 150, 200 and 300 bar, and a Q value of 220. All simulations used the geometrical spreading model determined in Section 3.1, which was based on the segmentation distances from full waveform modelling. Source to NS_B amplification, based on the network-average, was relatively small, but non-negligible. The simulations were compared to the individual horizontal component response spectra at the NS_B horizon for all 20 spectral periods for which recorded data were available (0.01 to 2.5 s).

In order to assess the fit of each model the inter-event terms are calculated at each of the 20 periods. As for the V4 GMM, random-effect terms are calculated using:

$$\eta_i = \frac{\tau^2 \sum_{j=1}^{n_i} y_{ij} - \mu_{ij}}{n_i \tau^2 + \phi^2} \qquad (3.1)$$

(Abrahamson & Youngs, 1992) with arbitrary starting values of the intra-event term ϕ=0.5 and inter-event term τ=0.5 ($\log_{10}$) and iterating until convergence. n_i is the number of records (y_{ij}) for the j^{th} event and μ_{ij} is the mean value of the j records for the i^{th} event. From the inter-event terms the average model bias is measured from the N events:

$$bias(T) = \frac{1}{N} \sum_{i=1}^{N} \eta_i (T) \qquad (3.2)$$

As for the V4 GMM, the root-mean-square (RMS bias) and standard deviation [σ(RMS bias)] over the period-specific values is taken after each simulation to provide a simulation specific (period independent) measure of model bias. Note that the RMS misfit will only be 0 in the case that the model is perfectly unbiased at all periods. Low σ(RMS bias) indicates that the residual misfit is consistent (either

consistently biased or unbiased), high values indicate period-to period differences in the bias are present. EXSIM performs time-domain simulation, and is significantly slower than SMSIM, which can use random-vibration theory to speed up the process when only peak-amplitude ordinates (*e.g*., SA) are required. For small magnitude events, EXSIM_dmb has been shown to produce the same results as SMSIM (Boore, 2009), as verified in the V4 GMM.

The results in terms of mean RMS bias is shown in Figure 3.5 versus stress parameter and κ_0. The contour plot clearly shows the trade-off between the source and site terms, with increasing stress-parameter being accompanied by increased κ_0 to provide similar bias. The best fitting model for the motions at the NU_B horizon is found to have the following parameter combination based on the smallest RMS average misfit (bias) and sigma: $\Delta\sigma$ = 70 bar; κ_0 = 0.010 s (RMS bias = 0.058 ± 0.087). The stress-parameter determined from the response spectra is higher than the average of ~35 bars determined from spectral analysis. It is noted, however, the approach here is to determine a full set of simplified parameters that reproduce the observed SA (and variability), rather than replicating the mean observed for the individual events.

Calibration to global GMPEs

The aim of the *upper* branch of the Groningen ground-motion model is to reflect ground motions observed for small **M** events in the gas field, while producing ground motions comparable with global tectonic seismicity when extrapolating to larger **M**. In order to calibrate the model at large magnitude we have performed a similar process to that described above for matching models with locally observed events. However, we now set the target as the PSA at 6 spectral periods (PGA, 0.1, 0.2, 0.3, 1 and 2 s) at magnitudes **M** = 5, 6 and 7, for logarithmically spaced distances of 0, 2.5, 5, 10 and 20 km and with V_{S30} = 1500 m/s (consistent with NS_B rock velocities). Normal faulting is assumed, with a dip of 75°. Six GMPEs were used as the target: three NGA-W2 models (BSSA14: Boore *et al*., 2014; CY14: Chiou & Youngs, 2014; CB2014: and Campbell & Bozognia, 2014) in addition to the Eastern North America model YA15: Yenier & Atkinson (2015) and the European (RESORCE) models Aetal14: Akkar *et al*. (2014) and Betal14: Bindi *et al.* (2014). Due to the larger stress-drops expected for normal tectonic events, the grid-search was expanded to include 20 values between 50 and 1600 bars. Based on the work of Boore (2009), who compared SMSIM against EXSIM_dmb, and the comparisons undertaken here, SMSIM (with the R_{EFF} distance metric used for finite-fault approximation) was again used for the calibration.

Models with low bias (over the range of κ_0) and period-to-period variability in bias σ(RMS bias) use 200-400 bars (Figure 3.6). Assessing the fit was somewhat subjective due to the strong attenuation in the Groningen model, which was not exhibited in the GMPEs and leads to a greater spread of SA at moderate and short periods with distance (Figure 3.7).

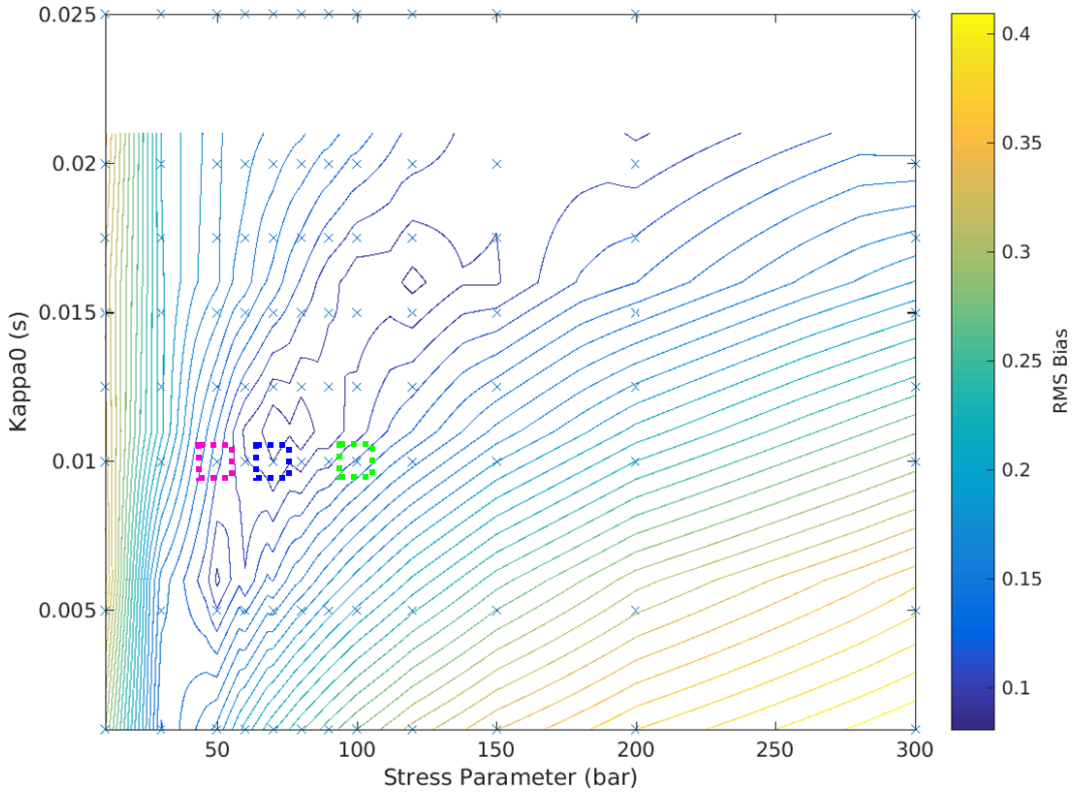

Figure 3.5. RMS bias contoured against stress parameter and κ_0 for Q=220. Dashed lines indicate the selected central (blue), lower (purple) and upper (green) model parameters for M ≤ 3.6.

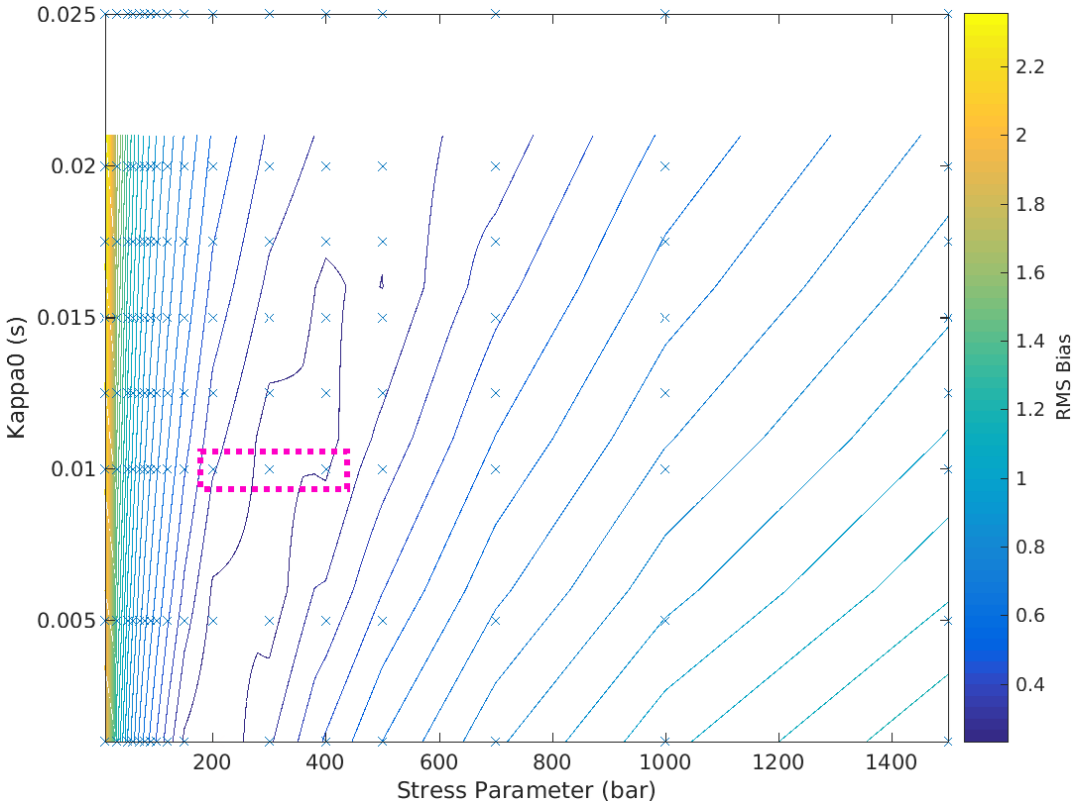

Figure 3.6. RMS bias against stress parameter and κ_0 for the NGA-W2 GMPE target PSA.

To be conservative, a model with ~300 bars was selected after inspection of the residual misfit plots to ensure that predicted motions for the upper model are consistent with (or, if necessary, exceed) tectonic seismicity across the range of periods. Effectively this means accepting a small positive model bias (*i.e.*, overestimation of long-period ground-motion) in order not to underestimate the short-period motions. A comparison of the simulated ground motions in terms of period, distance and magnitude is shown in Figure 3.7 for a 300 bar model. From these plots i7 can be appreciated that the upper branch of the V5 GMM does indeed mimic the GMPEs derived from tectonic earthquakes. The exception to this is most clearly visible in the middle frame of Figure 3.7, where is can be seen that the Groningen GMM predicts values lower than those obtained from the ENA model of Yenier & Atkinson (2015) as distance from the source increases, which is to be expected because Q values in the upper crust in Groningen are about an order of magnitude smaller than those typically found in ENA.

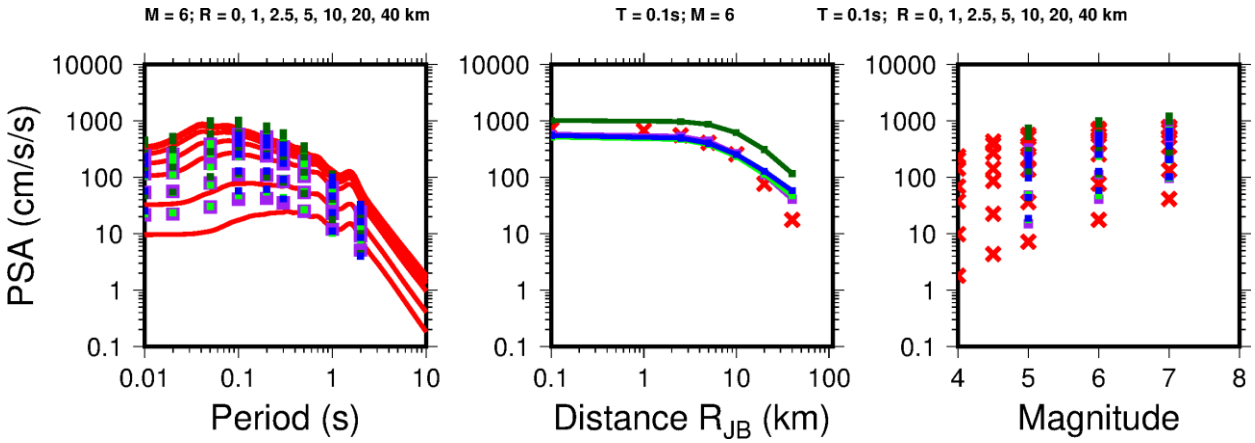

Figure 3.7. Comparison of simulations (upper model) using SMSIM RVT (R_{eff} version) (red) and the six GMPEs (blue: average NGA; purple/light green: RESORCE; dark green: ENA, Z_{hyp}=10 km). *Left*: SA vs. period. *Middle*: SA vs. distance. *Right*: SA vs. magnitude. All for scenarios indicated above panels.

Selection of lower, central and upper models

As for previous GMMs, for the forward simulations it was decided to use alternative values of the stress parameter to reflect the considerable epistemic uncertainty associated with extrapolation to much larger magnitudes. In the magnitude range covered by data (**M** ≤ 3.6) the two central branches have a stress parameter of 70 bars (the best-fit model to local data, minimum bias), the lower branch 50 bars [with median bias to local data at moderate to short periods (0 to 0.2 s) $\sim -0.5\tau$ *to* $-\tau$] and—reflecting the possibility of the motions being similar to those from normal tectonic earthquakes—the upper branch has 100 bars [median bias to local data at short periods $\sim +0.5\tau$ *to* $+\tau$]. All models exhibit an increase of stress-parameter

with magnitude, reflecting the belief that for larger events, increasingly sampling greater depths of the crust, the low Δσ values observed in the reservoir at low **M** are unrealistic. For the two central models (central *a* and central *b*), Δσ rises to 140 bars and 220 bars at **M** 5, respectively, then remains constant. Similarly, the lower and upper models rise to 75 bars and 330 bars, respectively (Figure 3.8). The latter is designed to produce motions, given the Groningen-specific attenuation and site characteristics, which are similar to those observed globally, as shown previously. The lower model, with stress drops increasing to 75 bars for **M** ≥ 5, is designed to reflect the fact that we do not believe that median stress drops at moderate and large magnitude could be lower than those observed for local seismicity in the reservoir. The overall spread of the models is designed to be consistent—increasing by a factor ~1.5 for each branch, apart from the lowermost branch, where 75 bars is chosen as the upper level for the lower model—with a 'self-similar' magnitude scaling (*i.e.*, consistent with the central models at low magnitude).

Table 3.1 summarises the full set of inputs to the simulations used to generate the motions at the NS_B reference for the derivation of the median GMPEs. For each of the model branches (lower, central *a*/*b*, and upper), response spectra were simulated using EXSIM_dmb for 2100 scenario events with **M** = 2.0 to 7.0 in steps of 0.25. For each scenario event a random epsilon was selected to define the length and width of the rupture. Recording locations were placed radially above the centre of the fault's top edge at 0 km and then 25 distances logarithmically spaced between 1.0 and 79.5 km. For each distance, 8 sites were located, at 0 to 315° (in 45° steps). In total 1.75 million response spectra were calculated, or 436,800 for each of the model branches.

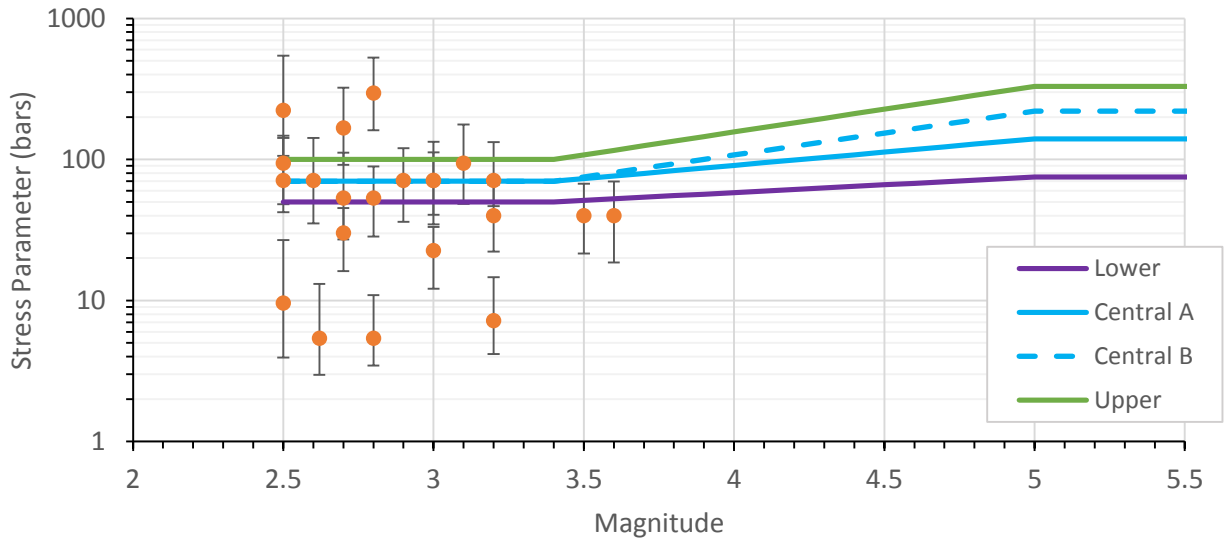

Figure 3.8. Estimates of stress drop together with confidence intervals as a function of magnitude, together with the four median models adopted for the simulations.

Table 3.1. EXSIM_dmb parameter values used in simulations for NS_B motions

Parameter	Symbol (units)	Value(s)	Notes
Density	ρ (g/cm^3)	2.6	
Shear-wave velocity	β (km/s)	2 3.5	**M** ≤ 4.5 (in reservoir) **M** ≥ 5.5 (Carboniferous)
Horizontal partition		0.707	
Radiation coefficient	θ	0.55	
Free surface	F	2	
Sub-fault source type		Brune (1970, 1971) ω^{-2}	
Top of rupture depth	Z_{top} (km)	3	
Seismogenic depth	Z_{seis} (km)	13	
Fault dip	Dip (degrees)	75	Average of observed 60 – 90 degrees.
Fault mechanism		Normal	
Fault width	W (km)	min(W(W&C'94), [Z_{seis}-3]/sin(dip)]	W(W&C'94): Width from Wells & Coppersmith (1994)
Fault length	L (km)	L(W&C'94)*(W/ W&C'94))	L(W&C'94): Length from Wells & Coppersmith (1994) Conserve area of fault A given by LxW in case limited by Z_{seis}
Hypocentre location	H(ΔL, ΔW) (km, km)	Random, 0	Located randomly along strike, at 3 km depth (top of fault).
Slip velocity	V_{slip} (km/s)	0.8β	
Stress parameter (Lower, Central, Upper)	$\Delta\sigma$ [**M** ≤ 3.4] (bars)	50, 70, 70, 100	Linear interpolation of log($\Delta\sigma$) with **M**
	$\Delta\sigma$ [**M** ≥ 5.0] (bars)	75, 140, 220, 330	
Geometrical spreading distances (R_{hyp})	R1, R2, R3 (km)	7, 12, 25	
Geometrical decay rates	λ1, λ2, λ3, λ4	-1.55, -0.23, -1.43, -1.00	
Path attenuation	Q	220	
Site attenuation	κ_0 (s)	0.010	
Source duration	T_S (s)	$1/0.4906\beta(\Delta\sigma/M_0)^{1/3}$	SI units
Path duration for sub-fault signals	T_P [R (km)]	$T_{5,75}/0.383$	V3 Groningen $T_{5,75}$ model for **M** = 3.0, Vs30=1500.
Rise time	T_S (s)	$1/f_0$	
Site amplification	A(f)	Network average NS_B	
Dynamic, pulsing percentage		50%	
Sub-fault averaging		RMS	
Scaling		(Acceleration FAS)^2	

Simulated NS_B motions

Figures 3.9 to 3.11 show simulated response spectral ordinates at the NS_B rock horizon for three different distances and, in each case, three different earthquake magnitudes. Each plot shows the simulations obtained with each of the four stress parameter branches that define the four branches of the median ground-motion logic-tree for the reference rock motions.

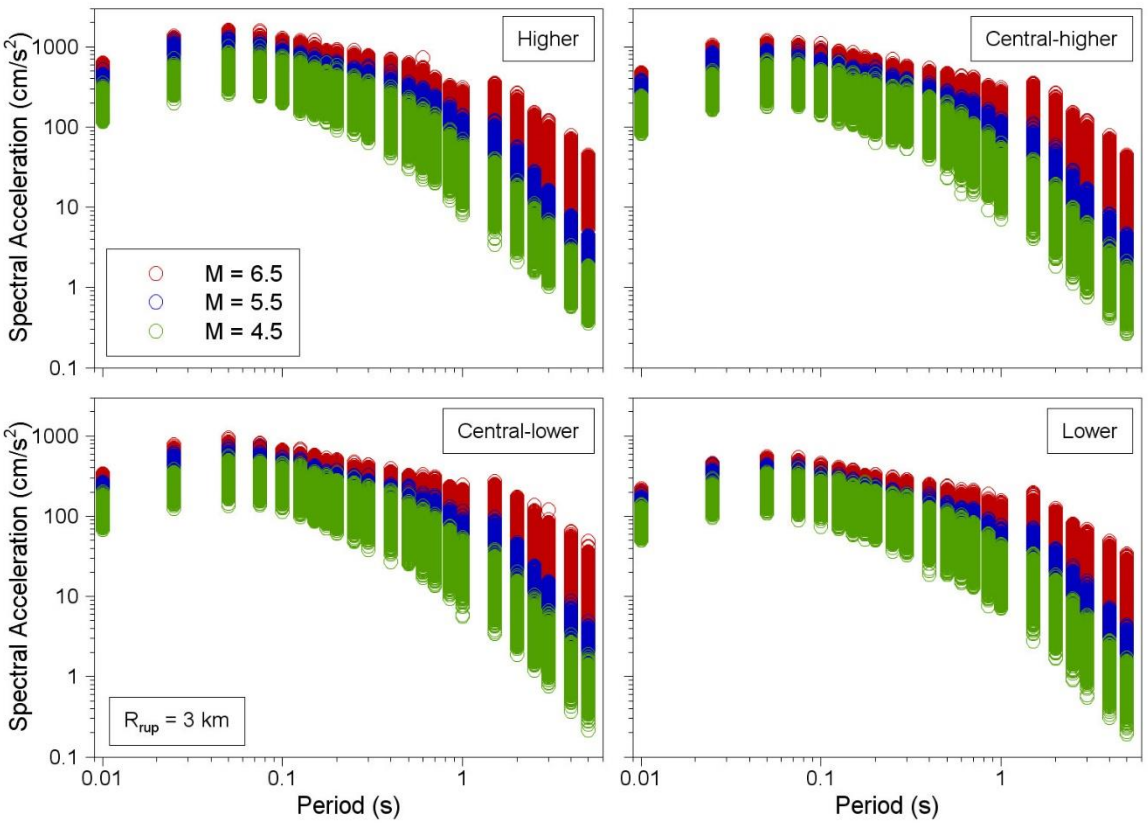

Figure 3.9. Simulated response spectra at NS_B at a rupture distance of 3 km

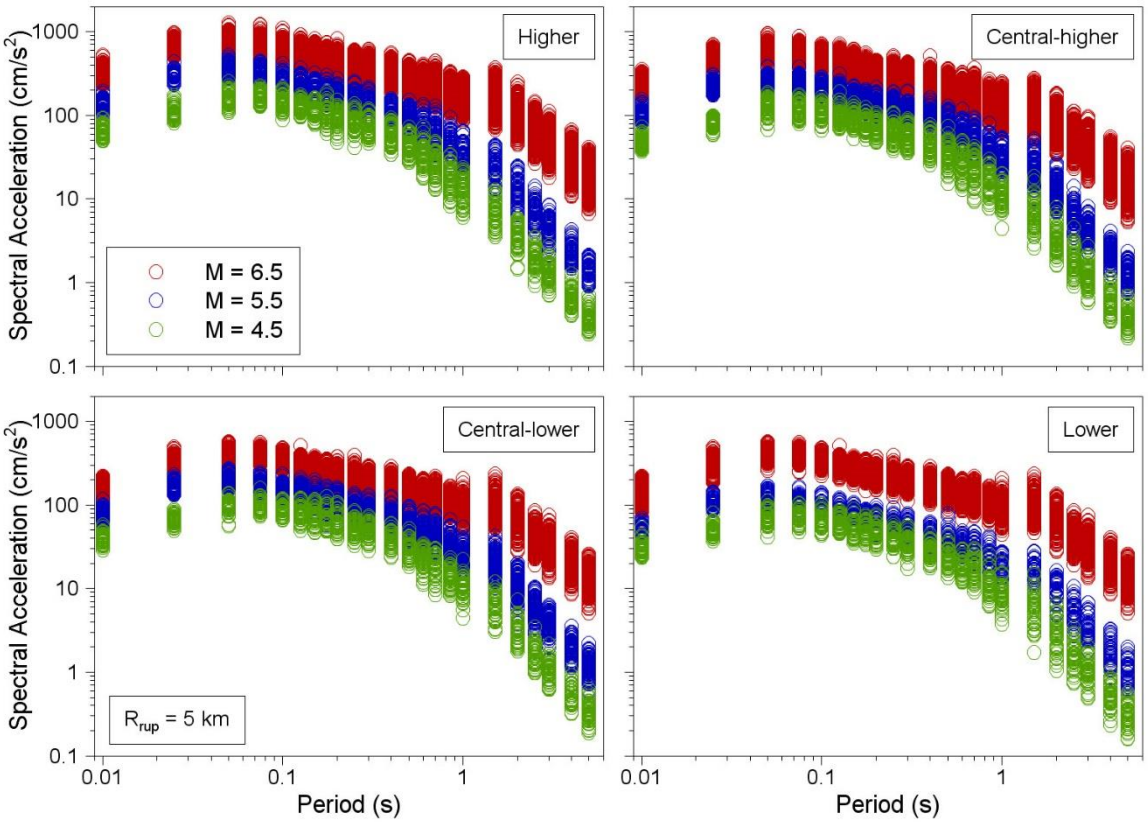

Figure 3.10. Simulated response spectra at NS_B at a rupture distance of 5 km

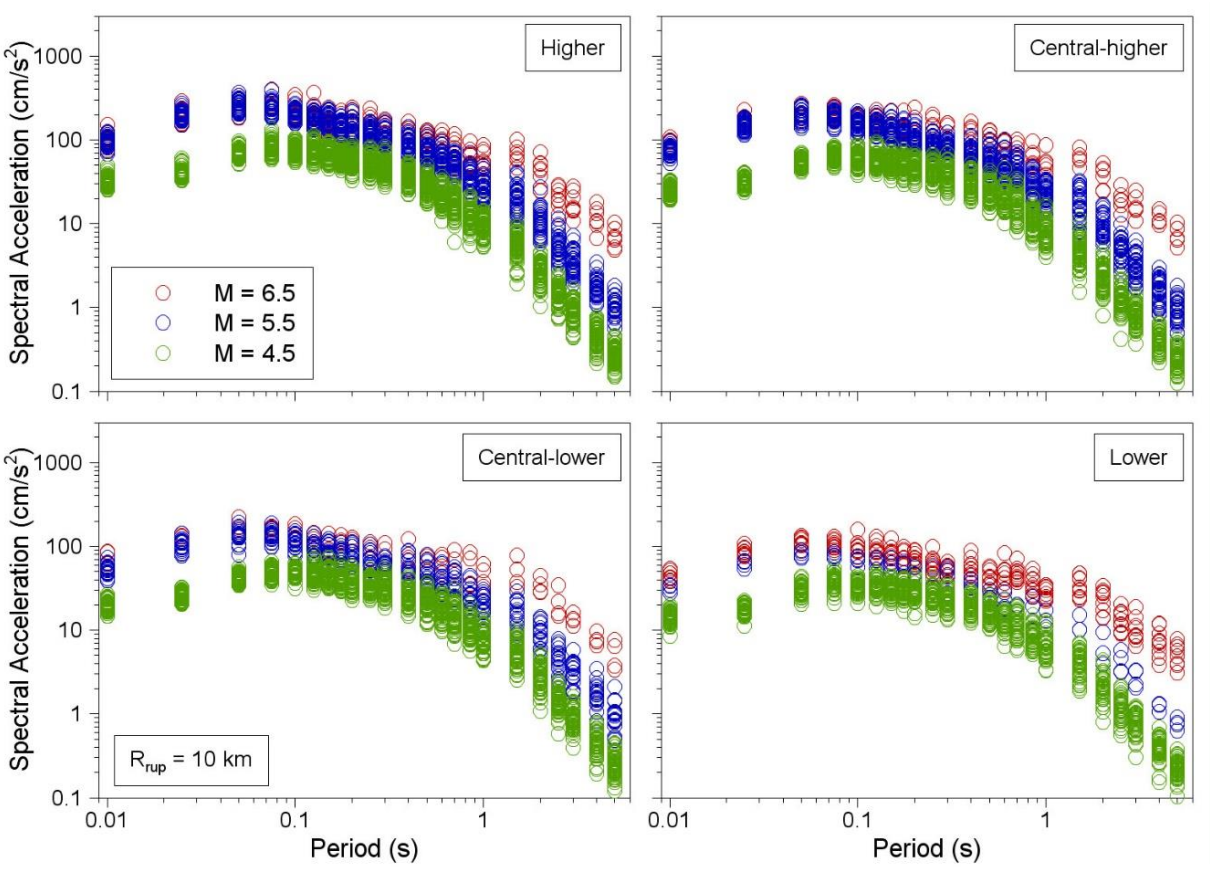

Figure 3.11. Simulated response spectra at NS_B at a rupture distance of 10 km

3.3. Parametric GMPEs for NS_B

The parametric GMPEs for Sa(T) and PGV at the NS_B were derived in exactly the same way as in the V4 model, performing simple regressions on the simulated motions. The functional form relating these ground-motion parameters to the local magnitude and the rupture distance is identical to that used for the V4 model, including the values of the hinging magnitudes for the changes in scaling and the hinging distances that control the changes in spreading functions.

The functional forms and their coefficients are all presented in Section 6.1 of this report. The equations are presented only in Chapter 6 to avoid unnecessary inflation of the length of the report and to thus provide a complete description of the GMM in a single section, for the convenience of potential users.

Figures 3.12 and 3.13 show plots of the outcomes from the regression against the simulations, for Sa(0.01s). The figures illustrate how well the regression fits the simulated motions at the NS_B horizon over the full range of magnitudes and distances for which the simulations were performed.

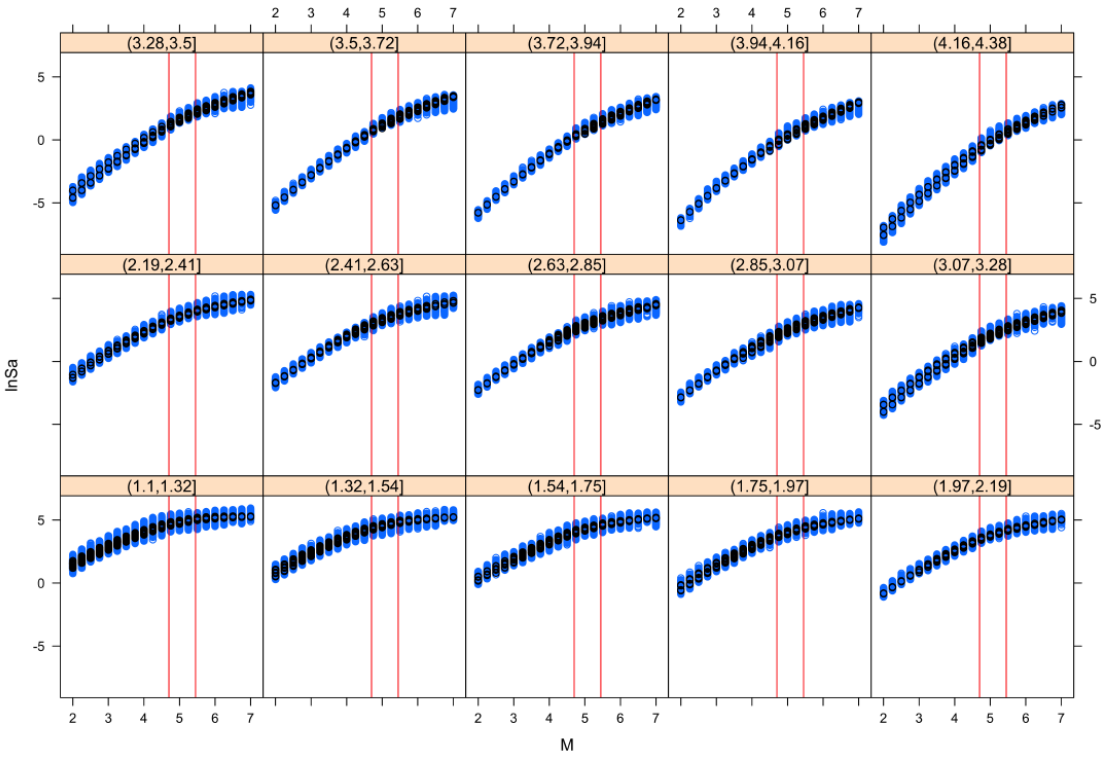

Figure 3.12. Comparison of regression results (*black*) with ESXIM simulations (*blue*) for PGA for different distances (ranges indicated by logarithmic values in header of each frame) against magnitude

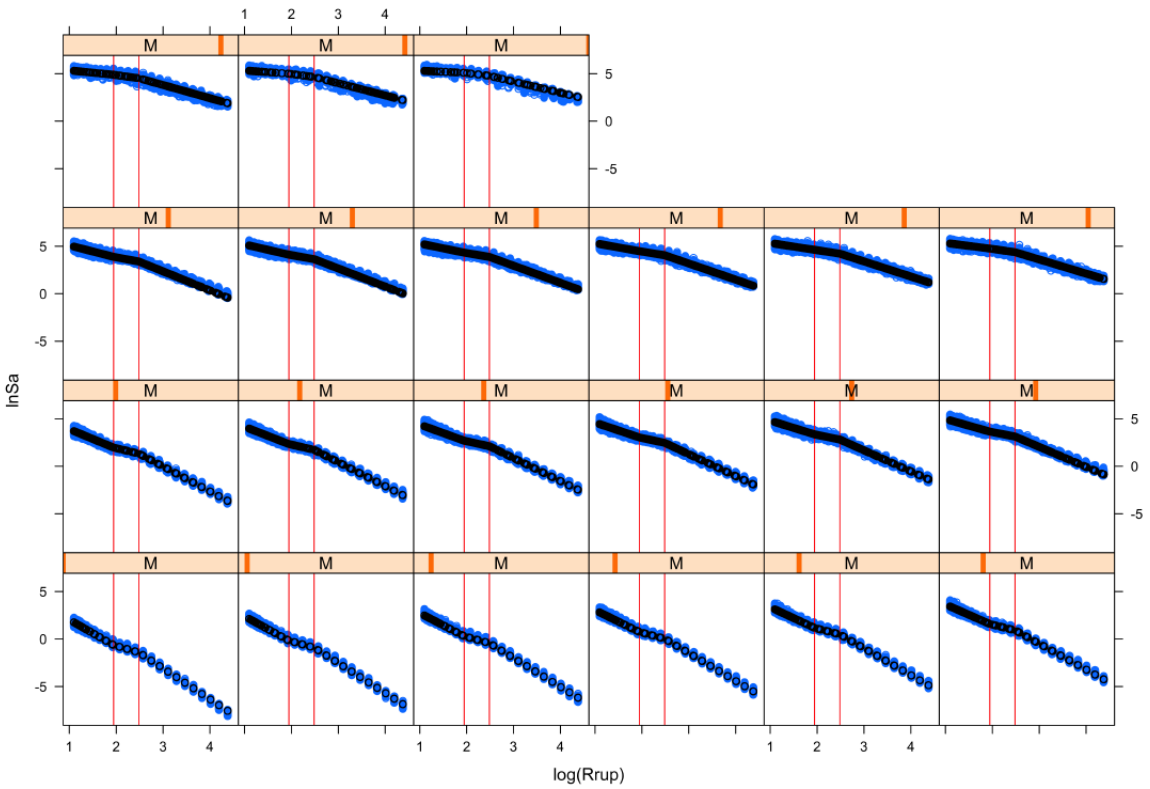

Figure 3.13. Comparison of regression results (*black*) with ESXIM simulations (*blue*) for PGA for different magnitudes (indicated by thick orange bars in header, with M increasing left to right) and distance; vertical red lines indicate control points for change of spreading function

3.4. Variability components

As for the V4 model, the variability components for the V5 model are primarily based upon an analysis of the small-magnitude data obtained in the Groningen field. The main exception to this statement is the use of comprehensive databases of tectonic earthquakes to place constraints upon the non-ergodic within-event variability.

The process followed to determine the between-event standard deviation is the same as that for the V4 model. Once the median model predictions were developed by running non-linear ordinary least squares regression analysis on the EXSIM simulation outputs, these model predictions were used to compute total residuals of the Groningen data. These field-specific data (either surface or borehole recordings) were transformed to the NS-B horizon. The total residuals are then partitioned into components using an advanced mixed effects regression approach that accounted for both magnitude uncertainties and spatial correlation, as well as crossed random effects for repeatable event and site effects. A more elaborate discussion of the approach taken, as well as the underlying mathematical framework, is provided in the V4 model report.

The mixed effects regression procedure was applied to each of the four model branches and the results obtained in each case are shown in Figure 3.14.

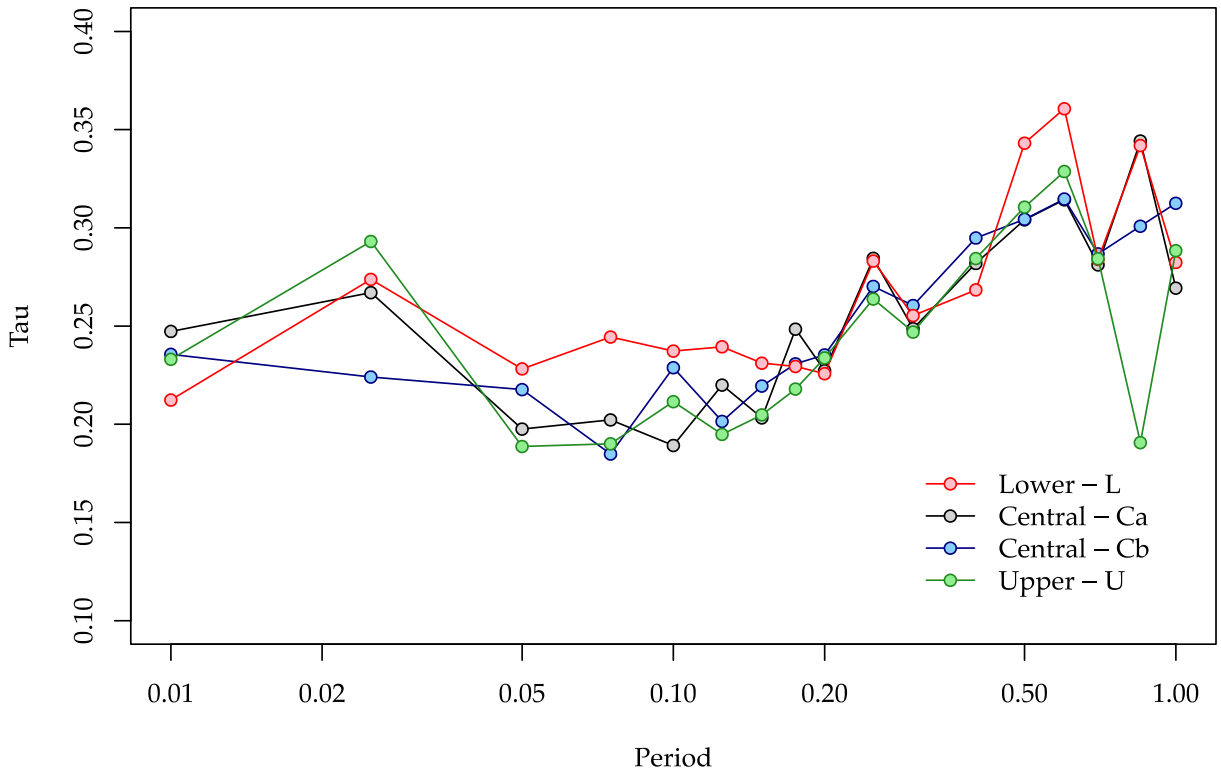

Figure 3.14. Estimates of the between-event standard deviation for each of the four branches at the NS-B horizon.

The variation in the estimates of between-event variability arise from two primary sources. The first is associated with the fact that the stress parameter values are different for each of the four considered branches and so the median model predictions over the magnitude range for which data from the Groningen field exists differ from branch to branch. This difference in medians leads to differences in total residuals that then influence the way these residuals are decomposed in the regression analysis. The second reason is related to the stochastic nature of the advanced regression analysis that is performed. A Markov-chain Monte Carlo approach is adopted within a Bayesian framework to obtain estimates of the variance components. While multiple simulations are run for each branch, there will still be some degree of variability from simulation-to-simulation. Rather than being a negative point, for the present study this is viewed as an advantage as it allows some degree of epistemic uncertainty to be implicitly incorporated into the specification of the between-event standard deviations.

In order to develop a model for the between-event variability, the functional form adopted previously for the V4 model was again utilised. This function is a continuous function of response period as shown in Eq.(3.3):

$$\tau(T) = \sqrt{\tau_0^2 + [g(T)\tau_1]^2 + g(T)\tau_0\tau_1\tau_3} \tag{3.3}$$

where the function $g(T)$ is defined as in Eq.(3.4).

$$g(T) = \frac{2}{3}\left[\frac{1}{1+\left(\frac{T}{\tau_2}\right)^2}\right]. \tag{3.4}$$

Independent fits of this model to the results shown in Figure 3.14 were made and this resulted in the set of parameters defined in Table 3.2.

Table 3.2. Parameters of the between-event standard deviation model

Branch	τ_0	τ_1	τ_2	τ_3
Lower, L	0.3335	0.4789	0.1982	-1.4434
Central, Ca	0.3068	0.6240	0.1028	-1.5605
Central, Cb	0.3132	0.5322	0.1299	-1.5269
Upper, U	0.3088	0.6348	0.1134	-1.5833

This model is able to capture the general variation of the between-event standard deviation well for all of the branches, as can be appreciated from the comparison between the regression outputs and the fitted models shown in Figure 3.15.

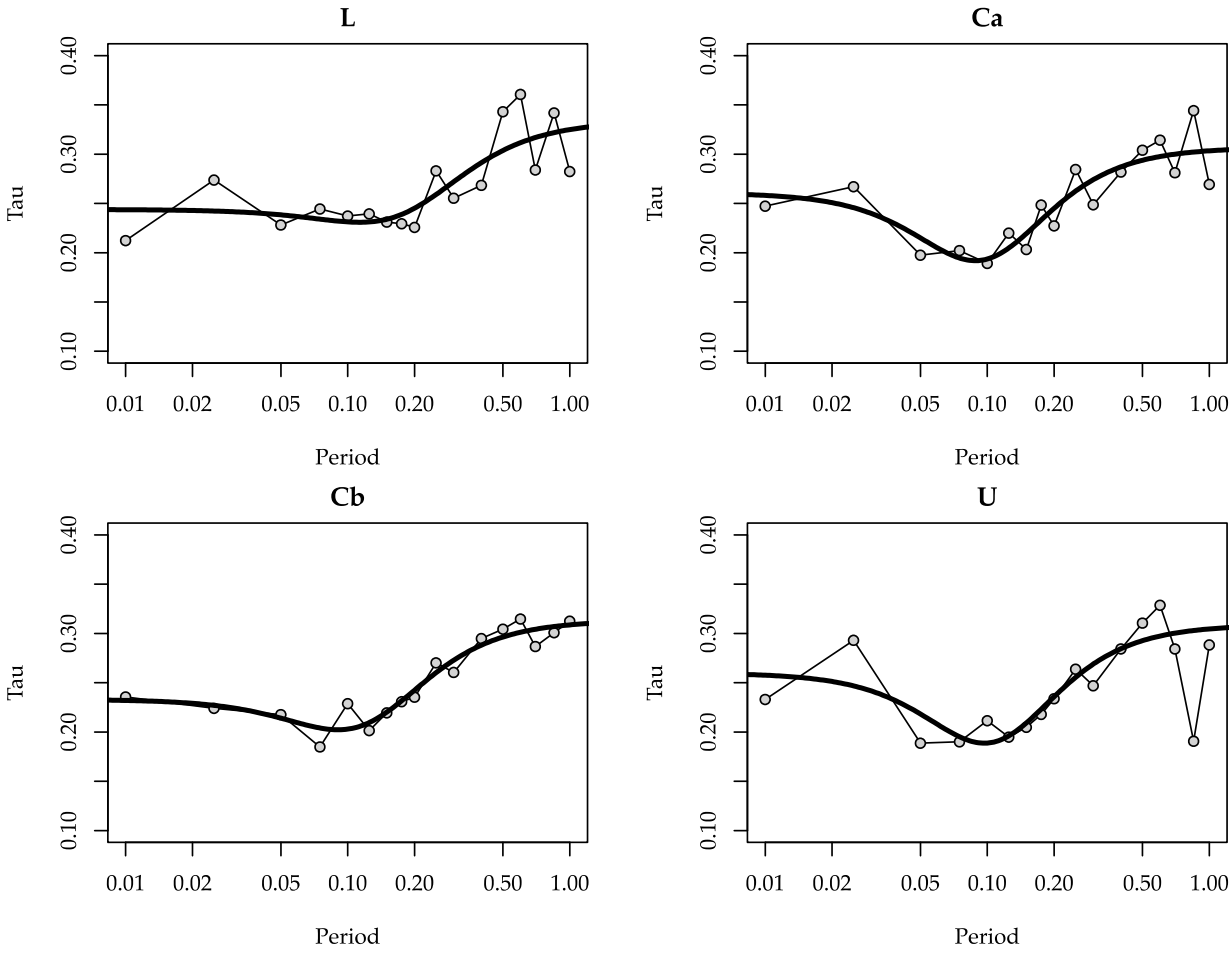

Figure 3.15. Model fits to the estimated between-event standard deviations. Note that for the upper branch, the anomalously low estimate at T=0.85 s is not used for the fitting.

The values of the between-event standard deviation for the V5 model have changed from those in the V4 model, as shown in Figure 3.16. For most periods of interest in the risk model for Groningen, the between-event standard deviations have increased, while at very short periods the model is now predicting lower values of between-event standard deviation. As the methodology remains consistent with that adopted for the V4 model, these differences are primarily attributed to the effect of the additional ground-motion records that have been added to the empirical database since the V4 model.

For the risk calculations, the geometric mean horizontal component of motion is transformed to the arbitrary horizontal component. This does not affect the median prediction but it requires the addition of the component-to-component variance to the variance associated with the geometric mean component. The strong polarisation of several of the Groningen ground-motion recordings led to values of component-to-component variability in previous versions of the model that are appreciably higher than those generally found from datasets of recordings from tectonic earthquakes.

The model for the component-to-component variability has been updated in the derivation of the V5 model to capture the distance dependence of the polarisation and also to diminish with increasing magnitude to become similar to tectonic models at the magnitude level beyond which triggered Groningen earthquakes would be assumed to have the characteristics of tectonic events. The derivation of this new model is presented in Appendix III.

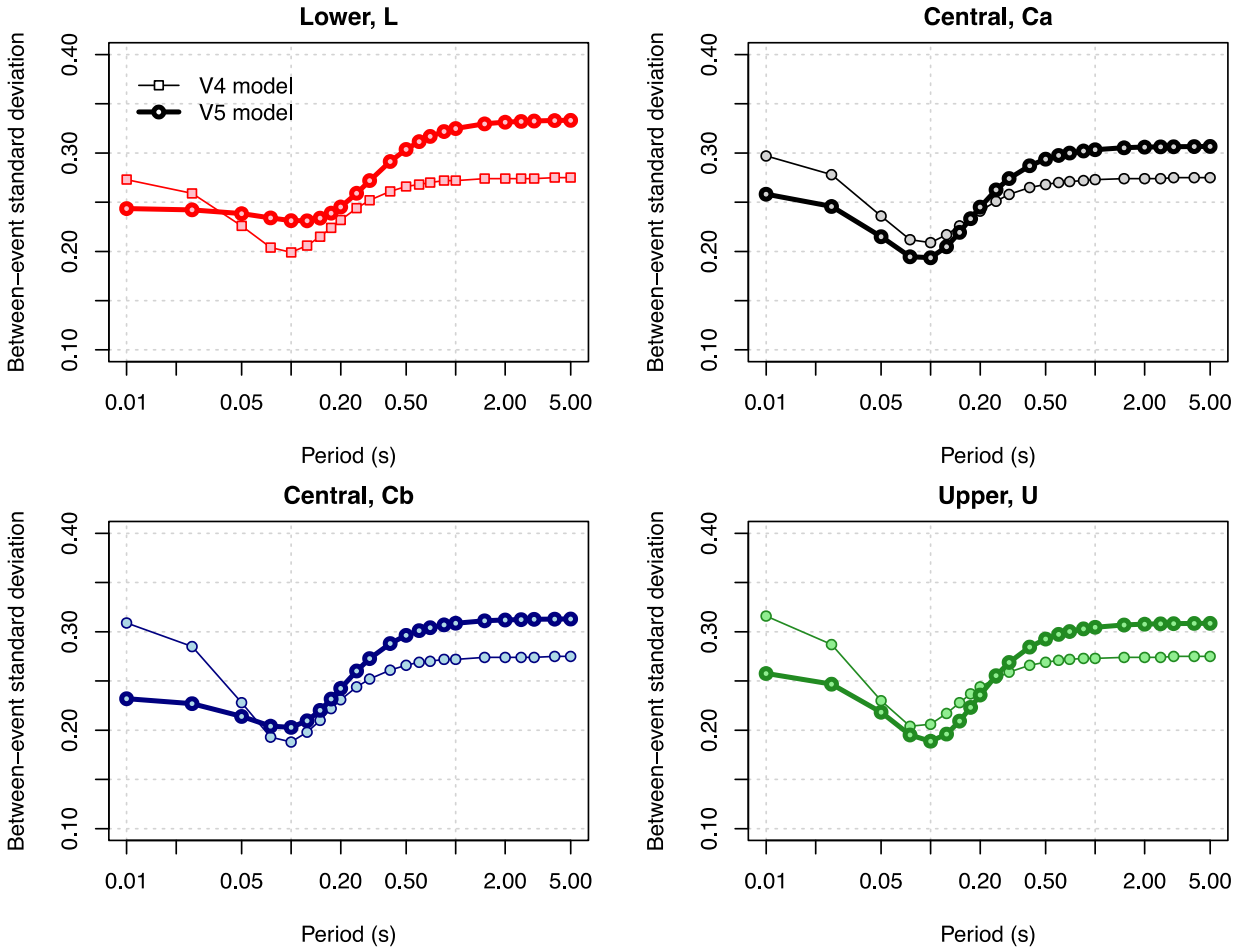

Figure 3.16. Comparison of the between-event standard deviations for the V4 and V5 models.

3.5. Comparison with V4 NS_B GMM

The derivation of the V5 model for NS_B motions followed exactly the same steps as used for the V4 model, but differences have arisen due to changes in the data. The variability model has altered slightly; while the within-event non-ergodic standard deviation remains unchanged the addition of the Slochteren data resulted in a modest increase in the between-event standard deviation except at the shortest oscillator periods, as shown in Figure 3.16.

The weights on the logic-tree branches carrying these four GMPEs were also unchanged from the V4 model since the rationale underlying the choice of those weights has not changed. The median predictions, however, have changed much more dramatically. The predictions from both models are compared in several plots presented in Appendix IV, from which it can be appreciated that except for short response periods and large earthquake magnitudes, the amplitudes predicted by the V5 model are appreciably lower than those from the V4 model. This is shown more clearly in Figures 3.17 and 3.18, which plot ratios of the predicted accelerations from the central-higher (Cb) and upper (U) models. The reduction in amplitudes is up to 20-30% in some cases. This is partly the result of the addition of the large number of recordings from the 2017 Slochteren earthquake to the database since the recorded amplitudes from that event were exceptionally low, leading to a reduction of about 10% with respect to the V4 GMM in the intermediate period range (see Appendix I for a detailed discussion of these data and their impact on the model derivation).

The primary cause for the change in NS_B amplitudes from V4 to V5, however, is the change in the relationship between local and moment magnitudes. Preliminary work on the relationship between **M** and M_L in the Groningen field indicated that for events larger than M_L 2.5 (in other words, those of relevance to the derivation of the GMM), values of **M** were, on average, consistently 0.2 units smaller than M_L. This relationship was implemented in the V4 inversions and caused a marked change in the estimates of the stress parameters and the near-source geometric spreading rate; in previous versions of the model, it has been assumed that the two magnitude scales were equivalent in the range of interest. Subsequent work, using a larger database of Groningen earthquakes and more detailed analyses, demonstrated conclusively that in fact the previous assumption that **M** = M_L was in fact valid (see Appendix II). Therefore, for the V5 model derivation, the assumption of equivalence of the two magnitude scales was once again invoked, now supported by empirical data from the region. Figure 3.19 shows the ratio of simulated motions obtained from the V5 model to those that would have been obtained had the 0.2 magnitude unit difference been retained; for the magnitude-distance combinations generally found to dominate the hazard and risk estimates in Groningen, the change in the magnitude relationship clearly caused a significant reduction. However, it is important to emphasise that the current model is well supported and it is the V4 model that was subject to a change that is not supported by local data (an occurrence that can be attributed to the very aggressive schedule on which the different versions of the model have been generated; see Section 2.1). Although the models are not directly comparable because of the change of distance metric associated with moving from point-source earthquake representations to finite rupture modelling, the GMM has actually been quite stable from V3 to V5, as illustrated in Figures 3.20 to 3.22. These plots also compare the models with predictions from two NGA-West2 models, confirming that for larger events the models predict motions similar to those from tectonic GMPEs (except at longer distances because of the lower Q values).

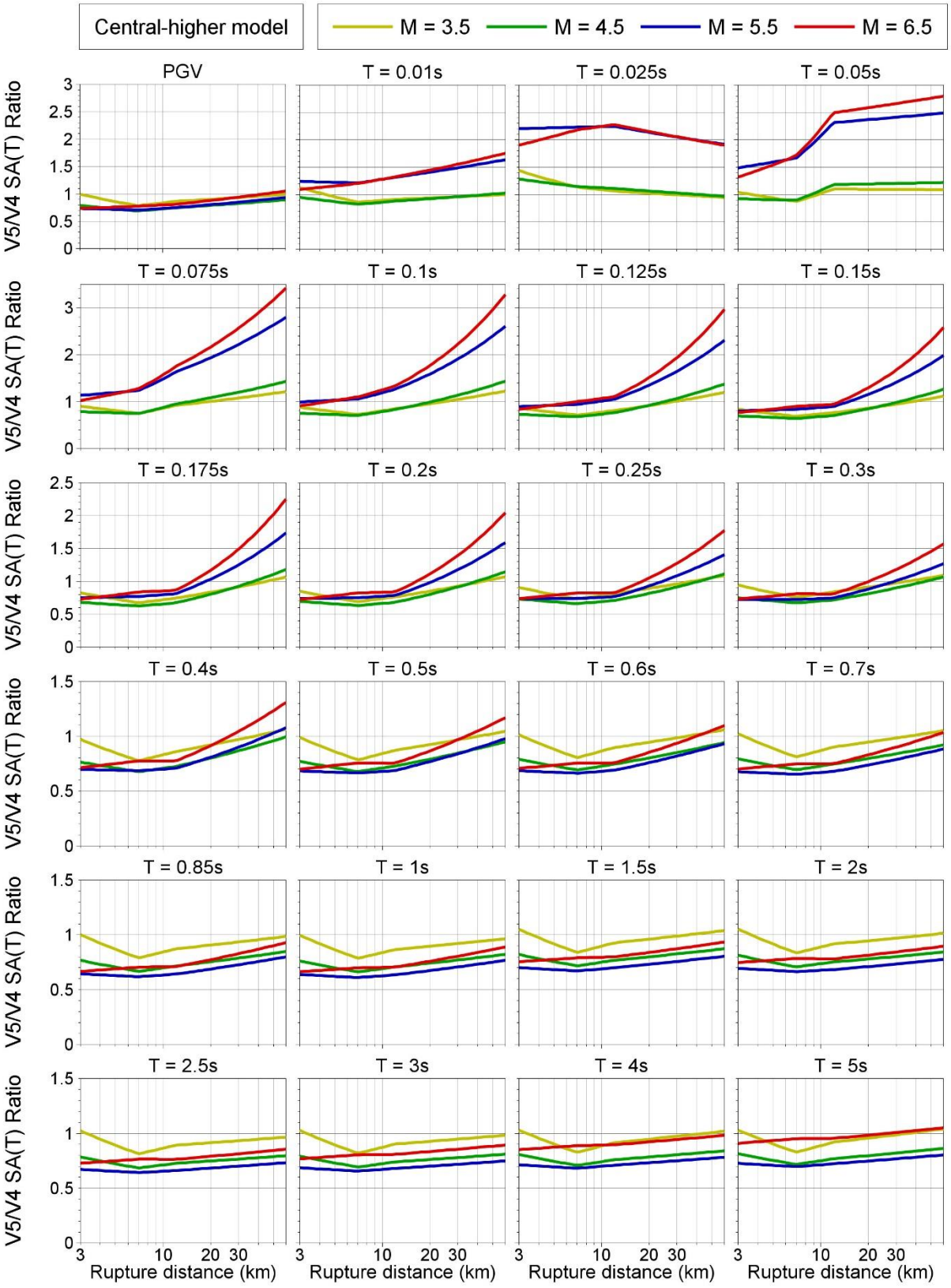

Figure 3.17. Ratios of predicted medians at NS_B from the central-higher (Cb) branch of the V5 to V4 models, plotted against distance for four magnitudes

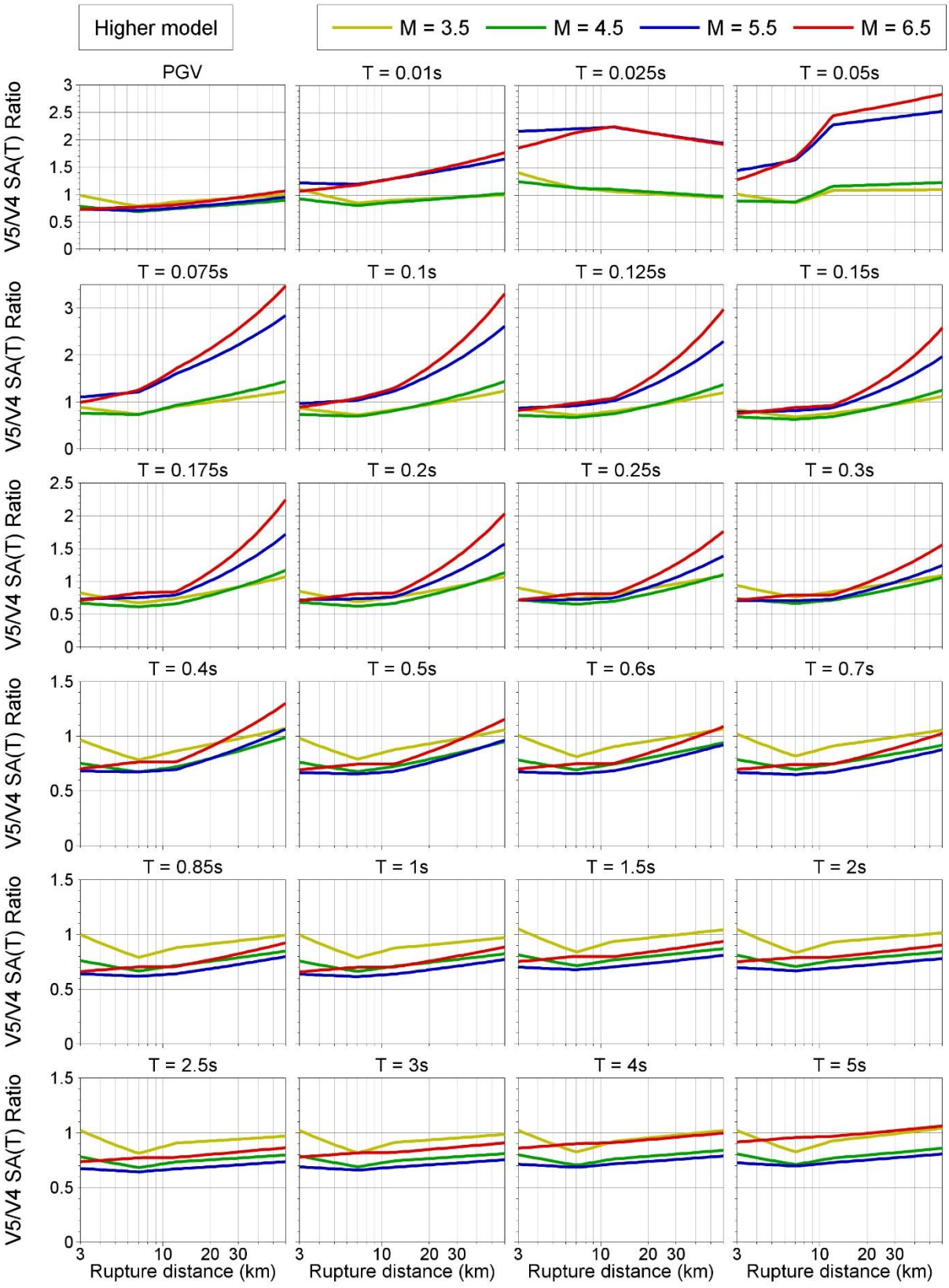

Figure 3.18. Ratios of predicted medians at NS_B from the upper (U) branch of the V5 to V4 models, plotted against distance for four magnitudes

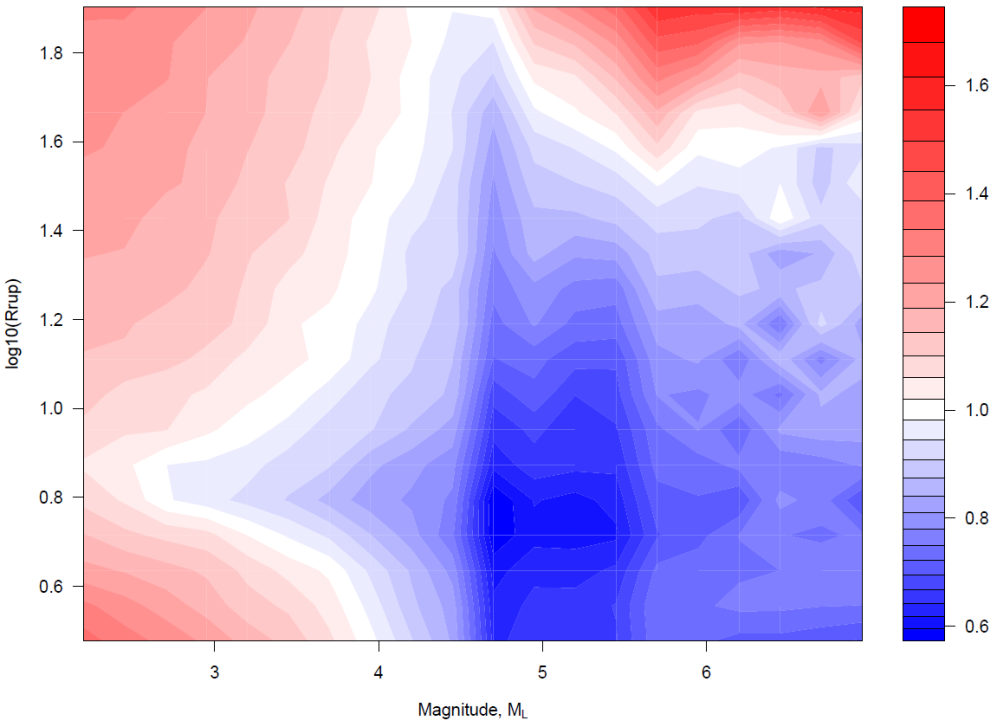

Figure 3.19. Ratios of V5 Sa(0.5s) at NS_B to those obtained invoking the **M** = M_L - 0.2 relationship in the inversions, as a function of magnitude and distance

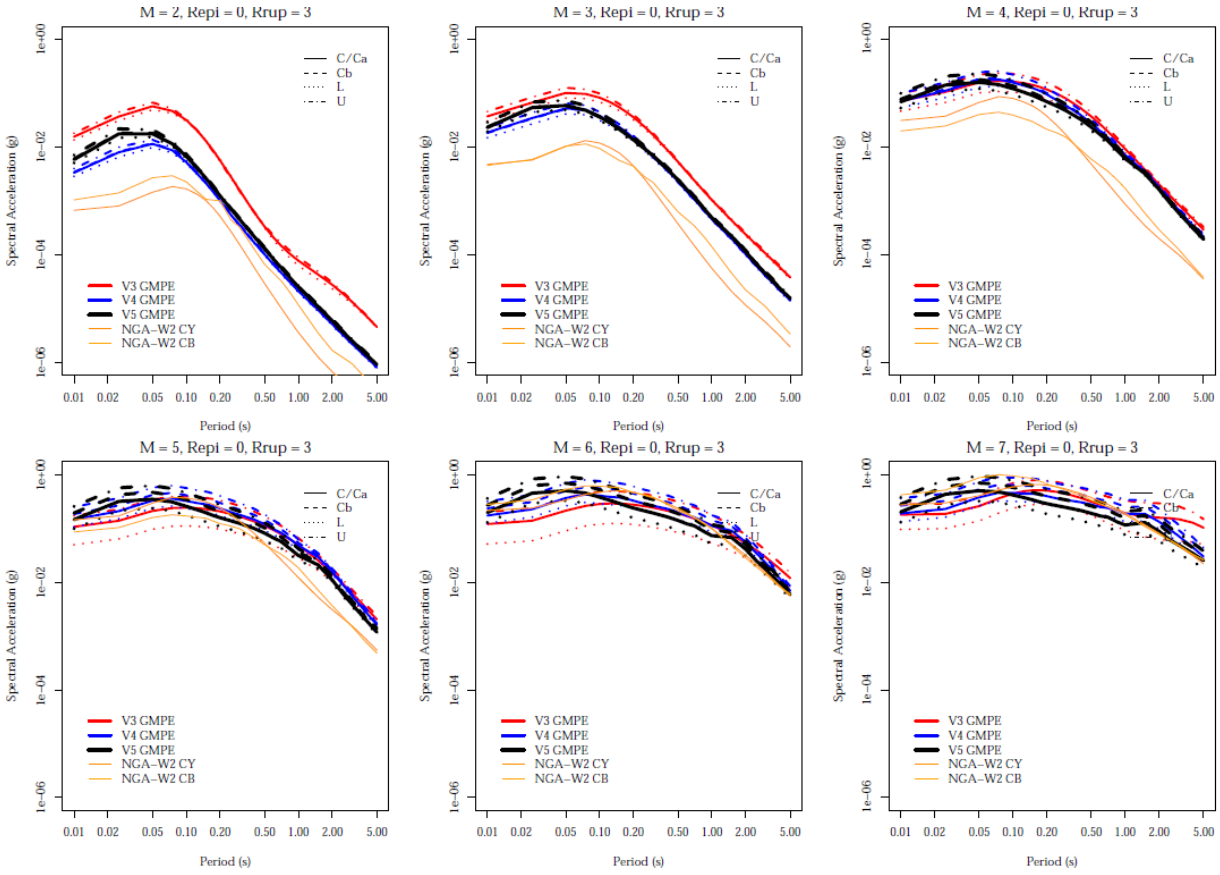

Figure 3.20. Comparison of predicted median spectral ordinates from the V3, V4 and V5 for an epicentral distance of 0 km, together with predictions from two NGA-West2 models.

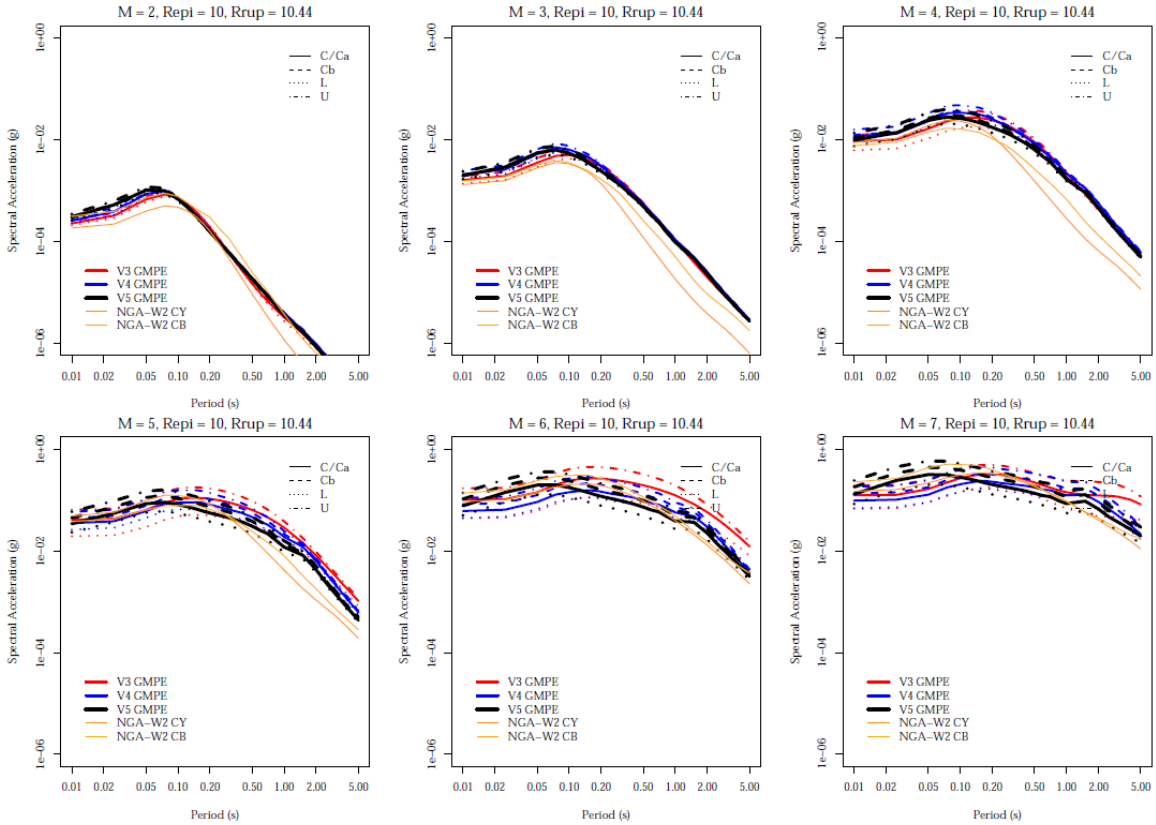

Figure 3.21. Comparison of predicted median spectral ordinates from the V3, V4 and V5 for an epicentral distance of 10 km, together with predictions from two NGA-West2 models.

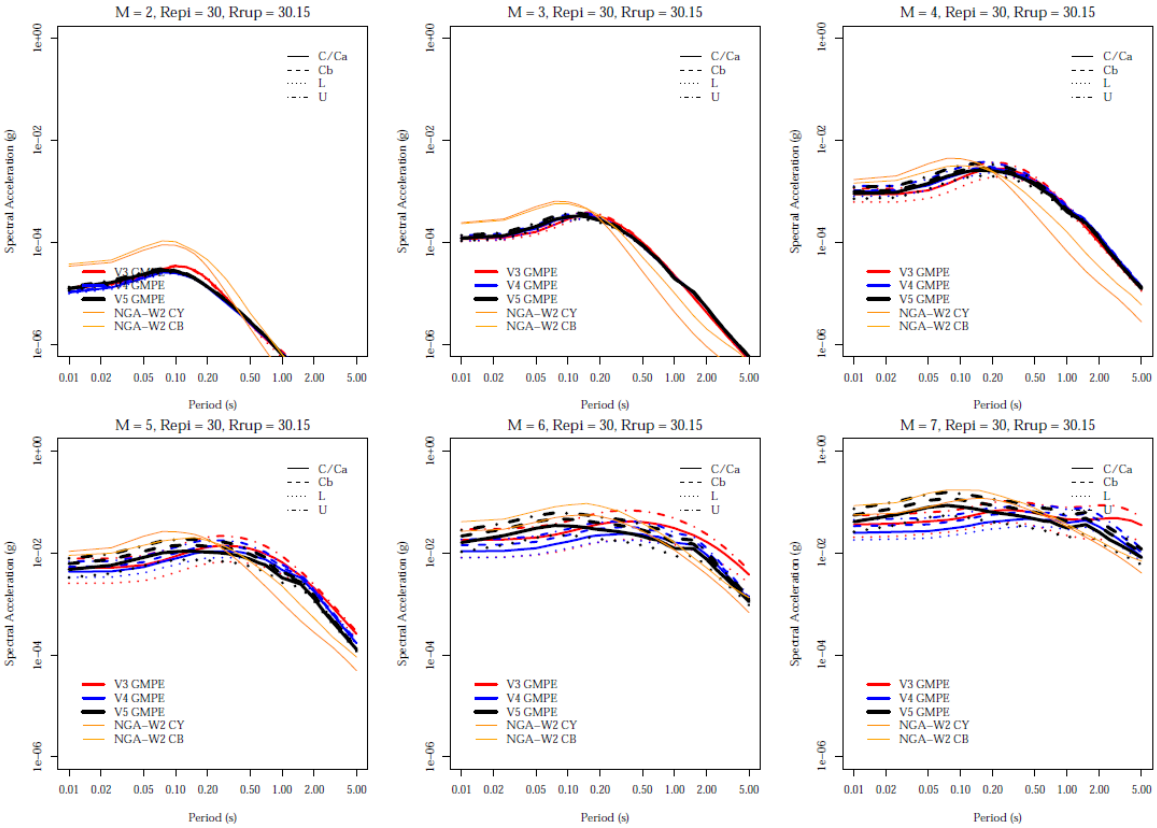

Figure 3.22. Comparison of predicted median spectral ordinates from the V3, V4 and V5 for an epicentral distance of 30 km, together with predictions from two NGA-West2 models.

4. Site Amplification Model

The site amplification model transforms the ground-motion predictions at the NS_B horizon to the ground surface. The framework of the V5 site response model—including the field zonation—is very similar to that of the V4 model, but some subtle differences are discussed in the first three sections of this Chapter. Thereafter, the residuals of the recorded surface motions with respect to the new model are discussed and the chapter closes with a brief comparison between the site response characteristics of the V4 and V5 models.

4.1. Site response analyses

The site response analyses were performed according to the same set-up as for GMM V4 (Bommer *et al*., 2017b). Several adjustments were made with respect to the input FAS motions at NU_B and their sampling, and to the geomechanic look-up table.

Input motions

A new set of 3,600 input FAS motions at NU_B was used as input for the STRATA site response calculations. These motions span a magnitude **M** range from 1.5 to 7.5 with steps of 0.1 (**M**=1.5-5.0) and 5.25, 5.5, 5.75, 6.0, 6.25, 6.5, 7.0, 7.25, 7.5. The rupture distance ranges from 3.0 to 60 km in 20 log-spaced steps. These ranges enable the derivation of the M-R dependence of AF (section 4.2). The derivation of the new FAS motions is described in Chapter 3.

The set of 3,600 FAS motions was ranked according to their PGA and subsequently divided into 10 groups instead of the 5 groups in GMM V4, because of the much larger number of motions. The FAS motions per group are shown in Figure 4.1 and 4.2.

The required inputs to the STRATA analyses are both an FAS and an estimate of the duration, for which the significant duration corresponding to 5-75% of the total Arias intensity is used. The durations are modelled using the equation of Boore & Thompson (2014) and the averages reported for 50 time-histories randomly generated for each FAS. The significant durations for the corresponding magnitudes in V4 and V5 are similar, ranging from 1.1 to 14 s (median 4.8 s) for V4 and 0.6 to 12 s (median 3.9 s) for V5. The significant durations of the higher magnitudes (**M** 6.25 – 7.5) which were added in V5 are longer, ranging from 5 to 37 s (median 11 s).

The duration was adjusted such that the PGV of the input FAS motion in the RVT-FAS analysis using STRATA corresponded to the PGV of the simulated time signals

($D_{75\text{-}5}$) using EXSIM that were input for the FAS. The corrected duration D_{corr} is given by:

$$D_{corr} = \frac{D_{75-5}}{0.64} \qquad \text{(Eq. 4.1)}$$

This correction produces PGVs in STRATA that are a few percent too low for low ranks and a few percent too high for high ranks, apart from the strongest motions (maximum 19%). The median relative difference between PGVs from EXSIM and PGVs from corrected durations in STRATA for all ranks is -0.5%.

One motion per group of ranked motions was randomly selected as input motion for each voxel stack, corresponding to 10 STRATA calculations per voxel stack as compared to 5 in GMM V4. The sampling of all signals for all calculations is shown in Figure 4.3. On average, each motion is sampled 391±20 times. The sampling of FAS motions of two small and two large zones is shown in Figure 4.4. Because of the much larger number of motions divided into 10 groups, not all motions are sampled in the smaller zones (top panels of Figure 4.4). All motions are sampled in the larger zones (bottom panel of Figure 4.4). Overall, the selection of the NS_B motions for input to the site response analyses was judged to be sufficiently random.

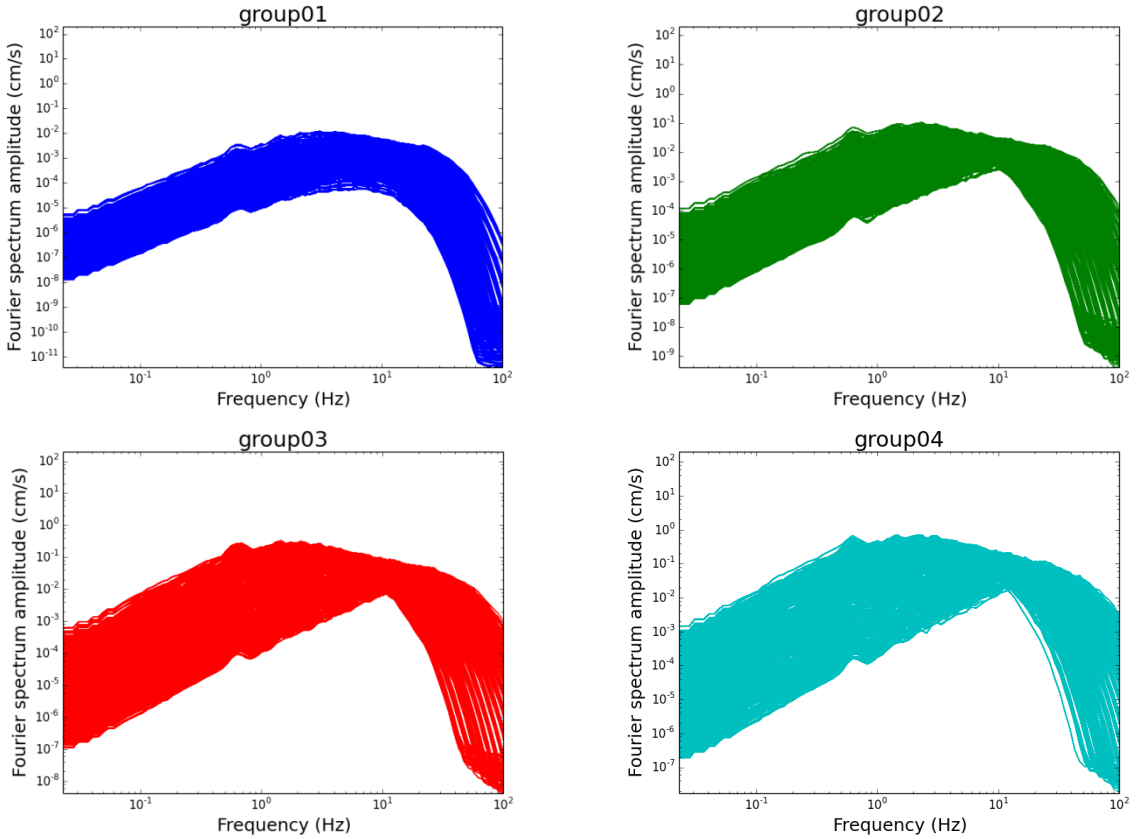

Figure 4.1. FAS generated at the NS_B horizon for use in RVT-based site response analyses for groups 1 to 4

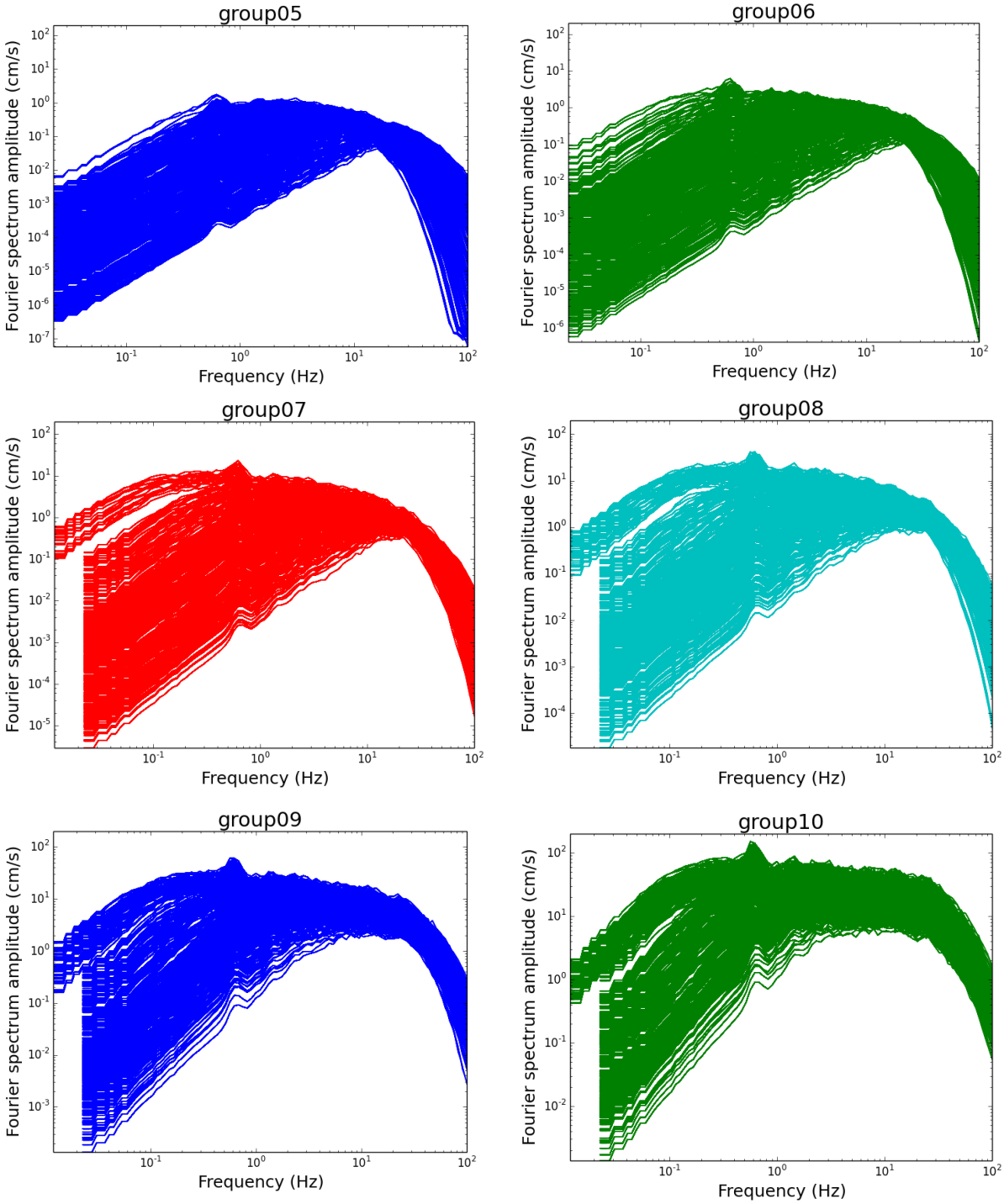

Figure 4.2. FAS generated at the NS_B horizon for use in RVT-based site response analyses for groups 5 to 10.

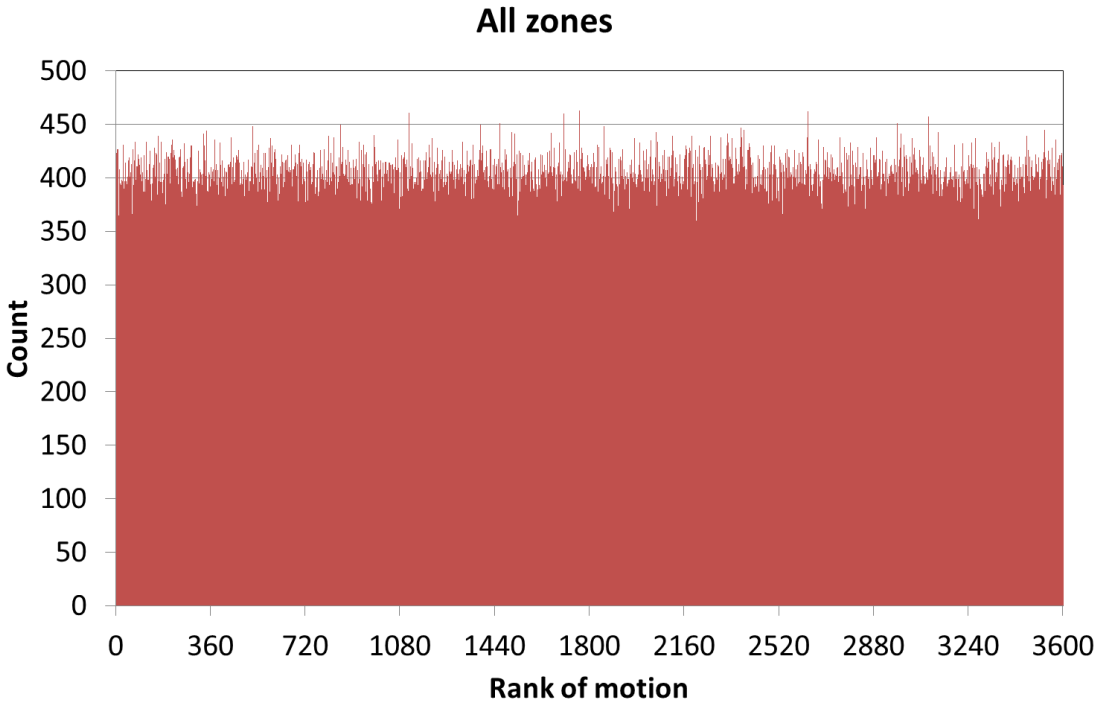

Figure 4.3. Sampling of the 3,600 NS_B FAS in the site response analyses over the whole field

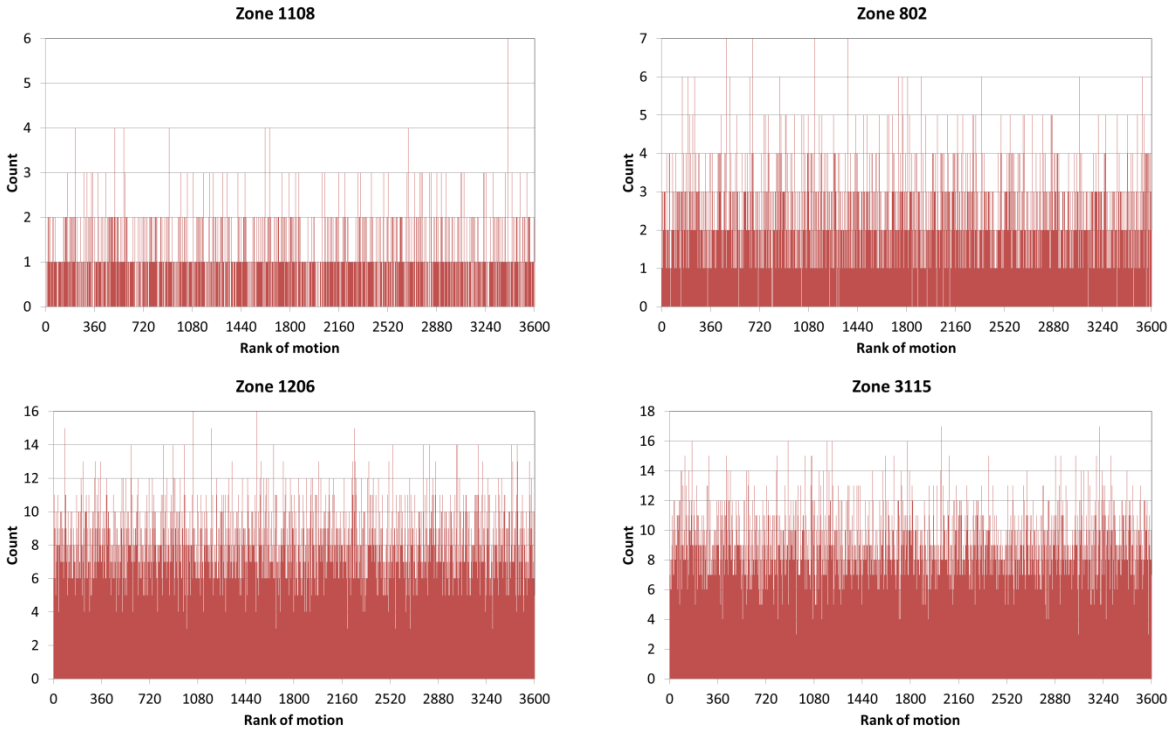

Figure 4.4. Sampling of the 3,600 NU_B FAS in the site response analyses for four of the geological zones. Top panels show the sampling for two small zones, bottom panels the sampling for two large zones.

Update of geomechanic look-up table

Results from laboratory test from Groningen samples became recently available (van Essen, 2017). The samples were taken at the Eemskanaal levee in the province of Groningen, in the toe and the crest of the levee. Cone penetration tests were also performed at these locations. The combination of laboratory data and CPT soundings enables the calibration of empirical relations between CPT parameters and undrained shear strength S_u for Groningen for the sampled stratigraphy-lithology combinations. The empirical relations were updated for three soil types: Naaldwijk clay, Holland peat and Basal peat.

For Naaldwijk clay, the relation $S_u = q_{net}/17$ follows the laboratory derived S_u much better than the earlier assumed $S_u = q_{net}/14$ (Figure 4.5). The empirical relation between S_u and vertical effective stress σ'_{vo} for V5 has been based on the CPT data set using $S_u = q_{net}/17$. The CPT based data were used rather than the laboratory data, because the CPT data represent a much larger data set and cover a larger vertical effective stress range.

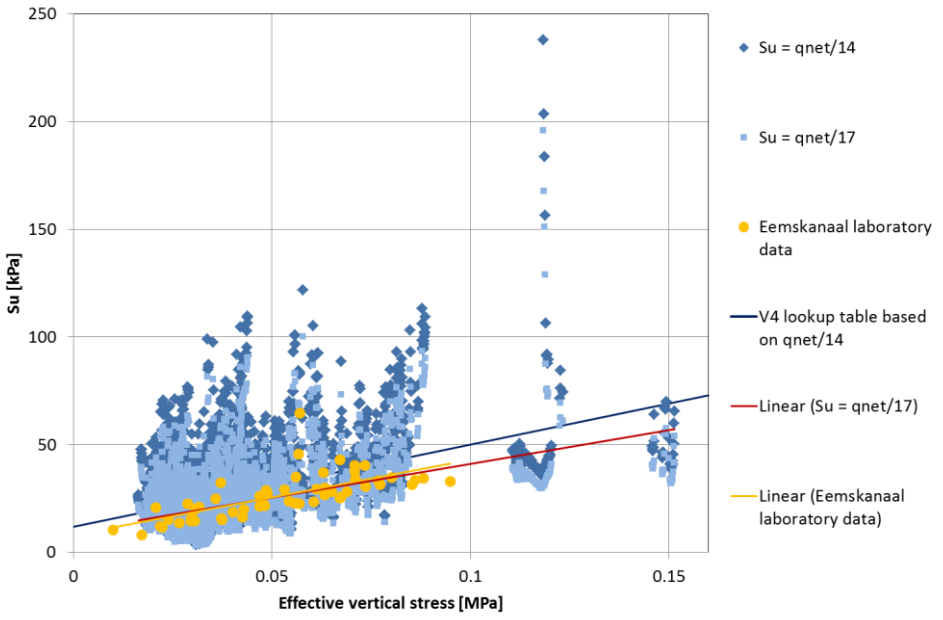

Figure 4.5. CPT derived and laboratory data for Su for Naaldwijk clay (NA), including linear regression lines.

For other types of clay, the laboratory data were insufficient to justify a deviation from earlier assumed $S_u = q_{net}/14$. Therefore, no changes relative to GMM V4 were made for clays, other than Naaldwijk clay.

The Holland peat and Basal peat are well represented in the laboratory data and less abundant in the CPT data set. The data are shown in Figure 4.6 and 4.7 for Holland peat and Basal peat respectively. In both cases, the laboratory data are regarded as

better representatives of S_u values than the CPT-derived S_u. Therefore, the updated empirical relation between S_u and vertical effective stress σ'_{vo} for V5 has been based on the linear regression through the laboratory data.

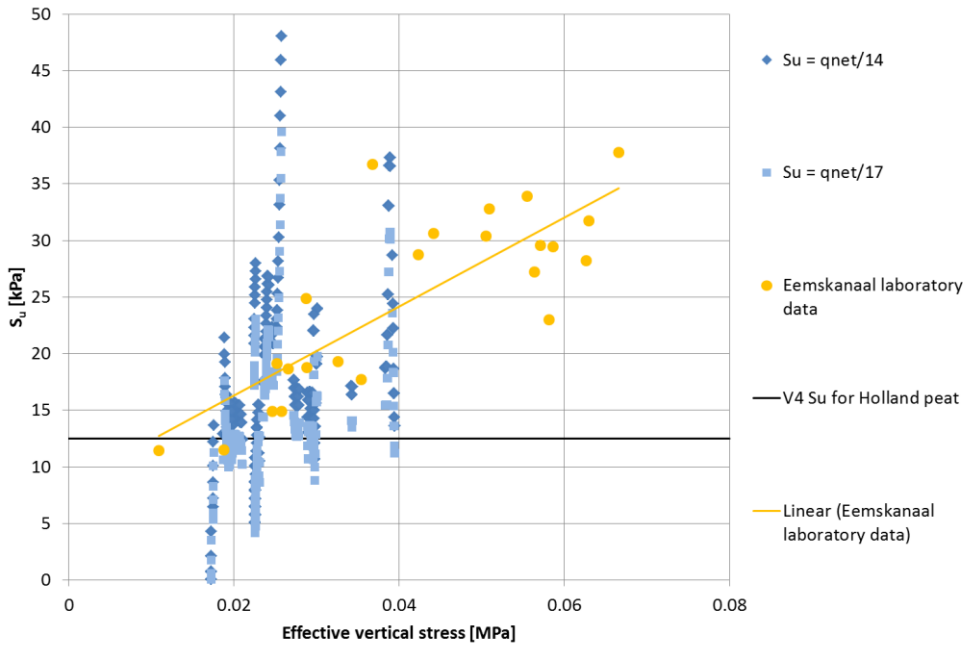

Figure 4.6. CPT derived and laboratory data for Su for Holland peat (NIHO), including V4 relation and linear regression line through laboratory data for V5.

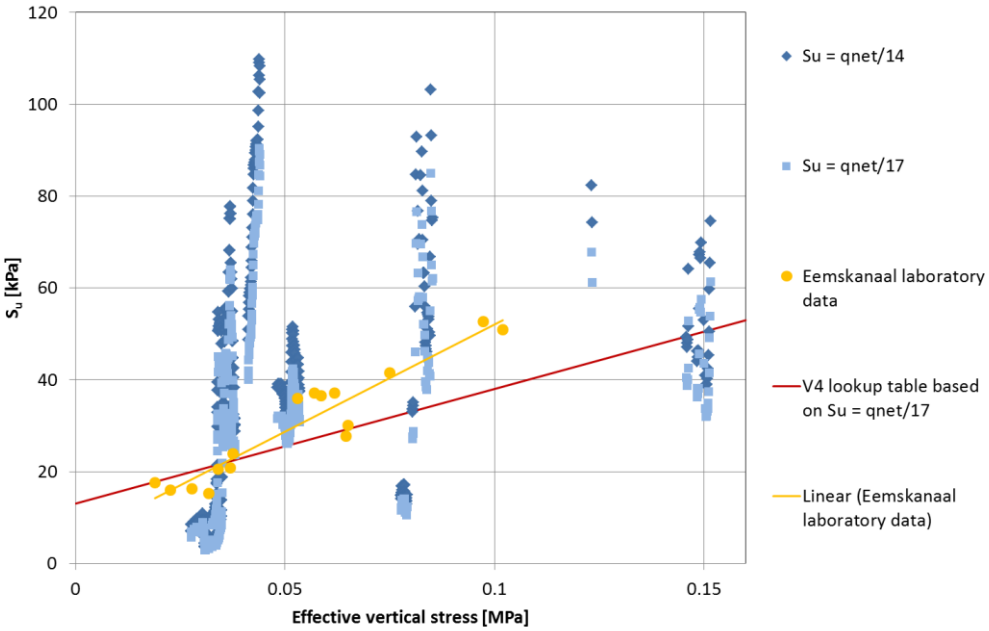

Figure 4.7. CPT derived and laboratory data for Su for Basal peat (NIBA), including V4 relation and linear regression line through laboratory data for V5.

The updated empirical relations are summarised below and replace the equations in Tables V.3 and V.4 in Appendix V of the GMM V4 report (Bommer *et al*., 2017b):

- Naaldwijk clay (NA): $S_u = 0.31\ \sigma'_{v0} + 10$ [in kPa]
- Holland peat (NIHO): $S_u = 0.39\ \sigma'_{v0} + 8$ [in kPa]
- Basal peat (NIBA): $S_u = 0.47\ \sigma'_{v0} + 5$ [in kPa]

4.2. Zonation and amplification factors

The V4 zonation was preserved for the V5 GMM. Moreover, the approach used to compute the amplification functions for the zones was similar to that for the V4 GMM, with the only change being the functional form of the linear part of the amplification factors (AF). These changes were introduced because the analyses performed in the V4 GMM led to persistent biases between the AFs computed for the stations and the AFs computed for the zones. This bias was determined to arise from a poor characterisation of the magnitude and distance dependence of the AFs.

The magnitude and distance dependence in the AFs is discussed at length in Stafford *et al*. (2017), who suggest that for magnitudes between about 2.5 and 4.5, the elastic AFs have a nearly linear dependence on magnitude and distance. These conclusions are based on numerical and theoretical analyses and are backed by empirical data from the KiK-net array. In the V4 GMM, the magnitude and distance dependence for the zones could not be fully captured because the sampling of magnitude and distance of the input motions was not sufficiently broad. In the V5 GMM model, the sampling of magnitude and distance covers the entire range of interest for the hazard model (see Section 4.1).

The model for the AF of the zones is given below. These equations replace Eqs.(8.4) to (8.7) of the V4 GMM report. For each zone and each response period (including PGV), the median amplification factor is given by:

$$\ln(AF) = f_1^* + f_2 \ln\left(\frac{Sa_{NS\_B,g} + f_3}{f_3}\right) \qquad (4.2)$$

where f_2 and f_3 are model parameters, and $Sa_{NS\_B,g}$ is the spectral acceleration at the NS_B horizon and is given in units of g (the acceleration of gravity). When the equation is applied to PGV, $Sa_{NS\_B,g}$ is replaced by PGV_{NS_B} in units of cm/s. The parameter f_1^* is magnitude-and distance-dependent. For spectral acceleration, it is given by:

$$f_1^* = [a_o + a_1 \ln(R)] + [b_0 + b_1 \ln(R)]\left[\min\left(M, M_{ref}\right) - M_{ref}\right] \qquad (4.3)$$

where M is moment magnitude, R is closest distance in km, a_o, a_1, b_0, and b_1 are model parameters, and M_{ref} is given by:

$$M_{ref} = M_1 - \frac{\ln(R)-\ln(3)}{\ln(60)-\ln(3)}(M_1 - M_2) \quad (4.4)$$

where M_1 and M_2 are model parameters.

For PGV, the parameter f_1^* is given by:

$$f_1^* = \begin{cases} [a_o + a_1 \ln(R)] + [b_0 + b_1 \ln(R)](M - M_{ref}) & \text{for } M \le M_{ref} \\ [a_o + a_1 \ln(R)] + d(M - M_{ref}) & \text{for } M > M_{ref} \end{cases} \quad (4.5)$$

where $M_{ref} = M_1$ and a_o, a_1, b_0, b_1, d, and M_1 are model parameters. Each of the model parameters in Eqs.(4.3) to (4.5) are oscillator-period dependent. The model is only applicable for M≥2. In addition, the amplification factor ln(AF) in Eq.(4.2) is subject to both upper and lower limits, AF_{max} and AF_{min}. These limits are the same as those applied to the AFs in the V4 GMM model. The linear portion of the model (Eqs. 4.3 and 4.5) was also used to compute the linear AFs for the stations (see Figure 2.7).

The parameters of Eqs.(4.2) to (4.5) were obtained in a similar manner as in the derivation of the V4 GMM. The parameters were obtained from maximum likelihood regressions of the AFs computed from the site response analyses described in Section 4.1. Since some of the parameters have interdependences, some constraints were placed on these parameters. Namely, parameter f_3 is chosen from a preliminary analysis and is assumed to be the same for all zones. Parameters M_1, M_2, a_1, b_1, and f_2 were smoothed sequentially (one at a time) after initial regressions. Parameters M_1, M_2, a_1, and b_1 were also constrained to be within the 5th and 95th percentiles of their respective values computed for all the stations. After each smoothing, the regression analyses were repeated.

Figure 4.8 shows the amplification factors for all the zones for a magnitude of 4.5 and a distance of 5 km. These AFs can be compared with the V4 AFs shown in Figure 9.5 from the V4 GMM report (Bommer *et al*., 2017b). Figure 4.9 plots the ratios of AFs of the V5 divided by the V4 model for four magnitude-distance combinations. The lower AFs at short periods were expected because of the positive bias with respect to recorded motions that was seen in the residuals of the V4 GMM model and which has been addressed in the V5 model development. For periods longer than about 0.2 seconds, the AFs in the V5 GMM are only slightly (less than 5%) lower than in the V4 GMM model.

Figure 4.10 plots the AFs for all the zones in the Groningen field for a fixed scenario (M = 4.5 and R = 5 km) and selected periods. The spatial distribution of AFs is similar to that observed in the V4 GMM (Figure 9.18 in Bommer *et al*., 2017b).

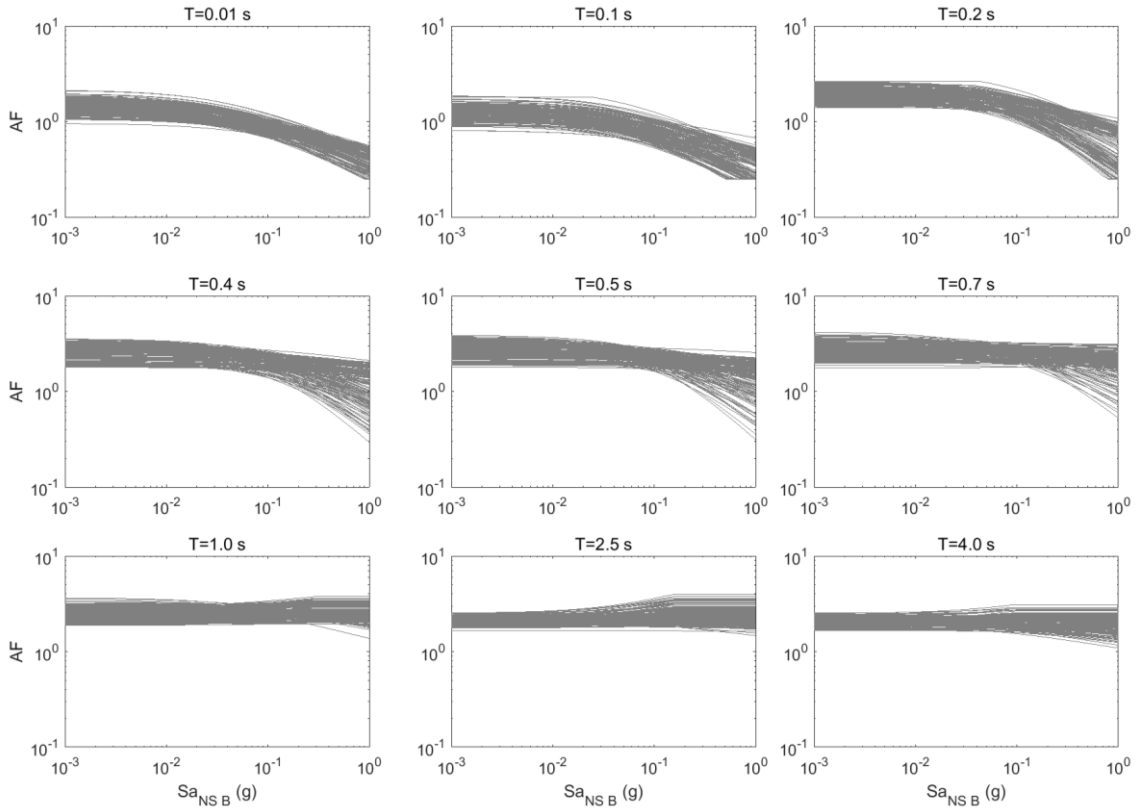

Figure 4.8. Fitted AF functions for all zones for selected periods (for M=4.5 and R=5 km)

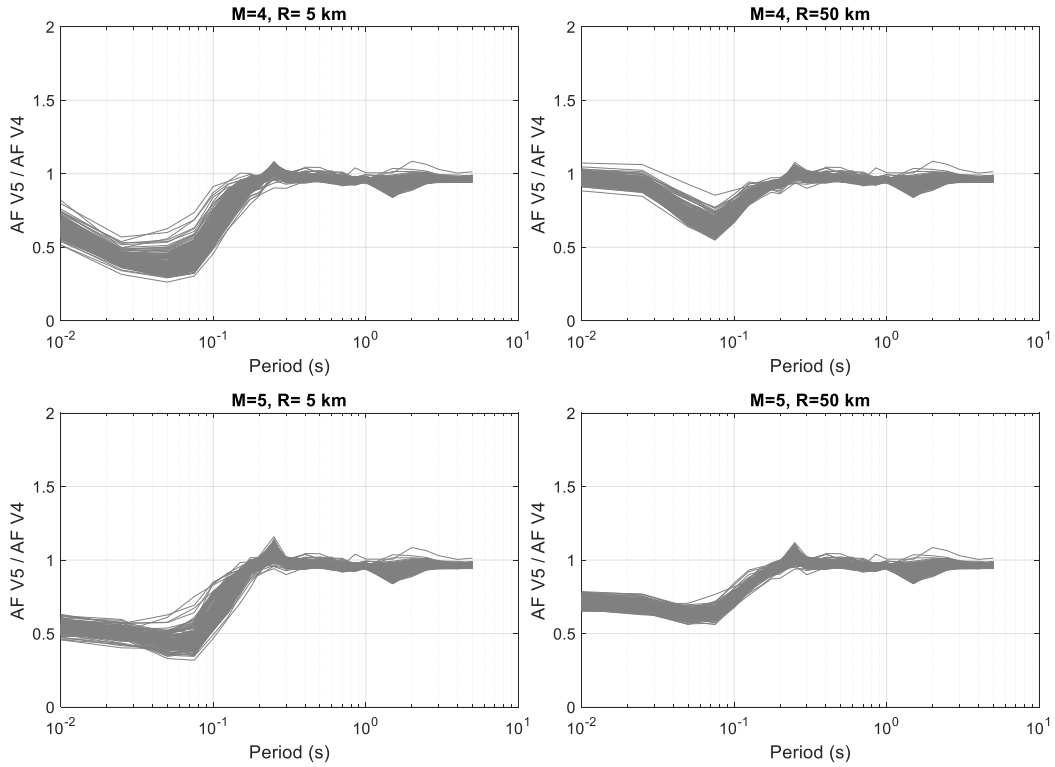

Figure 4.9. Ratios of AFs of V5 GMM over V4 GMM for all the zones. Each plot corresponds to a selected magnitude/distance combination. Spectral accelerations at rock were selected using the V5 GMM rock model.

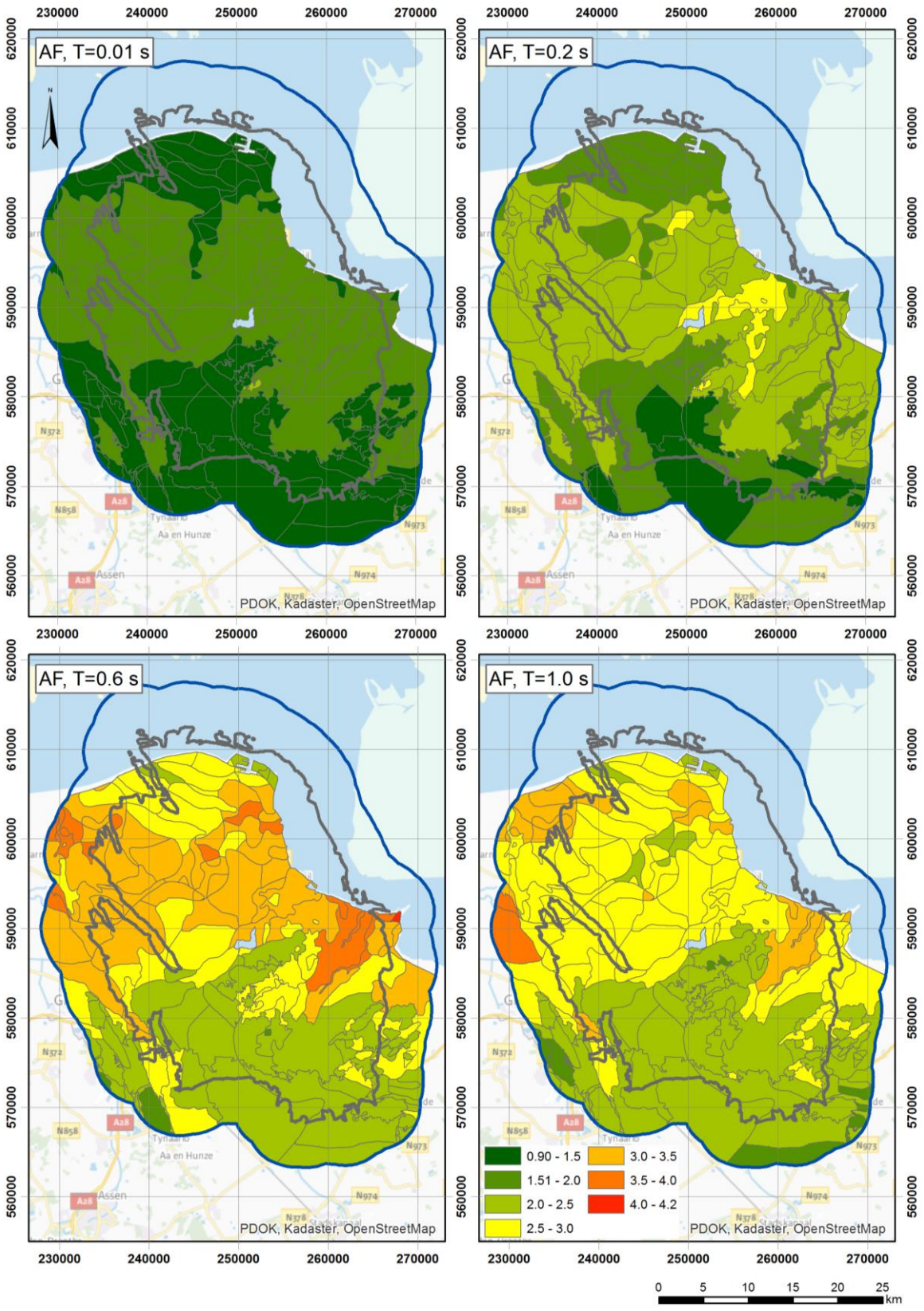

Figure 4.10. Weak motion AFs (e^{f1*}) for the zones in the Groningen region. The AFs are shown for a M=4.5, R=5 km scenario and selected periods

An important check for the model validity is that the AFs computed for a station for the magnitude-distance combinations of recorded motions should fall within the range of site-to-site variability of the corresponding zone AFs. Figure 4.11 shows this comparison for two selected stations. Additional figures for other station/zone combinations are given in Appendix V. In general, the station AFs are within a range of two standard deviation of the zone AFs, however, there are some biases that are seen at very low periods (zone AFs are lower than station AFs), and at a period of about 0.1 seconds (zone AFs are higher than station AFs). These differences occur because of deviations from the assumed linearity of AFs with respect to magnitude and distance.

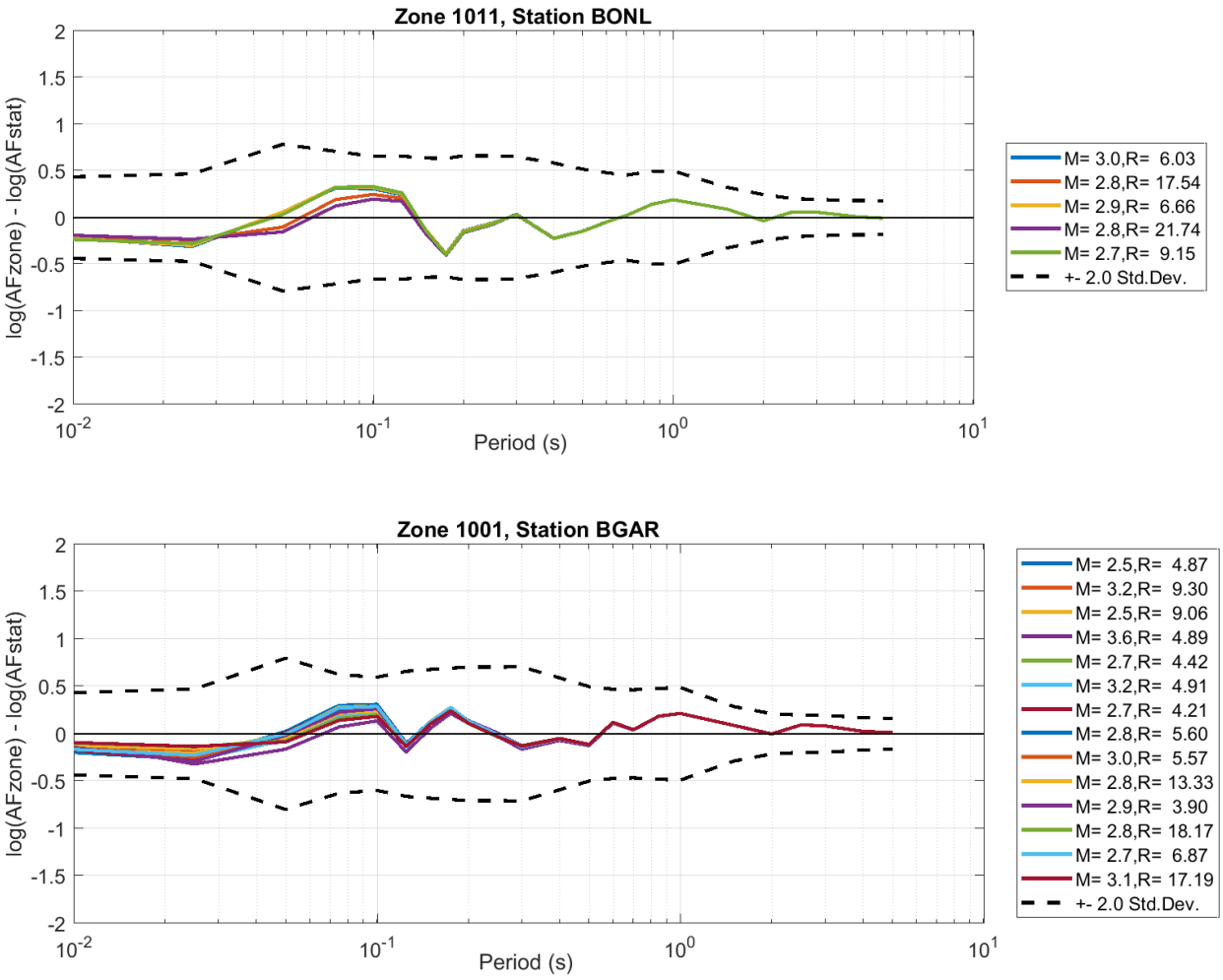

Figure 4.11. Comparison of linear AF for selected stations and the corresponding zone where the station is located. AFs are shown for the magnitude and distance pairs that correspond to recorded motions at each station. Similar plots for all other B-station recordings are given in Appendix V.

4.3. Variability associated with AFs

The model for site-to-site variability (ϕ_{S2S}) was developed in a similar way as for the V4 GMM, with the only difference being that in the V4 GMM model, the ϕ_{S2S} for large values of Sa_{NS_B} ($\phi_{S2S,2}$) was constrained to always be higher than or equal to the value for low values of Sa_{NS_B} ($\phi_{S2S,1}$). This constraint was not applied in V5 GMM because often the uncertainty at low intensities was larger than at high intensities because of the complexity resulting from magnitude and distance dependence. Figure 4.12 plots the difference in ϕ_{S2S} values between V5 GMM and V4 GMM. Overall, the values of $\phi_{S2S,1}$ for periods lower than about 0.2 seconds increased with respect to the V4 GMM. On the other hand, values of $\phi_{S2S,2}$ are generally the same for both models at longer periods.

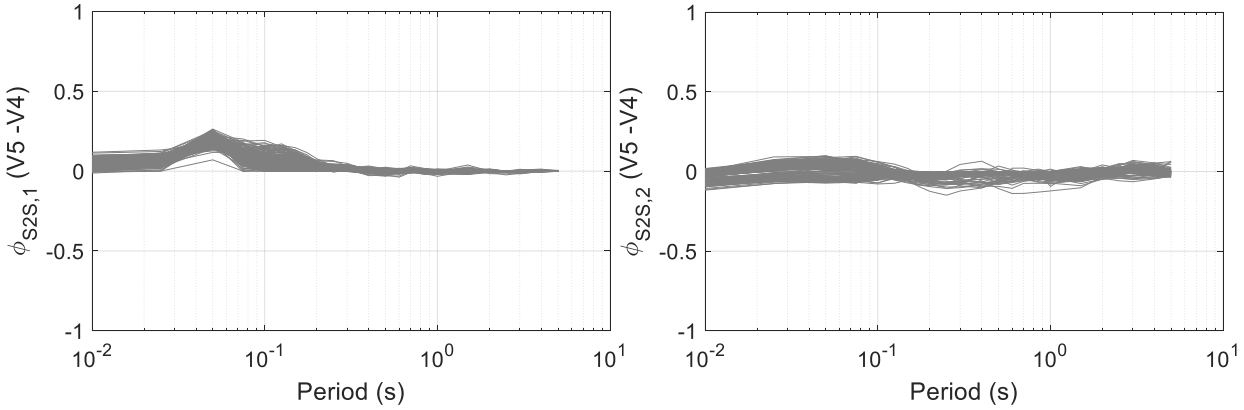

Figure 4.12. Difference in ϕ_{S2S} values between the V5 GMM and the V4 GMM. The plot on the left is for low intensity values ($\phi_{S2S,1}$), and the plot on the right is for high intensity values ($\phi_{S2S,2}$).

The values of $\phi_{S2S,1}$ for all the zones in the Groningen region are shown in Figure 4.13. The spatial distribution of these values is similar to the distribution in the V4 GMM (see Figure 9.19 in Bommer *et al*., 2017b).

4.4. Surface residuals of Groningen recordings

Residuals have been calculated at the surface by first calculating the residuals at the NS_B horizon (see Section 3.4) and then subtracting these from the total residuals. Plots showing the residuals de-composed into between-event and within-event components at the NS_B, and the site response residual at the surface, are shown for all 24 amplitude-based parameters in Appendix VI. Overall, the residuals are well behaved, showing no trends and, at longer periods, rather small scatter. Bearing in mind the process of building the model and the use of zone-wide AFs in forward modelling, the fit to the surface recordings is remarkably good.

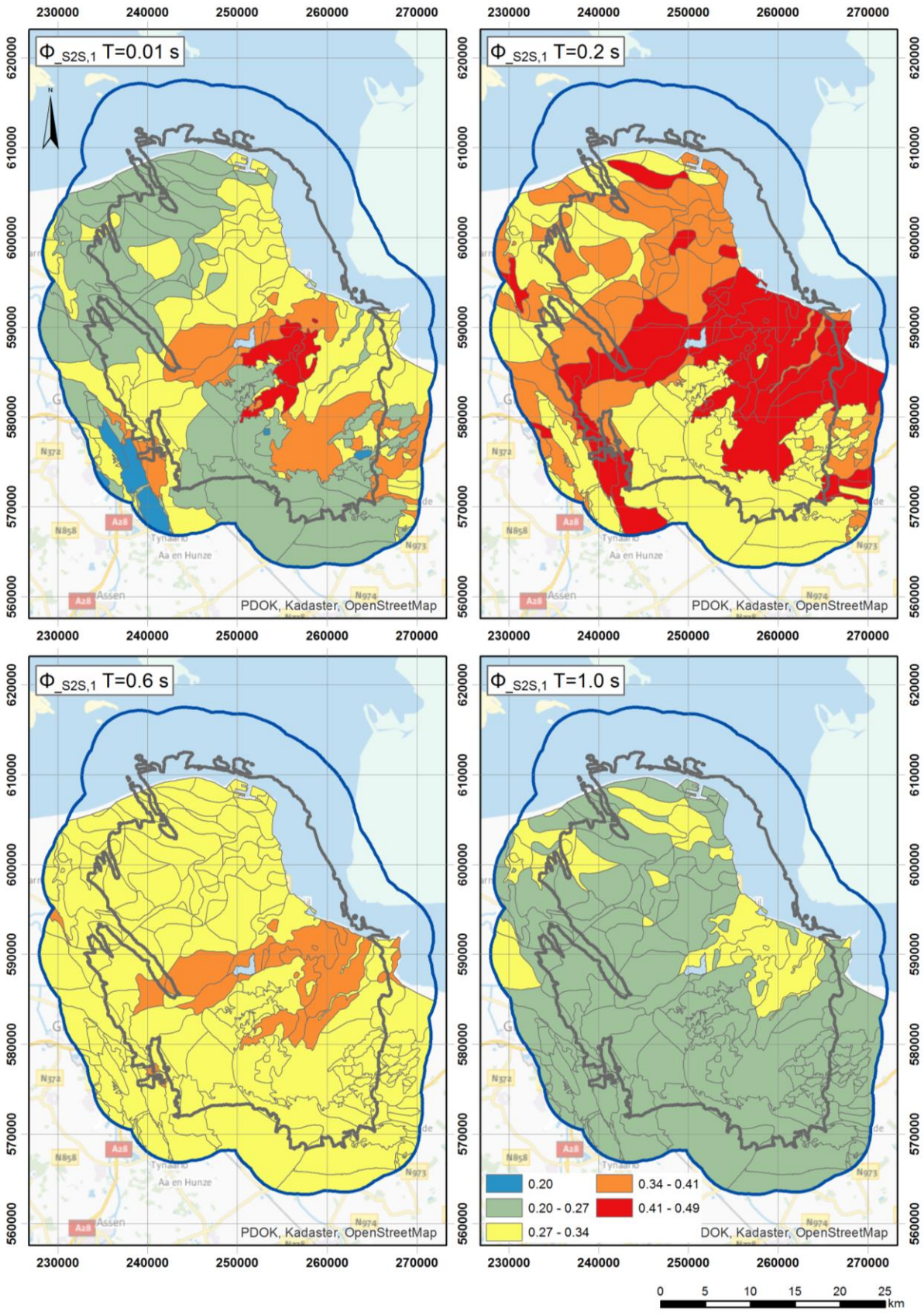

Figure 4.13. $\phi_{S2S,1}$ values for selected period and for all zones in the Groningen region

In the V4 model, it was noted that at short periods, there was overestimation due to M-R dependence of the AFs not being well captured; Figure 4.14 shows that in the V5 model, this issue has been resolved. This was a key objective of V5 GMM development stage.

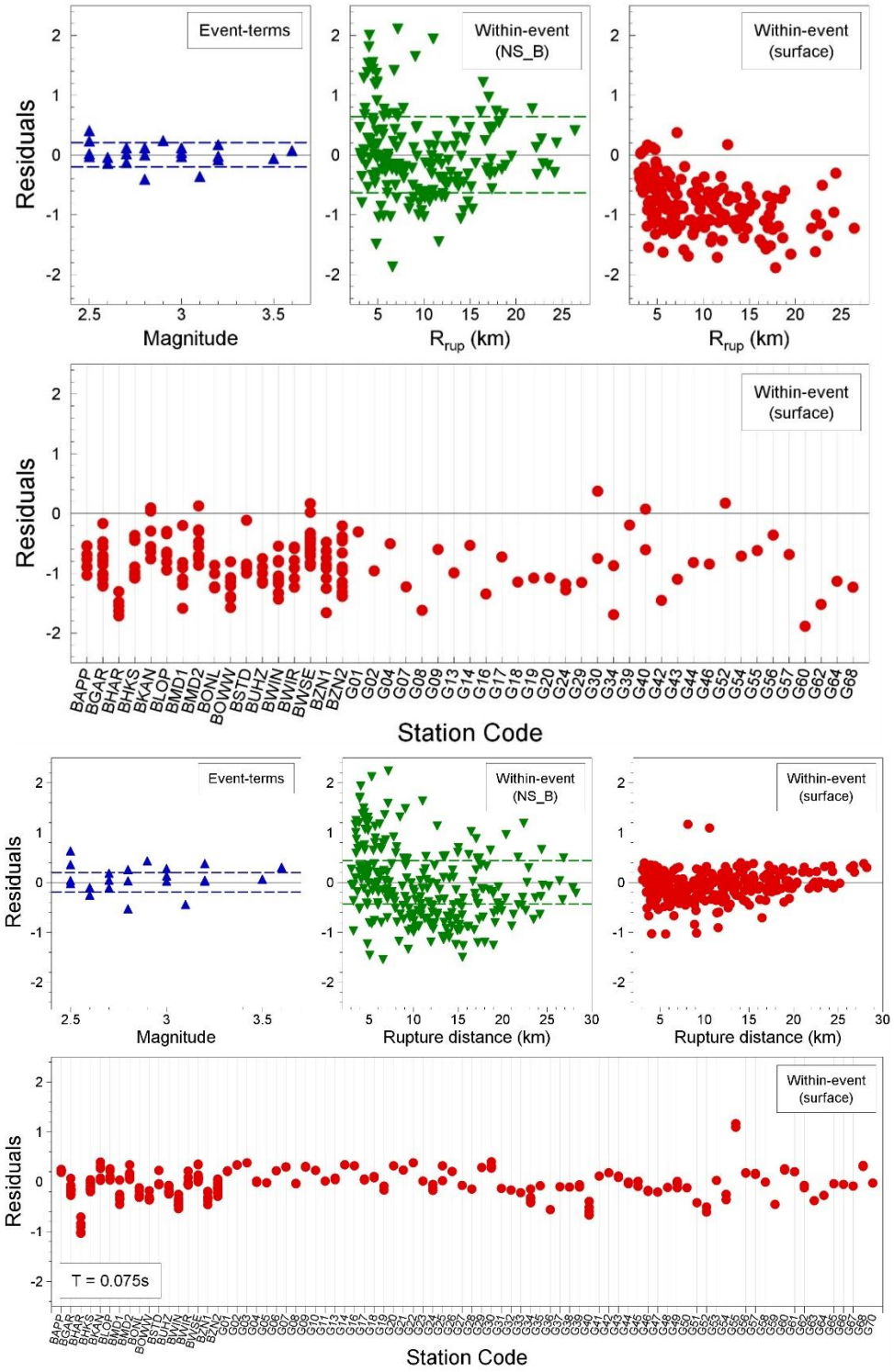

Figure 4.14. Decomposed residuals of surface motions for Sa(0.075s) from the V4 (*upper*) and V5 (*lower*) models

4.5. Comparison with V4 AFs and GMM

Appendix VII shows plots of the predicted median response spectra from the V5 model at the ground surface together with the motions at the NS_B horizon, the latter to illustrate the effects of the amplification factors. In each of these plots, the surface motions from the V4 GMM are also shown for comparison. For the smaller magnitudes, predictions from the V3 are also included; however, because that model was based on point source representation of earthquakes, larger magnitudes require assumptions regarding the conversion from R_{epi} to R_{rup} that make meaningful comparisons very difficult.

The general pattern observed between the predictions from the V4 and V5 models is that the latter predicts lower amplitudes at the surface. This reduction is not primarily due to changes in the site amplification model since median AFs have mostly reduced slightly (see Figure 4.9 and specific examples in Figure 4.15) and the site-to-site variability has increased a little (see Figure 4.10 and specific examples in Figure 4.16); these two changes will, to some extent, cancel each other out. The main reason for the lower predicted surface motions is the changes to the NS_B model (Section 3.5), in which amplitudes dropped mainly because of the updated magnitude scale correlation and, to a lesser extent, because of the inclusion of the data from the 2017 Slochteren earthquake.

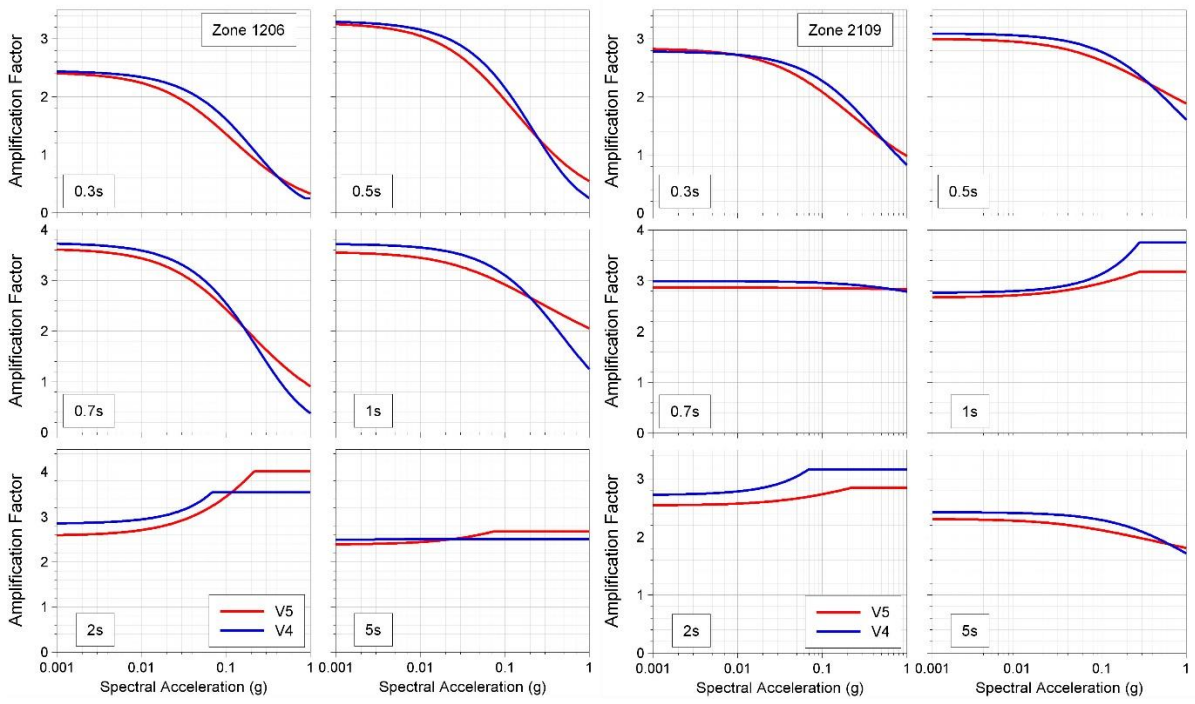

Figure 4.15. Comparison of median AFs from the V4 (blue) and V5 (red) models at six response periods. *Left*: Zone 1206, *Right*: Zone 2109.

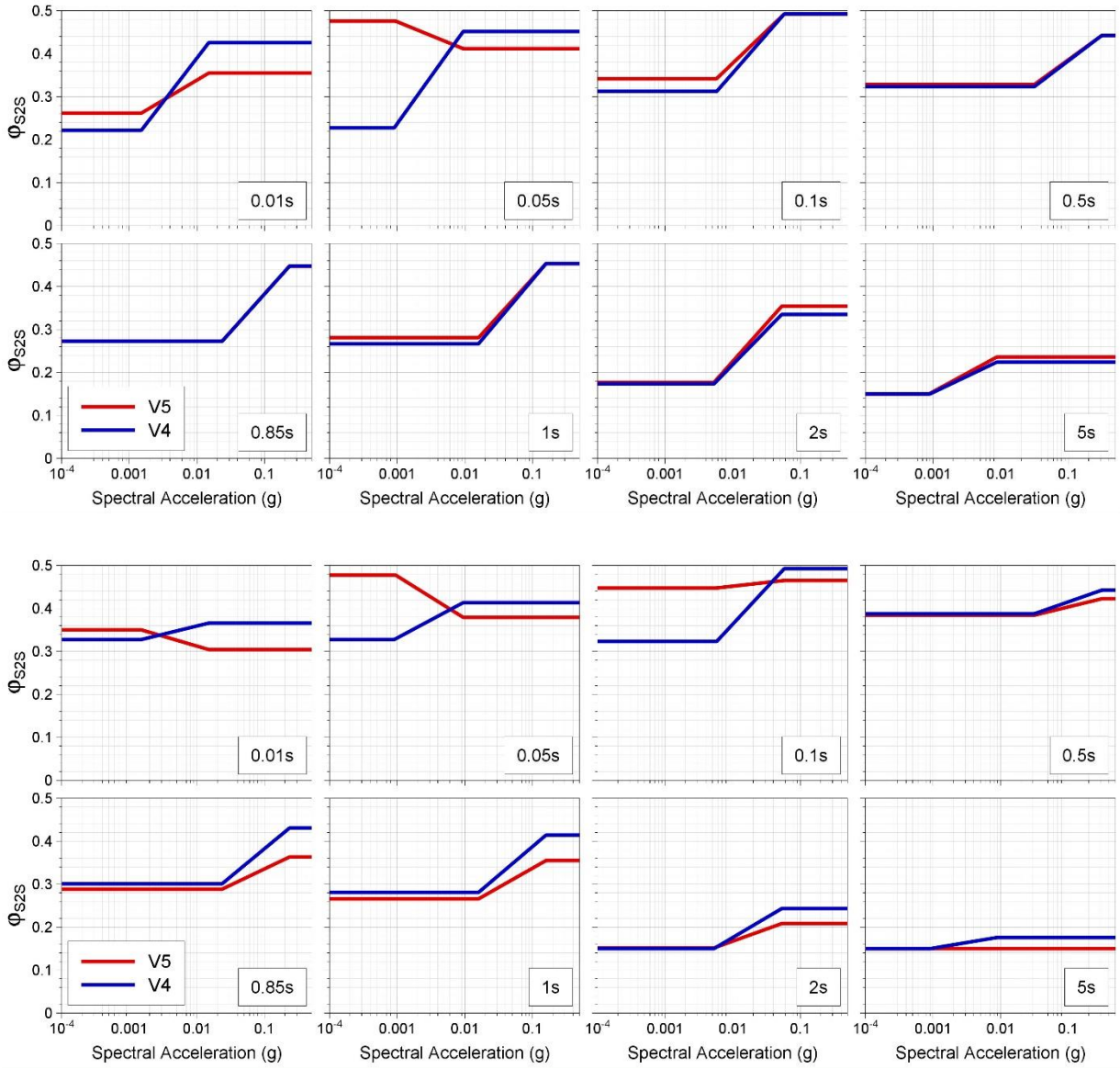

Figure 4.16. Comparison of site-to-site variability from the V4 (blue) and V5 (red) models at six response periods. *Upper*: Zone 1206, *Lower*: Zone 2109.

5. Duration Model

As has been noted earlier in Chapter 2, for some building types in the Groningen exposure database the fragility functions are defined in terms of both spectral accelerations and the duration of the ground shaking, for which the significant duration defined between 5% and 75% of the total Arias intensity is adopted as the preferred definition.

The general approach used to derive the V5 duration model was essentially the same as that used in the V4 model development; this chapter briefly explains the subtle differences and then compares the results from the two models.

5.1. Derivation of updated model

The duration model was developed by performing regression analyses directly upon the outputs of the EXSIM simulations. This is the same process as was followed during the development of the V4 duration model. The EXSIM simulations use the prediction equation originally developed for use in the V3 model to describe the durations of time-series originating from each sub-source of the finite fault ruptures represented by EXSIM. This V3 model has previously been shown to work well for small events and is able to capture some important field-specific attributes of the path scaling. However, the V3 duration model performed poorly when extrapolated to the prediction of large-magnitude, long-distance scenarios. The approach of using EXSIM to generate synthetic accelerograms and fitting the duration model to these outputs performed well for the V4 duration model and so the approach was retained for the V5 model.

Figure 5.1 presents an example of the duration values derived from the EXSIM simulations plotted against distance for three magnitude values. A key feature of the durations arising from EXSIM is the decreasing rate of duration increase with distance that exists as magnitudes increase. This scaling is consistent with what is commonly observed from tectonic earthquakes.

The simulated duration values shown in Figure 5.1 represent part of a much larger database of simulated duration values. In total, 436,800 simulated durations were generated for each of the four model branches and these simulated data and thereafter regarded as ‘empirical data’ for the purposes of developing the V5 duration model. That is, the duration model arises from a regression analysis conducted treating the EXSIM duration outputs as observed duration values. However, the variance components for the duration model are obtained by making use of the real observed duration values from the Groningen field.

As the overall process adopted for the development of the V5 duration model is the same as that for the V4 model, the main differences arising between the V4 and V5 duration models therefore relate to the fact that source durations are sensitive to level of stress drop. As the V5 model adopts a new set of stress drop branches the duration model is updated to reflect these new branches. Furthermore, the additional ground-motion recordings used in the V5 database dictates that the estimates of the variance components differ between the V4 and V5 models.

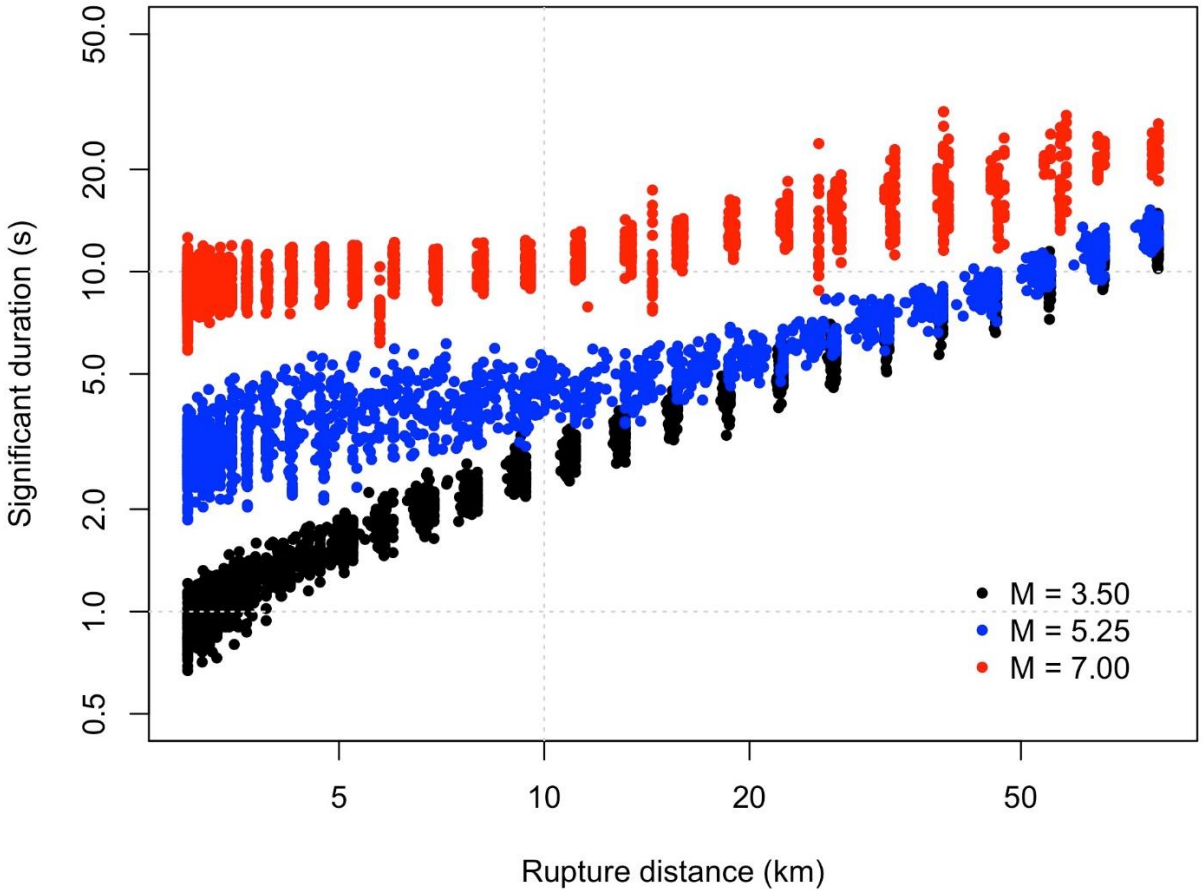

Figure 5.1. Example significant duration values derived from EXSIM simulations for three magnitude values.

The functional form used for the duration model remains the same as that in the V4 model, but the magnitudes at which fundamental changes in scaling take place have been modified slightly. This modification reflects the adjustment to the relationship between local and moment magnitudes used in the V5 model. For both the V4 and V5 models the EXSIM simulations were performed in terms of moment magnitude (which is the natural magnitude scale to use for that software). Therefore, when changes in the duration predictions arose as a result of changes to the expected scaling of rupture dimensions, changes in stress parameter with magnitude, or changes in the rupture velocity with magnitude, the points at which these changes

occurred were defined as a function of moment magnitude. For the V4 duration model, the functional form was defined in a piecewise manner to reflect differences in scaling associated with these points, but the particular locations where scaling changed was converted to be defined in terms of local magnitude. For the V5 model, the adopted equivalence between local and moment magnitudes means that the points at which scaling changes are now slightly adjusted to be more directly aligned with the breaks in scaling incorporated into the EXSIM simulations.

The overall functional form for the V5 duration model is defined in terms of contributions from the source, path and site:

$$\ln D_{5-75\%} = g_{src}(M) + g_{path}\left(R_{rup}, M\right) + g_{site}(V_{S,30}) \tag{5.1}$$

The inclusion of the site response term reflects the fact that durations are directly predicted to the surface horizon rather than being predicted to NS_B first and then mapped to the surface.

The source scaling is a function of magnitude only and is defined in Eq.(5.2):

$$g_{src}(M) = \begin{cases} m_6 + m_7(M - 5.25) & \text{for } M \leq 5.25 \\ m_6 + m_8(M - 5.25) + m_9(M - 5.25)^2 & \text{for } M > 5.25 \end{cases} \tag{5.2}$$

where the magnitude used for the source term is constrained to not be less than 3.25, *i.e.*, $M \equiv \max(M, 3.25)$.

The path scaling is linear in log-rupture distance for distances beyond 12km (informed by the numerical waveform modelling), while at closer distances there is a degree of nonlinear scaling. The overall path function is defined as:

$$g_{path}\left(R_{rup}, M\right) = \begin{cases} (r_6 + r_7 M)\left[\ln\left(\frac{R_{rup}}{3}\right)\right]^{r_8} & \text{for } R_{rup} \leq 12\text{km} \\ (r_6 + r_7 M)\left[\ln\left(\frac{12}{3}\right)\right]^{r_8} + (r_9 + r_{10} M)\ln\left(\frac{R_{rup}}{12}\right) & \text{for } R_{rup} > 12\text{km} \end{cases} \tag{5.3}$$

In a similar manner to the source scaling, the magnitude value that is passed into the path scaling function is constrained to equal a value within the range 3.25 to 6.0. Hence, the magnitude in Eq.(5.3) can be expressed as $M \equiv \min[\max(M, 3.25), 6.0]$.

The site scaling is adopted from the model of Afshari & Stewart (2016), but is adjusted to simply reflect the difference in shear-wave velocity that exists between the NS_B horizon, to which the EXSIM durations correspond, and the surface. The

parameterisation of the surface velocity is made using the average shear-wave velocity over the uppermost 30 m. The site scaling is therefore:

$$g_{site}\left(V_{S,30}\right) = \phi_1 \ln\left[\frac{\min\left(V_{S,30}, V_1\right)}{V_1}\right] \tag{5.4}$$

with $\phi_1 = -0.2246$ and $V_1 = 600$ m/s. These site response parameters are kept constant for all of the four model branches.

The model coefficients for the magnitude and distance scaling for each of the four branches is presented in Table 5.1. The computation of the variance components is made using the same procedure outlined in Section 3.4, but as the total residuals are computed directly from the surface motions, the regression estimates τ and ϕ, rather than τ and ϕ_{SS}. These parameters are also included in Table 5.1.

Table 5.1. Coefficients of the median V5 duration model

Coefficient	Lower, L	Central, Ca	Central, Cb	Upper, U
m_6	1.0138	1.0077	0.9829	0.9444
m_7	0.6912	0.6864	0.6763	0.6627
m_8	0.9453	0.9247	0.9143	0.9513
m_9	-0.1202	-0.1314	-0.1335	-0.1567
r_6	2.4617	2.4515	2.4537	2.4752
r_7	-0.3998	-0.3982	-0.3970	-0.4004
r_8	0.7099	0.7105	0.7078	0.7106
r_9	1.1584	1.1545	1.1370	1.1200
r_{10}	-0.1207	-0.1192	-0.1143	-0.1090
τ	0.3937	0.3961	0.3922	0.3935
ϕ	0.5400	0.5401	0.5398	0.5399

In applications to the risk model, the arbitrary rather than geometric mean component of the duration is required, which necessitates the addition of the component-to-component variance. The derivation of this quantity is presented in Appendix III.

The general scaling of the V5 duration model is shown with respect to distance for a number of magnitude values in Figure 5.2 and with respect to magnitude for a number of distances in Figure 5.3. It is clear from both figures that the impact of the stress parameter branches is typically modest at small to intermediate magnitude values, but that there is some non-negligible dependence for larger magnitudes.

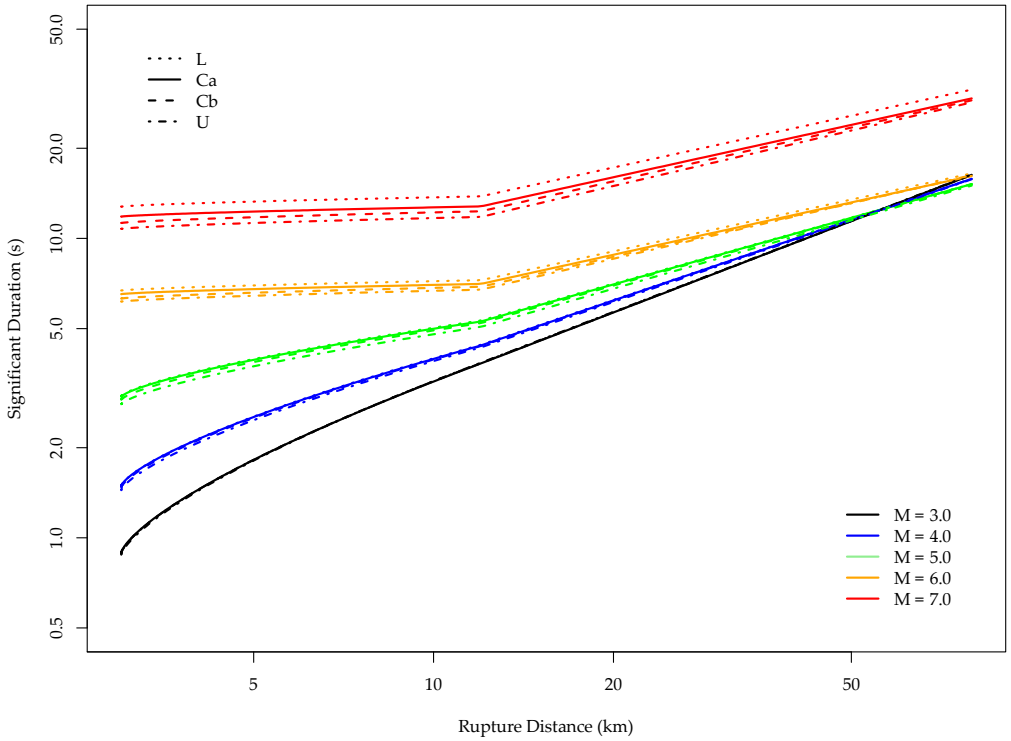

Figure 5.2. Predicted scaling of significant duration with distance for a number of magnitude values. V_{S30} is taken at 200m/s in all cases.

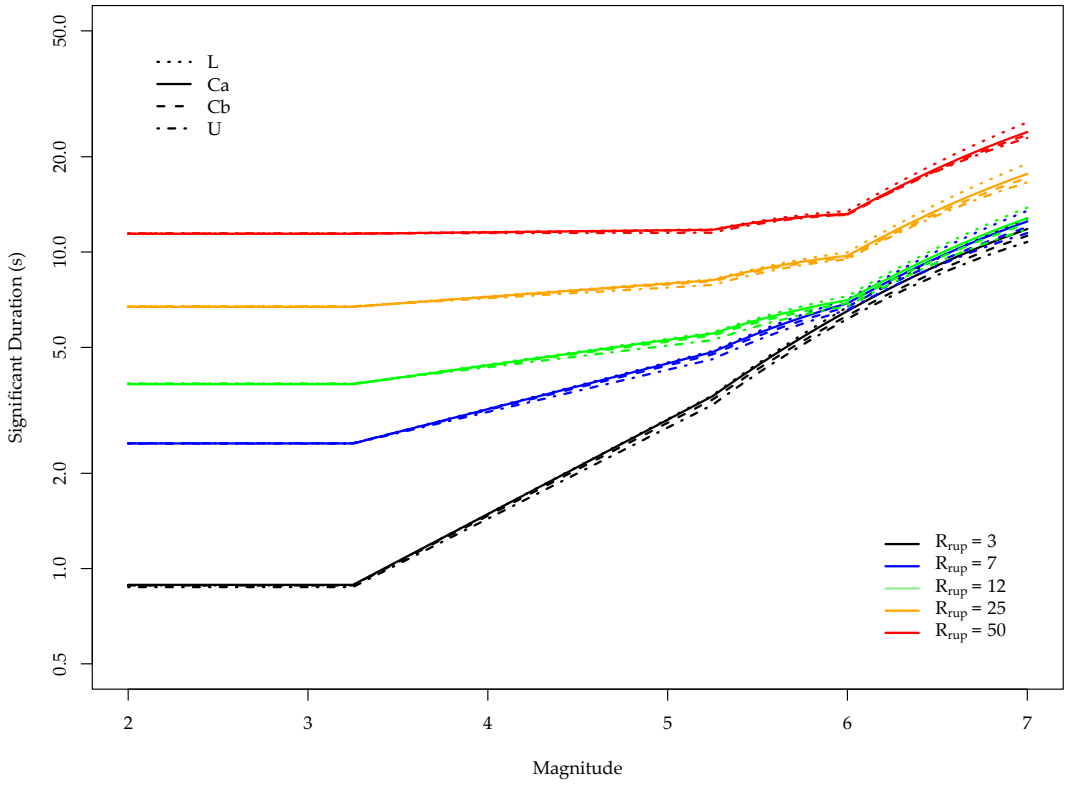

Figure 5.3. Predicted scaling of significant duration with magnitude for a number of distance values. V_{S30} is taken at 200m/s in all cases.

5.2. Comparison with V4 model

The predictions of the V5 duration model are broadly consistent with those of the V4 model for many scenarios of relevance to the Groningen risk model. Given that both models make use of the V3 prediction model to define the sub-source duration values and the scaling of these sub-source contributions with distance, it is not surprising to see very consistent predictions of both magnitude and distance scaling in both the V4 and V5 models. This consistency can be appreciated for each of the four branches in Figure 5.4.

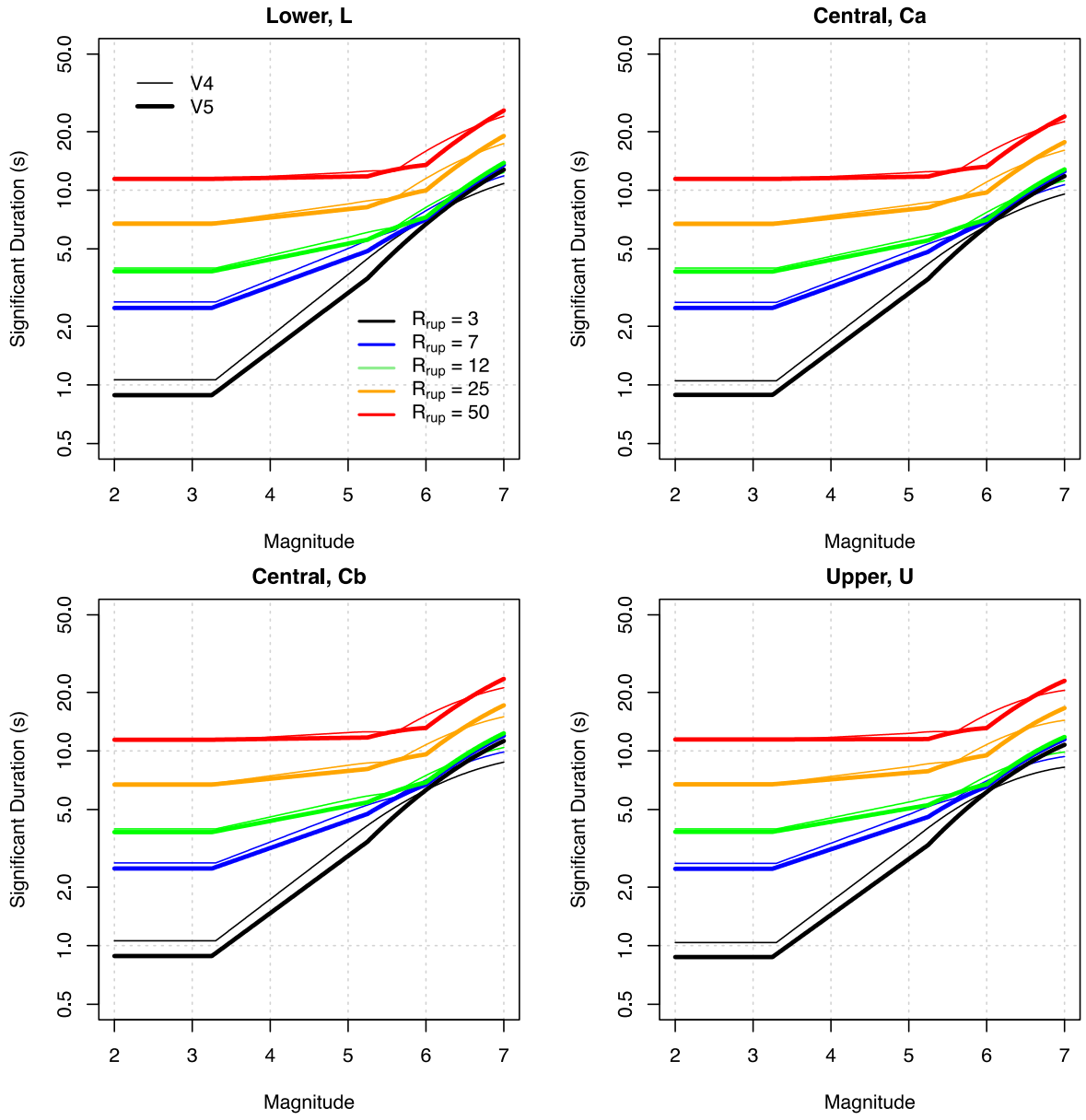

Figure 5.4. Comparison of duration predictions from the V4 and V5 models with respect to magnitude for a number of different distances. Note that predictions are shown here for a consistent value of moment magnitude, *i.e.*, the V4 model predictions are converted from local magnitude to moment magnitude.

However, there are non-trivial differences between the V4 and V5 model predictions for the shortest distances where the effects of the changes in stress parameter between these models is most significant. Figure 5.4 shows that the V5 duration model consistently predicts shorter durations at short distances than its V4 counterpart. These shorter durations reflect the higher values of stress parameter that have been adopted in the V5 model. At larger distances the influence of the source duration is not as strong and so the predictions for both V4 and V5 become more aligned. Similarly, the distance scaling shown in Figure 5.5 reinforces this point showing that differences tend to reduce as one moves farther away.

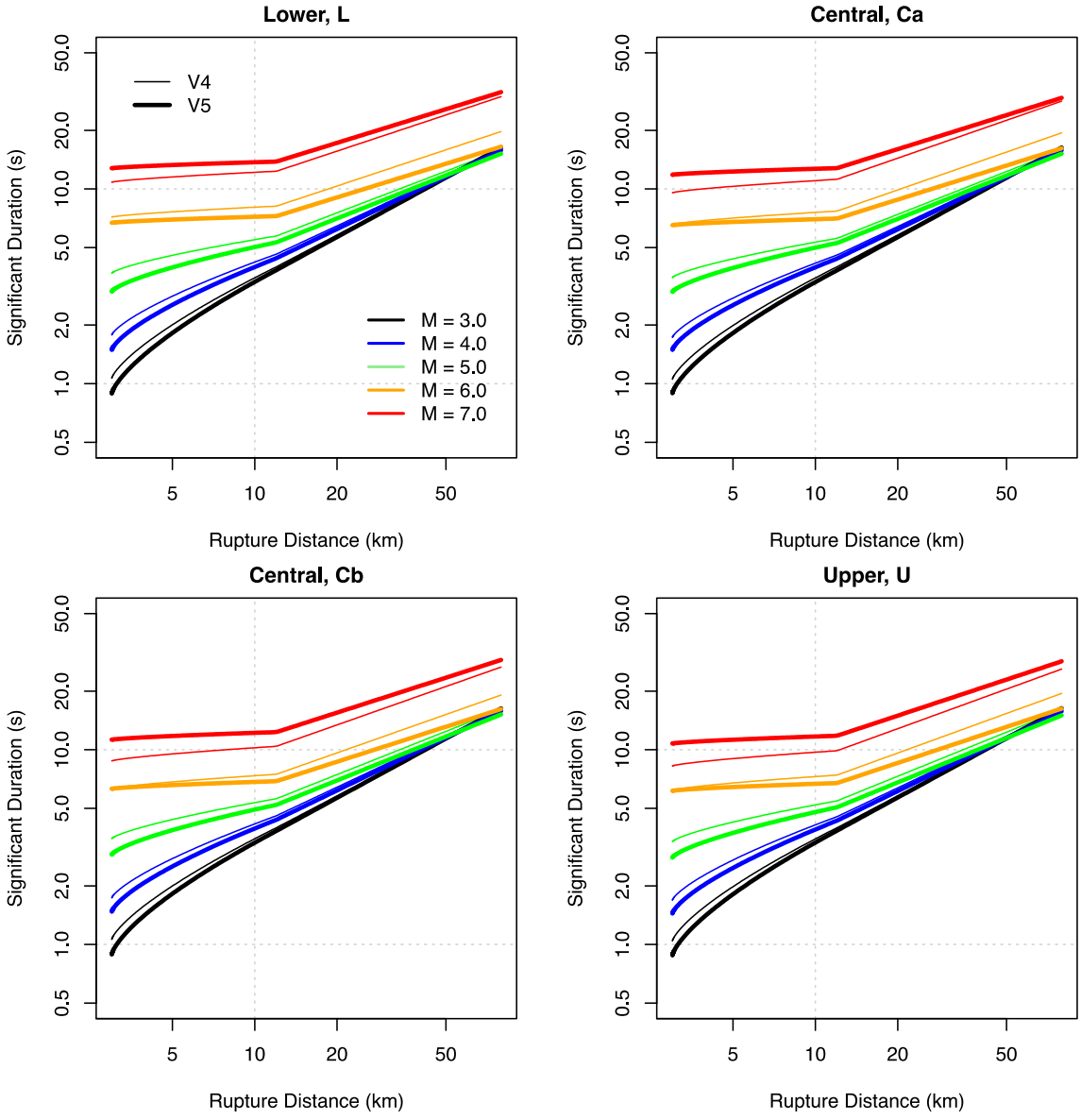

Figure 5.5. Comparison of duration predictions from the V4 and V5 models with respect to rupture distance for a number of different magnitude values. Note that predictions are shown here for a consistent value of moment magnitude, *i.e.*, the V4 model predictions are converted from local magnitude to moment magnitude.

The variance components for the duration model are treated differently between the V4 and V5 models. As discussed in Section 6.2, the V5 risk model computes ground-motion fields (of both spectral amplitude and duration) at the NS_B horizon, and then propagates these through to the surface. In the V4 model the correlations that exist between the spectral amplitudes and duration was handled in an approximate manner that allowed only the total standard deviation of durations at the surface to be modelled. In the more correct approach adopted in V5, it becomes necessary to decompose the total standard deviation into between-event and within-event components.

Since there is almost no magnitude scaling in the duration predictions over the magnitude range spanning the Groningen data, the total residuals for duration computed in each branch are very similar. The variance components are also similar as a result. As can be seen from Table 5.1, the average between-event standard deviation over the four model branches in V5 is 0.3939, while the average within-event standard deviation is 0.5400. The corresponding total standard deviation is 0.6683 for the V5 model and this is slightly larger than the value of 0.6354 obtained from the V4 model.

6. MODEL SUMMARY and IMPLEMENTATION

As noted in Chapter 1, this chapter provides a concise summary of the complete model for those interested in its implementation. This means that some information is repeated from previous chapters but for the convenience of the user the complete model is presented here in its entirety. Section 6.1 presents the basic model elements, including the equations and their coefficients, as well as identifying all of the electronic supplements where the model parameters are listed; in previous GMM reports, similar information was included as an Executive Summary. Section 6.2 provides instructions for the sampling of the variance components.

6.1. Complete GMM logic-tree

The V5 Groningen ground-motion model (GGMM) has the same basic structure as the V4 model: equations for the prediction of accelerations at the NS_B rock horizon combined with frequency-dependent non-linear site amplification factors (AF) assigned to zones defined throughout the study area (onshore gas field plus 5 km buffer). As for the V4 model, the model provides predictions of 5%-damped spectral accelerations [Sa(T)], at 23 periods and peak ground velocity (PGV); in all cases, the geometric mean of the horizontal components is predicted. As in V4, the predictions at the NS_B horizon are a function of local magnitude (M_L) and rupture distance (R_{rup}). Additionally, the model predicts the duration of shaking ($D_{S5\text{-}75}$) directly at the ground surface, as a function of M_L, R_{rup} and V_{S30}.

The functional form of the predictive equations is essentially the same as in V4 (apart from the model for AF) and the logic-tree structure is also the same, with four branches for the median predictions and two branches for the within-event variability. The field zonation is identical with exactly the same 160 zones defined by the X-Y coordinates of the voxels included within each zone. The median V_{S30} values for each zone are also unchanged from the V4 model.

This section summarises the basic elements of the V5 model as required for its implementation in hazard and risk calculations. The coefficients and additional values (such as the site amplification zonation) are included in supplementary CSV files identified in the text.

Equations for Median Motions at NS_B Rock Horizon

The equations for predicting the median ground-motion parameters at the NS_B rock horizon are a function of only magnitude (M_L) and distance (R_{rup}); hereafter, these are specified simply as M and R, the latter measured in km. The model has exactly the same functional form as the V4 model for motions at the NS_B horizon and can

be represented as comprising a source component and a path component, the latter being a function of magnitude and distance:

$$\ln(Y) = g_{source}(M) + g_{path}(R,M) \qquad (6.1)$$

where Y is either Sa(T) in cm/s^2 or PGV in cm/s. The source-related terms are segmented into three ranges of magnitude:

$$g_{source}(M) = m_0 + m_1(M-4.7) + m_2(M-4.7)^2 \qquad M \le 4.7 \qquad (6.2a)$$

$$g_{source}(M) = m_0 + m_3(M-4.7) \qquad 4.7 < M \le 5.45 \qquad (6.2b)$$

$$g_{source}(M) = m_0 + m_3(5.45-4.7) + m_4(M-5.45) + m_5(M-5.45)^2 \qquad M > 5.45 \qquad (6.2c)$$

Similarly, the path terms are also segmented into ranges of rupture distance:

$$g_{path}(R,M) = (r_0 + r_1 M)\ln\left(\frac{R}{3}\right) \qquad R < 7 \qquad (6.3a)$$

$$g_{path}(R,M) = (r_0 + r_1 M)\ln\left(\frac{7}{3}\right) + (r_2 + r_3 M)\ln\left(\frac{R}{7}\right) \qquad 7 \le R < 12 \qquad (6.3b)$$

$$g_{path}(R,M) = (r_0 + r_1 M)\ln\left(\frac{7}{3}\right) + (r_2 + r_3 M)\ln\left(\frac{12}{7}\right) + (r_4 + r_5 M)\ln\left(\frac{R}{12}\right) \qquad R \ge 12 \qquad (6.3c)$$

There are four versions of the median equations for Y at the NS_B horizon, as summarised in Table 6.1; these models correspond to different values of the stress parameter, $\Delta\sigma$. There are two central models, both having the same value of the stress parameter in the magnitude range of the existing Groningen data; at larger magnitudes, the stress parameters rise to a lower (Ca) and higher (Cb) values.

Table 6.1. Weights on the four branches for median predictions at NS_B.

Branch	Model	Code	Weight
1	Lower	L	0.1
2	Central – lower	Ca	0.3
3	Central – upper	Cb	0.3
4	Upper	U	0.3

The coefficients of equations (6.2) and (6.3) for the four individual models are presented in the file **gmpe_medians_NS_B_20170724_v5.csv**.

Sigma Model for NS_B Rock Horizon GMPEs

The sigma model representing the aleatory variability in the values of ln(Y) from Eq.(6.1) includes a between-earthquake component, τ, and a within-earthquake component, ϕ_{SS}. If Y_μ is the median value obtained from Eqs.(6.1)-(6.3), then two different quantities may be predicted by sampling from the components of variability: Y_{GM}, the geometric mean component (to be used for hazard mapping), and Y_{arb}, the arbitrary component (to be used in risk calculations):

$$\ln(Y_{GM}) = \ln(Y_\mu) + \varepsilon_E \tau + \varepsilon_S \phi_{SS} \quad (6.4a)$$

$$\ln(Y_{arb}) = \ln(Y_\mu) + \varepsilon_E \tau + \varepsilon_S \phi_{SS} + \varepsilon_C \sigma_{C2C} \quad (6.4b)$$

The ε values are standard normal variates that represent the numbers of standard deviations from the each of the normal distributions; σ_{C2C} is the component-to-component variability. The component-to-component variability model has changed appreciably from the V4 model and now includes dependence on both magnitude and distance. The component-to-component variance is defined by the following equations for the value at different periods, T:

$$\sigma^2_{c2c}(M,R) = 0.026 + 1.03[5.6 - \min(5.6, \max[M, 3.6])]R^{-2.22} \qquad T \le 0.1s \quad (6.5a)$$

$$\sigma^2_{c2c}(M,R) = 0.045 + 5.315[5.6 - \min(5.6, \max[M, 3.6])]R^{-2.92} \qquad T \ge 0.85s \quad (6.5b)$$

For periods in between 0.1 and 0.85 seconds, the following interpolation is used:

$$\sigma^2_{c2c}(T,M,R) = \sigma^2_{c2c}(0.1,R) + \left[\frac{\log(T) - \log(0.1)}{\log(0.85) - \log(0.1)}\right]\left[\sigma^2_{c2c}(0.85,R) - \sigma^2_{c2c}(0.1,R)\right] \quad (6.6)$$

The component-to-component variability of duration is also defined and presented later in this section.

A unique value of between-earthquake variability is associated with each period (and PGV) and there are two equally-weighted branches for the within-event variability. The between-earthquake variability values are modified from V4 but the values of the within-event variability are identical to those used in the previous model. The complete logic-tree for motions at the NS_B horizon is illustrated in Figure 6.1. The values of the sigma components are presented in the file **gmpe_sigmas_NS_B_20170831_v5.csv**.

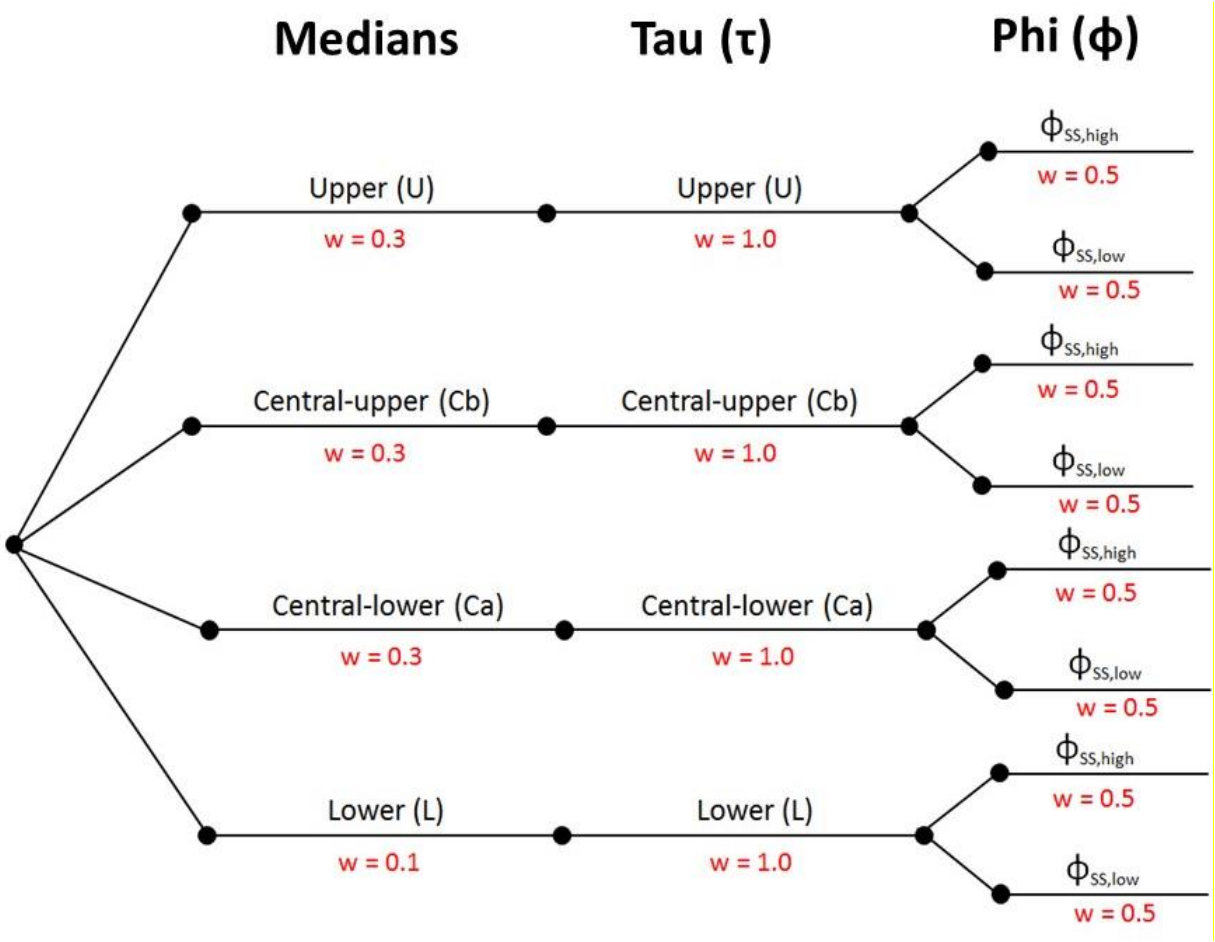

Figure 6.1. Logic-tree structure for model for motions at the NS_B horizon

Field Zonation

The study area is divided into **160** zones having a common set of AFs for both Sa(T) and PGV (Figure 6.2). The zones are defined by a numerical code; the zones and their geographical limits are identical to those defined for the V4 model. A list of 140,862 voxel squares of 100 x 100 m—each identified by the RD coordinates of their centre—and the zone to which each voxel is identified is provided in the following file: **gmpeSurfaceZonation_20170824_v5.csv**. The content of the file is identical to that in **gmpeSurfaceZonation_20170131_v4.csv**, but a new file has been created in order to have a consistent set of CSV files defining the parameters of the V5 model.

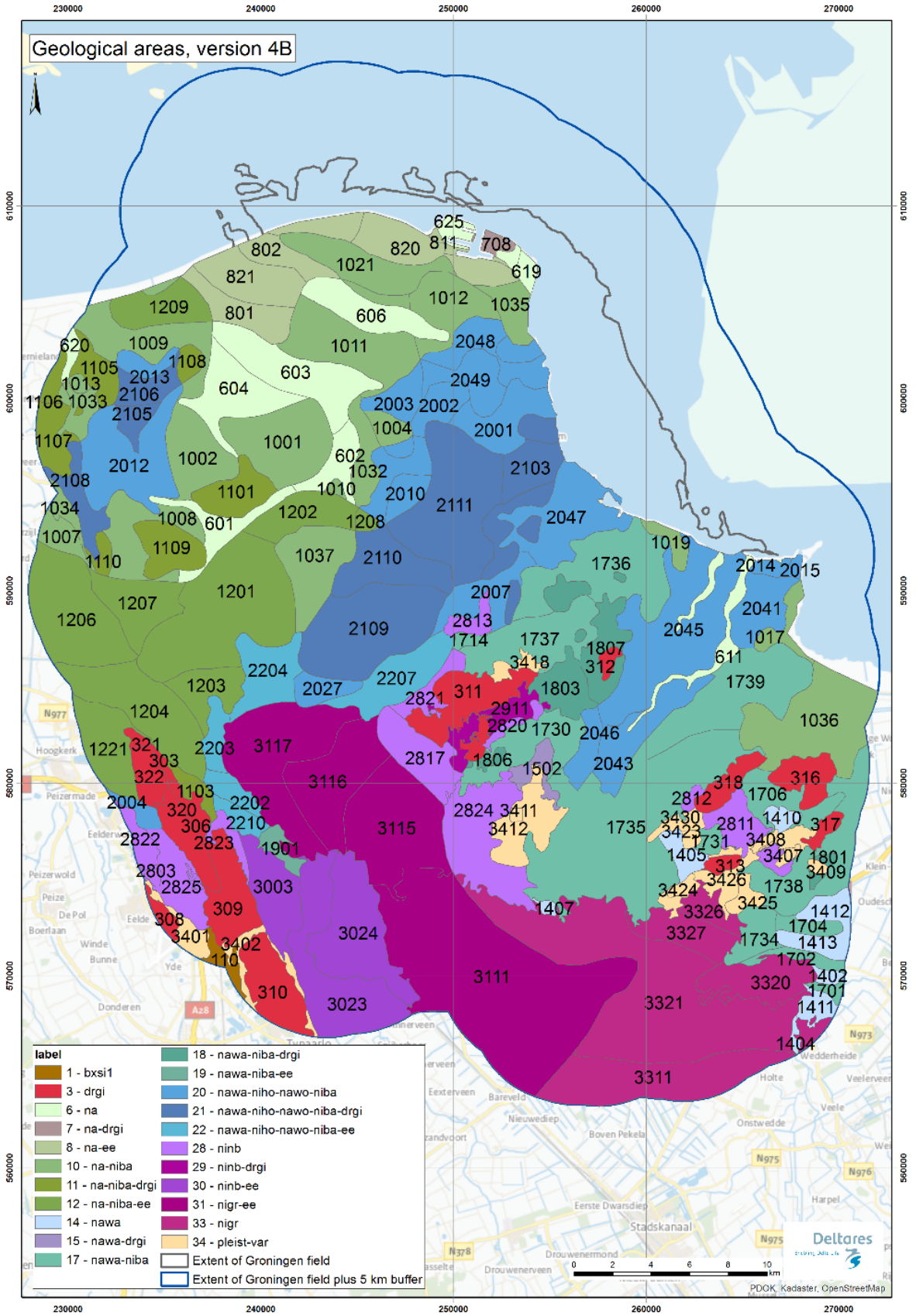

Figure 6.2. V5 zonation of the Groningen field for site amplification factors

Median Non-Linear Soil Amplification Factors

For each of the 160 zones and each ground-motion parameter (spectral acceleration at 23 periods and PGV), the amplification factors, AF, are defined as follows:

$$\ln[AF(Sa)] = f_1^* + f_2 \ln\left(\frac{Sa_{NS\_B,g} + f_3}{f_3}\right) \qquad (6.7a)$$

$$\ln[AF(PGV)] = f_1^* + f_2 \ln\left(\frac{PGV_{NS\_B} + f_3}{f_3}\right) \qquad (6.7b)$$

In Eq.(6.7a), $Sa_{NS\_B,g}$ is the spectral acceleration at the NS_B horizon, expressed in units of *g* (981 cm/s^2); in Eq.(6.7b), PGV_{NS_B} is the PGV value at the same reference rock horizon, in units of cm/s. This general formulation in unchanged from the V4 model, but the functional form for the first term on the right-hand side has been modified, as explained below.

The first term on the right-hand side of Eq.(6.7), f_1^*, is the exponent of the linear part of the amplification factors. The term is magnitude- and distance-dependent and for Sa(T) this dependence is defined by the following equation:

$$f_1^* = [a_0 + a_1 \ln(R)] + [b_0 + b_1 \ln(R)][\min(M, M_{ref}) - M_{ref}] \qquad (6.8)$$

where M_{ref} is given by:

$$M_{ref} = M_1 - \left[\frac{\ln(R) - \ln(3)}{\ln(60) - \ln(3)}\right](M_1 - M_2) \qquad (6.9)$$

where M_1 and M_2 are model parameters.

For PGV, f_1^*, is given by:

$$f_1^* = [a_0 + a_1 \ln(R)] + [b_0 + b_1 \ln(R)](M - M_1) \qquad M \le M_1 \qquad (6.10a)$$

$$f_1^* = [a_0 + a_1 \ln(R)] + d(M - M_1) \qquad M > M_1 \qquad (6.10b)$$

The model parameters a_0, a_1, b_0, b_1, M_1 and M_2 are all given for all periods and all zones in the file **gmpeSurfaceAmplificationModel_20170826_v5.csv**. For PGV, the same parameters are given but M_2 is given as -99 since this coefficient is not used for this ground-motion parameter. The coefficient *d* used in Eq.(6.10b) is also included in the file, and is entered as 0 for Sa(T). The values of ln(AF) in Eqs.(6.7a) and (6.7b) are subject to upper and lower limits of AF_{max} and AF_{min}, which are also

included in the same file. It should be noted that the model for AF is only applicable for magnitudes greater than or equal to M_L 2.

Site-to-Site Variability Model

The variability in the site amplification factors is given by the standard deviation ϕ_{S2S}, which is defined as a tri-linear function as defined in the following equations (and illustrated in Figure 6.3):

$$\phi_{S2S} = \phi_{S2S,1} \qquad Sa_{NS\_B,g} < Sa_{Low} \qquad (6.11a)$$

$$\phi_{S2S} = \phi_{S2S,1} + (\phi_{S2S,2} - \phi_{S2S,1})\left[\frac{\ln(Sa_{NS\_B,g}) - \ln(Sa_{low})}{\ln(Sa_{high}) - \ln(Sa_{low})}\right] \qquad Sa_{Low} \le Sa_{NS\_B,g} \le Sa_{High} \qquad (6.11b)$$

$$\phi_{S2S} = \phi_{S2S,2} \qquad Sa_{NS\_B,g} > Sa_{High} \qquad (6.11c)$$

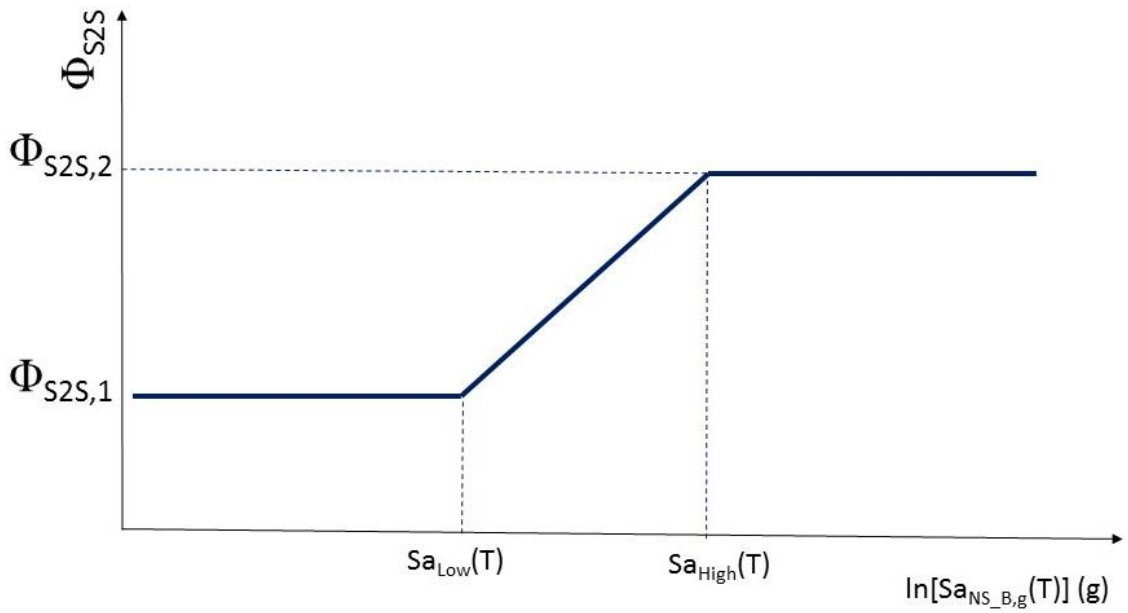

Figure 6.3. Schematic illustration of the site-to-site variability model. The values on the *x*-axis is the spectral acceleration at the NS_B, expressed in units of *g*, or the PGV value in cm/s. In either case, the value is obtained by application of Eqs.(6.1) to (6.4)

The four parameters defining the site-to-site variability model for Sa(T) at all 23 periods and also for PGV in each of the 160 site amplification zones are listed in the file **gmpeSurfaceAmplificationModel_20170826_v5.csv**.

Period-to-Period Correlation of Residuals of Sa(T)

For the risk calculations, values of Sa(T) calculated at a given location for different periods, T, must account for the period-to-period correlations of the residuals. The correlation coefficients, to be applied to all components of variability, for Sa(T) at all 23 periods are exactly the same as those used in the V4 model and these are provided in the CSV file: **gmpe_period2period_correlations_20170824_v5.csv**. The content of this file is identical to the file provided with the V4 model (**gmpe_period2period_correlations_20170131_v4.csv**) but a new file has been created to create a consistent suite of input files for the V5 model.

For convenience, an additional file (**gmpe_im2im_correlations_20170901_v5.csv**) has been provided that includes the full correlation matrix for both spectral ordinates and durations (as discussed in Section 6.2).

Duration Model

The model for the prediction of durations has the same functional form as the V4 model, only the magnitudes at which the breaks in scaling occur and the actual coefficients having been changed. As before, the model has four branches that should each be used in conjunction with the corresponding median branch on the predictions for Sa(T) and PGV. The median predictions of the duration, $D_{S5\text{-}75}$ (significant duration based on the accumulation from 5% to 75% of the total Arias intensity), is comprised of a source component and a path component to obtain the NS_B motions, plus a site component that transforms the rock motions to the ground surface:

$$\ln(D_{S5-75}) = f_{source}(M) + f_{path}(R,M) + f_{site}(V_{S30}) \qquad (6.12)$$

The source function is defined as:

$$f_{source} = m_6 + m_7(\max[M,3.25] - 5.25) \qquad M \le 5.25 \qquad (6.13a)$$

$$f_{source} = m_6 + m_8(M - 5.25) + m_9(M - 5.25)^2 \qquad M > 5.25 \qquad (6.13b)$$

The path function is dependent on both distance and magnitude:

$$f_{path} = (r_6 + r_7 M')\left[\ln\left(\frac{R}{3}\right)\right]^{r_8} \qquad R \le 12 \qquad (6.14a)$$

$$f_{path} = (r_6 + r_7 M')\left[\ln\left(\frac{12}{3}\right)\right]^{r_8} + (r_9 + r_{10} M')\ln\left(\frac{R}{12}\right) \qquad R > 12 \qquad (6.14b)$$

where, $$M' = \min[\max(M, 3.25), 6.0] \quad (6.14c)$$

The site term is very simple:

$$f_{site}(V_{S30}) = -0.2246 \ln\left(\frac{\min(V_{S30}, 600)}{600}\right) \quad (6.15)$$

The duration model requires V_{S30} as an input parameter. The median V_{S30} value for each of the 160 site amplifications zones is listed in the supplementary electronic file **gmpeSurfaceZonationVs30_20170826_v5.csv** (which contains exactly the same information as **gmpeSurfaceZonationVs30_20170131_v4.csv**). A map showing these median V_{S30} values is presented in Figure 6.4. Since the largest value of V_{S30} for any zone is 270 m/s, the logarithmic term in Eq.(6.15) will always be the ratio $V_{S30}/600$.

The coefficients of Eqs.(6.13) and (6.14) are all listed, for all four branches, in the file **gmpeDuration_20170903_v5.csv**. The total variability in the duration predictions is given by the sigma values in Table 6.2; the component-to-component variability for the duration is given by:

$$\sigma^2_{c2c} = 0.0299 + 2.434[5.6 - \min(5.6, \max[M, 3.6])]R^{-1.95} \quad (6.16)$$

this variability is sampled conditioned on the residual of the amplitude-based parameter, using the correlation coefficients in Table 6.3. The sigma values are also provided in the file **gmpeDuration_20170903_v5.csv** and the correlation coefficients are provided in the additional supplementary electronic file **gmpeDuration_Sa_Correlations_20170826_v5.csv** (which contains the same values as **gmpeDuration_Sa_Correlations_20170131_v4.csv**). The four duration branches are to be implemented in combination individually with the corresponding median branch for spectral accelerations and PGV.

Table 6.2. Sigma components for $\ln(D_{S5\text{-}75})$

Branch	1	2	3	4
Model	Lower	Central-lower	Central-upper	Upper
τ**[ln($D_{S5\text{-}75}$)]**	0.3937	0.3961	0.3922	0.3935
ϕ**[ln($D_{S5\text{-}75}$)]**	0.5400	0.5401	0.5398	0.5399

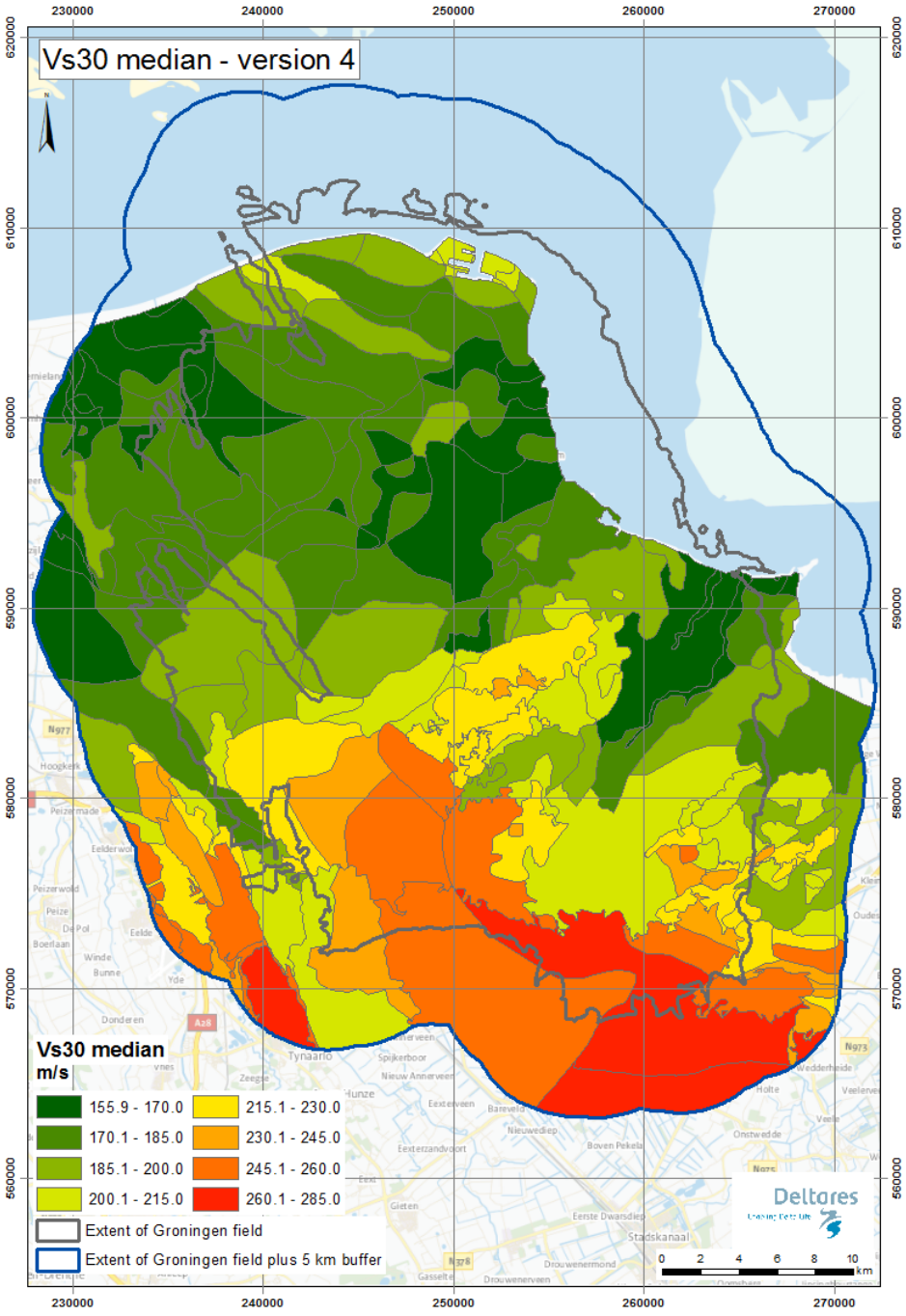

Figure 6.4. Median V_{S30} values of each zone

Table 6.3. Correlation coefficients for the residuals of duration and Sa(T) or PGV (applicable for both between event and within event correlations)

T [s]	**0.01**	**0.025**	**0.05**	**0.075**	**0.1**	**0.125**	**0.15**	**0.175**	**0.2**	**0.25**	**0.3**	**0.4**
ρ	-0.45	-0.45	-0.45	-0.45	-0.39	-0.39	-0.39	-0.39	-0.39	-0.39	-0.39	-0.33
T [s]	**0.5**	**0.6**	**0.7**	**0.85**	**1**	**1.5**	**2**	**2.5**	**3**	**4**	**5**	**PGV**
ρ	-0.28	-0.24	-0.21	-0.17	-0.13	-0.05	-0.01	0.02	0.05	0.09	0.12	-0.26

Summary List of Electronic Supplements

1. gmpe_medians_NS_B_20170724_v5.csv
2. gmpe_sigmas_NS_B_20170831_v5.csv
3. gmpeSurfaceZonation_20170824_v5.csv
4. gmpeSurfaceAmplificationModel_20170826_v5.csv
5. gmpe_period2period_correlations_20170824_v5.csv
6. gmpeDuration_20170903_v5.csv
7. gmpeSurfaceZonationVs30_20170826_v5.csv
8. gmpeDuration_Sa_Correlations_20170826_v5.csv
9. gmpe_im2im_correlations_20170901_v5.csv

These files are all contained in the folder “V5 GMM electronic supplements”, which is made available as a zipped file of the same name.

6.2. Sampling of variance components

The ground-motion model (GMM) developed for induced seismicity in the Groningen gas field predicts spectral accelerations (SA) at 23 response periods (T), peak ground velocity (PGV) and significant duration (D) at the ground surface as a function of local magnitude (M), rupture distance (R) and site classification. For all intensity measures the motion is first predicted at a bedrock horizon (NS_B) and then amplification factors (AF) are applied to these rock amplitudes to obtain the surface motions. While field-specific probabilistic AFs (functions defining the distribution of amplification) are developed for SA and PGV, in the case of significant duration a global deterministic V_{S30}-dependent AF is adopted and applied throughout the field. The AFs are defined for PGV and for SA at each period and for each of the 160 zones defined over the field. Values of duration are predicted using a unique value of V_{S30} for each of the zones. Note that SA for an oscillator period of 0.01 s is assumed equivalent to peak ground acceleration (PGA).

The prediction of the median values of SA, PGV and D is relatively straightforward, simply applying the relevant values of M and R for each earthquake-site combination, and then applying the relevant AF or V_{S30} depending on the zone within which the site is located. However, the models predict distributions of values rather than unique estimates of SA, PGV and D. In all cases, the intensity measures (SA, PGV and D) are log-normally distributed and their joint distribution is assumed to be multivariate log-normal. For both model development and sampling it is convenient to work with the log-transformed intensity measures such that variation about the median motion for a given scenario is defined by a symmetric normal distribution (or multivariate normal). The scale of the variation in this transformed space is defined by a standard deviation. The total standard deviation in ground-motion prediction models is usually represented by the symbol sigma (σ) and the total residuals are

then defined by the product of σ and epsilon (ε) the number of standard deviations sampled (and a standard normal variate).

The purpose of this document is to define the procedures for sampling the aleatory variability in the prediction of the ground-motion parameters. The hazard and risk model for the Groningen field uses Monte Carlo simulations and therefore the focus is on the random sampling of ε values in each ground-motion realisation. The process is schematically illustrated in Figure 6.5, which depicts the estimation of SA for a single value of T at three locations (over two zones) as a result of a single earthquake. In practice, however, the implementation is somewhat more complicated because the sampling of variance components must also respect correlations between parameters and spatial correlation as well. The first section of the document defines the different components of variability and then the issue of spatial correlation is discussed. After that, the sampling is discussed for different applications of increasing complexity with regards to the variability.

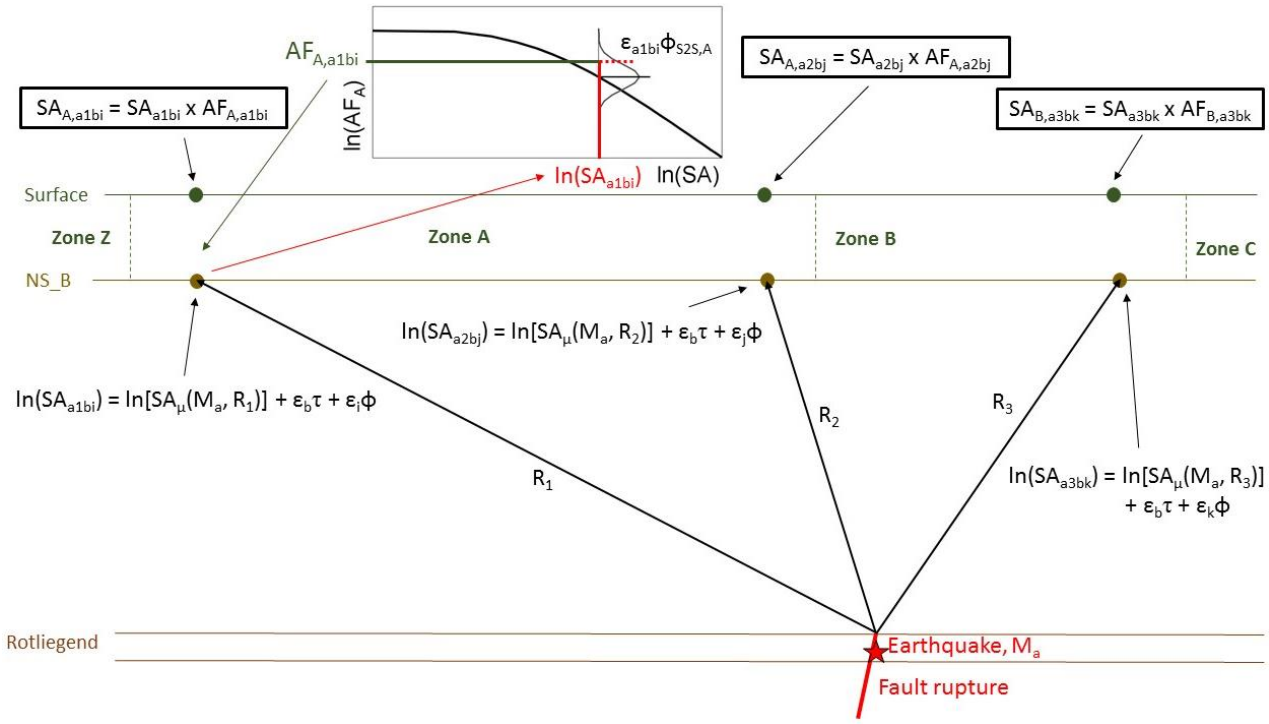

Figure 6.5. Schematic illustration of the calculation of SA at three surface points, in two zones, for an earthquake of magnitude M_a and an event-term of $\varepsilon_b\tau$; in this simple example, the within-event variability is sampled without considering spatial correlation (Bommer *et al*., 2017c).

Components of Variability in the Groningen GMM

The components of variability defined in the Groningen GMM are listed in Table 6.4, indicating also which ground-motion parameters they are related to and where they

are applied both in terms of a reference horizon and in the calculation of hazard or risk.

Table 6.4. Elements of ground-motion variability in the Groningen GMM

Symbol	Description	GM Parameter[1]	Horizon[2]	H or R[3]	Epsilon[4]
σ_{GM}	Standard deviation of geometric mean of ground-motion parameters	SA(T), PGV	NS_B	Hazard	ε_{GM}
σ_{arb}	Standard deviation of arbitrary component of ground-motion parameters	SA(T), PGV, D	NS_B	Risk[5]	ε_{arb}
τ	Between-event variability of ground-motion parameters	SA(T), PGV, D	NS_B	H & R[5]	ε_E
ϕ_{ss}	Within-event non-ergodic variability of amplitude-based parameters	SA(T), PGV, D	NS_B	H & R[5]	ε_S
σ_{c2c}	Component-to-component variability of spectral accelerations	SA(T), D	NS_B	Risk	ε_c
ϕ_{S2S}	Site-to-site variability associated with AFs	SA(T)	Surface	H & R	ε_Z

Notes: 1 – The ground-motion parameters to which it applies; 2 – Reference elevation at which applied; 3 – Whether used in hazard or risk calculations; 4 – Symbol for normalised residual used to sample distribution; 5 – PGV is not currently employed in probabilistic risk calculations, while D is not employed in hazard calculations.

The total variability on the geometric mean ground-motion amplitudes is given by:

$$\sigma_{GM} = \sqrt{\tau^2 + \phi_{SS}^2 + \phi_{S2S}^2} \qquad (6.17)$$

whereas the total variability of the arbitrary component of motion is given by:

$$\sigma_{arb} = \sqrt{\tau^2 + \phi_{SS}^2 + \phi_{S2S}^2 + \sigma_{c2c}^2} \qquad (6.18)$$

The total variability on the duration is conceptually also decomposed into these different elements, but because the amplification effects are treated as being known and deterministic $\phi_{S2S} \equiv 0$ and $\phi = \phi_{SS}$, noting that normally $\phi^2 \equiv \phi_{SS}^2 + \phi_{S2S}^2$.

There are two correlation functions defined for ground-motion residuals as well, and their characteristics are summarised in Table 6.5. Both of these correlation models are used to construct the full correlation matrix that is required for the sampling process within the risk calculations.

Table 6.5. Correlations of residuals in the Groningen GMM

Symbol	Description	GM Parameter[1]	Horizon[2]
ρ_{T2T}	Period-to-period correlation of spectral accelerations	SA at multiple T	NS_B
ρ_{SA-D}	Correlations of spectral acceleration and duration	SA(T) and D	NS_B

Notes: 1 – The ground-motion parameters to which it applies; 2 – Reference elevation at which employed.

Spatial Correlation of Ground Motions

Another correlation of ground-motion residuals is that which occurs spatially since observations from dense recording networks have revealed that epsilon values at closely-spaced locations tend to be correlated rather than being entirely random.

For the calculation of Group Risk or any other aggregate measure of the seismic risk, the spatial correlation of ground motions is important since it leads to pockets of higher-than-average and lower-than-average ground motions rather than simply random spatial variation of the amplitudes. The coincidence of a pocket of higher-than-average ground motions with a group of seismically vulnerable structures will result in higher estimates of Group Risk than when spatial correlation of the ground motions is ignored. Although the primary focus of the risk modelling is Individual Local Personal Risk (ILPR, which is a location-specific measure), Group Risk estimates may be needed and for this reason, spatial correlation does need to be considered.

A Groningen-specific model for spatial correlation of ground motions has not yet been derived (see Chapter 7). For the current (V5) risk modelling purposes, it is proposed to approximate the spatial correlation not with a function that varies continuously with the distance separating two points but with a simpler model that assumes perfect correlation within each of the 160 site amplification zones (although in practice the NS_B motions, the AFs and σ_{c2c} all depend on M and R, and the value of R will vary for different grid points within a zone, hence the while the correlation is perfect, the actual ground-motion amplitudes over the zone will vary spatially.) and no within-event correlation between one zone and another. Once the field-specific model is ready, the degree to which this approximation mimics the real spatial correlation will be explored, but for the current phase of risk modelling it is proposed to constrain the sampling of variability elements such as to approximate spatial correlation in the simplified manner indicated above. However, there is no requirement to invoke spatial correlation in the hazard calculations.

Sampling Variability in Hazard Calculations for PGV and SA(T)

When hazard maps are generated in terms of these 24 parameters, they are treated completely independently. The uniform hazard response spectra (UHRS) at specified location are obtained from individual hazard curves for SA at the 23 response periods. The hazard is calculated at grid points defined across the field, usually with several grid points located within each site response zone.

The sequence of sampling of variability to be followed in generating the hazard estimates is therefore as follows:

1. For each earthquake and GM parameter, a value of ε_E is randomly sampled.
2. For each grid point, the NS_B motion is calculated randomly sampling ε_S; this means that spatial correlation is ignored at the reference rock horizon.
3. For each grid point, the median surface motion is estimated by applying the AF value conditioned on the realisation of the NS_B motion (including the two components of variability sampled in steps #1 and #2).
4. The final surface motion at each location is then calculated by randomly sampling ε_Z; here again, spatial correlation is ignored and the site-to-site variability is therefore interpreted as being due to spatial variability of the soil profiles and dynamic soil properties within the zone.

Sampling Variability in Ground-motion Values for Risk Calculations

When ground-motions at the surface are predicted for the purpose of providing inputs to risk calculations, a number of differences arise when compared to the same predictions within the hazard calculations. One of these is that the component-to-component variability needs to be added in order to obtain estimates of the arbitrary component of motion rather than the geometric mean. Secondly, spatial correlation needs to be approximated as was described earlier. And finally, since the risk calculations are made for several structural typologies at a given location—which have different vibration periods and some of which have different vibration periods along their two axes—the period-to-period correlations of the spectral accelerations also need to be sampled. Similarly, as fragility curves for some typologies utilise both spectral amplitude and duration, the correlation between these intensity measures must also be taken in to account. The sampling sequence now becomes as follows:

1. For each earthquake, the covariance matrix for between-event residuals is sampled in order to obtain a vector $\boldsymbol{\varepsilon}_E$ that contains between-event residuals for all 23 spectral ordinates as well as duration. This can be expressed mathematically as $\boldsymbol{\varepsilon}_E = [\varepsilon_E(T_1) \quad \cdots \quad \varepsilon_E(T_{23}) \quad \varepsilon_E(D)]^T$. The correlation matrix can be defined as:

$$\boldsymbol{\rho} = \begin{bmatrix} \boldsymbol{\rho}_{Sa(\boldsymbol{T}),Sa(\boldsymbol{T})} & \boldsymbol{\rho}_{Sa(\boldsymbol{T}),D} \\ \boldsymbol{\rho}_{D,Sa(\boldsymbol{T})} & \rho_{D,D} \end{bmatrix} = \begin{bmatrix} \rho_{Sa(T_1),Sa(T_1)} & \rho_{Sa(T_1),Sa(T_2)} & \cdots & \rho_{Sa(T_1),D} \\ \rho_{Sa(T_2),Sa(T_1)} & \rho_{Sa(T_2),Sa(T_2)} & \cdots & \rho_{Sa(T_2),D} \\ \vdots & & \ddots & \vdots \\ \rho_{D,Sa(T_1)} & \rho_{D,Sa(T_2)} & \cdots & \rho_{D,D} \end{bmatrix} \quad (6.19)$$

2. For each zone, the NS_B motion for the arbitrary component needs to reflect both the variability suggested by ϕ_{SS} as well as the component-to-component variability associated with σ_{c2c}. Rather than sample separate sets of epsilon values for each of these components individually, a vector of epsilon values $\boldsymbol{\varepsilon}_A = [\varepsilon_A(T_1) \quad \cdots \quad \varepsilon_A(T_{23}) \quad \varepsilon_A(D)]^T$ is generated. For each ground-motion measure, the residual of the arbitrary component is given by $\varepsilon_A\sqrt{\phi_{SS}^2 + \sigma_{c2c}^2} \equiv \varepsilon_S\phi_{SS} + \varepsilon_c\sigma_{c2c}$. That is, the covariance matrix from which $\boldsymbol{\varepsilon}_A$ is sampled has diagonal elements that are defined by $\phi_{SS}^2 + \sigma_{c2c}^2$ (for all spectral ordinates and for duration). The off-diagonal elements of the covariance matrix make use of the same correlation matrix elements as used for the sampling of the between-event residuals. The sampled values of $\boldsymbol{\varepsilon}_A$ are used at all grid points within a zone to approximate spatial correlation.
3. For each grid point, the median surface motion is estimated by applying the AF value conditioned on the realisation of the NS_B motion (including the two components of variability $\boldsymbol{\varepsilon}_E$ and $\boldsymbol{\varepsilon}_A$ sampled in steps #1 and #2). Note that for the duration there is no conditioning and the AF for each zone depends purely upon the V_{S30} value for the zone.
4. The final surface motion at each location is then calculated by randomly sampling ε_Z; for a given period, the same value of ε_Z should be invoked at every grid point within a zone in order to represent spatial correlation.

7. CONCLUSIONS and FUTURE DEVELOPMENTS

The V5 model is the product of work conducted over many months and the outcome of several cycles of iteration and critical review. The model meets all of the objectives defined for ground-motion prediction in the Groningen field in terms of reflecting local source, path and site conditions, and also capturing the epistemic uncertainty associated with extrapolation from recordings of small-magnitude induced earthquakes to the estimation of ground motions generated by larger triggered earthquakes. The model also meets all of the requirements for hazard and risk modelling in terms of the predicted ground-motion parameters.

In this closing chapter, some features of the GMM—including the assumption of linear site response for the existing records—are briefly discussed and potential future developments are outlined.

Non-Linear Site Response in Current Database?

The basic framework for developing the Groningen GMMs, from V2 to V5, has involved removing linear site amplification from the recorded motions to transform the motions to the NS_B rock horizon, and then transferring predicted NS_B motions from larger earthquakes to ground surface using non-linear AFs (Figure 2.8). The assumption that the records in the Groningen database have only been affected by linear site amplification is reasonable considering that most of the earthquakes recorded in the field are smaller than M_L 3.2, and the largest earthquake is only M_L 3.6 (Figure 2.2). There are no direct means to verify that this assumption holds. However, this assumption seems to be corroborated by the comparison of site amplification functions obtained from the inversion of the seismological model with the linear surface-to-NS_B transfer functions (see Figures 5.16 and 5.17 in the V4 GMM report, Bommer *at al.,* 2017b).

In this section we explore this assumption using the V5 GMM zone amplification factors (AFs). Figure 7.1 plots the ratio of the zone AFs using the full model (see Section 4.2) and the AFs using only the linear portion of this model [*e.g.*, only f_1^*, see Eq.(4.2) in Section 4.2]. For each station, the AFs are computed for the magnitude-distance combinations that correspond to the recorded motions at these stations. Observe that the assumption of linearity holds for periods greater than about 0.2 seconds. For a period of 0.01 seconds, the largest deviation from linearity is for Station BMD1 for the M_L 3.6 Huizinge earthquake. The station is at a distance of only 3.59 km. In this case, the non-linear AF are 11% smaller than the linear factors. The largest deviations from the linear assumption occur at a period of 0.05 seconds. The largest deviation occurs also for the BMD1 Huizinge recording (the non-linear AF is 30% lower than the linear AF).

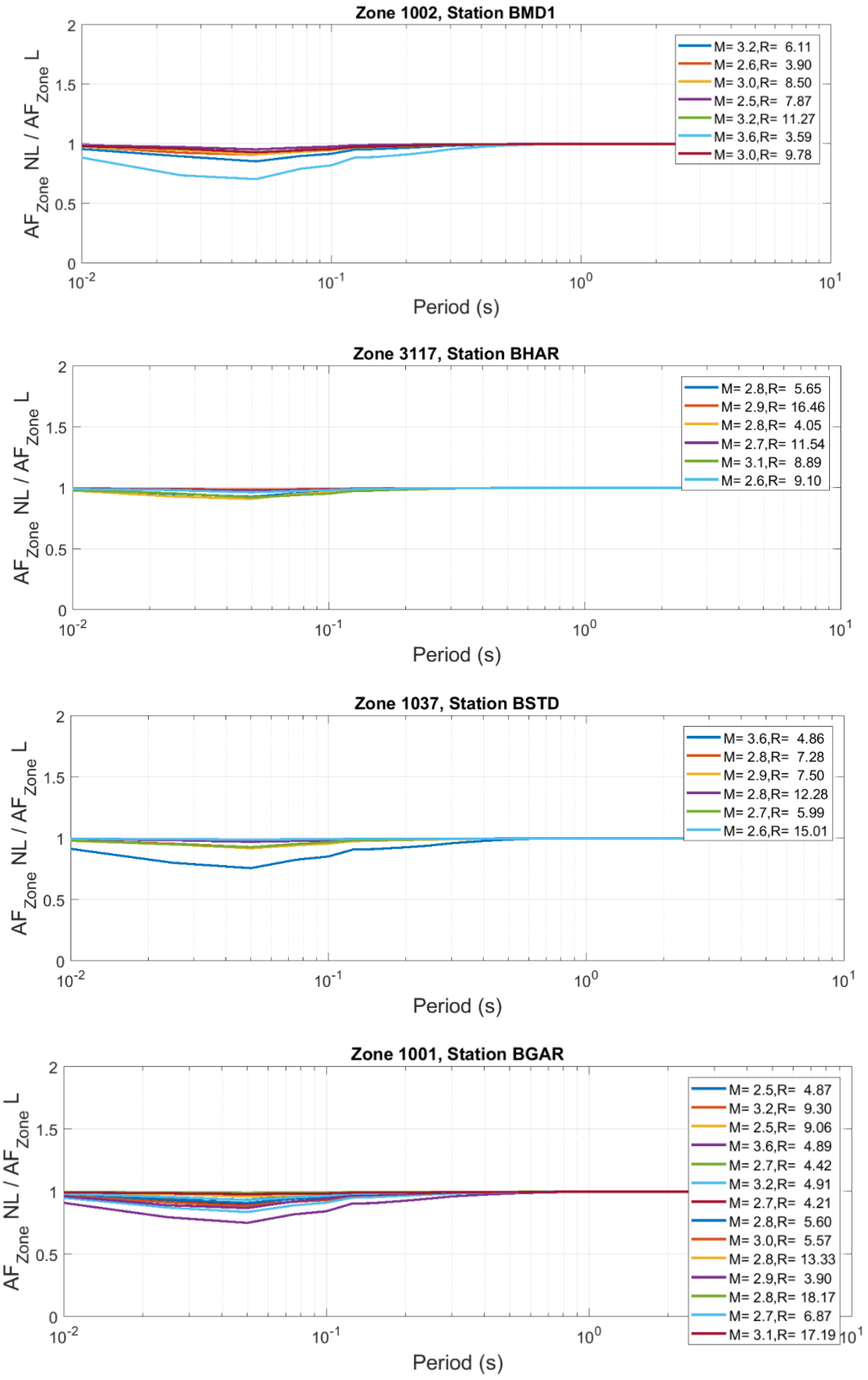

Figure 7.1. Ratios of nonlinear AFs (AF_{Zone} NL) to linear AFs (AF_{Zone} L) for selected stations. The AFs are computed using the Zone AF model. Spectral accelerations at the NS_B boundary are computed from the V5 GMM using the Central-upper branch.

The zone AFs are largely consistent with the assumption of linearity. The inversions that are conducted to develop the NS_B model use the full bandwidth of the recordings, hence the possible deviations from linearity at high frequencies (0.02 s ≤ T ≤ 0.075 s) should not affect the model greatly, other than possibly a slight over-estimation of kappa at the NS_B interface. However, only the recordings for the strongest earthquakes could lead to deviations from non-linearity. Since all the records are used in the inversion (Figure 2.2), it is unlikely that the value of kappa is affected too strongly. Equally, the stress parameter estimates may also have been affected by underestimation of the NS_B motions at a few short periods for a few of the records. However, since the stress parameters are estimated from inversion of all of the records using the full range of frequencies, the effect would not be large. The logic-tree structure, as discussed below, already allows for greater stress parameter values in the magnitude range of the field database.

Another effect of the deviation from non-linearity is that there may be an under-estimation of motions for the short periods where these deviations are observed. However, at these periods the site-to-site variability values have increased significantly from previous versions of the model (see Figures 4.12 and 4.15 in Section 4.3). Moreover, these periods are not of high relevance to the current risk model (see Figure 2.9).

The alternative approach of accounting for potential non-linear behaviour in the site response for the small-magnitude earthquakes recorded at the stations would necessitate an iterative approach for the development of the model. This approach would require multiple repetitions of the full suite of site response analyses and consequently would be computationally very costly. Considering that the small deviations from non-linearity are unlikely to have a large effect on the risk model and since uncertainty in the GMM logic-tree extends to the small-magnitude range of the data, the decision was made to maintain the framework assuming linear AFs for the existing database and to accept the potential bias in the model derivation.

Stability of the GMM and the NEN-NPR

The V5 GMM is the outcome of an iterative development process that has involved incremental evolution at each stage. In many regards the model has been stable since V2 or V3, when the basic framework of predicting motions at a buried rock horizon to be combined with non-linear AFs was established. Although it is difficult to compare the V3 and V5 models because of their use of different distance metrics, the model has been stable in several respects apart from the apparent fluctuations related to the use of an **M**-M_L relationship in the V4 model derivation that is now understood to be inappropriate to the Groningen region. The current model is considered to be stable and has sufficient uncertainty bounds to be used with confidence for the foreseeable future. As has been noted previously, the uncertainty range increases with earthquake magnitude but is non-trivial even in the small magnitude range (Figure 7.2). The lower and higher branches in the magnitude

range of the existing data cover such features as the reduction due to addition a new, low-stress parameter event, on the one hand, and the potential minor underestimation of the stress parameters due to the assumption of fully linear site response for all records in the existing database, on the other.

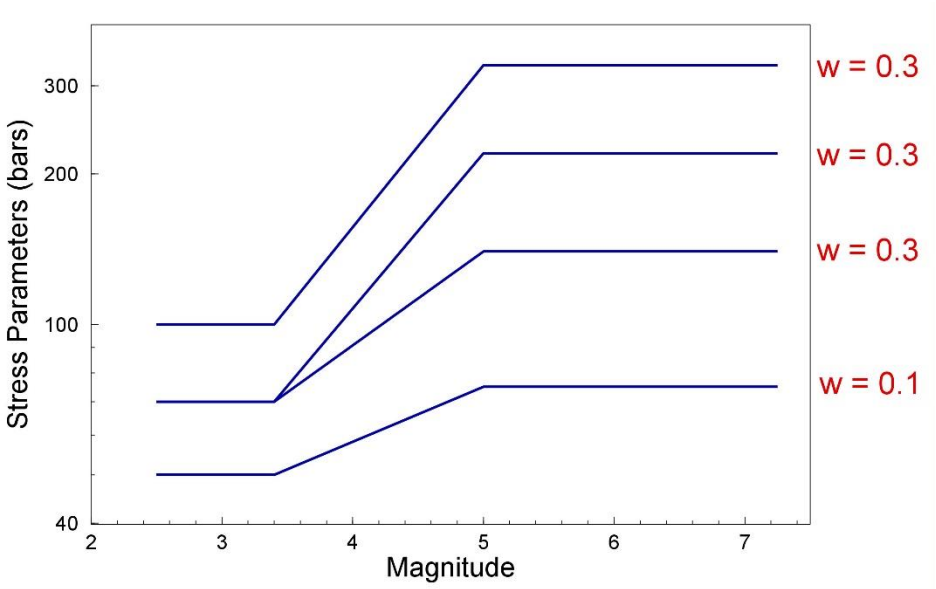

Figure 7.2. Stress parameters and associated weights underlying the V5 GMM logic-tree; note the range of uncertainty even in the magnitude interval covered by the data

Since the 2016 Winningsplan was based on the V2 model (see Figure 2.1), the V3 and V4 models would have no real significance other than staging posts in the model development, which while time-consuming in terms of documentation did facilitate review and feedback. However, the V4 GMM has acquired additional relevance because it was used in the recent update of the NEN-NPR building code for the Groningen region. This is one more consequence of the imposed schedule for responses to the Groningen earthquakes. However, it is now clear that the current version of the NEN-NPR code is based on a conservative ground-motion model, which is consistent with the purpose and objective of codes for earthquake-resistant design of buildings.

Spatial Correlation of Groningen Ground-Motions

The primary metric used to quantify seismic risk in the Groningen field is local personal risk (LPR), which is specific to individual buildings or locations. However, other metrics are also considered, including Group Risk (GR) that is an aggregate measure over the complete exposure database. The calculation of GR is sensitive to spatial correlation of the ground motions, for which reason the instructions for implementation of the GMM presented in Section 6.2 are aimed at ensuring an approximation to a realistic spatial correlation model. Work planned in the coming weeks will derive a Groningen-specific spatial correlation model, which will then be

compared to the implied distribution of spatial correlation lengths from the implementation of the variability sampling instructions within the framework of site amplification factors on non-uniform size. The expectation is that the comparison will confirm the current approximation as an acceptable and conservative approximation.

The data that will be used to derive the spatial correlation model will be partly obtained from the flexible network that is gathering closely-spaced recordings from dense arrays of geophones (Figure 7.3). These data will be added to the recordings from the three permanent accelerograph networks now operating in the region: the KNMI permanent surface accelerographs (B-stations), the KNMI operated borehole arrays of geophone plus surface accelerographs (G-stations), and the TNO-operated network of accelerographs in houses and public buildings (Figure 7.4). Records from instruments at the NAM facilities in the field may also be added to the dataset.

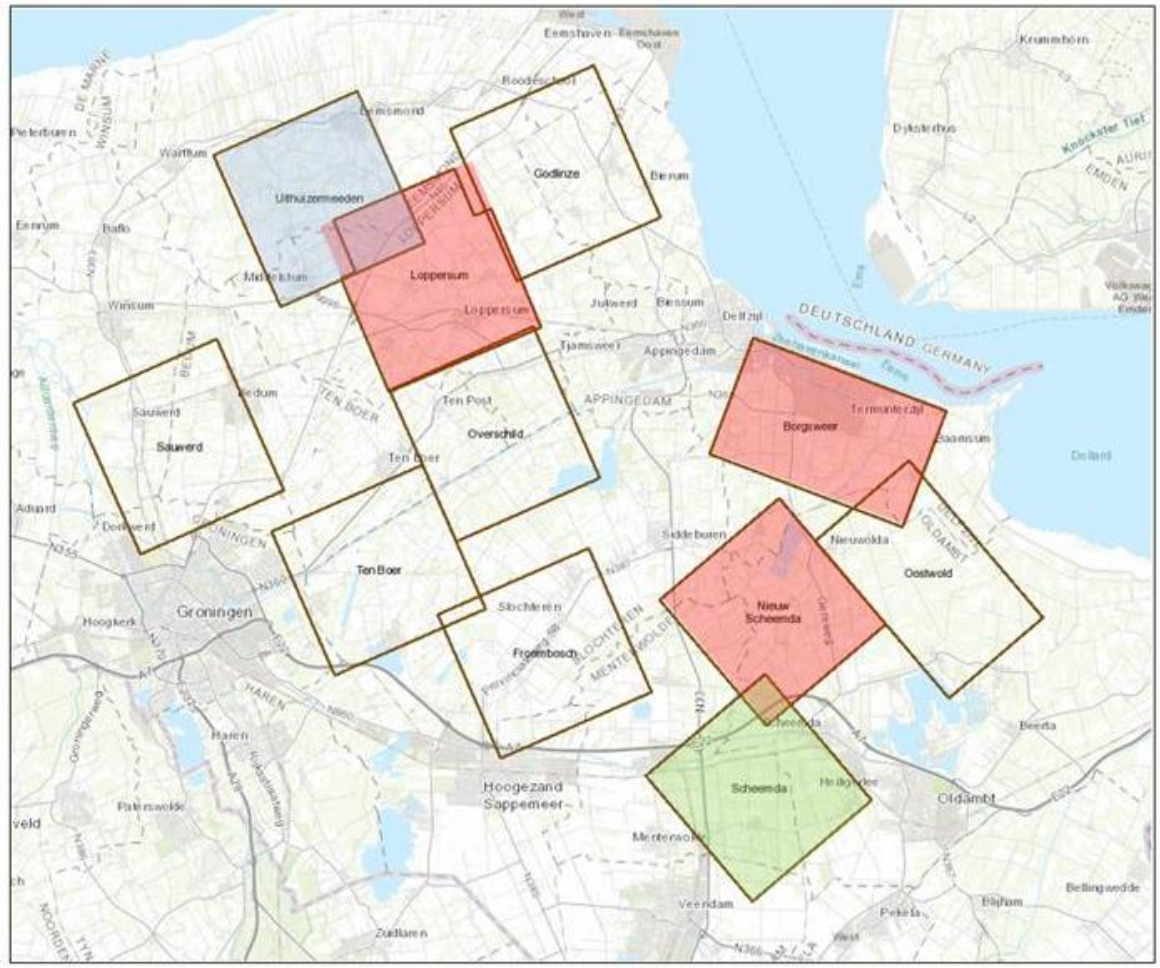

Figure 7.3. Deployment areas (“patches”) for the NAM flexible network of 400 geophones, where the instruments are installed for periods of about 6 weeks. The red areas have already been covered, the green was the most recent area of installation and the blue the next location to be targeted. The blank areas are planned deployment areas; the deployment has since progressed. (*Courtesy of Remco Romijn, NAM*).

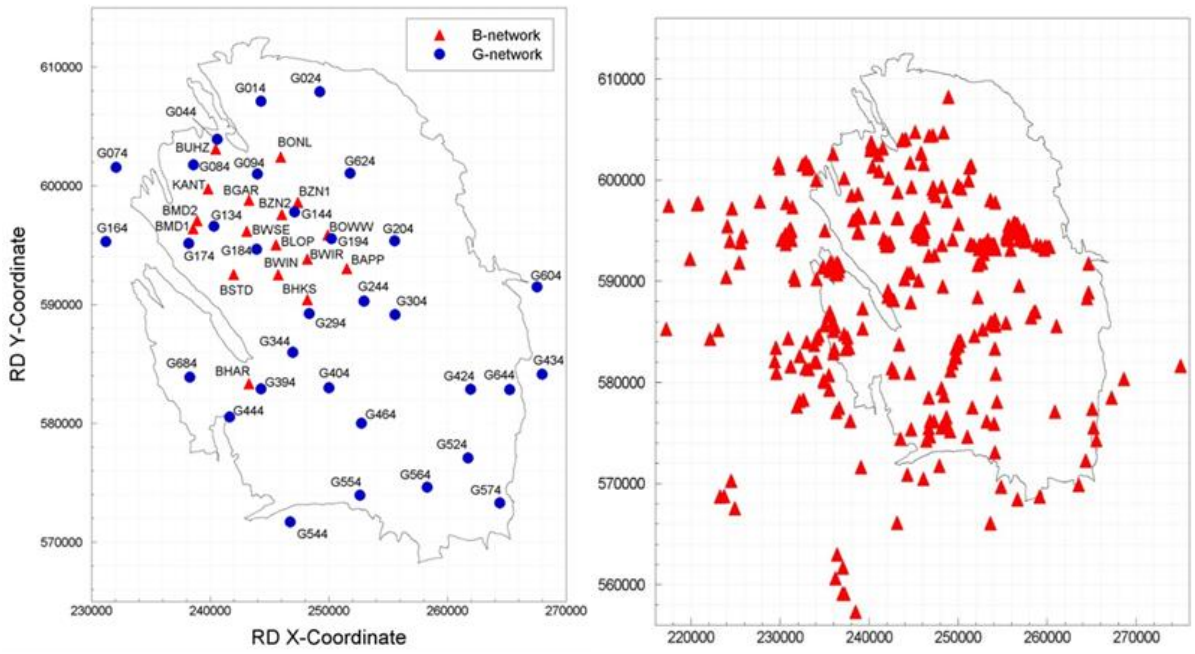

Figure 7.4. Accelerograph networks in Groningen: *Left*: B-station and G-station operated by KNMI; *Right*: TNO-operated instruments in houses and public buildings

Regarding the TNO network, to date these recordings have not been used in the model derivation because of concerns regarding the installation of many of the accelerographs above floor level (Figure 7.5.). In order to investigate the degree to which the structural response of these buildings may have influenced the recordings—and therefore the degree to which they can be used as representations of the actual ground motion—experiments have been conducted. In full-scale shaking table tests on a model of a Groningen house conducted at LNEC in Lisbon, the installation of TNO instruments on wall brackets was reproduced together with a second instrument correctly installed at the base of the building (Figure 7.6). Recordings obtained from these instruments are now being processed and will be analysed over the coming weeks to ascertain whether recordings from instruments such as those depicted in Figure 7.5 can be used for the derivation of the spatial correlation model.

Future Updates of the Groningen GMM

While it has been necessary to develop the GMM for Groningen through a series of short and intense iterations, with each development stage lasting about 7 months on average, there is no intention to produce a V6 model on a similar schedule. Having now reached a mature stage of model development, it is expected that the V5 model will be used for the coming period and any revision will be undertaken on a less rushed timetable. As new data becomes available—in the form of recordings from new earthquakes or improved characterisation of the shallow or deep sub-surface—sensitivity analyses will first be performed to gauge the likely impact on the model.

Figure 7.5. Examples of TNO instruments installed above ground level

Figure 7.6. Reproduction of the TNO installation of accelerographs at ground level and at a higher level on a full-scale model subjected to shake table testing at LNEC

8. References

Abercrombie, R.E. (1995). Earthquake source scaling relationships from -1 to 5 M_L using seismograms recorded at 2.5 km depth. *Journal of Geophysical Research* **100**, 24015-24036.

Abrahamson, N.A. & R.R. Youngs (1992). A stable algorithm for regression-analyses using the random effects model. *Bulletin of the Seismological Society of America* **82**, 505-510.

Afshari, K. & J.P. Stewart (2016). Physically parameterized prediction equations for significant duration in active crustal regions. *Earthquake Spectra* **32**(4), 2057-2081.

Akkar, S., M.A. Sandıkkaya & J.J. Bommer (2014). Empirical ground-motion models for point- and extended-source crustal earthquake scenarios in Europe and the Middle East. *Bulletin of Earthquake Engineering* **12**(1), 359-387. *Erratum*: **12**(1), 389-390.

Anderson, J.G. & S.E. Hough (1984). A model for the shape of the Fourier amplitude spectrum of acceleration at high frequencies. *Bulletin of the Seismological Society of America* **74**, 1969-1993.

Atkinson, G.M., J.J. Bommer & N.A. Abrahamson (2014). Alternative approaches to modeling epistemic uncertainty in ground motion in probabilistic seismic-hazard analysis. *Seismological Research Letters* **85**(6), 1141-1144.

Bindi, D., M. Massa, L. Luzi, G. Ameri, E. Pacor, R. Puglia & P. Augliera (2014). Pan-European ground-motion prediction equations for the average horizontal component of PGA, PGV, and 5%-damped PSA at spectral periods up to 3.0 s using the RESORCE dataset. *Bulletin of Earthquake Engineering* **12**(1), 391-430.

Bommer, J.J., H. Crowley & R. Pinho (2015a). A risk-mitigation approach to the management of induced seismicity. *Journal of Seismology* **19**(2), 623-464.

Bommer, J.J., B. Dost, B. Edwards, P.P. Kruiver, P. Meijers, M. Ntinalexis, B. Polidoro, A. Rodriguez-Marek & P.J. Stafford (2015c*). Development of Version 2 GMPEs for response spectral accelerations and significant durations from induced earthquakes in the Groningen field*. Version 2, 29 October 2016, 515 pp.

Bommer, J.J., B. Dost, B. Edwards, P.J. Stafford, J. van Elk, D. Doornhof & M. Ntinalexis (2016a). Developing an application-specific ground-motion model for induced seismicity. *Bulletin of the Seismological Society of America* **106**(1), 158-173.

Bommer, J.J., B. Dost, B. Edwards, P.P. Kruiver, P. Meijer, M. Ntinalexis, A. Rodriguez-Marek & P.J. Stafford (2016b). *Development of V3 GMPEs for response spectral accelerations and significant durations from induced earthquakes in the Groningen field*. Version 0, 8 July 2016, 476 pp.

Bommer, J.J., B. Dost, B. Edwards, P.P. Kruiver, P. Meijer, M. Ntinalexis, A. Rodriguez-Marek, E. Ruigrok, J. Spetzler & P.J. Stafford (2017b). *V4 Ground-Motion Model (GMM) for Response Spectral Accelerations, Peak Ground Velocity, and Significant Durations in the Groningen Field*. Version 2.1, 23 June 2017, 541 pp.

Bommer, J.J., B. Dost, B. Edwards, P.P Kruiver, M. Ntinalexis, A. Rodriguez-Marek, P.J Stafford & J. van Elk (2017c). Developing a model for the prediction of ground motions due to earthquakes in the Groningen gas field. *Netherlands Journal of Geoscience*, *in press.*

Bommer, J.J., P.J. Stafford & J.E. Alarcón (2009). Empirical equations for the prediction of the significant, bracketed and uniform duration of earthquake ground motion. *Bulletin of the Seismological Society of America* **99**(6), 3217-3233.

Bommer, J.J., P.J. Stafford, B. Edwards, B. Dost & M. Ntinalexis (2015b). *Development of version 1 GMPEs for response spectral accelerations and for strong-motion durations*. Version 2, 21 June 2015, 304 pp.

Bommer, J.J., P.J. Stafford, B. Edwards, B. Dost, E. van Dedem, A. Rodriguez-Marek, P. Kruiver, J. van Elk, D. Doornhof & M. Ntinalexis (2017a). Framework for a ground-motion model for induced seismic hazard and risk analysis in the Groningen gas field, The Netherlands. *Earthquake Spectra* **33**(2), 481-498.

Bommer, J.J. & J. van Elk (2017). Comment on "The maximum possible and maximum expected earthquake magnitude for production-induced earthquakes at the gas field in Groningen, The Netherlands" by Gert Zöller and Matthias Holschneider. *Bulletin of the Seismological Society of America* **107**(3), 1564-1567.

Boore, D.M. (2005a). *SMSIM – Fortran programs for simulating ground motions from earthquakes: Version 2.3—A revision of OFR 96-80*. US Geological Survey Open-File Report 00-509, 55 pp.

Boore, D.M. (2005b). Erratum: Equations for estimating horizontal response spectra and peak acceleration from western north American earthquakes: A summary of recent work, by D.M. Boore, W.B. Joyner and T.E. Fumal. *Seismological Research Letters* **76**(3), 368-369.

Boore, D.M. (2009). Comparing stochastic point-source and finite-source ground-motion simulations: SMSIM and EXSIM. *Bulletin of the Seismological Society of America* **99**, 3202-3216.

Boore, D.M., J.P. Stewart, E. Seyhan & G.M. Atkinson (2014). NGA-West2 equations for predicting PGA, PGV, and 5% damped PSA for shallow crustal earthquakes. *Earthquake Spectra* **30**(3).

Boore, D.M. & E.M. Thompson (2014). Path durations for use in the stochastic-method simulations of ground motions. *Bulletin of the Seismological Society of America* **104**(5), 2541-2552.

Bourne, S.J., S.J. Oates, J. van Elk & D. Doornhof (2014). A seismological model for earthquakes induced by fluid extraction from a subsurface reservoir. *Journal of Geophysical Research Solid Earth* **119**, doi: 10.1002/201JB011663.

Bourne, S.J., S.J. Oates, J.J. Bommer, B. Dost, J. van Elk & D. Doornhof (2015). A Monte Carlo method for probabilistic hazard assessment of induced seismicity due to conventional natural gas production. *Bulletin of the Seismological Society of America* **105**(3), 1721-1738.

Brune, J.N. (1970). Tectonic stress and spectra of seismic shear waves from earthquakes. *Journal of Geophysical Research* **75**, 4997-5009.

Brune, J.N. (1971). Correction. *Journal of Geophysical Research* **76**, 5002.

Butcher, A., R. Luckett, J.P. Verdon, J.-M. Kendall, B. Baptie & J. Wookey (2017). Local magnitude discrepancies for near-event receivers: Implications for the U.K. traffic-light scheme. *Bulletin of the Seismological Society of America* **107** 532-541.

Campbell, K.W. & Y. Bozorgnia (2007). *Campbell-Bozorgnia NGA Ground Motion Relations for the Geometric Mean Horizontal Component of Peak and Spectral Ground Motion Parameters.* PEER Report 2007/02, Pacific Earthquake Engineering Research Center, University of California at Berkeley, 240 pp.

Campbell, K.W. & Y. Bozorgnia (2014). NGA-West2 ground motion model for the average horizontal components of PGA, PGV, and 5%-damped elastic pseudo-acceleration response spectra. *Earthquake Spectra* **30**(3), 1087-1115.

Chiou, B.S.J. & R.R. Youngs (2014). Update of the Chiou and Youngs NGA model for the average horizontal component of peak ground motion and response spectra. *Earthquake Spectra* **30**(3), 1117-1153.

Deichmann, N. (2006). Local magnitude, a moment revisited. *Bulletin of the Seismological Society of America* **96**, 1267-1277.

Deichmann, N. (2017). Theoretical basis for the observed break in M_L/M_W scaling between small and large earthquakes. *Bulletin of the Seismological Society of America* **107**, 505-520.

Dost, B., B. Edwards & J.J. Bommer (2017b). The relationship between M_w and M_L – a review and application to induced seismicity in Groningen, the Netherlands. *Submitted to Seismological Research Letters.*

Dost, B. & D. Kraaijpoel (2013). *The August 16, 2012 earthquake near Huizinge (Groningen)*. KNMI. http://www.knmi.nl/knmilibrary/miscellaneousreport.html

Dost, B., E. Ruigrok & J. Spetzler (2017a). Development of probabilistic seismic hazard assessment for the Groningen gas field. *Netherlands Journal of Geoscience*, *in press.*

Dost, B., T. van Eck & H. Haak (2004). Scaling of peak ground acceleration and peak ground velocity recorded in the Netherlands. *Bolletino di Geofisica Teorica ed Applicata* **45**(3), 153-168.

Edwards, B., B. Allmann, D. Fäh & J. Clinton (2010). Automatic computation of moment magnitudes for small earthquakes and the scaling of local to moment magnitude. *Geophysical Journal International* **183**, 407-420.

Edwards, B. & J. Douglas (2014). Magnitude scaling of induced earthquakes. *Geothermics* **52**, 132-139.

Edwards, B., T. Kraft, C. Cauzzi, P. Kästli & S. Wiemer (2015). Seismic monitoring and analysis of deep geothermal projects in St Gallen and Basel, Switzerland. *Geophysical Journal International* **201**, 1020-1037.

Grünthal, G., R. Wahlstrom & D. Stromeyer (2009). The unified catalogue of earthquakes in central, northern, and northwestern Europe (CENEC)-updated and expanded to the last millennium. *Journal of Seismology* **13**, 517-541.

Hanks, T. C. & D. M. Boore (1984). Moment-magnitude relations in theory and practice. *Journal of Geophysical Research* **89**, 6229-6235.

Kempton, J.J. & J.P. Stewart (2006). Prediction equations for significant duration of earthquake ground motions considering site and near-source effects. *Earthquake Spectra* **22**(4), 985-1013.

Kraaijpoel, D. & B. Dost (2013). Implications of salt-related propagation and mode conversion effects on the analysis of induced seismicity. *Journal of Seismology* **17**(1), 95-107.

Kruiver, P. P., E. van Dedem, E. Romijn, G. de Lange, M. Korff, J. Stafleu, J.L. Gunnink., A. Rodriguez-Marek, J.J. Bommer, JJ
. van Elk & D. Doornhof (2017). An integrated shear-wave velocity model for the Groningen gas field, The Netherlands. *Bulletin of Earthquake Engineering* **15**(9), 3555-3580.

Motazedian, D. & G.M. Aktinson (2005). Stochastic finite-fault modelling based on a dynamic corner frequency. *Bulletin of the Seismological Society of America* **95**, 995-1010.

Munafò, I., L. Malagnini & L. Chiaraluce (2016). On the relationship between M_w and M_L for small earthquakes. *Bulletin of the Seismological Society of America* **106**, 2402-2408.

Noorlandt, R.P., P.P. Kruiver, M.P.E. de Kleine, M. Karaoulis, G. de Lange, A. Di Matteo, J. von Ketelhodt, E. Ruigrok, B. Edwards, A. Rodriguez-Marek, J.J. Bommer, J. van Elk & D. Doornhof (2017). Characterisation of ground-motion recording stations in the Groningen gas field. *Re-submitted to Journal of Seismology following review and revision.*

Rodriguez-Marek, A., P.P. Kruiver, P. Meijers, J.J. Bommer, B. Dost, J. van Elk & D. Doornhof (2017). A regional site-response model for the Groningen gas field. *Bulletin of the Seismological Society of America* **107**(5), 2067-2077.

Spetzler, J. & B. Dost (2017b) *Probabilistic Seismic Hazard Analysis for Induced Earthquakes in Groningen*; Update June 2017. KNMI report.

Stafford, P.J., Rodriguez-Marek, A., B. Edwards, P.P. Kruiver & J.J. Bommer (2017). Scenario dependence of linear site effect factors for short-period response spectral ordinates. *Bulletin of the Seismological Society of America*, doi: 10.1785/0120160123.

van Essen, H. (2017). *Proevenverzameling Noorderzijlvest - Deelverzameling ten behoeve van dijkversterking Eemskanaal*. Deltares report 1220173-024-GEO-0071, 30 May 2017 (in Dutch).

Wells, D.L. & K.J. Coppersmith (1994). New empirical relationships among magnitude, rupture length, rupture width, rupture area, and surface displacement. *Bulletin of the Seismological Society of America* **84**, 974-1002.

Yenier, E. & G.M. Atkinson (2015). Regionally adjustable generic ground-motion prediction equation based on equivalent point-source simulations: Application to central and eastern North America. *Bulletin of the Seismological Society of America* **105**, 1989-2009.

APPENDIX I

Slochteren Earthquake Recordings

A magnitude M_L 2.6 earthquake occurred towards the south of the Groningen field on 27 May 2017 near the town of Slochteren (Figure A1.1). This was the first event of $M_L \geq 2.5$ to contribute records to the ground-motion database used for the derivation of the GMM since the V3 database was established with 178 accelerograph recordings obtained from 22 earthquakes with local magnitude in the range from M_L 2.5 to M_L 3.6; the database remained unchanged for the V4 GMM.

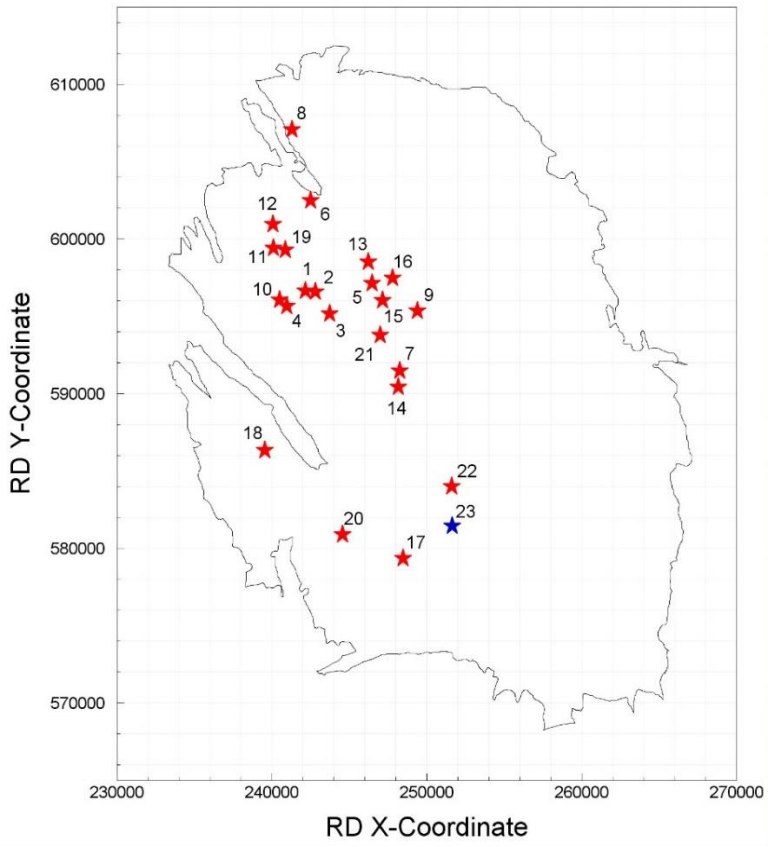

Figure A1.1. Epicentres of the 22 earthquakes in the V3-V4 Groningen ground-motion database and the May 2017 Slochteren event (*blue star*)

The recordings from the Slochteren event were processed rapidly in order to be incorporated to the database used for the derivation of the V5 GMM. The earthquake added 68 new recordings to the database—and increase of almost 40% compared to the V3 and V4 versions—predominantly from the G-stations, including several stations that had not contributed to the database previously. Before this event, the

largest number of recordings from a single event were the 44 accelerograms of the M_L 3.1 Hellum earthquake, which was the last event added to the V3 database. With the expansion of the recording networks in the region, it can now be expected that future earthquakes will routinely generate similar numbers of recordings.

The PGA values recorded in the Slochteren earthquake are compared with those from previous earthquakes in Figure A1.2. The largest horizontal PGA value was 0.035*g*. While this is much smaller than the maximum value of 0.082*g* recorded in the 2012 Huizinge earthquake—in itself a very low level of motion compared to those observed in destructive earthquakes in tectonically active regions—it did appear large in comparison to previous earthquakes of comparable magnitude. The value of 0.035*g* has been exceeded in five previous earthquakes, the smallest of which was of magnitude M_L 2.9. This highest PGA was recorded at less than 2 km from the earthquake epicentre. As can be appreciated from Figure A1.2, the majority of the recorded amplitudes were rather low, even compared to the existing database.

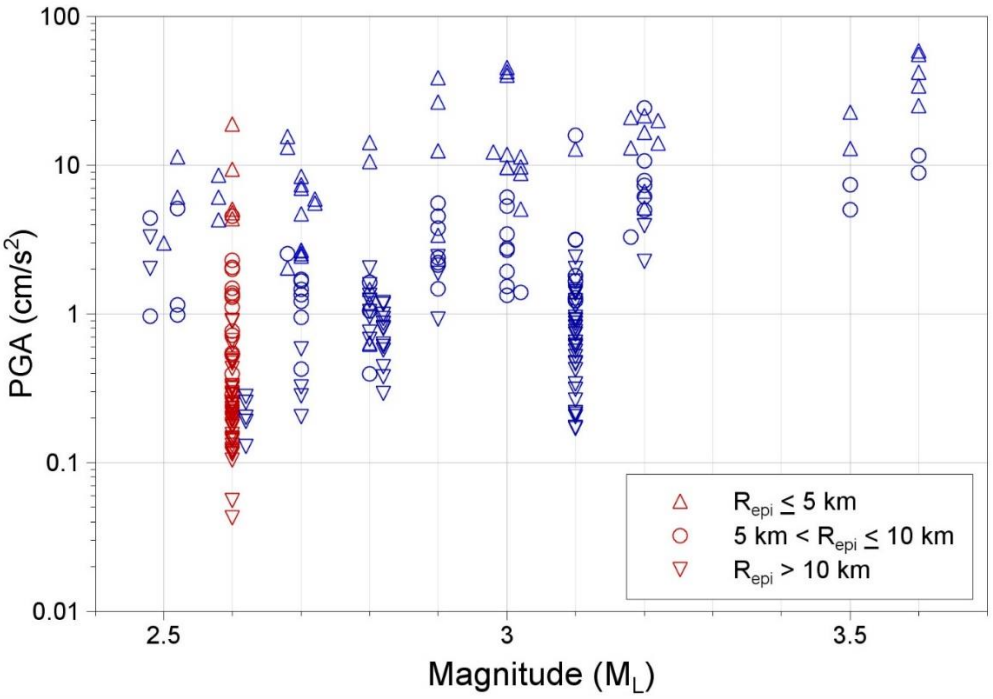

Figure A1.2. Geometric mean horizontal PGA values against magnitude in the Groningen database, with symbols indicating ranges of epicentral distance. The blue symbols correspond to the May 2017 Slochteren event. Where two or more events have the same magnitude, the symbols are displaced slightly left and/or right for clarity.

The recording exhibiting the largest peak acceleration of 0.035*g* displays features typical of the Groningen data, namely highly-polarised horizontal components with the high PGA value associated with a pronounced and isolated peak in the motion (Figure A1.3). As already observed in the database, for individual components of

motion the values of PGA and duration exhibit a strong inverse correlation (Figure A1.4).

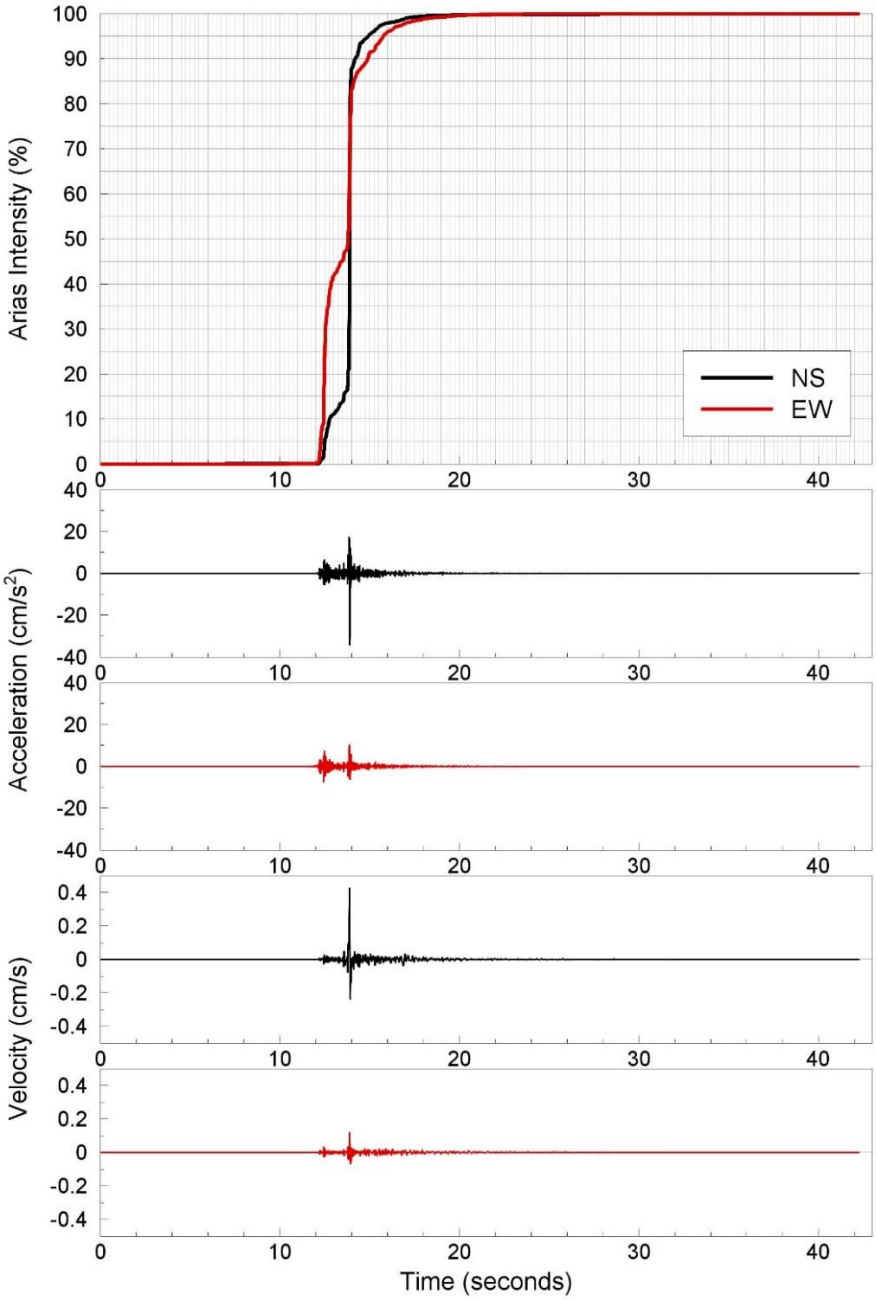

Figure A1.3. Horizontal acceleration and velocity components from the G46 station recordings of the Slochteren earthquakes and the Husid plots showing the distribution of the energy in the motion over time

The degree of polarization of the horizontal motions at short epicentral distances is illustrated in Figure A1.5, in which it can be seen that for two recording stations (G46 and G50), the ratios of the two horizontal peaks—of both acceleration and velocity—is about 3.

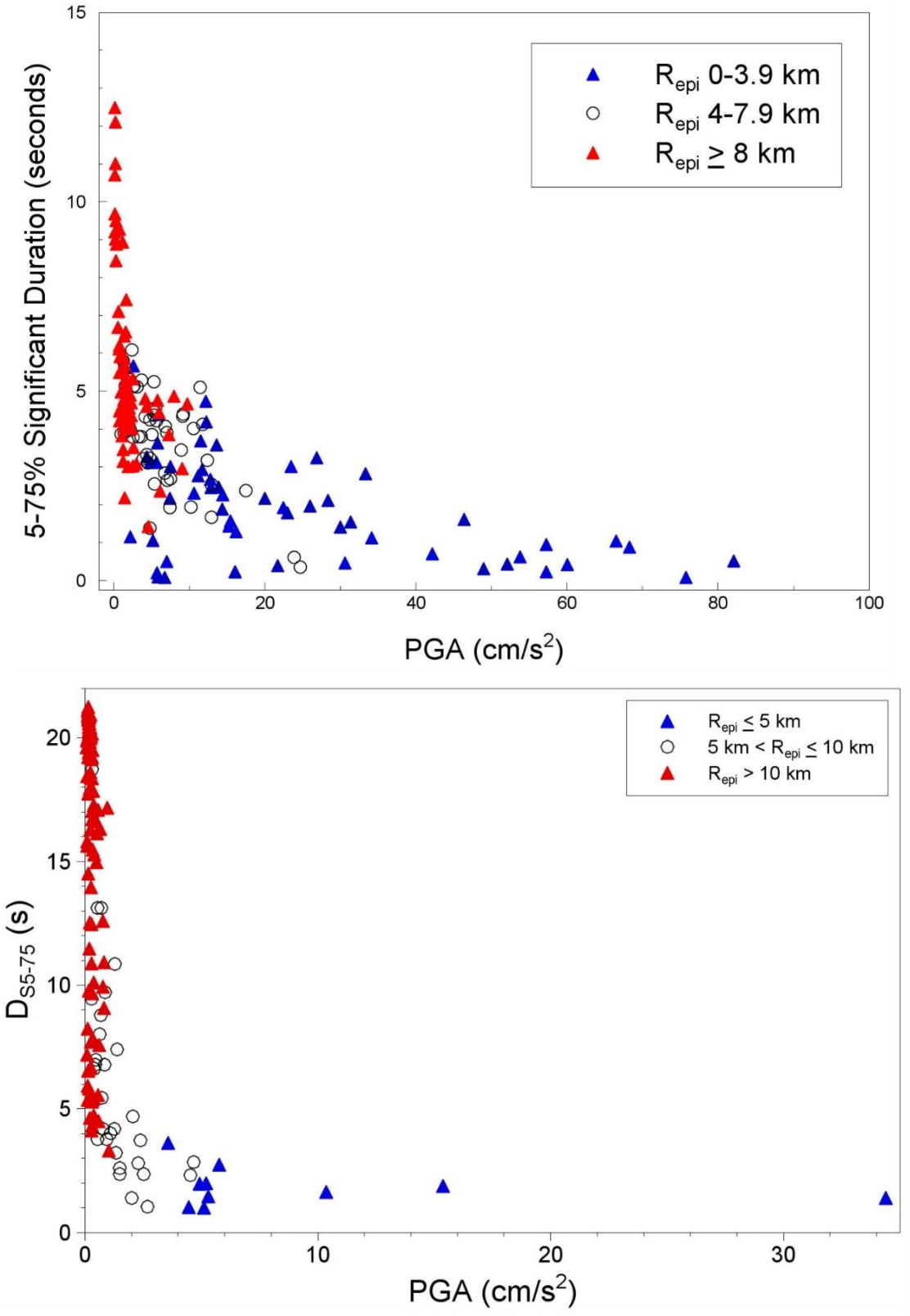

Figure A1.4. *Upper*: Individual component values of PGA and significant duration in the Groningen ground-motion database, showing the strong inverse relationship between these two parameters; *Lower*: Similar plot using only the Slochteren data.

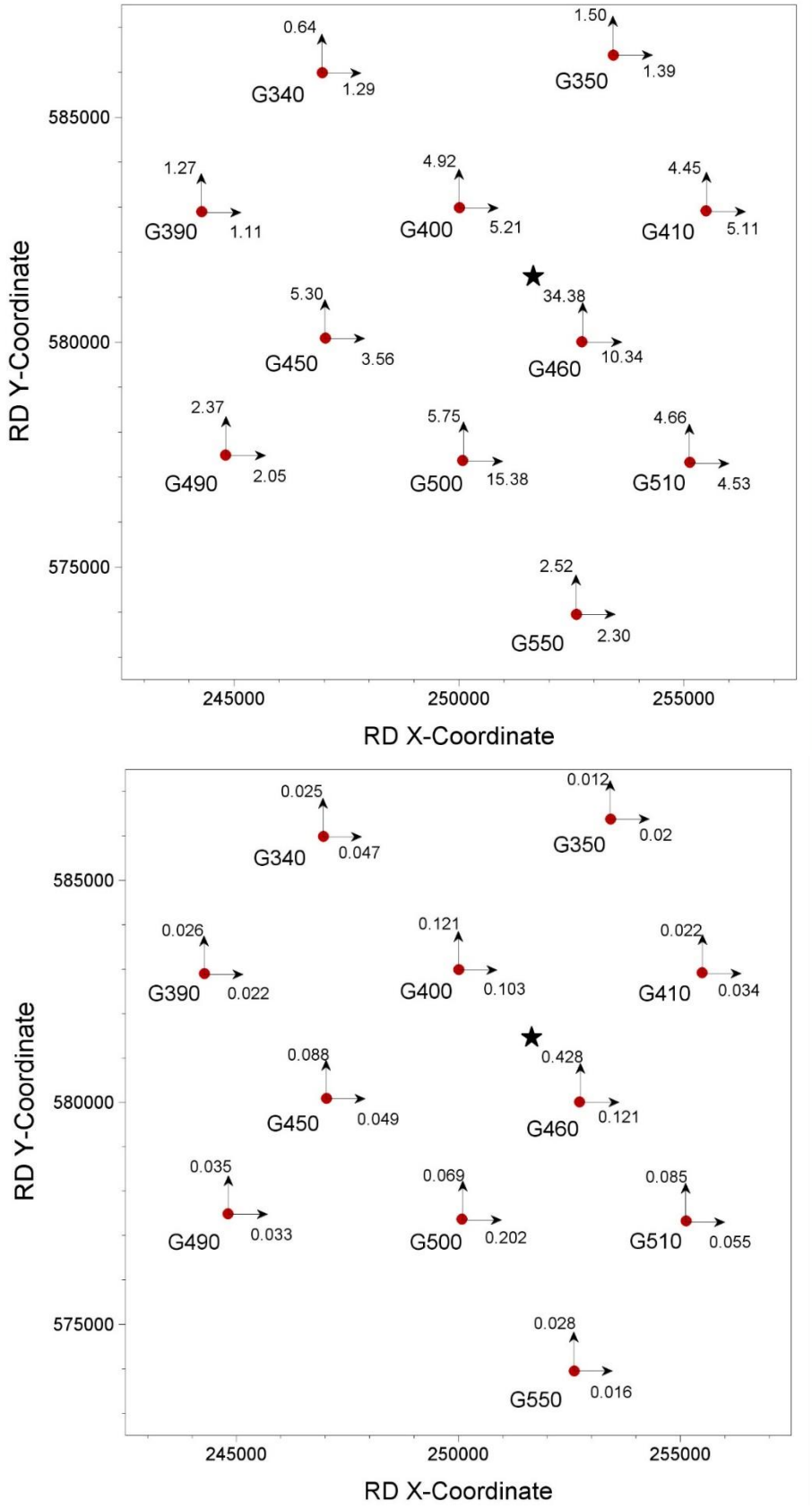

Figure A1.5. *Upper*: Accelerograph stations within ~8 km of the epicentre (*black star*) of the Slochteren earthquake, showing the PGA values (cm/s^2) on the NS and EW components; *Lower*: Similar plot for PGV (cm/s).

Despite the relatively high peaks of the strongy-polarised near-source recordings, as noted earlier the overall pattern observed is that on average the amplitudes of motion from this earthquake are rather low. Calculating the residuals of geometric mean PGV with respect to the V4 GMM, the event-term is found to be one inter-event standard deviation below the median level for that model. The relatively weak nature of this earthquake is also confirmed by the event terms found from the simulations for the V5 model (Figure A1.6).

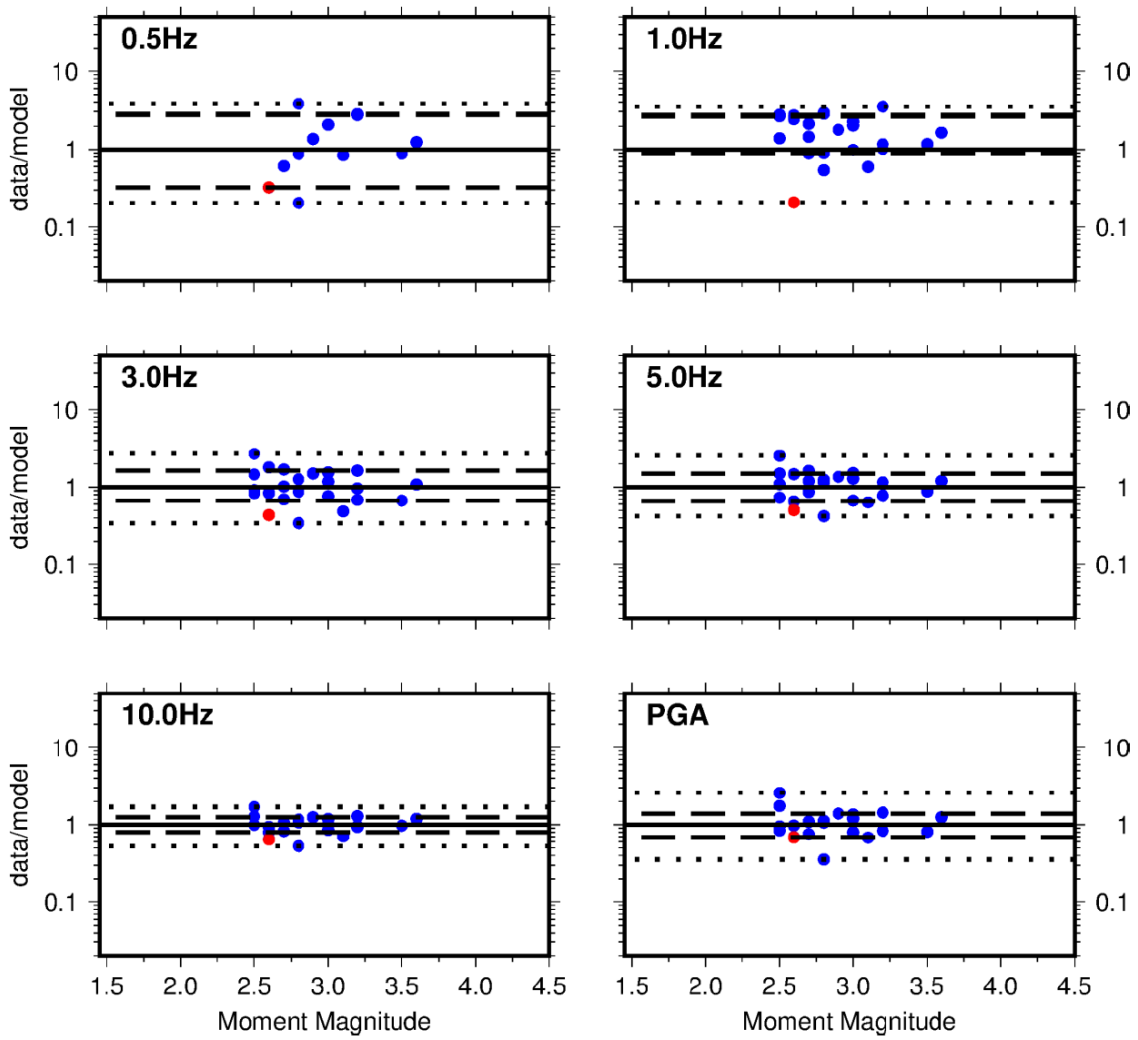

Figure A1.6. Between-event terms for the Central-lower (Ca) simulations with the V5 model; the red dots correspond to the Slochteren earthquake. The solid line indicates equivalence, the dashed and dotted lines indicate the one and two standard deviation levels.

Figure A1.7 shows the effect of repeating the V5 inversions without the Slochteren recordings, which leads to an optimal solution with a higher kappa value at the NS_B horizon and a higher value of the stress parameter, if it assumed that this applies to both of the central branches. The combined effect of these two changes is shown in Figure A1.8, which shows that in the range of intermediate periods (0.1-0.5 s) the

reduced stress parameter leads to a ~10% reduction in amplitudes, while at shorter periods the kappa increase appears to cancel out the effect.

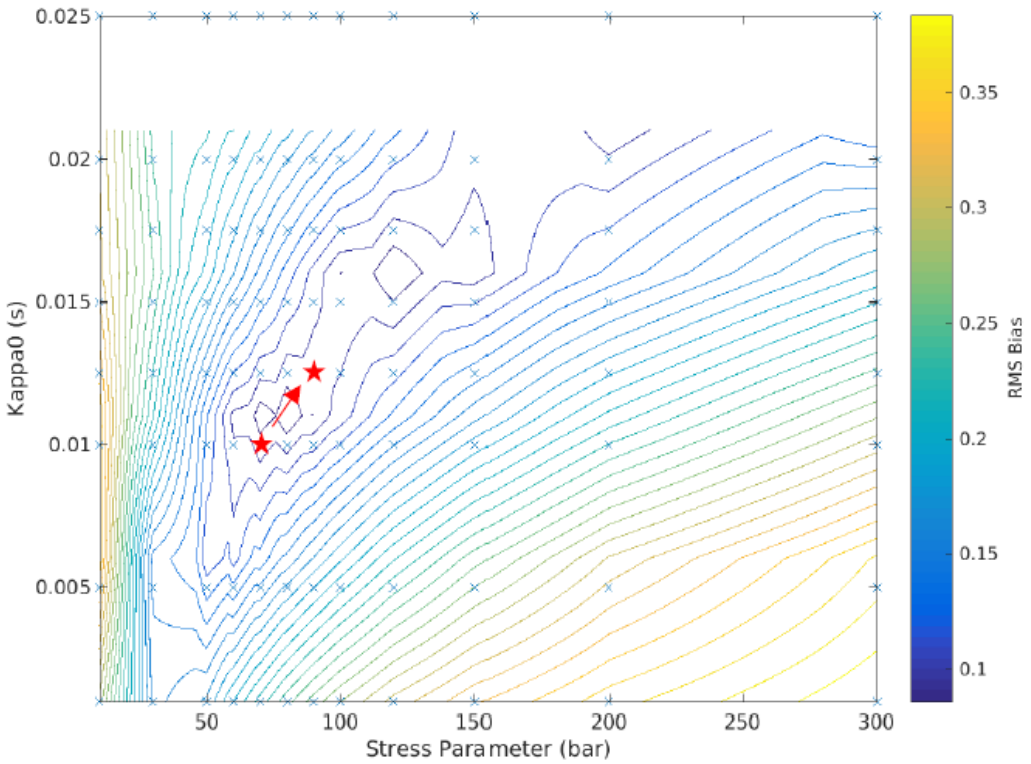

Figure A1.7. Change in optimal model parameters caused by removal of Slochteren data

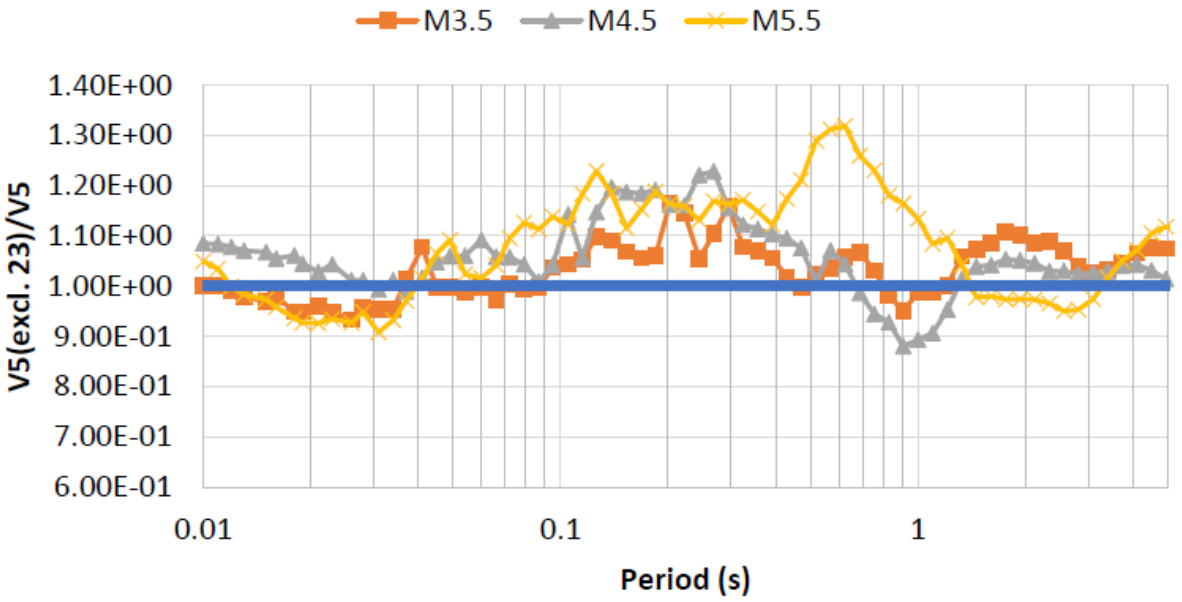

Figure A1.8. Ratios of simulated motions from V5 inversions excluding and including the recordings of the Slochteren event

APPENDIX II

M_L-M Relationship for Groningen

A2.1. Summary

The use of local magnitude (M_L) in seismic hazard analyses is a topic of recent debate. In regions of weak- or moderate-seismicity, small earthquakes (characterized by M_L) are commonly used to determine frequency-magnitude distributions (FMD) for probabilistic hazard calculations. However, empirical and theoretical studies on the relation between moment magnitude (**M**) and M_L for small earthquakes show a systematic difference between the two below a region-dependent magnitude threshold. This difference may introduce bias in the estimation of the frequency of larger events with given **M**, and consequently seismic hazard. For induced seismicity related to the Groningen gas field, this magnitude threshold is determined to be **M** ~2, with equality between **M** and M_L at higher magnitudes. A quadratic relation between **M** and M_L is derived for $0.5 < M_L < 2$, in correspondence to recent theoretical studies.

A2.2. Introduction

Magnitudes of the induced earthquakes in the Groningen field are assigned by the official seismological service of the Netherlands, which is part of KNMI. These are local magnitudes, M_L. Within the context of the Groningen seismic hazard and risk models, both the compaction-based seismicity model (*e.g.*, Bourne *et al*., 2014) and the ground-motion models (GMM) are being developed in terms of local magnitude but with the assumption of these magnitudes being equivalent to moment magnitude, **M**. Although this assumption represents a reasonable starting point (Deichmann, 2006), it has been a clear goal since the beginning of the project to either confirm this assumed equivalence or else to replace it with a validated relationship.

Local Magnitudes in Groningen

Based on a dataset of 157 records, recorded in 1995 and the first half of 1996, an equation for M_L in the Netherlands was established as:

$$M_L = \log_{10}A + 1.33 \log(R) + 0.00139\, R + 0.424 \qquad \text{(A2.1)}$$

and has been used in the determination of magnitudes in the Groningen gas field.

Moment magnitude

Seismic moment, M_o, can be derived from the Fourier spectra of S waves, as shown, for example, in Abercrombie (1995) and Edwards *et al*. (2010). Methods rely on determining the long-period displacement plateau of the Fourier spectrum,

accounting for anelastic attenuation and site effects. The recorded plateau values are subsequently used to determine geometrical spreading, amplification and seismic moment. The latter is then used to determine moment magnitude, **M**.

Comparison of M

In order to explore the sensitivity of event-to-event variability in calculated **M** depending on the approach we calculated **M** using the approach of Dost & Kraaijpoel (2013) and Edwards *et al.* (2010). Identical material properties were assumed in both methods. The primary difference between the methods is the spectral fitting technique and formulation of the geometrical spreading function. In the latter method, the entire S-wave train (as opposed to the direct S-wave pulse) is taken as signal and an 'apparent' geometrical decay determined. This rate of decay was found to be $1/R^{1.58}$ from 3 to 7 km, and $1/R^{0.09}$ from 7 to 12 km. In the method of Dost & Kraaijpoel (2013), a stronger decay ($R^{-1.9}$) was observed due to strong wave-guide effects of the subsurface on the S-wave pulse. The resulting **M** values are nevertheless similar and, considering the error, follow a 1:1 trend (Figure A2.1). The results presented henceforth use the Dost & Kraaijpoel (2013) approach.

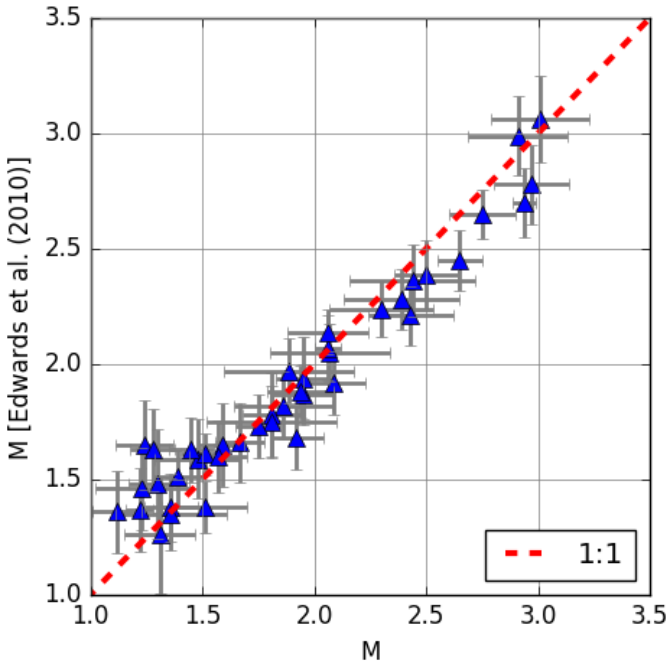

Figure A2.1. Comparison of **M** determined using the approach detailed here, and those calculated following the approach detailed in Edwards *et al*. (2010)

A2.3. Relationship between M and M_L

A total of 116 events, listed in Table A2.1, have been processed to calculate **M** and compare these values to measured M_L. In general the uncertainties in M_L are larger than uncertainties in **M.** This may be caused by the fact that the original borehole

network used to calculate M_L has a large inter-station distance, on average 20 km, while covering a heterogeneous upper crustal structure. The distance between the accelerometer stations used to calculate **M** is less and, being located at the surface, do include the highly heterogeneous uppermost 200 m.

For events of magnitude M_L>2 both M_L and **M** are similar (Figure A2.2). For smaller events a quadratic relation was fit to the data using a least-squares optimization:

$$\mathbf{M} = 0.056262 * M_L^2 + 0.65553 * M_L + 0.4968 \qquad \text{(A2.2)}$$

This relation is close to the relation derived by Grünthal et al. (2009). Munafò et al. (2016) showed that for small events $M = 2/3 * M_L + C$. In Figure A2.2 this relation is close to the quadratic fit for small events ($M_L < 1.5$) with C = 0.53. These results confirm the validity of the assumed equality between **M** and M_L for **M** ≥ 2.5.

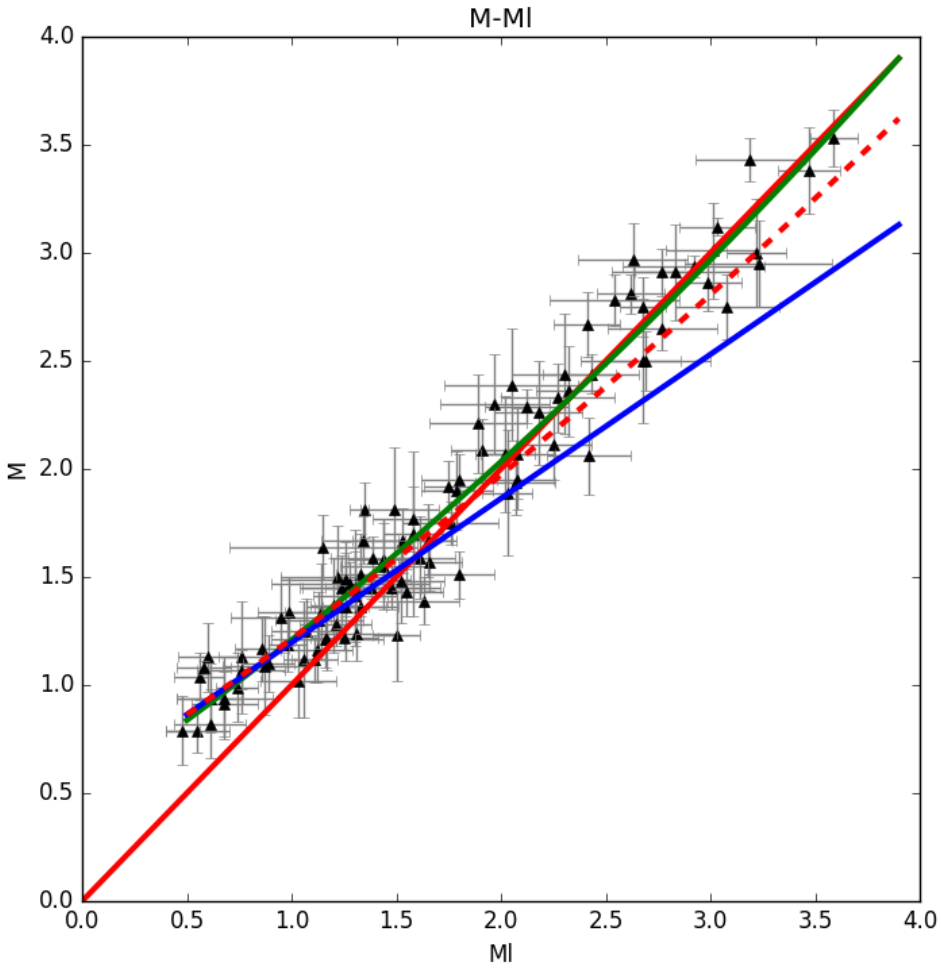

Figure A2.2. Moment magnitude **M** as a function of local magnitude M_L. In green the proposed quadratic relation is shown [Eqn.(A2.2)]. In red-dashed the Grünthal *et al.* (2009) relation and in blue the Munafò *et al*. (2016) relation

A2.4. Conclusions

Numerous empirical studies have shown that 1:1 scaling between M_L and **M** does not extend to low magnitudes. For M_L > 2-3, the average of the studies seems to conform with **M** ≈ M_L, albeit with significant scatter of the scaling relations between individual regions. For M_L < 2, and for studies spanning a broader magnitude range, it is observed that **M** > M_L. The difference, furthermore, tends to increase for increasingly small magnitudes, with up to a unit of difference for M_L = 0 events. Three studies compiling data over a broad magnitude range: in Europe, Switzerland and neighbouring regions, and in California, show a distinct curve in the M_L versus **M** scaling below M_L = 2.5. This is consistent with simulation-based studies (Deichmann, 2006, 2017; Edwards *et al*., 2010; Hanks & Boore, 1984; Munafò *et al*., 2016), which show that when accounting for the effect of attenuation (Q and κ_0) *and* the Wood-Anderson instrument response, we should expect a curvilinear scaling relation between M_L and **M**. This is due to a complex interaction of the earthquake source signal and the filtering effects of the propagation medium (low-pass) and instrument response (displacement high-pass).

In the Groningen case it has been shown that **M** is approximately equal to M_L above M_L = 2.5, confirming the assumption of equality between the magnitude scales in the hazard assessment for induced seismicity in the region. A systematic trend, best described by a quadratic relation between **M** and M_L and similar in form to those observed in other empirical and theoretical studies, is seen for magnitudes smaller than M_L = 2.5. The **M**-M_L relation for Groningen is close to the relation Grünthal *et al*. (2009) published for the central, northern and northwestern Europe. However, Edwards & Douglas (2014) showed a large variation in published catalogue magnitudes with respect to **M** for induced earthquakes worldwide, demonstrating the need for a proper definition and calibration of magnitudes for each region of interest.

Table A2.1. Events used in the **M**-M_L calculations with their corresponding magnitudes. From 01-01-2014 onward, all events of M_L≥ 2.0 are selected, before that time only events of M_L>3.0 and some additional smaller events have been selected. Starting in 2015 some events could be added with M_L<2.0. The last column shows the number of records available for analysis.

yymmdd	time	lat	lon	M_L	#	M	#	Name
060808	05:04:00	53.350	6.697	3.47 ± 0.15	8	3.38 ± 0.20	4	Westeremden
081030	05:54:29	53.337	6.720	3.22 ± 0.14	7	3.00 ± 0.25	6	Westeremden
090414	21:05:26	53.345	6.680	2.62 ± 0.16	7	2.81 ± 0.09	3	Huizinge
090508	05:23:12	53.354	6.762	2.99 ± 0.16	7	2.86 ± 0.13	5	Zeerijp
100814	07:43:20	53.403	6.703	2.32 ± 0.15	5	2.36 ± 0.21	5	Uithuizen
110119	19:39:32	53.319	6.645	2.43 ± 0.23	7	2.40 ± 0.09	4	Westerwijtw.
110627	15:48:10	53.303	6.787	3.19 ± 0.26	9	3.49 ± 0.07	7	Garrelsweer
110831	06:23:57	53.444	6.687	2.54 ± 0.31	8	2.78 ± 0.12	3	Uithuizen
120816	20:30:33	53.345	6.672	3.59 ± 0.11	8	3.53 ± 0.13	7	Huizinge

yymmdd	time	lat	lon	M_L	#	M	#	Name
130119	20:10:07	53.285	6.790	2.41 ± 0.16	6	2.67 ± 0.15	3	Overschild
130207	22:31:58	53.375	6.667	2.68 ± 0.18	8	2.50 ± 0.29	3	Zandeweer
130207	23:19:09	53.389	6.667	3.23 ± 0.35	7	2.95 ± 0.20	3	Zandeweer
130209	05:26:10	53.366	6.758	2.68 ± 0.11	5	2.75 ± 0.14	2	Zeerijp
130702	23:03:56	53.294	6.785	3.03 ± 0.18	7	3.12 ± 0.04	2	Garrelsweer
130904	01:33:32	53.344	6.772	2.77 ± 0.13	6	2.91 ± 0.11	5	Zeerijp
131126	23:54:53	53.327	6.845	2,02 ± 0.14	6	2.07 ± 0.27	6	Appingedam
140203	06:30:48	53.334	6.757	1.53 ± 0.13	3	1.86 ± 0.22	6	Loppersum
140213	02:13:14	53.357	6.782	3.01 ± 0.22	6	3.01 ± 0.22	14	Leermens
140228	04:38:52	53.279	6.750	1.15 ± 0.45	4	1.64 ± 0.15	6	Ten Post
140310	03:39:10	53.351	6.768	0.95 ± 0.24	4	1.31 ± 0.16	8	Zeerijp
140311	09:08:23	53.228	6.822	2.30 ± 0.25	9	2.44 ± 0.28	5	Schildwolde
140318	21:15:18	53.390	6.618	2.05 ± 0.32	5	2.39 ± 0.26	7	Rottum
140417	20:18:35	53.327	6.723	1.34 ± 0.20	5	1.67 ± 0.11	8	Loppersum
140420	08:36:03	53.351	6.743	1.35 ± 0.02	4	1,81 ± 0.13	9	Zeerijp
140513	18:16:05	53.333	6.640	1.39 ± 0.20	4	1.59 ± 0.10	5	Westerwijtwerd
140616	15:16:40	53.349	6.710	1.80 ± 0.18	4	1.95 ± 0.12	9	Westeremden
140702	17:34:17	53.214	6.790	2.12 ± 0.20	5	2.29 ± 0.08	5	Slochteren
140707	23:13:44	53.269	6.752	1.05 ± 0.09	2	1.39 ± 0.10	4	Overschild
140809	15:55:33	53.325	6.835	1.97 ± 0.26	5	2.30 ± 0.23	6	Oosterwijtwerd
140819	19:25:24	53.376	6.725	1.22 ± 0.27	4	1.50 ± 0.24	8	Garsthuizen
140901	07:17:43	53.194	6.787	2.63 ± 0.26	6	2.97 ± 0.17	6	Froombosch
140930	11:42:03	53.258	6.655	2.83 ± 0.30	8	2.91 ± 0.22	12	Garmerwolde
141021	06:49:15	53.358	6.747	1.53 ± 0.24	4	1.67 ± 0.15	6	Zeerijp
141105	01:12:35	53.374	6.678	2.92 ± 0.34	6	2.94 ± 0.05	14	Zandeweer
141122	04:09:03	53.355	6.698	1.28 ± 0.38	4	1.47 ± 0.10	6	Westeremden
141130	01:03:48	53.360	6.672	1.38 ± 0.33	4	1.45 ± 0.05	4	Middelstum
141228	15:13:06	53.350	6.753	1.26 ± 0.31	4	1.49 ± 0.17	10	Zeerijp
141230	02:37:37	53.208	6.728	2.77 ± 0.26	7	2.65 ± 0.10	11	Woudbloem
150106	06:55:28	53.324	6.768	2.69 ± 0.31	4	2.50 ± 0.14	14	Wirdum
150111	23:05:24	53.171	6.797	1.53 ± 0.36	3	1.34 ± 0.15	5	Sappemeer
150118	10:54:10	53.233	6.720	1.49 ± 0.21	5	1.81 ± 0.29	7	Lageland
150122	03:44:16	53.245	6.822	0.60 ± 0.32	2	0.84 ± 0.12	3	Hellum
150123	11:45:37	53.175	6.797	1.24 ± 0.13	4	1.36 ± 0.10	3	Sappemeer
150202	23:15:33	53.268	6.743	0.93 ± 0.08	2	1.06 ± 0.32	5	Overschild
150225	10:02:57	53.323	6.857	2.33 ± 0.13	3	2.43 ± 0.19	10	Appingedam
150324	13:27:57	53.322	6.855	2.27 ± 0.27	5	2.33 ± 0.16	9	Appingedam
150516	14:14:49	53.306	6.847	1.58 ± 0.19	4	1.77 ± 0.15	7	Appingedam
150521	21:08:48	53.244	6.810	1.75 ± 0.12	5	1.92 ± 0.12	5	Schildwolde
150527	10:52:10	53.404	6.668	2.01 ± 0.33	3	2.06 ± 0.06	8	Uithuizen
150606	23:39:15	53.340	6.750	1.91 ± 0.15	8	2.09 ± 0.14	12	Loppersum
150610	02:26:07	53.344	6.753	1.76 ± 0.23	8	1.75 ± 0.10	12	Zeerijp
150707	03:09:01	53.262	6.631	2.08 ± 0.17	26	1.95 ± 0.14	11	Thesinge
150818	07:06:13	53.185	6.754	2.03 ± 0.12	20	1.89 ± 0.29	8	Kolham
150930	18:05:37	53.234	6.834	3.08 ± 0.25	41	2.75 ± 0.15	13	Hellum
151030	18:49:01	53.285	6.920	2.25 ± 0.18	42	2.11 ± 0.16	6	Meedhuizen
151115	23:01:42	53.357	6.743	0,86 ± 0.13	9	1,17 ± 0.15	5	Zeerijp
151202	06:40:02	53.240	6.831	1,61 ± 0.17	21	1,59 ± 0.19	6	Hellum

yymmdd	time	lat	lon	M_L	#	M	#	Name
151225	04:19:36	53.315	6.735	1,33 ± 0.18	8	1,36 ± 0.12	6	Ten Post
160107	05:25:55	53.168	6.814	1,63 ± 0.17	31	1,39 ± 0.11	6	Zuidbroek
160113	06:41:42	53.248	6.855	1,31 ± 0.19	47	1,24 ± 0.13	6	Siddeburen
160117	11:57:33	53.258	6.840	1,52 ± 0.21	51	1,48 ± 0.19	6	Siddeburen
160126	22:22:33	53.203	6.720	1.50 ± 0.11	11	1,23 ± 0.21	4	Harkstede
160219	21:48:37	53.260	6.617	1.30 ± 0.20	20	1,41 ± 0.21	5	Zuidwolde
160225	22:26:30	53.184	6.781	2.42 ± 0.20	73	2.06 ± 0.18	10	Froombosch
160304	13:00:29	53.372	6.685	0.87 ± 0.20	8	1.09 ± 0.23	6	Eppenhuizen
160307	10:16:53	53.268	6.826	1.20 ± 0.11	11	1.37 ± 0.22	6	Steendam
160325	09:46:39	53.244	6.645	1.80 ± 0.17	32	1.51 ± 0.11	5	Garmerwolde
160402	00:47:53	53.249	6.657	1.13 ± 0.21	15	1.30 ± 0.13	7	Garmerwolde
160424	15:36:47	53.231	6.825	1.12 ± 0.17	6	1.16 ± 0.15	5	Schildwolde
160506	17:27:39	53.342	6.694	0.68 ± 0.23	7	0,94 ± 0.19	6	Westeremden
160515	11:57:15	53.268	6.989	0.98 ± 0.09	5	1.19 ± 0.13	3	Woldendorp
160516	20:38:41	53.291	6.916	1.11 ± 0.11	7	1.12 ± 0.11	5	Meedhuizen
160528	02:08:20	53.237	6.635	1.21 ± 0.17	20	1.28 ± 0.10	5	Groningen
160529	14:27:54	53.286	6.835	1.07 ± 0.17	8	1.25 ± 0.15	5	Overschild
160601	08:02:54	53.361	6.750	1.24 ± 0.20	10	1.45 ± 0.15	5	Zeerijp
160602	18:43:13	53.249	6.924	1.48 ± 0.14	12	1.45 ± 0.10	4	Wagenborgen
160618	23:58:25	53.184	6.766	1.25 ± 0.16	28	1.22 ± 0.06	4	Kolham
160622	13:10:10	53.344	6.811	0.74 ± 0.10	4	0.99 ± 0.16	4	Oosterwijtwerd
160718	08:58:11	53.378	6.709	1.66 ± 0.15	20	1.57 ± 0.13	7	Eppenhuizen
160726	14:02:10	53.277	6.907	0.93 ± 0.17	3	0.88 ± 0.10	3	Tjuchem
160728	15:57:28	53.250	6.824	0.76 ± 0.11	7	1.13 ± 0.26	5	Hellum
160807	20:40:22	53.374	6.644	1.33 ± 0.12	24	1.51 ± 0.19	5	Kantens
160824	23:44:03	53.354	6.950	1.06 ± 0.10	22	1.12 ± 0.27	4	Eems-Dollard
160828	03:27:53	53.401	6.636	1.26 ± 0.19	25	1.36 ± 0.25	5	Uithuizen
160902	13:16:00	53.218	6.844	2.07 ± 0.19	46	1.94 ± 0.15	8	Schildwolde
160909	12:21:23	53.337	6.811	0.76 ± 0.21	11	1.07 ± 0.09	7	Oosterwijtwerd
160921	14:21:32	53.254	6.945	1.16 ± 0.14	22	1.21 ± 0.13	5	Wagenborgen
160927	23:22:14	53.244	6.616	0.89 ± 0.12	5	1.10 ± 0.13	4	Groningen
161012	07:12:46	53.305	6.725	0.48 ± 0.08	8	0.79 ± 0.16	5	Ten Post
161101	00:12:28	53.301	6.807	1.89 ± 0.23	41	2.21 ± 0.23	9	Wirdum
161101	00:57:46	53.306	6.809	2.18 ± 0.21	54	2.26 ± 0.24	10	Wirdum
161108	11:23:17	53.331	6.795	1.44 ± 0.21	11	1.55 ± 0.20	10	Eenum
161120	15:20:07	53.299	6.744	0.99 ± 0.16	3	1.11 ± 0.09	4	Ten Post
161120	17:58:40	53.300	6.802	1.17 ± 0.27	6	1.21 ± 0.14	5	Wirdum
161120	18:57:56	53.336	6.838	1.65 ± 0.14	26	1.67 ± 0.17	10	Appingedam
161126	13:18:35	53.343	6.805	0.56 ± 0.12	4	1.04 ± 0.11	7	Leermens
161126	17:03:34	53.261	6.909	1.03 ± 0.18	11	1.02 ± 0.17	5	Siddeburen
161207	01:52:49	53.333	6.774	1.79 ± 0.17	34	1.90 ± 0.18	10	Loppersum
161212	11:28:07	53.264	6.977	0.61 ± 0.16	7	0.94 ± 0.16	4	Woldendorp
161215	04:44:48	53.343	6.807	0.60 ± 0.14	5	1.13 ± 0.16	4	Leermens
161215	10:45:30	53.378	6.934	1.58 ± 0.14	30	1.70 ± 0.38	6	Eems-Dollard
161216	19:55:23	53.254	6.984	0.55 ± 0.15	15	0.79 ± 0.10	5	Nieuwolda
161217	11:56:47	53.211	6.652	0.58 ± 0.13	8	1.08 ± 0.03	3	Groningen
161220	16:15:39	53.215	6.696	1.14 ± 0.17	26	1.34 ± 0.22	3	Harkstede
161222	23:41:01	53.345	6.867	0.45 ± 0.16	3	0.66 ± 0.15	4	Holwierde

yymmdd	time	lat	lon	M_L	#	M	#	Name
161230	03:05:53	53.301	6.802	0.99 ± 0.15	19	1.34 ± 0.16	8	Wirdum
161230	03:06:07	53.292	6.810	0.64 ± 0.13	3	1.03 ± 0.20	6	Overschild
170114	12:47:19	53.214	6.840	0.61 ± 0.17	5	0.82 ± 0.16	4	Schildwolde
170117	18:53:10	53.248	6.839	0.68 ± 0.16	18	0.91 ± 0.15	7	Hellum
170204	02:56:52	53.371	6.739	0.90 ± 0.14	3	1.15 ± 0.13	6	Garsthuizen
170204	03:27:37	53.371	6.736	0.60 ± 0.02	2	0.81 ± 0.08	6	Garsthuizen
170226	21:39:48	53.328	6.778	1.44 ± 0.17	24	1.58 ± 0.19	11	Wirdum
170306	11:35:13	53.327	6.571	1.55 ± 0.17	9	1.43 ± 0.11	6	Onderdendam
170311	12:52:48	53.350	6.761	2.08 ± 0.18	54	2.07 ± 0.21	12	Zeerijp
170314	05:22:36	53.319	6.886	1.30 ± 0.14	33	1.45 ± 0.27	11	Delfzijl
170404	10:00:44	53.271	6.991	1.82 ± 0.18	36	1.72 ± 0.09	9	Woldendorp

APPENDIX III

Component-to-Component Variability Model

A3.1 Introduction

The risk calculations for the Groningen field require the use of the arbitrary instead of the geometric mean component of spectral acceleration and duration. This is predicted by sampling a normal distribution considering the geometric mean predictions of the Groningen GMMs as the mean and the component-to-component variability as the standard deviation. Previous estimates of the component-to-component variability of the Groningen ground-motion database yielded significantly larger values than those observed in published ground-motion models and calculated for other strong-motion databases. Research into the cause of this difference during the development of the V3 model (Bommer *et al*., 2016b) showed that the variability values obtained are related to the distances of the records considered. The derivation of a new distance-dependent model is therefore important to take this effect into account. Additionally, a component-to-component variability model for duration was also derived to estimate the arbitrary component of duration. The following work is summarised in this Appendix: (a) the derivation of a new field-averaged model similar to the V3/V4 model, (b) the derivation of a distance- and magnitude- dependent model, and (c) the derivation of the model for duration.

A3.2 Field-averaged model for c2c variability of spectral acceleration

The component-to-component variability with respect to the geometric mean at each period is given by the following equation (Boore, 2005b):

$$\sigma_{c2c}^2 = \frac{1}{N}\sum_{j=1}^{N}\left(\frac{\ln Y_{1j} - \ln Y_{2j}}{2}\right)^2 \qquad \text{(A3.1)}$$

where Y1 and Y2 are the spectral accelerations at that period from the two horizontal components of the j^{th} record, and N is the total number of records.

Because of the scarcity of data beyond the period of 1 s, it was decided by Bommer *et al.* (2015c) for the V2 and V3/V4 models to use the values of Campbell & Bozorgnia (2007), scaled to match the Groningen values up to a period of 1 second. A simple tri-linear fit was then applied to the values to produce the final model, in order to eliminate erratic period-to-period variations.

Figure A3.1 shows the component-to-component variance calculated for the V3/V4 Groningen ground-motion database, the values reported by Boore (2005b) and by

Campbell & Bozorgnia (2007) as well as the final model used in the V3 and V4 GMMs. An equivalent V5 model (referred to as "V3 updated") derived by repeating the process identically – but with the inclusion of the data recorded during the 26 May 2017 M_L 2.6 Slochteren earthquake – is also shown.

The variances calculated with the updated model are between 10% and 15% lower than those corresponding to the V3/V4 database. As a result, the best fit to the data is provided by scaling the Campbell & Bozorgnia (2007) values by 2.05 instead of 2.25. The value calculated for PGV is 0.283 and coincides with the value obtained by scaling the Campbell & Bozorgnia (2007) value for PGV by 2.05.

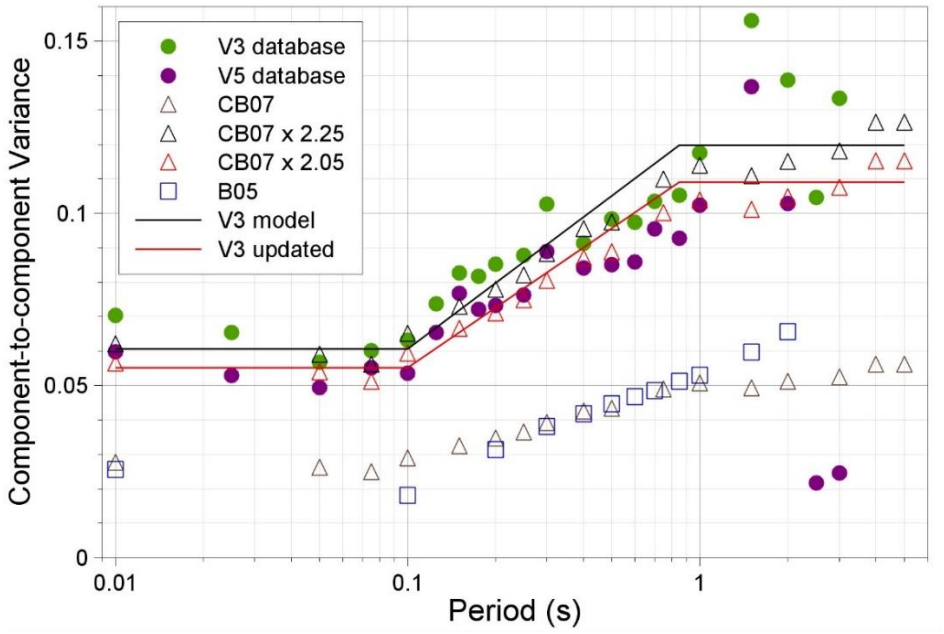

Figure A3.1. The component-to-component variances of the Groningen data (*solid circles*) and their approximation by the scaled values from Campbell & Bozorgnia (2007), simplified by a trilinear trend

A3.3 Distance-dependent model for c2c variability of spectral acceleration

The decrease of variability observed from V3/V4 to V5 in Figure A3.1 is most likely due to the change in the distance distribution of the database due to the inclusion of the Slochteren data, which generally consist of more distant recordings than the existing database. Using a field-averaged model when distance has significant influence has the disadvantage that the component-to-component variability is underestimated in the short distances and overestimated in longer distances.

Figure A3.2 shows the individual component-to-component variances of the arbitrary components of each record with respect to the geometric-mean acceleration, against distance, the values of the model presented in Section A3.2 (in red), the values of Campbell & Bozorgnia (2007) and the values of several functional forms of which the

fit to the data was tested. The functional form in orange is finally selected for the V5 distance-dependent model because it matches the observations of high polarisation at short distances and quickly converges to the tectonic values in longer distances. This functional form is:

$$\sigma_{c2c}^2 = s_1 + s_2 e^{s_3 + s_4 \ln(R)} \quad \text{(A3.2)}$$

This expression can be re-written more simply as:

$$\sigma_{c2c}^2(R) = c_1 + c_2 R^{c_3} \quad \text{(A3.3)}$$

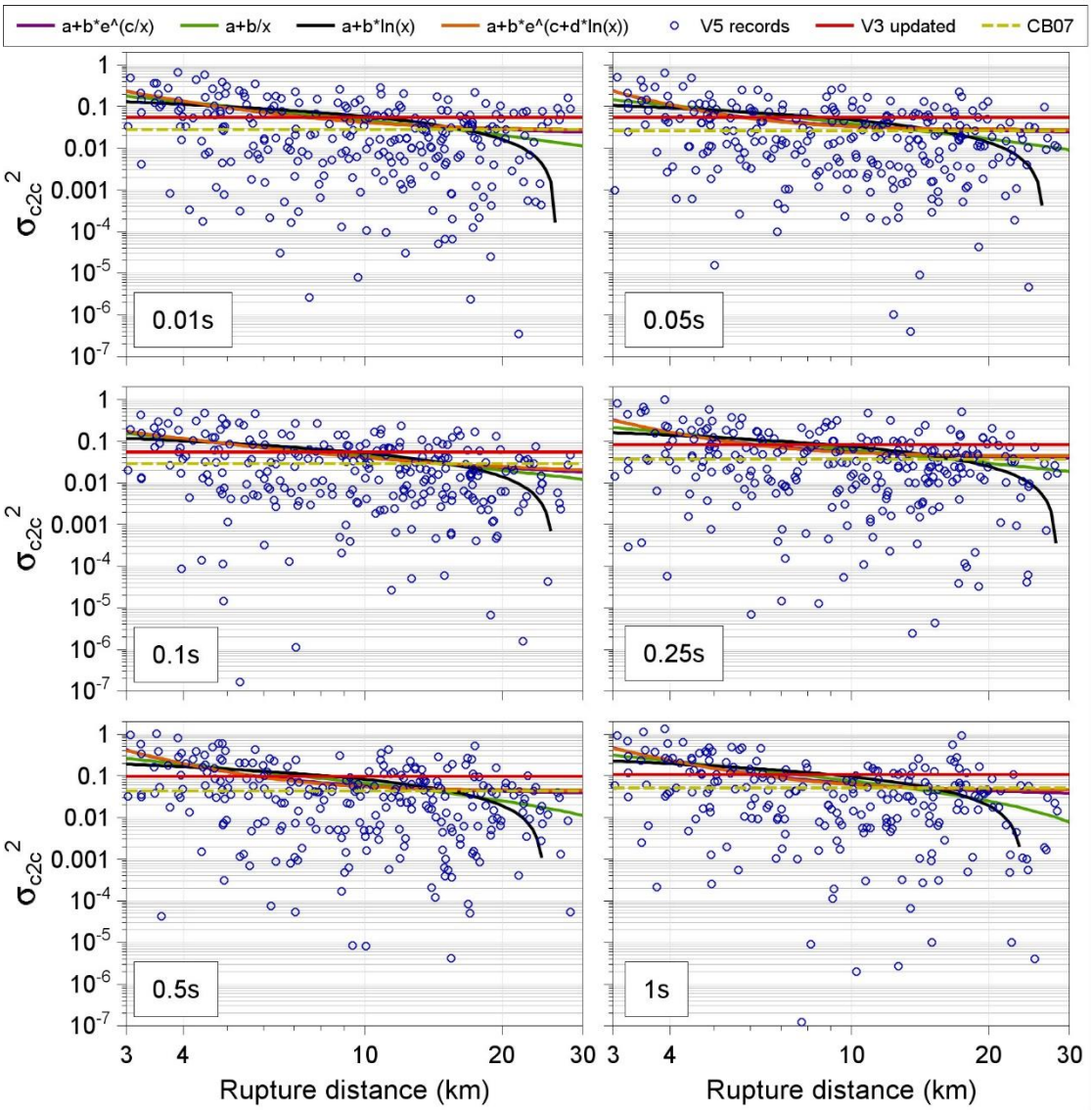

Figure A3.2. The component-to-component variances of the Groningen records at six periods compared to possible functional forms of a distance-dependent model

Figure A3.3 presents the component-to-component variance calculated by Eq.(A3.3)

for different distances and using coefficients obtained from regressions performed for each period individually. In order to eliminate erratic period-to-period fluctuations, we fix the model to a tri-linear form similar to the V3/V4 model, whereby a constant value will be used for periods below 0.1s and another for periods greater than 0.85s, and the values for intermediate periods will be a result of linear interpolation of the two in the log(T) space. Figure A3.4 shows the new model that results from this simplification.

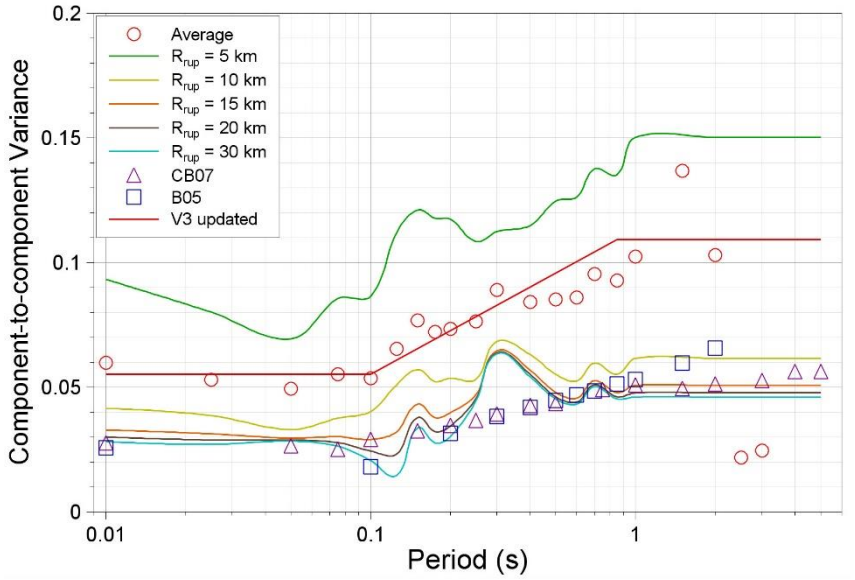

Figure A3.3. The component-to-component variability model for Groningen as obtained by individual regressions at each period, at different distances, compared to the data average, the updated V3 model and the tectonic models.

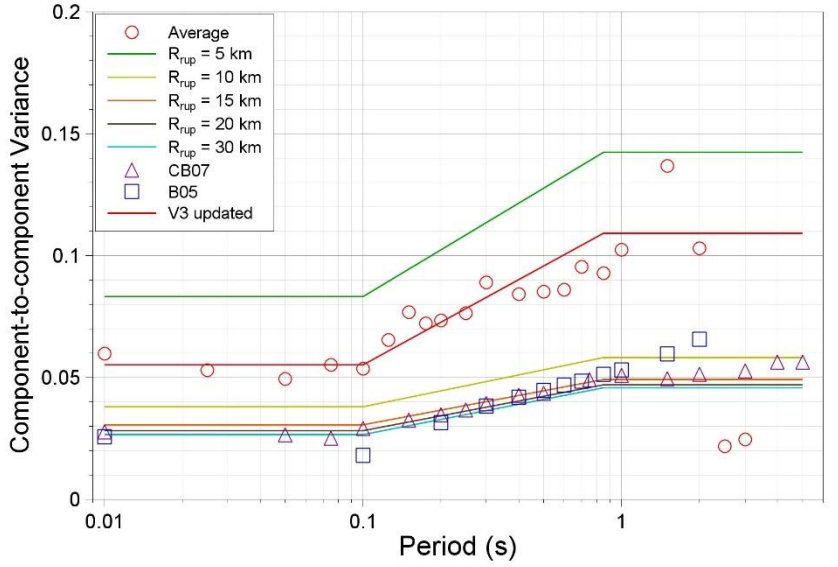

Figure A3.4. The component-to-component variability model for Groningen at different distances, compared to the data average, the updated V3 model and the tectonic models.

The high values exhibited for short distances will have a significant impact on the risk calculations, which begs the question of whether this polarisation will also persist at larger magnitudes. The polarisation observed is very likely an effect of the clear radiation pattern emitted by the nearly-point sources of small magnitude events. As ruptures elongate and events acquire the characteristics of tectonic earthquakes with larger magnitudes, it is most likely that polarisation will diminish as multiple points with opposite and different radiation patterns contribute to the waveforms recorded. Hence, we do not expect the component-to-component variability at large magnitudes to be different from that presented by published tectonic models. Therefore, we apply a magnitude-dependence to the model, whereby it will be fully applicable as presented in Figure A3.4 for the magnitude range of the data (until M 3.6) and converge linearly to tectonic values over two units of magnitude (until M 5.6). The final form of the V5 component-to-component variability model is presented in Eqs.(A3.4-6) and is shown in Figures A3.5 and A3.6.

$$\sigma^2_{c2c}(M,R) = 0.026 + 1.03\left[5.6 - \min\left(5.6, \max\left[M, 3.6\right]\right)\right]R^{-2.22} \qquad \text{for T} \leq 0.1\text{s} \quad \text{(A3.4)}$$

$$\sigma^2_{c2c}(M,R) = 0.045 + 5.315\left[5.6 - \min\left(5.6, \max\left[M, 3.6\right]\right)\right]R^{-2.92} \qquad \text{for T} \geq 0.85\text{s} \quad \text{(A3.5)}$$

$$\sigma^2_{c2c}(T,M,R) = \sigma^2_{c2c}(0.1,M,R) + \left[\frac{\log(T) - \log(0.1)}{\log(0.85) - \log(0.1)}\right]\left[\sigma^2_{c2c}(0.85,M,R) - \sigma^2_{c2c}(0.1,M,R)\right]$$

for 0.1s < T < 0.85s (A3.6)

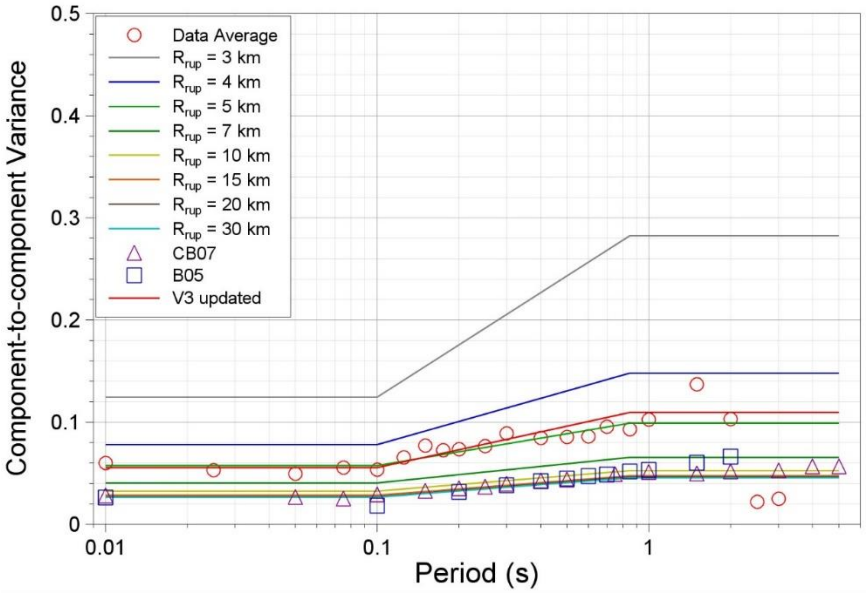

Figure A3.5. The component-to-component variance model for Groningen at different distances for M_L4.5 compared to the data average, the updated V3 model and the tectonic models.

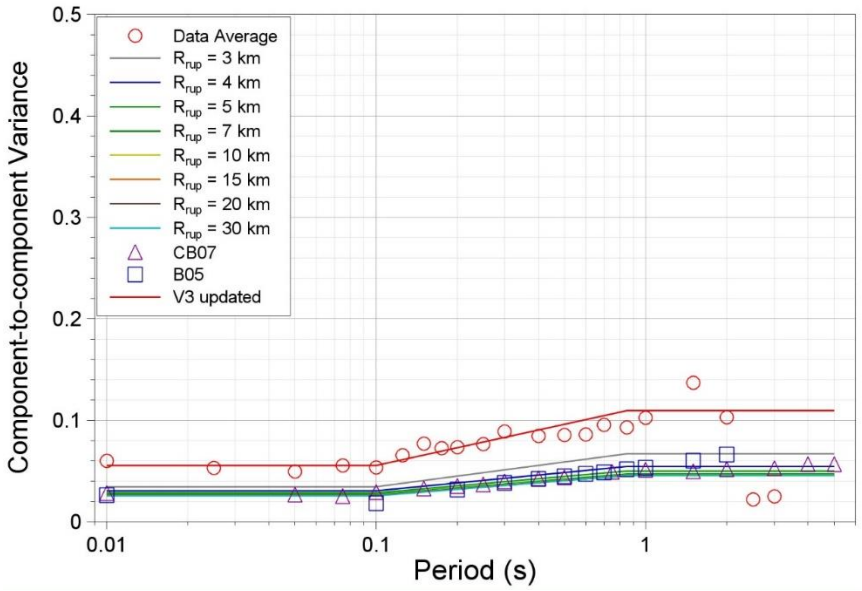

Figure A3.6. The component-to-component variance model for Groningen at different distances for M_L5.5 compared to the data average, the updated V3 model and the tectonic models.

A3.3 Distance-dependent model for c2c variability of duration

An equivalent model is derived for duration and presented in Eq. (A3.7). Figure A3.7 compares the model to the individual component-to-component variances of duration of the arbitrary components of the records.

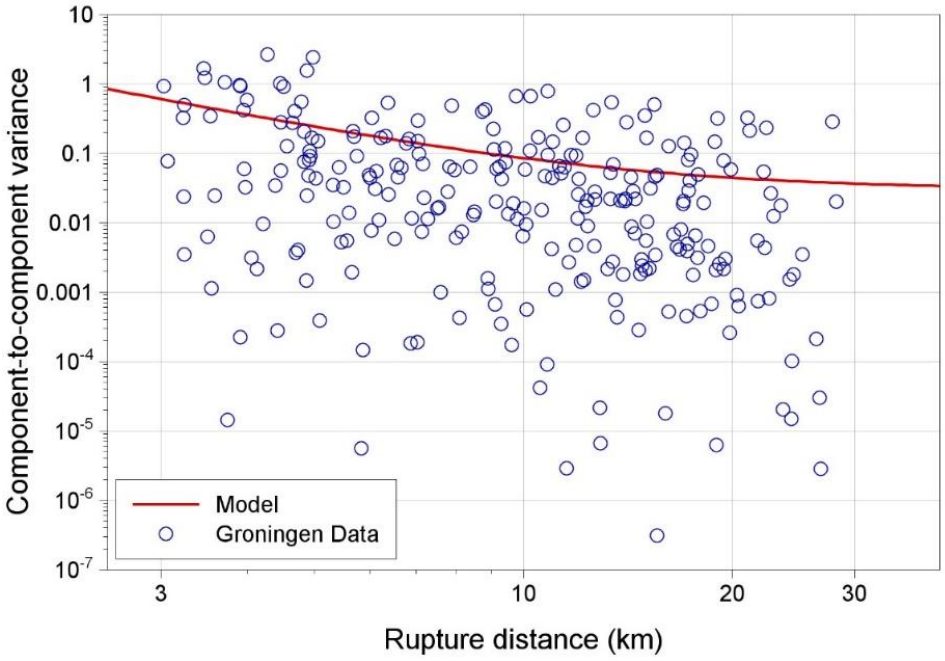

Figure A3.7. Comparison of the V5 durations c2c variability model and the component-to-component variances of the durations of the Groningen records

The model has the same functional form as the model for spectral acceleration, and has been fixed to converge to the values of the tectonic model of Bommer *et al*. (2009) at large magnitudes and longer distances:

$$\sigma^2_{c2c}(R) = 0.0299 + 2.434\left[5.6 - \min\left[5.6, \max(M, 3.6)\right]\right]R^{-1.95} \qquad \text{(A3.7)}$$

Figure A3.8 displays the magnitude scaling of the model at different distances.

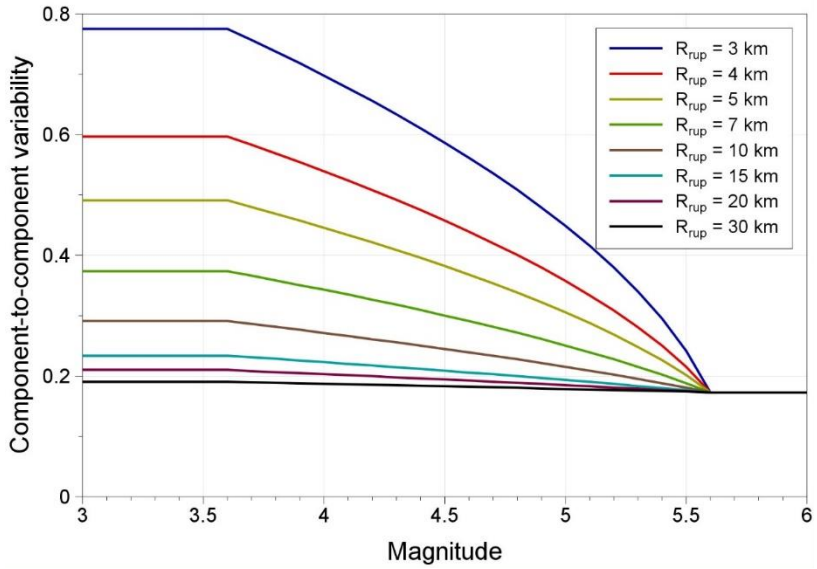

Figure A3.8. Comparison of the V5 durations c2c variability model and the component-to-component variances of the durations of the Groningen records

APPENDIX IV

Median Predictions of Motions at NS_B

The V4 model medians are shown in *dashed* while the V5 model medians in *full* lines.

A4.1 Plots of median predictions at NS_B shown with respect to distance

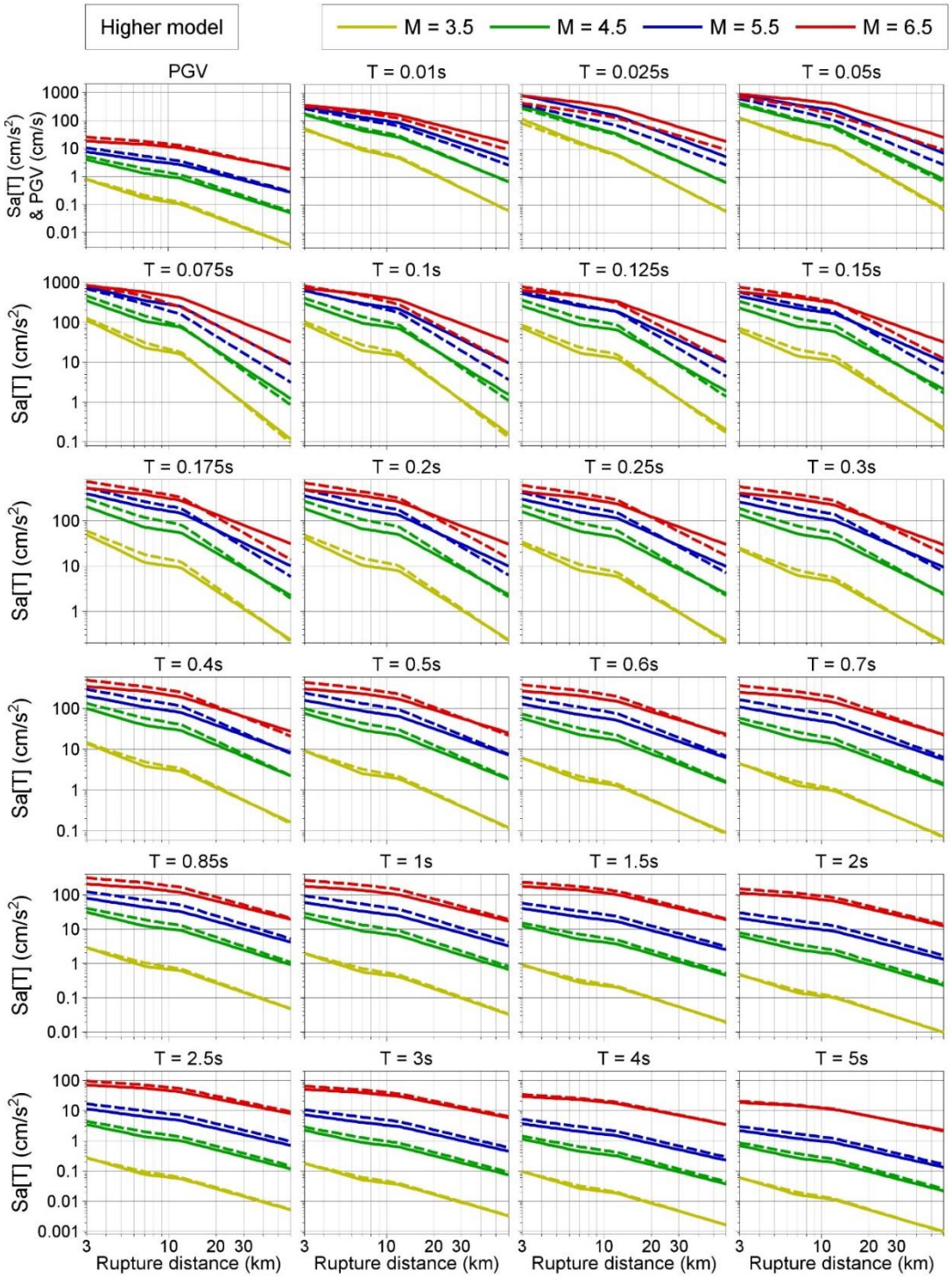

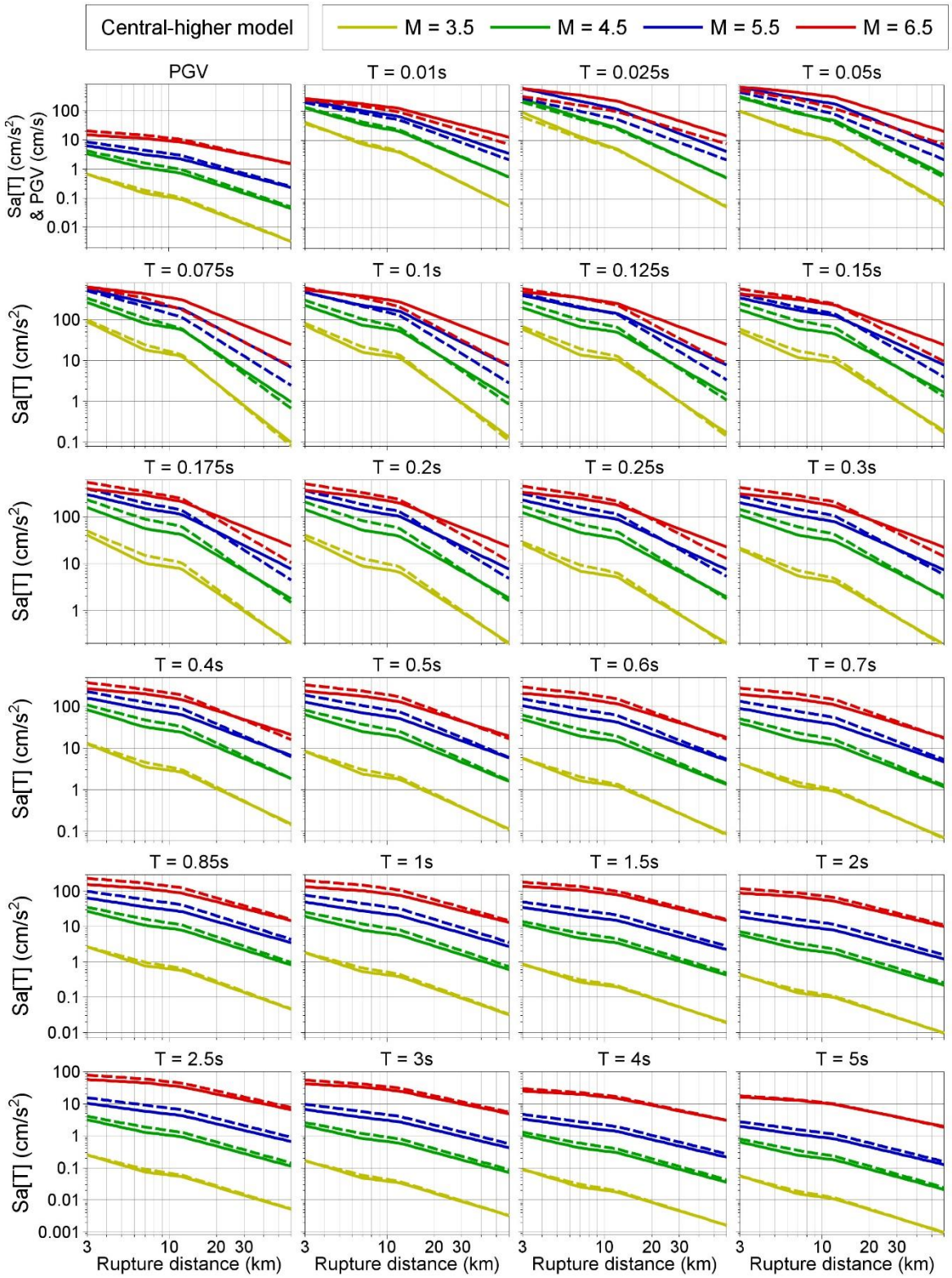
Central-higher model
M = 3.5
M = 4.5
M = 5.5
M = 6.5
PGV
T = 0.01s
T = 0.025s
T = 0.05s
T = 0.075s
T = 0.1s
T = 0.125s
T = 0.15s
T = 0.175s
T = 0.2s
T = 0.25s
T = 0.3s
T = 0.4s
T = 0.5s
T = 0.6s
T = 0.7s
T = 0.85s
T = 1s
T = 1.5s
T = 2s
T = 2.5s
T = 3s
T = 4s
T = 5s
Sa[T] (cm/s²) & PGV (cm/s)
Sa[T] (cm/s²)
Rupture distance (km)

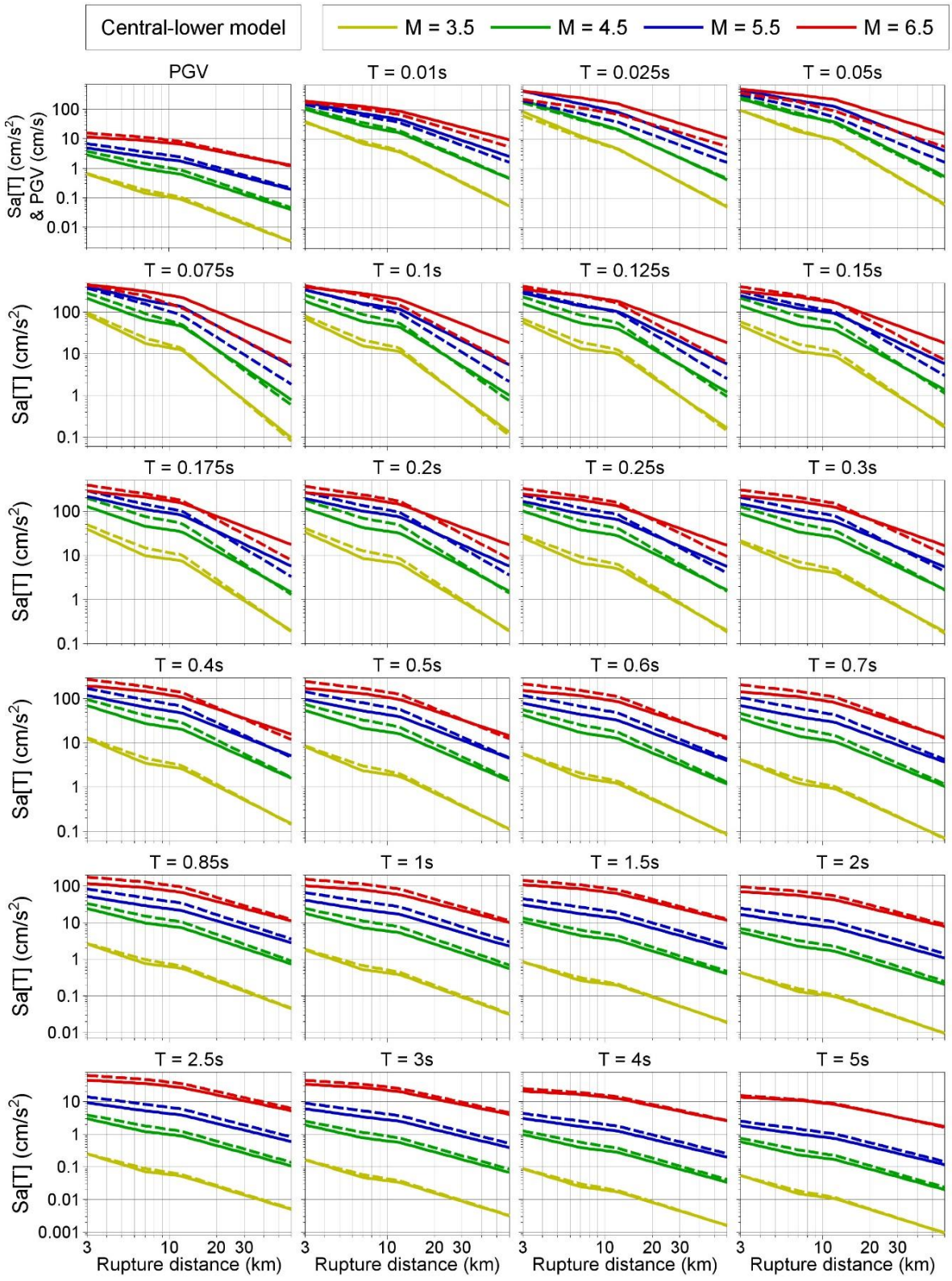
Central-lower model
M = 3.5
M = 4.5
M = 5.5
M = 6.5
PGV
T = 0.01s
T = 0.025s
T = 0.05s
T = 0.075s
T = 0.1s
T = 0.125s
T = 0.15s
T = 0.175s
T = 0.2s
T = 0.25s
T = 0.3s
T = 0.4s
T = 0.5s
T = 0.6s
T = 0.7s
T = 0.85s
T = 1s
T = 1.5s
T = 2s
T = 2.5s
T = 3s
T = 4s
T = 5s
Sa[T] (cm/s²) & PGV (cm/s)
Sa[T] (cm/s²)
Rupture distance (km)

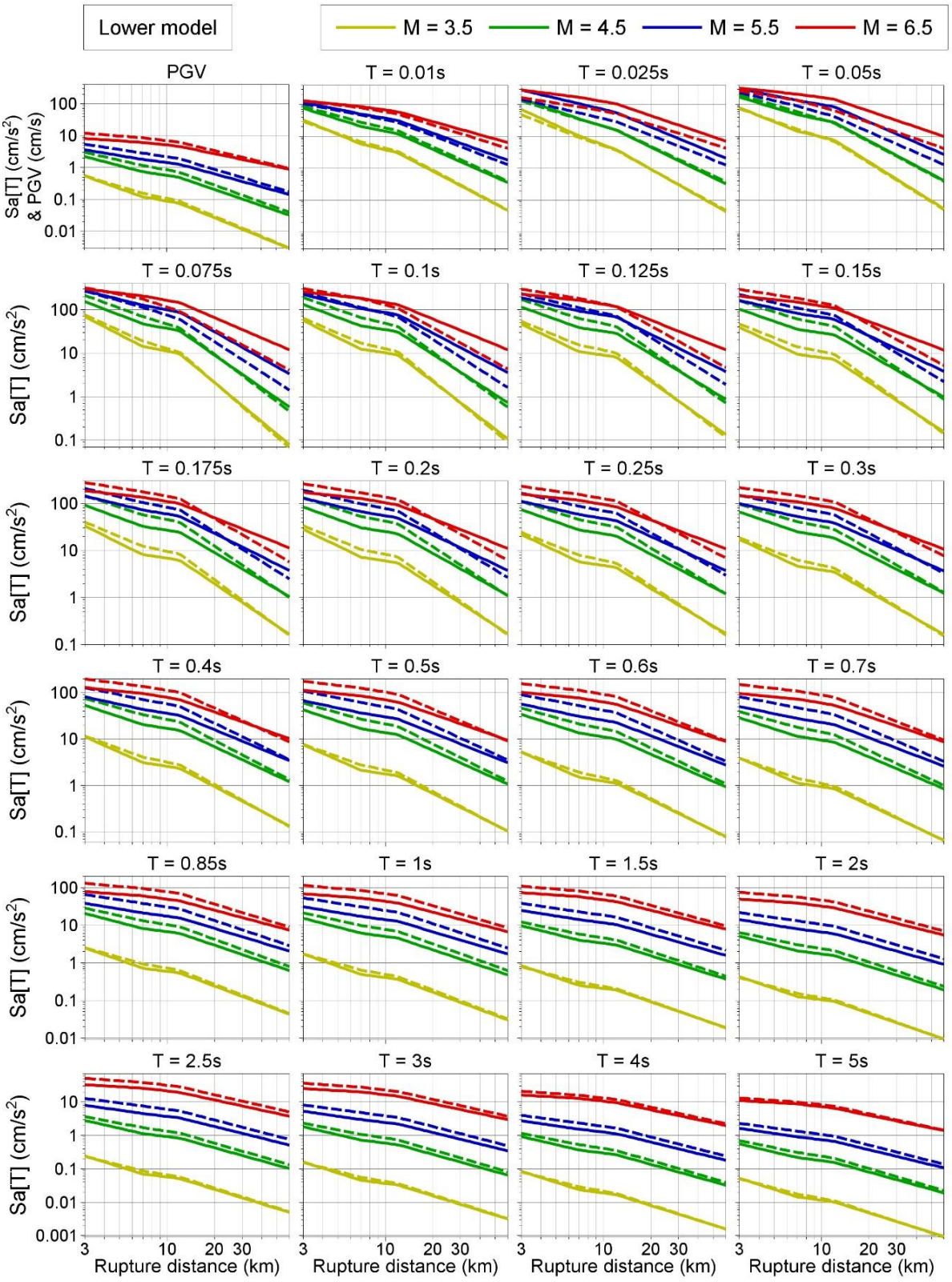
Lower model
M = 3.5
M = 4.5
M = 5.5
M = 6.5
PGV
T = 0.01s
T = 0.025s
T = 0.05s
T = 0.075s
T = 0.1s
T = 0.125s
T = 0.15s
T = 0.175s
T = 0.2s
T = 0.25s
T = 0.3s
T = 0.4s
T = 0.5s
T = 0.6s
T = 0.7s
T = 0.85s
T = 1s
T = 1.5s
T = 2s
T = 2.5s
T = 3s
T = 4s
T = 5s
Sa[T] (cm/s²) & PGV (cm/s)
Sa[T] (cm/s²)
Rupture distance (km)

A4.2 Response Spectra

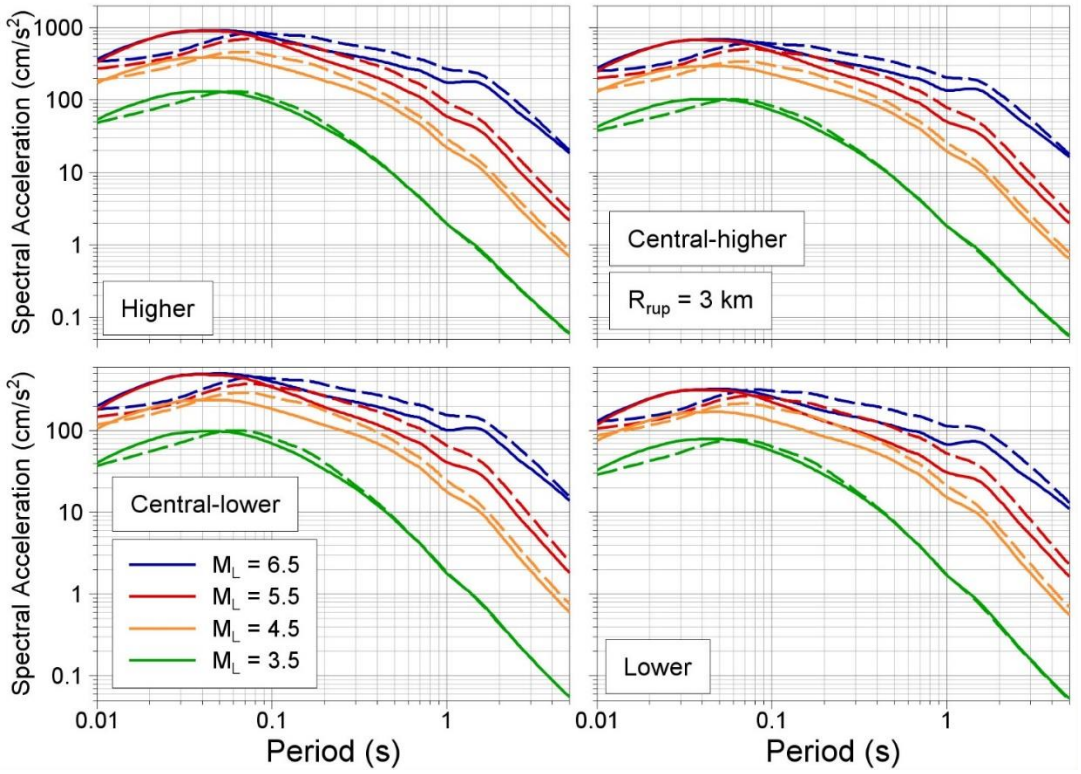

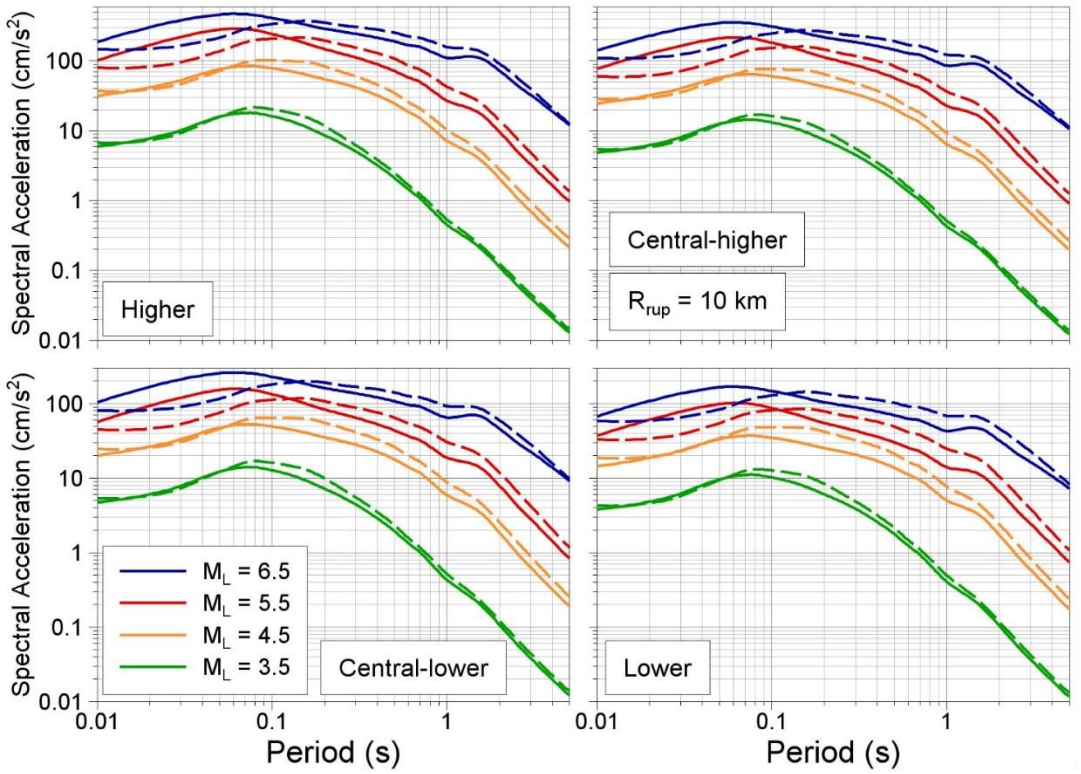

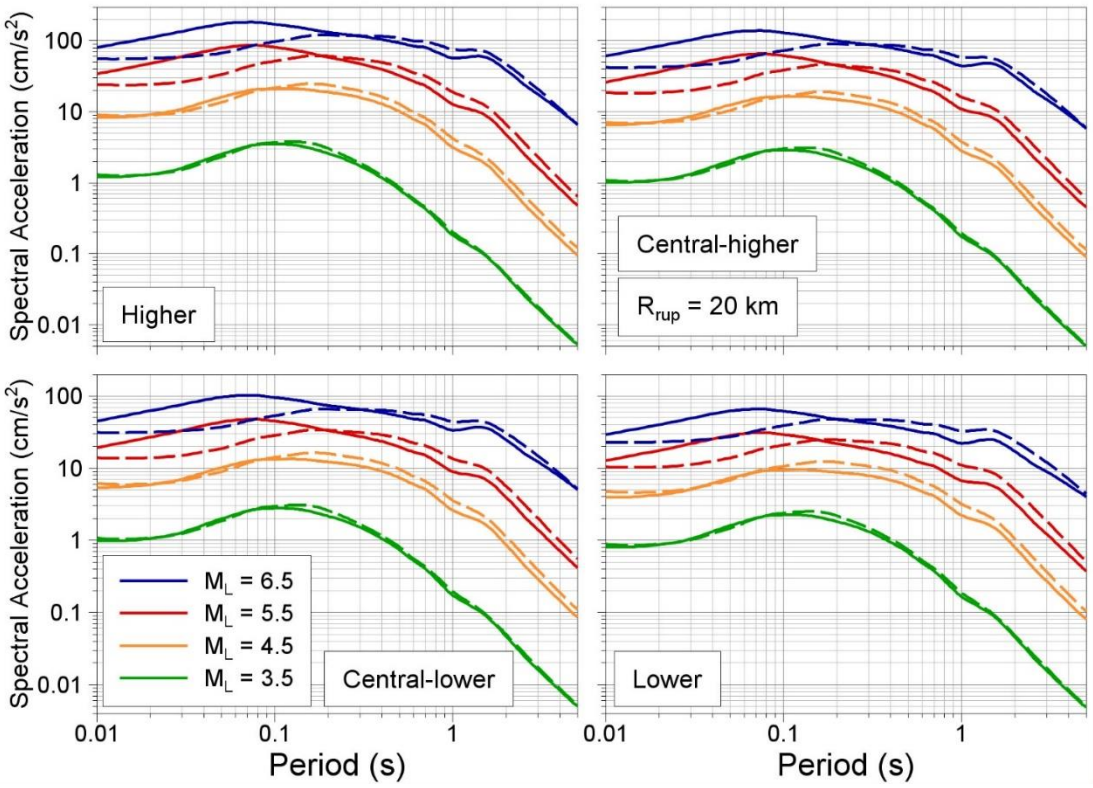
Spectral Acceleration (cm/s²)
100
10
1
0.1
0.01
Higher
Central-higher
R_rup = 20 km
M_L = 6.5
M_L = 5.5
M_L = 4.5
M_L = 3.5
Central-lower
Lower
0.01
0.1
1
Period (s)

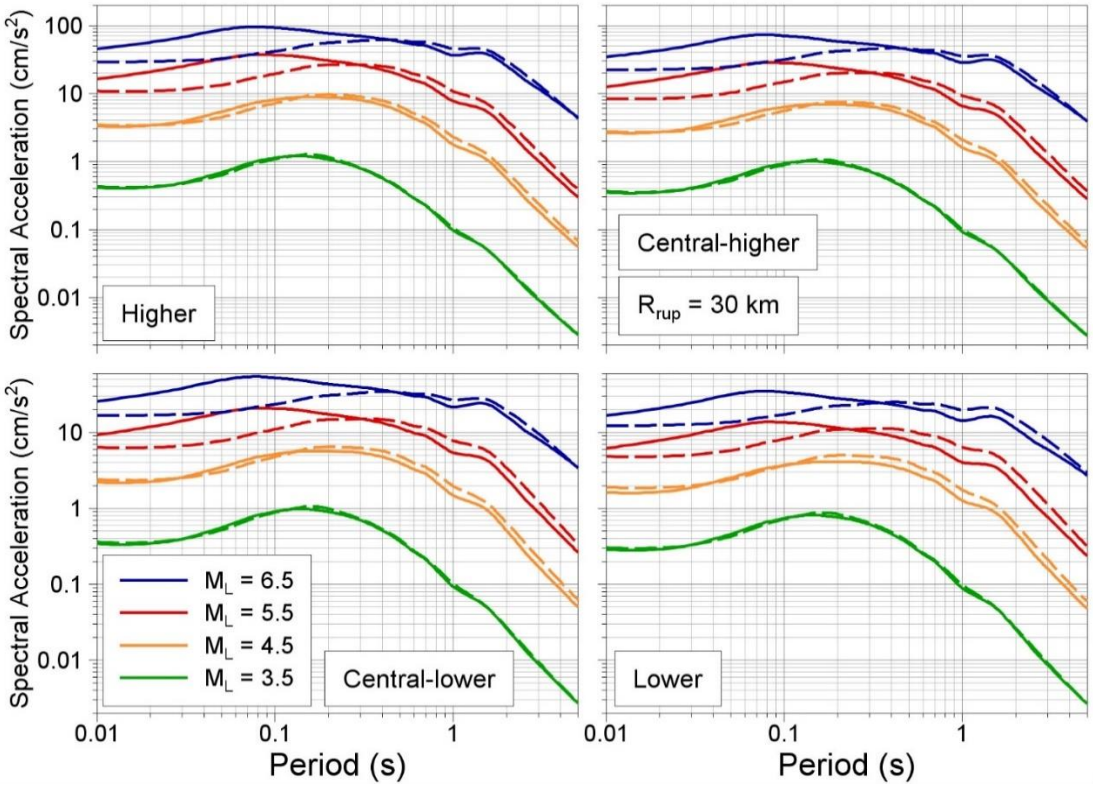
Spectral Acceleration (cm/s²)
100
10
1
0.1
0.01
Higher
Central-higher
R_rup = 30 km
M_L = 6.5
M_L = 5.5
M_L = 4.5
M_L = 3.5
Central-lower
Lower
0.01
0.1
1
Period (s)

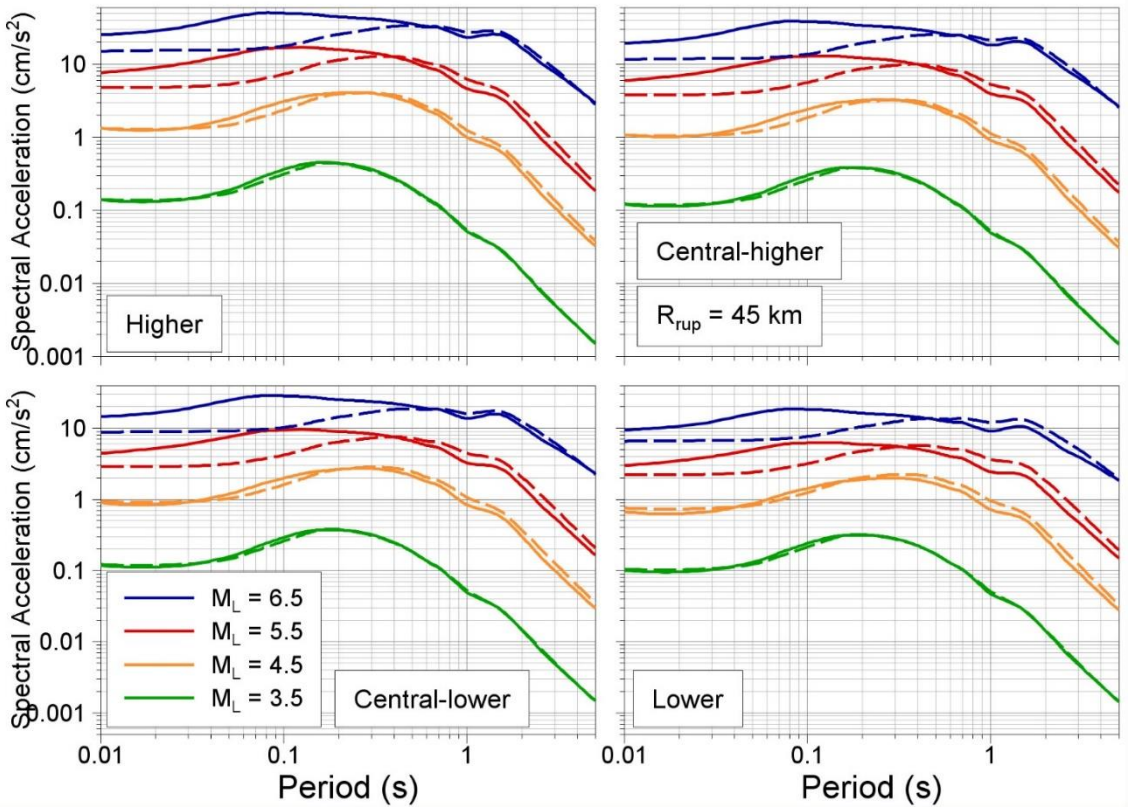
Spectral Acceleration (cm/s²)
10
1
0.1
0.01
0.001
Higher
Central-higher
R_rup = 45 km
M_L = 6.5
M_L = 5.5
M_L = 4.5
M_L = 3.5
Central-lower
Lower
0.01
0.1
1
Period (s)

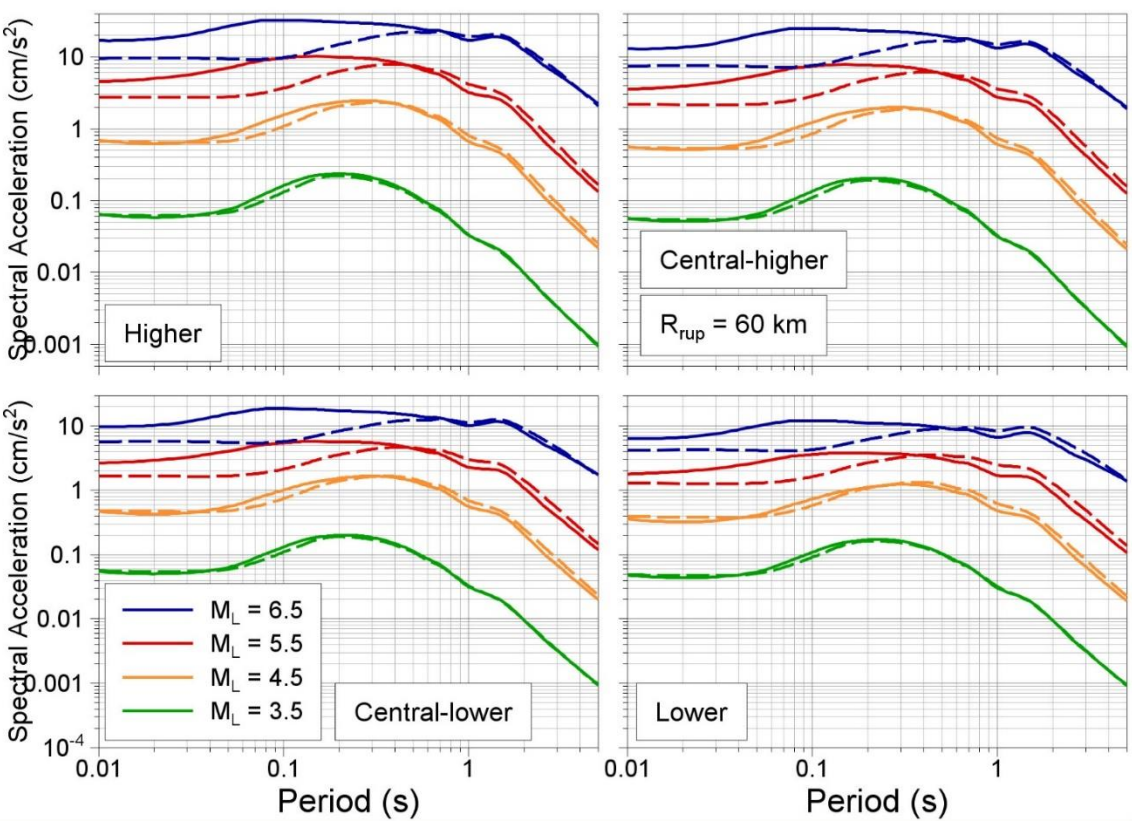
Spectral Acceleration (cm/s²)
10
1
0.1
0.01
0.001
10⁻⁴
Higher
Central-higher
R_rup = 60 km
M_L = 6.5
M_L = 5.5
M_L = 4.5
M_L = 3.5
Central-lower
Lower
0.01
0.1
1
Period (s)

A4.3 Plots of median predictions at NS_B shown with respect to magnitude

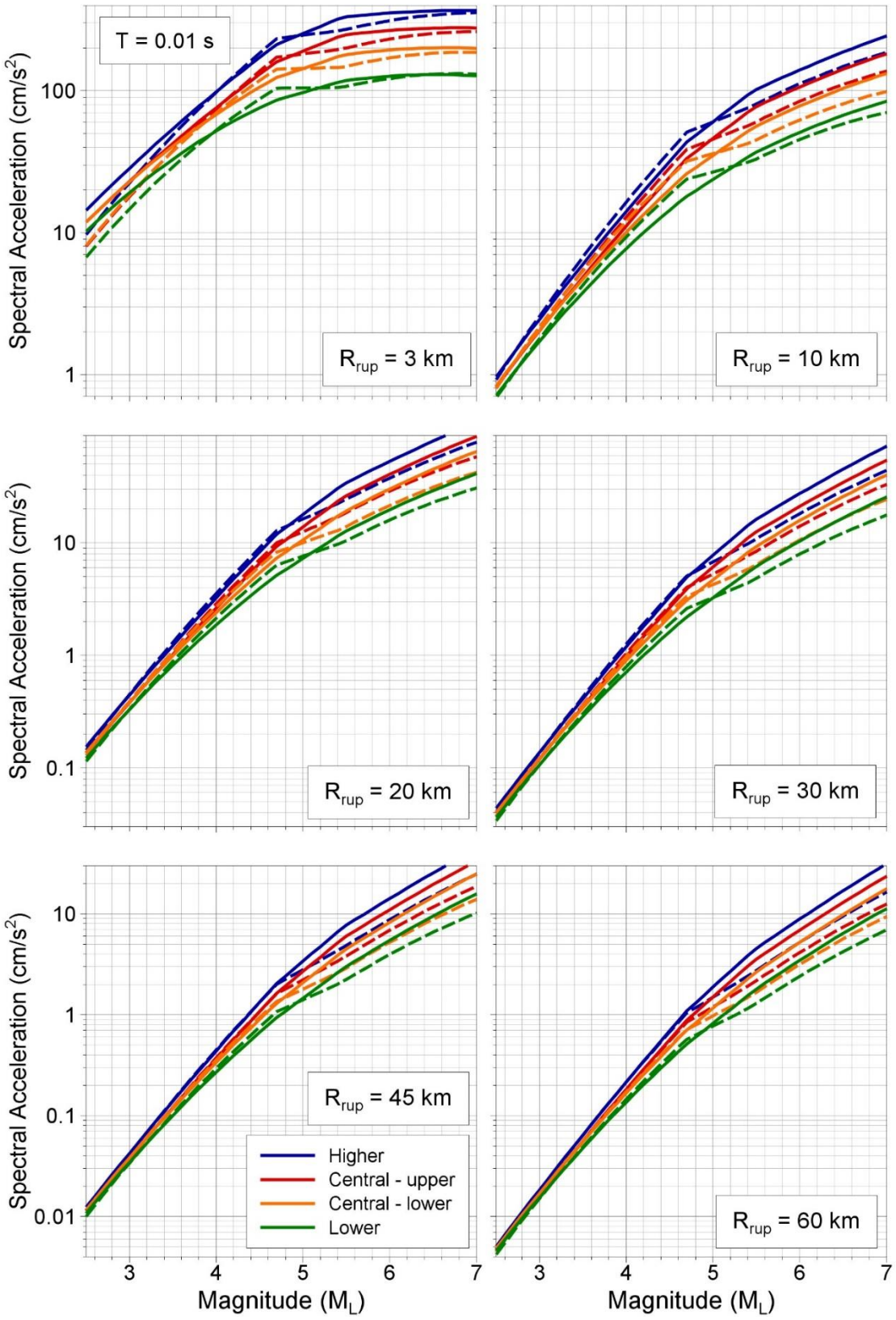

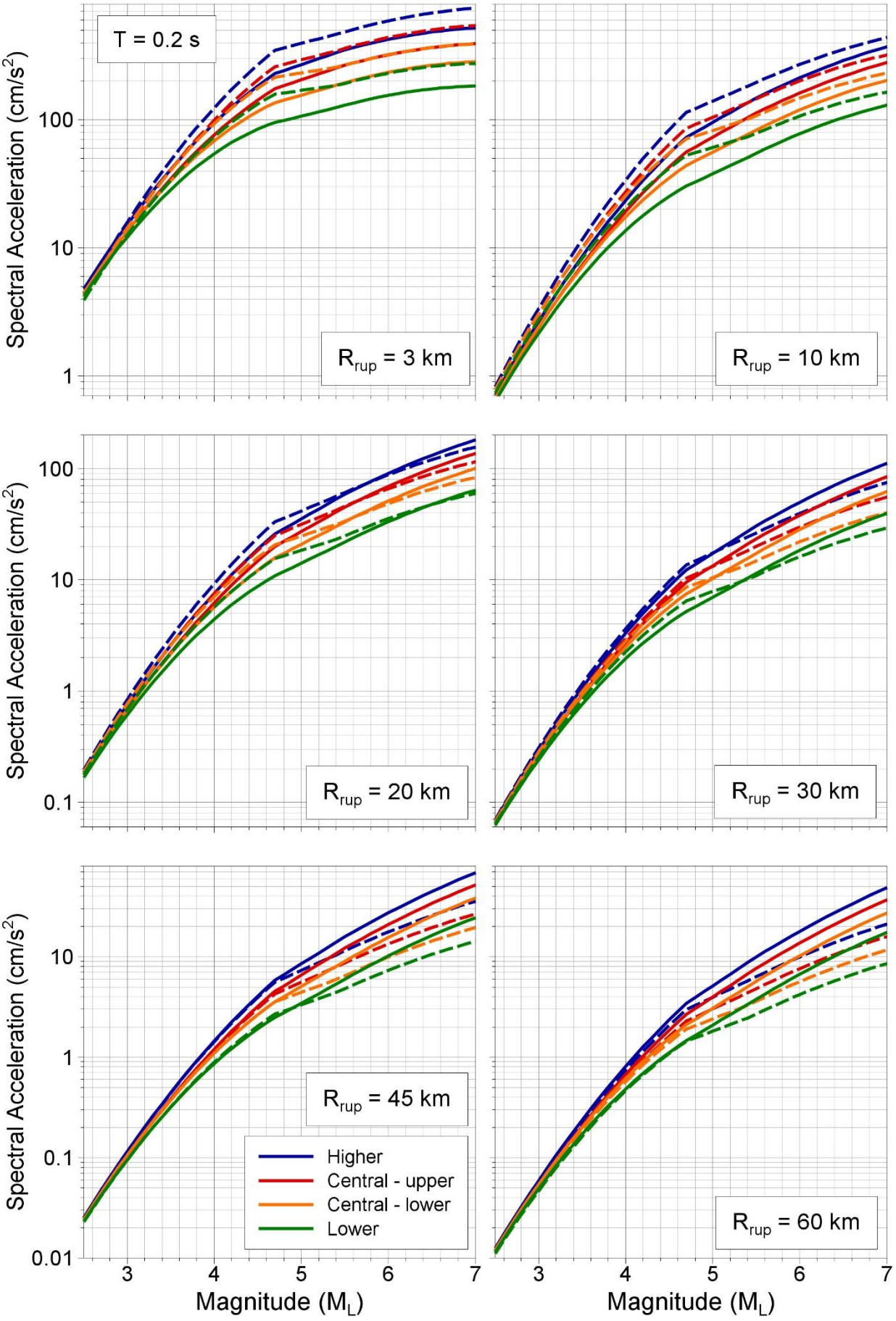
T = 0.2 s
R_rup = 3 km
R_rup = 10 km
R_rup = 20 km
R_rup = 30 km
R_rup = 45 km
R_rup = 60 km
Higher
Central - upper
Central - lower
Lower
Spectral Acceleration (cm/s²)
Magnitude (M_L)
100
10
1
0.1
0.01
3
4
5
6
7

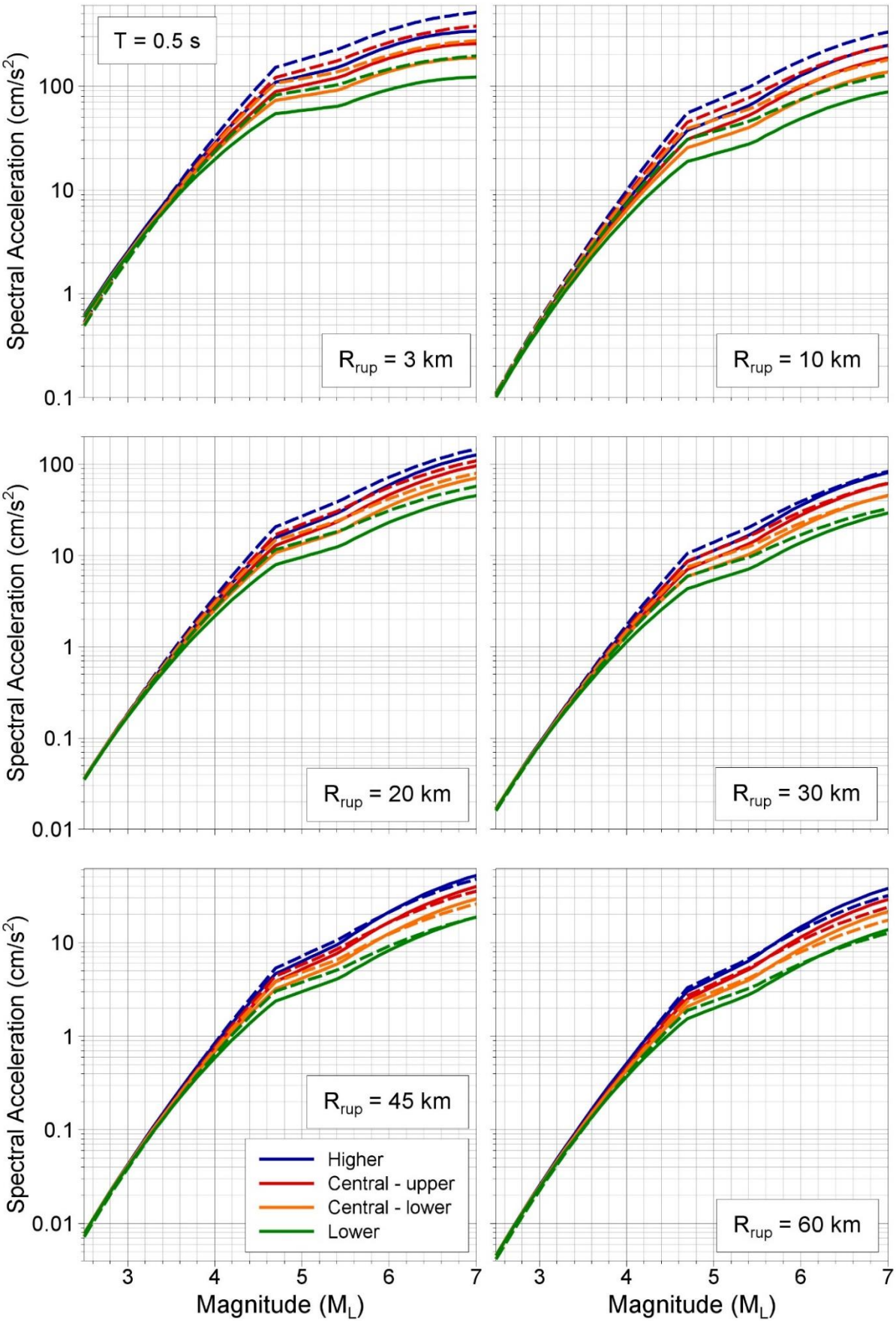
T = 0.5 s
R_rup = 3 km
R_rup = 10 km
R_rup = 20 km
R_rup = 30 km
R_rup = 45 km
R_rup = 60 km
Higher
Central - upper
Central - lower
Lower
Spectral Acceleration (cm/s²)
Magnitude (M_L)
0.01
0.1
1
10
100
3
4
5
6
7

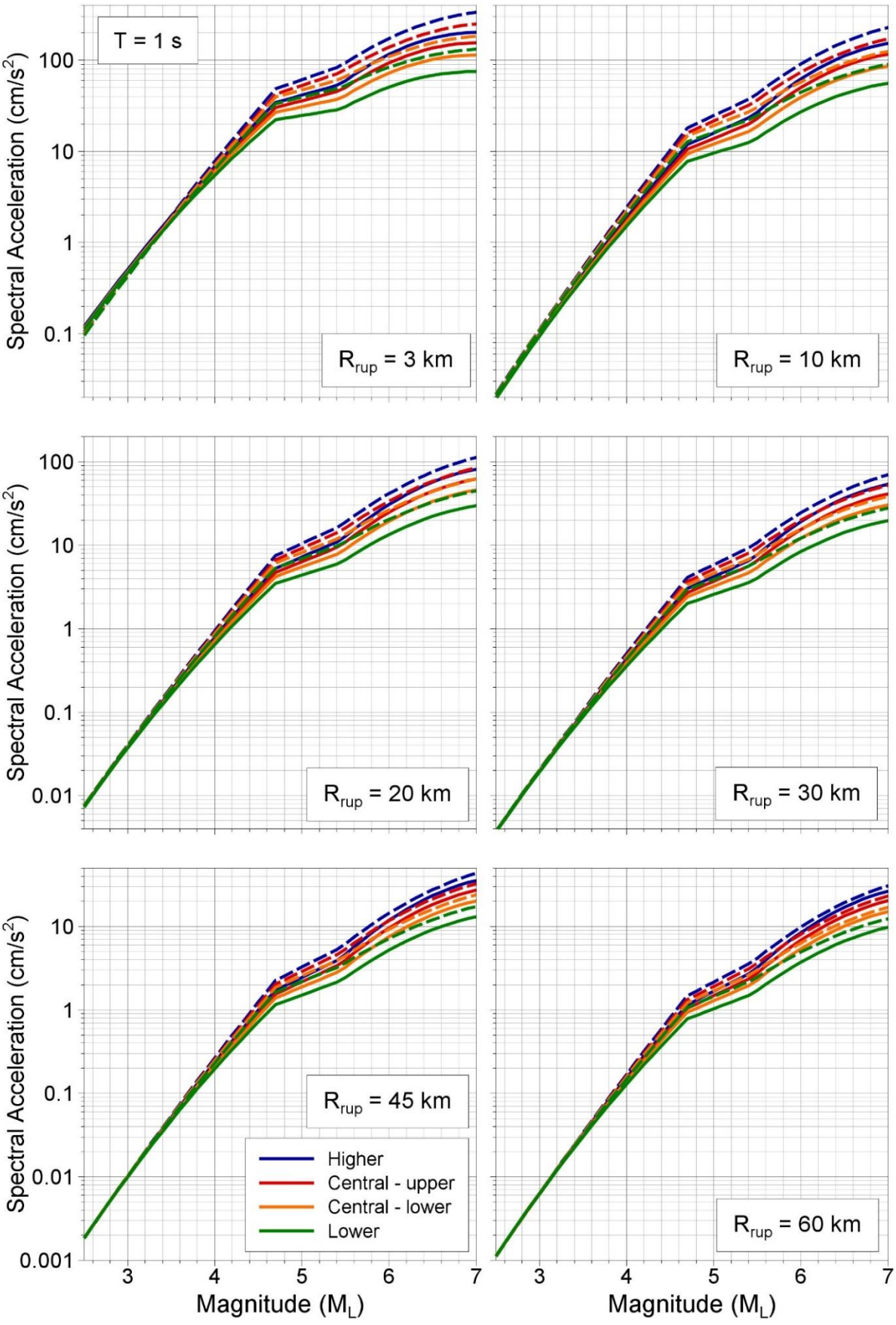
T = 1 s
R_{rup} = 3 km
R_{rup} = 10 km
R_{rup} = 20 km
R_{rup} = 30 km
R_{rup} = 45 km
R_{rup} = 60 km
Higher
Central - upper
Central - lower
Lower
Spectral Acceleration (cm/s^2)
Magnitude (M_L)
100
10
1
0.1
0.01
0.001
3
4
5
6
7

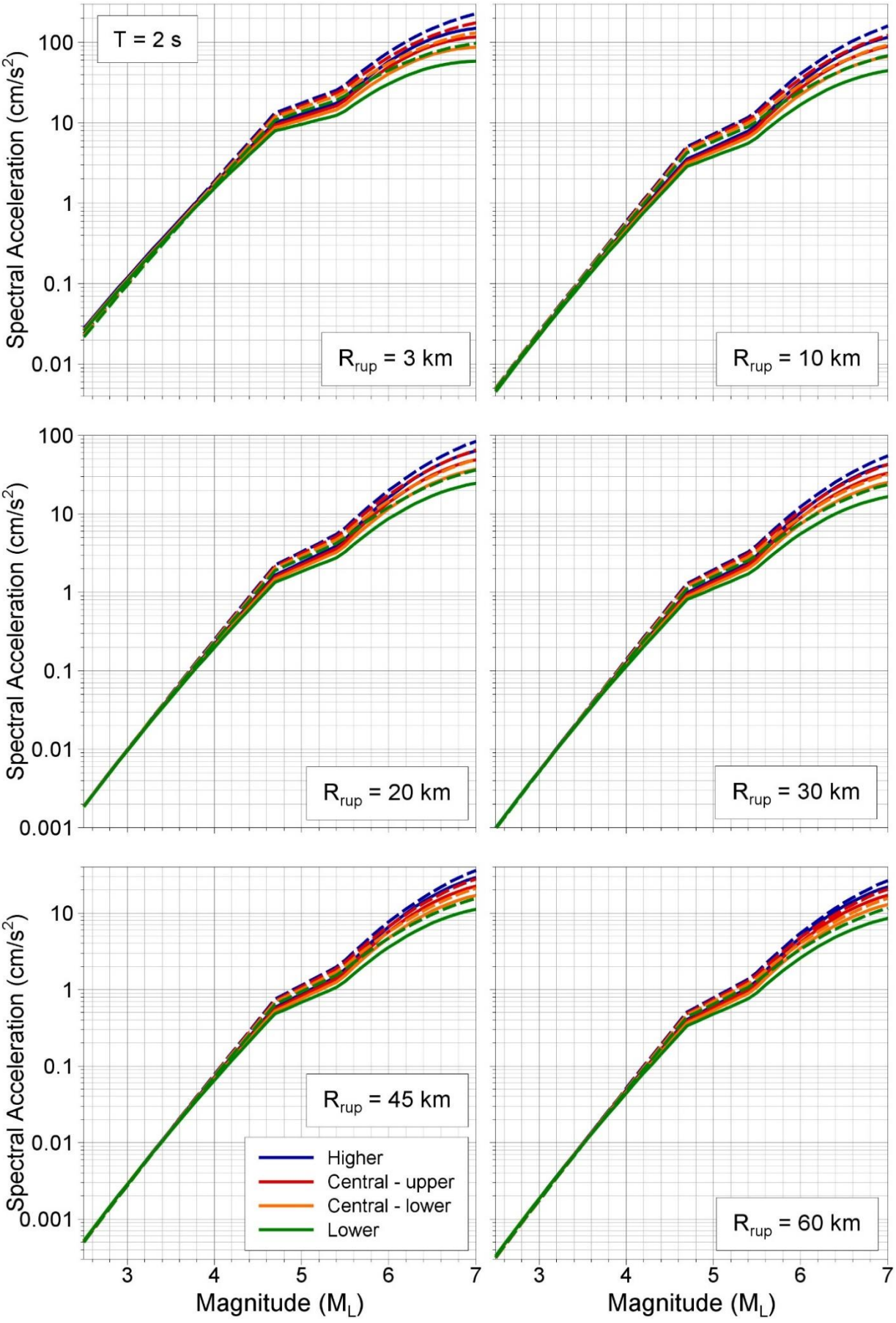
T = 2 s
R_rup = 3 km
R_rup = 10 km
R_rup = 20 km
R_rup = 30 km
R_rup = 45 km
R_rup = 60 km
Higher
Central - upper
Central - lower
Lower
Spectral Acceleration (cm/s²)
Magnitude (M_L)
100
10
1
0.1
0.01
0.001
3
4
5
6
7

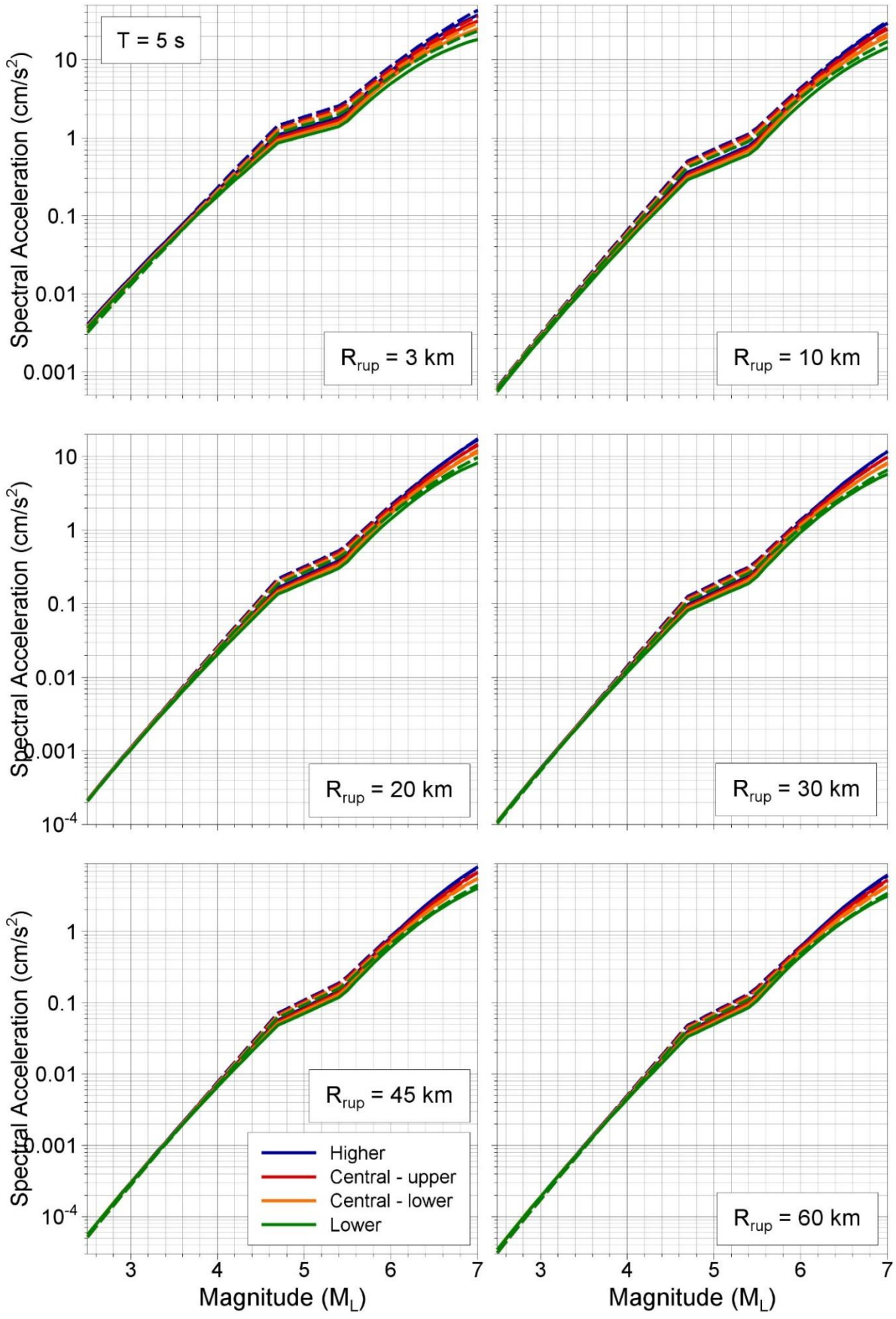
T = 5 s
R_{rup} = 3 km
R_{rup} = 10 km
R_{rup} = 20 km
R_{rup} = 30 km
R_{rup} = 45 km
R_{rup} = 60 km
Higher
Central - upper
Central - lower
Lower
Spectral Acceleration (cm/s^2)
Magnitude (M_L)

APPENDIX V

Stations *vs* Zone Linear AFs

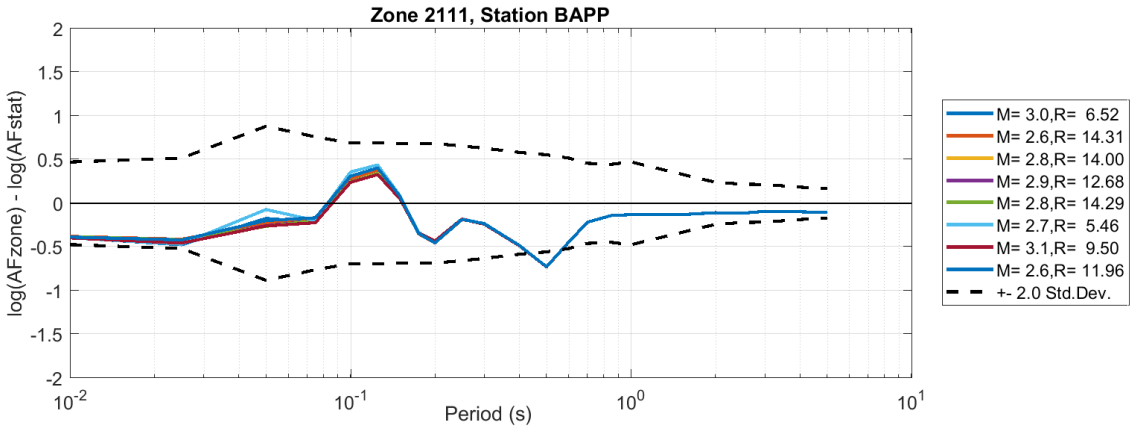

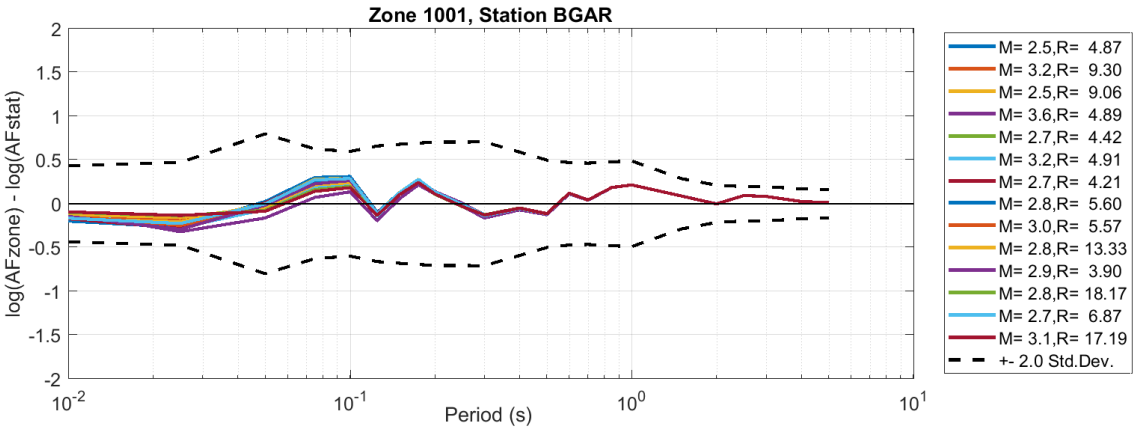

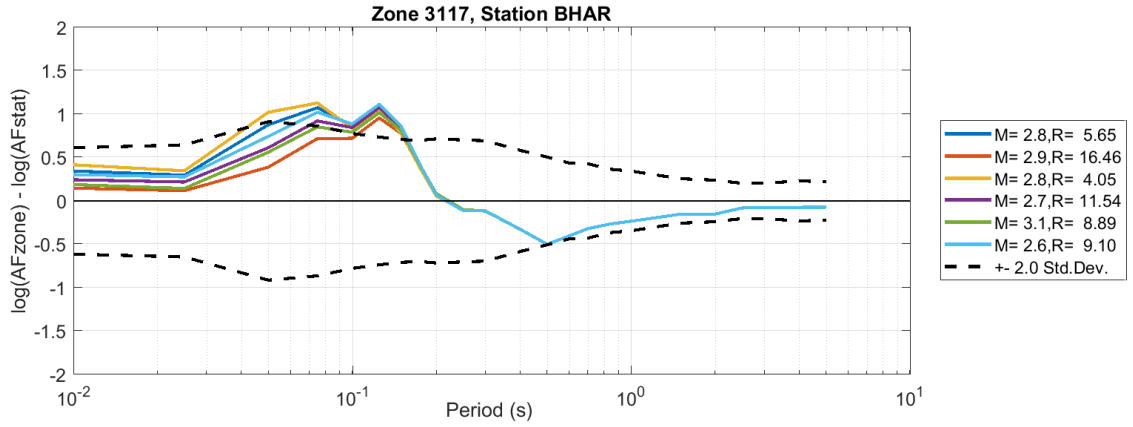

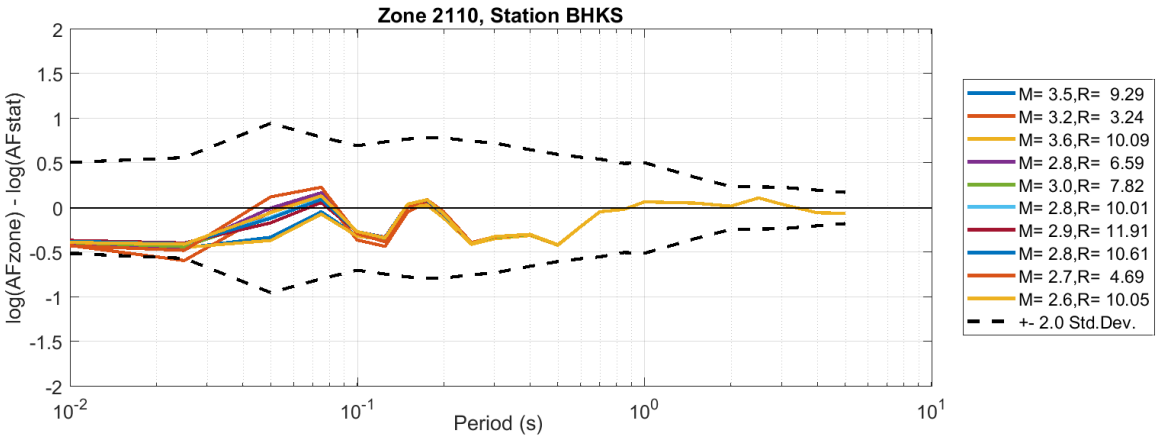
Zone 2110, Station BHKS
log(AFzone) - log(AFstat)
Period (s)
M= 3.5,R= 9.29
M= 3.2,R= 3.24
M= 3.6,R= 10.09
M= 2.8,R= 6.59
M= 3.0,R= 7.82
M= 2.8,R= 10.01
M= 2.9,R= 11.91
M= 2.8,R= 10.61
M= 2.7,R= 4.69
M= 2.6,R= 10.05
+- 2.0 Std.Dev.

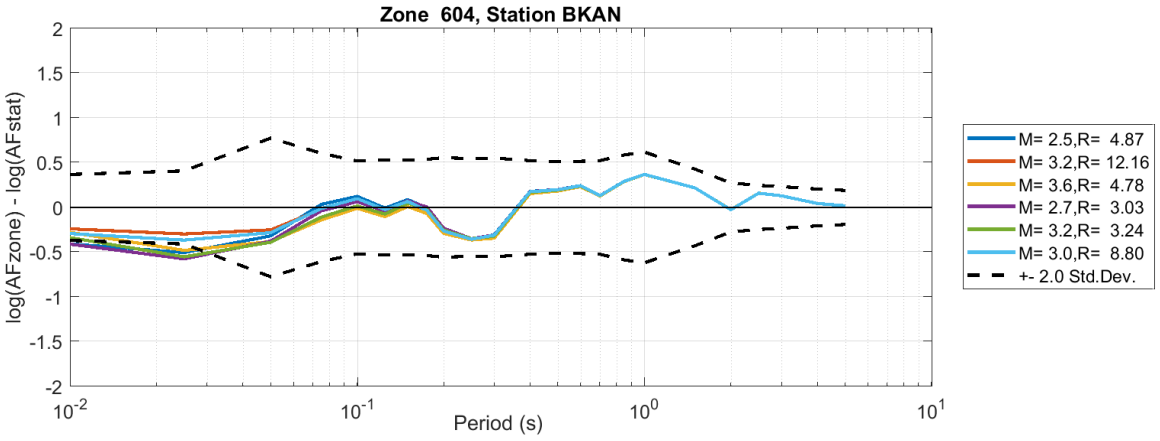
Zone 604, Station BKAN
log(AFzone) - log(AFstat)
Period (s)
M= 2.5,R= 4.87
M= 3.2,R= 12.16
M= 3.6,R= 4.78
M= 2.7,R= 3.03
M= 3.2,R= 3.24
M= 3.0,R= 8.80
+- 2.0 Std.Dev.

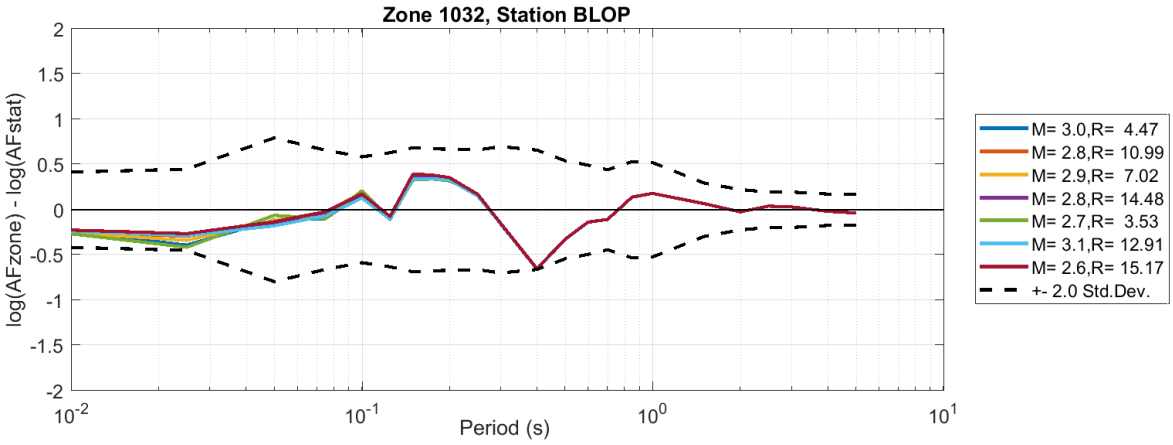
Zone 1032, Station BLOP
log(AFzone) - log(AFstat)
Period (s)
M= 3.0,R= 4.47
M= 2.8,R= 10.99
M= 2.9,R= 7.02
M= 2.8,R= 14.48
M= 2.7,R= 3.53
M= 3.1,R= 12.91
M= 2.6,R= 15.17
+- 2.0 Std.Dev.

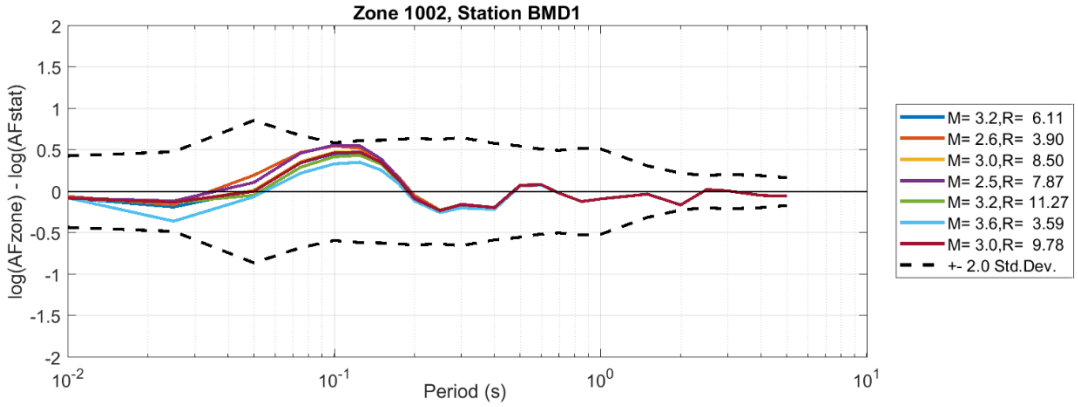
Zone 1002, Station BMD1
log(AFzone) - log(AFstat)
Period (s)
M= 3.2,R= 6.11
M= 2.6,R= 3.90
M= 3.0,R= 8.50
M= 2.5,R= 7.87
M= 3.2,R= 11.27
M= 3.6,R= 3.59
M= 3.0,R= 9.78
+- 2.0 Std.Dev.

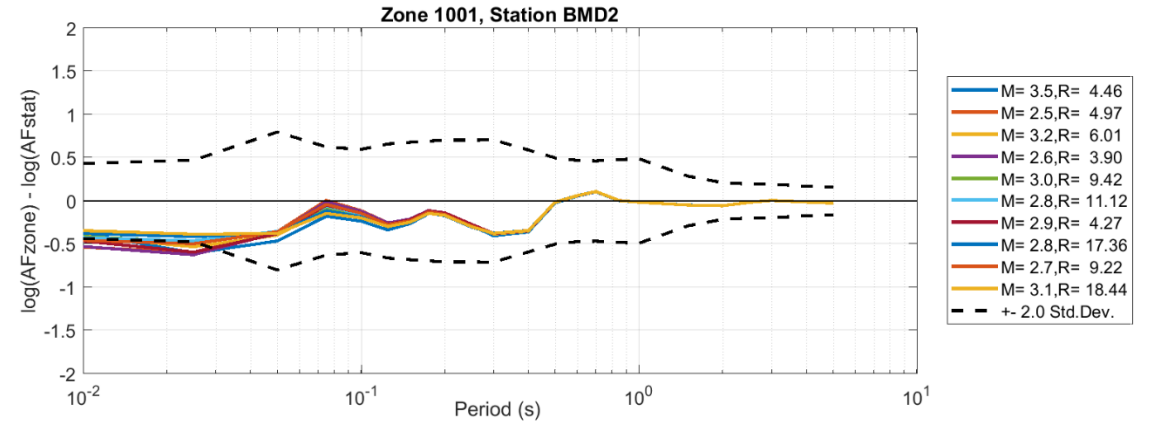
Zone 1001, Station BMD2
log(AFzone) - log(AFstat)
Period (s)
M= 3.5,R= 4.46
M= 2.5,R= 4.97
M= 3.2,R= 6.01
M= 2.6,R= 3.90
M= 3.0,R= 9.42
M= 2.8,R= 11.12
M= 2.9,R= 4.27
M= 2.8,R= 17.36
M= 2.7,R= 9.22
M= 3.1,R= 18.44
+- 2.0 Std.Dev.

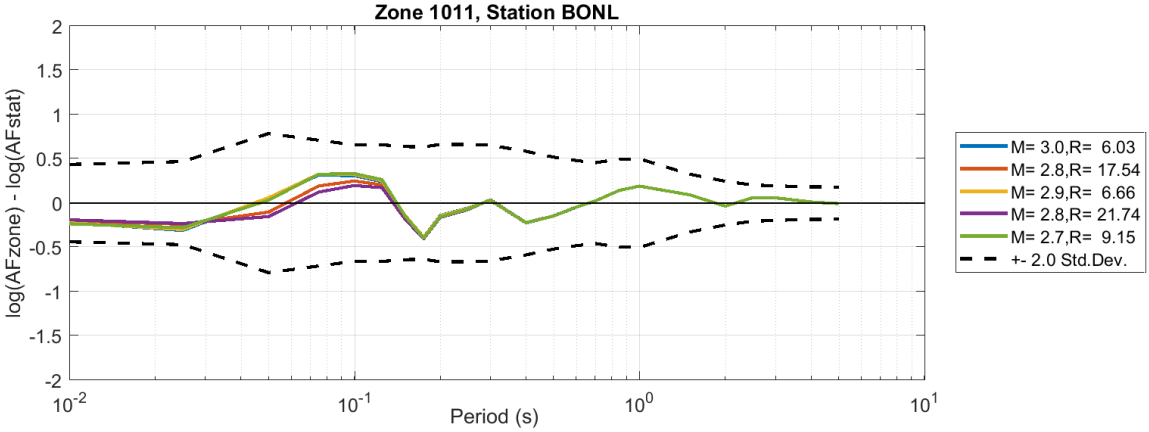
Zone 1011, Station BONL
log(AFzone) - log(AFstat)
Period (s)
M= 3.0,R= 6.03
M= 2.8,R= 17.54
M= 2.9,R= 6.66
M= 2.8,R= 21.74
M= 2.7,R= 9.15
+- 2.0 Std.Dev.

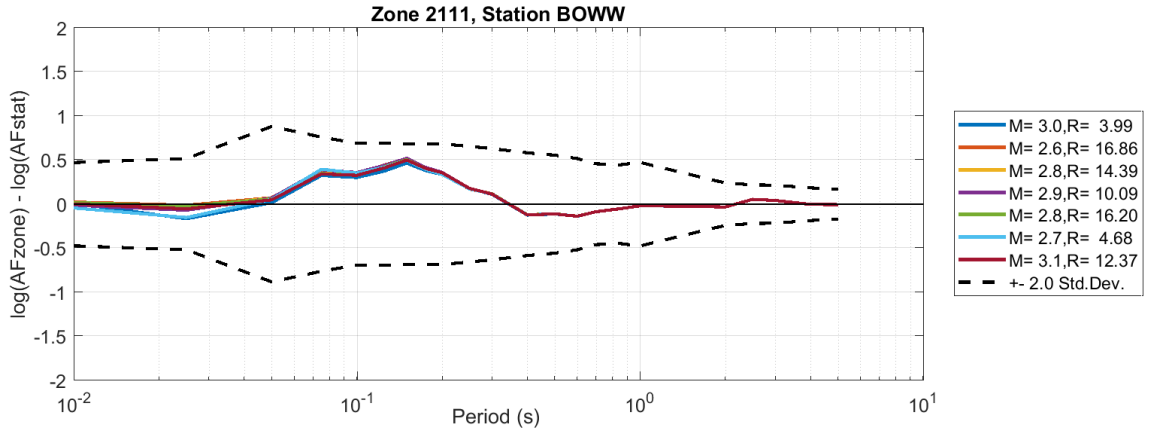
Zone 2111, Station BOWW
log(AFzone) - log(AFstat)
Period (s)
M= 3.0,R= 3.99
M= 2.6,R= 16.86
M= 2.8,R= 14.39
M= 2.9,R= 10.09
M= 2.8,R= 16.20
M= 2.7,R= 4.68
M= 3.1,R= 12.37
+- 2.0 Std.Dev.

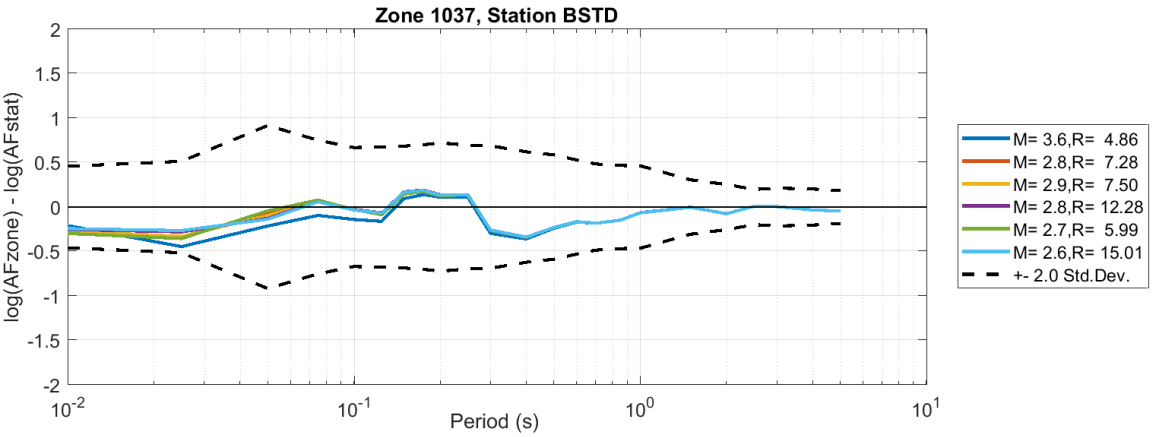
Zone 1037, Station BSTD
log(AFzone) - log(AFstat)
Period (s)
M= 3.6,R= 4.86
M= 2.8,R= 7.28
M= 2.9,R= 7.50
M= 2.8,R= 12.28
M= 2.7,R= 5.99
M= 2.6,R= 15.01
+- 2.0 Std.Dev.

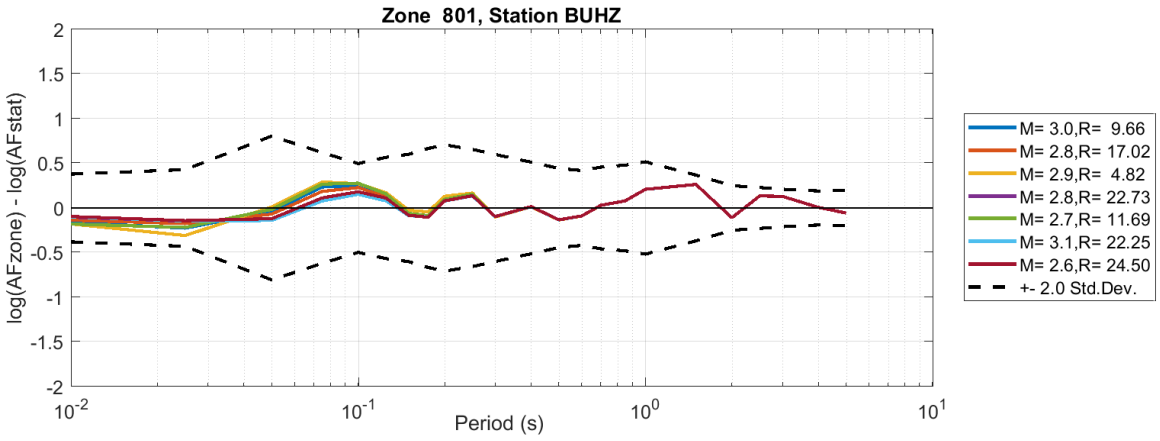
Zone 801, Station BUHZ
log(AFzone) - log(AFstat)
Period (s)
M= 3.0,R= 9.66
M= 2.8,R= 17.02
M= 2.9,R= 4.82
M= 2.8,R= 22.73
M= 2.7,R= 11.69
M= 3.1,R= 22.25
M= 2.6,R= 24.50
+- 2.0 Std.Dev.

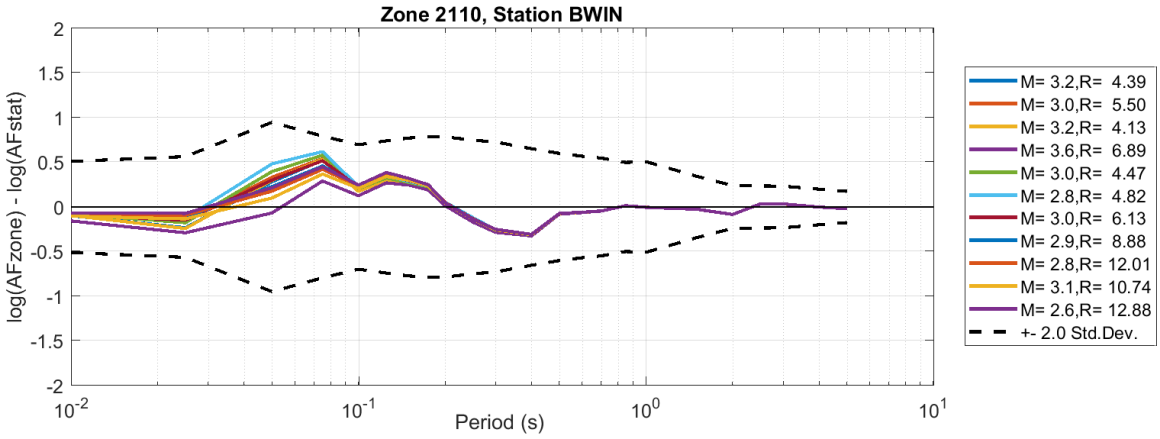
Zone 2110, Station BWIN
log(AFzone) - log(AFstat)
Period (s)
M= 3.2,R= 4.39
M= 3.0,R= 5.50
M= 3.2,R= 4.13
M= 3.6,R= 6.89
M= 3.0,R= 4.47
M= 2.8,R= 4.82
M= 3.0,R= 6.13
M= 2.9,R= 8.88
M= 2.8,R= 12.01
M= 3.1,R= 10.74
M= 2.6,R= 12.88
+- 2.0 Std.Dev.

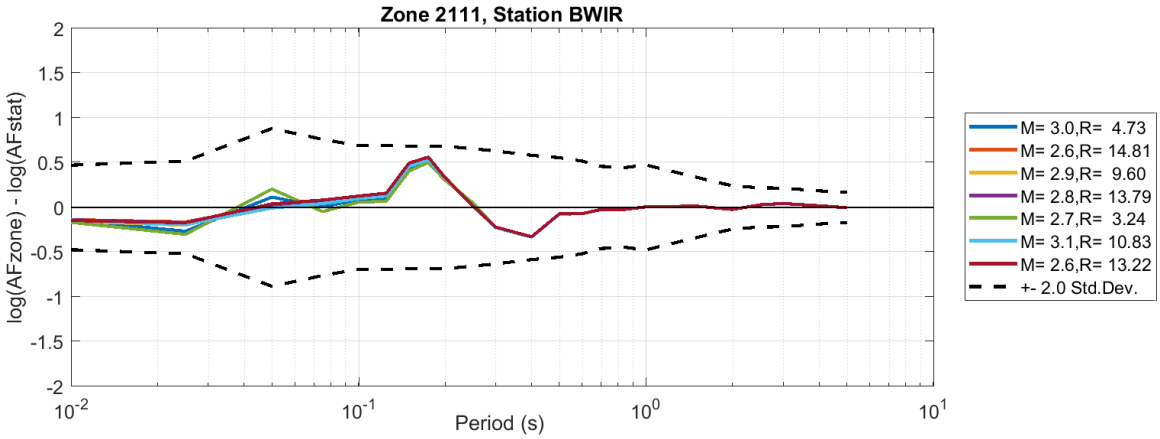
Zone 2111, Station BWIR
log(AFzone) - log(AFstat)
Period (s)
M= 3.0,R= 4.73
M= 2.6,R= 14.81
M= 2.9,R= 9.60
M= 2.8,R= 13.79
M= 2.7,R= 3.24
M= 3.1,R= 10.83
M= 2.6,R= 13.22
+- 2.0 Std.Dev.

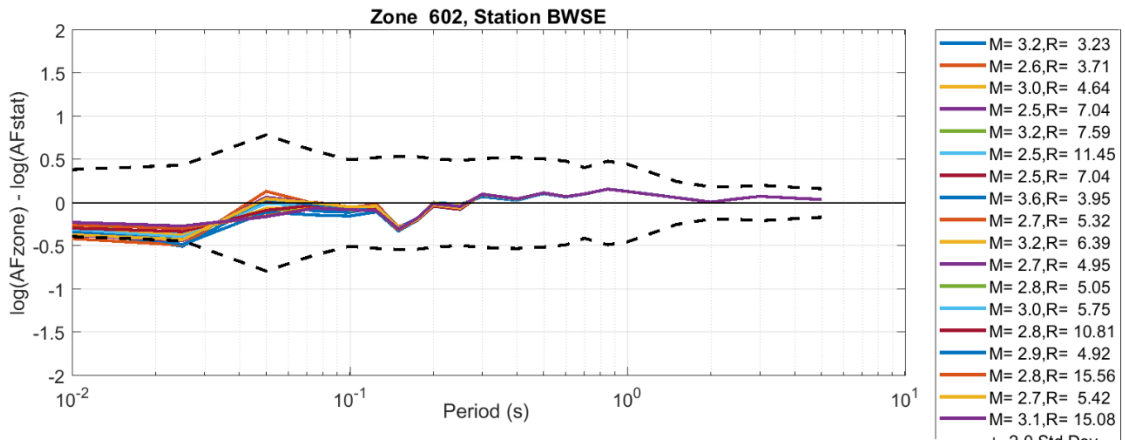
Zone 602, Station BWSE
log(AFzone) - log(AFstat)
Period (s)
M= 3.2,R= 3.23
M= 2.6,R= 3.71
M= 3.0,R= 4.64
M= 2.5,R= 7.04
M= 3.2,R= 7.59
M= 2.5,R= 11.45
M= 2.5,R= 7.04
M= 3.6,R= 3.95
M= 2.7,R= 5.32
M= 3.2,R= 6.39
M= 2.7,R= 4.95
M= 2.8,R= 5.05
M= 3.0,R= 5.75
M= 2.8,R= 10.81
M= 2.9,R= 4.92
M= 2.8,R= 15.56
M= 2.7,R= 5.42
M= 3.1,R= 15.08

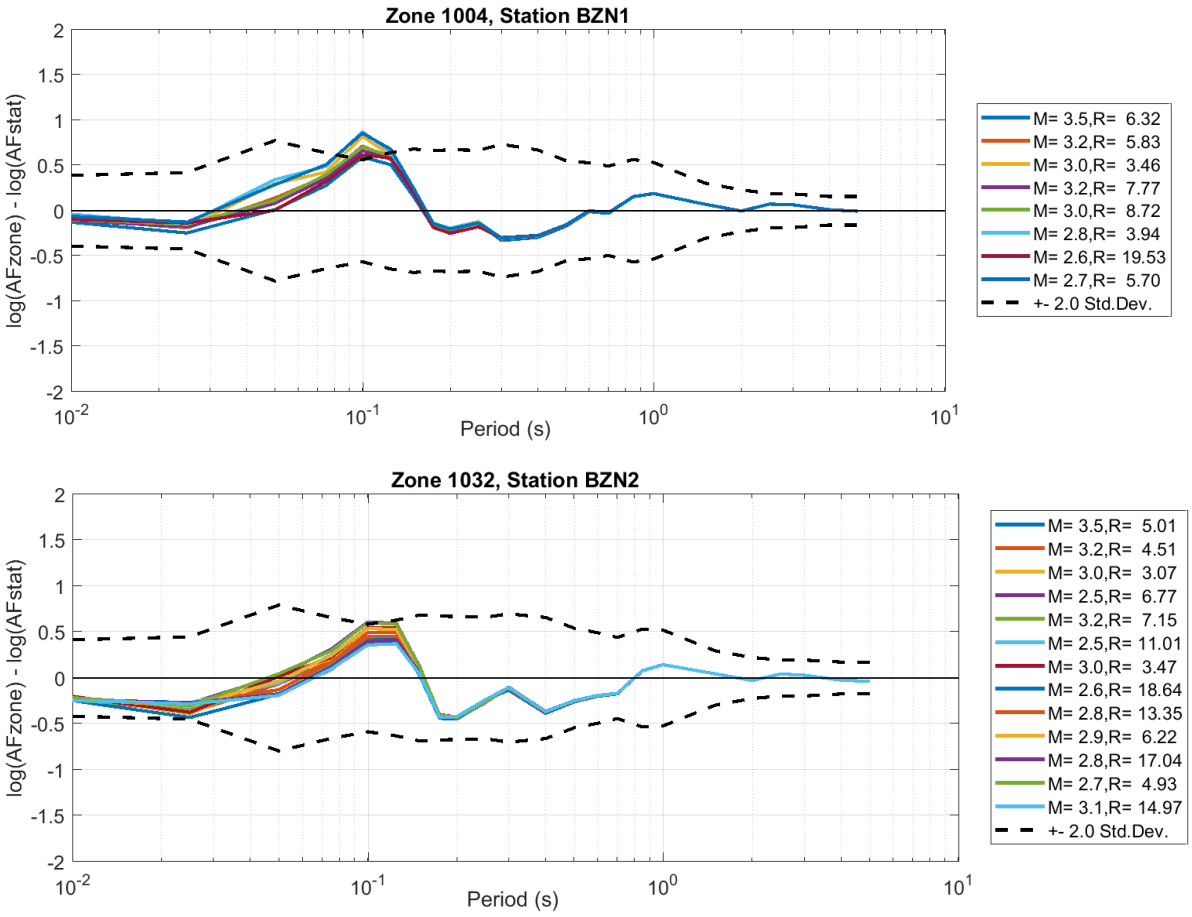
Zone 1004, Station BZN1
log(AFzone) - log(AFstat)
Period (s)
M= 3.5,R= 6.32
M= 3.2,R= 5.83
M= 3.0,R= 3.46
M= 3.2,R= 7.77
M= 3.0,R= 8.72
M= 2.8,R= 3.94
M= 2.6,R= 19.53
M= 2.7,R= 5.70
+- 2.0 Std.Dev.
Zone 1032, Station BZN2
log(AFzone) - log(AFstat)
Period (s)
M= 3.5,R= 5.01
M= 3.2,R= 4.51
M= 3.0,R= 3.07
M= 2.5,R= 6.77
M= 3.2,R= 7.15
M= 2.5,R= 11.01
M= 3.0,R= 3.47
M= 2.6,R= 18.64
M= 2.8,R= 13.35
M= 2.9,R= 6.22
M= 2.8,R= 17.04
M= 2.7,R= 4.93
M= 3.1,R= 14.97
+- 2.0 Std.Dev.

APPENDIX VI

Surface Residuals of Groningen Recordings

Presented in the plots are residuals of the Central-lower model obtained using $\phi_{SS,low}$.

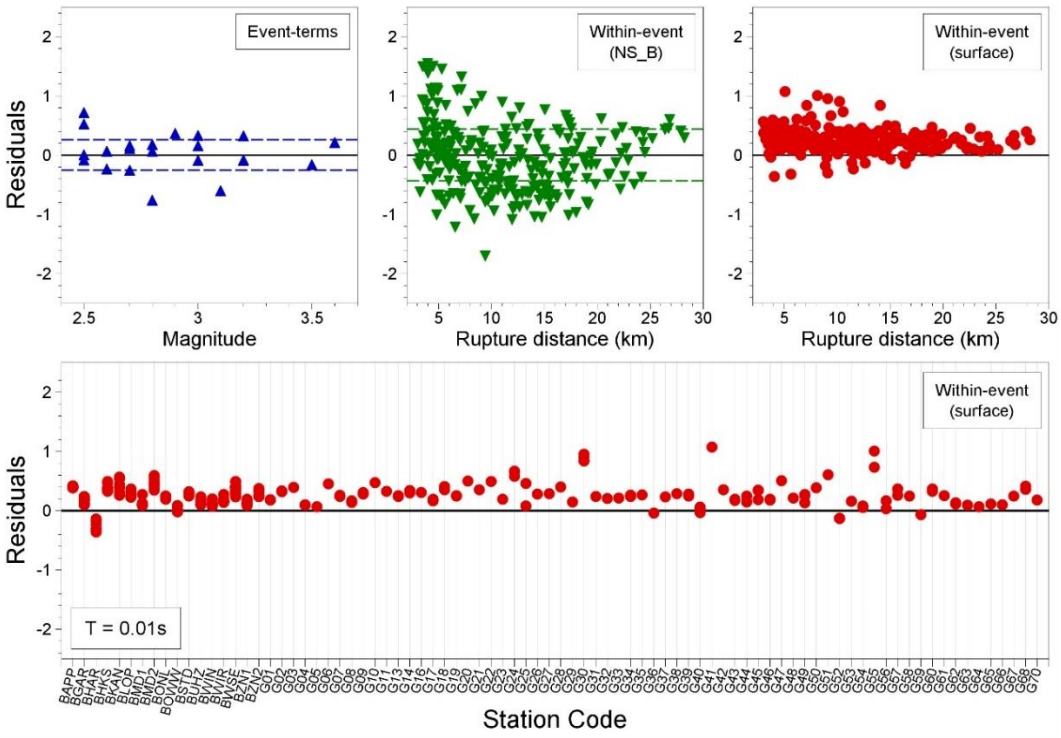

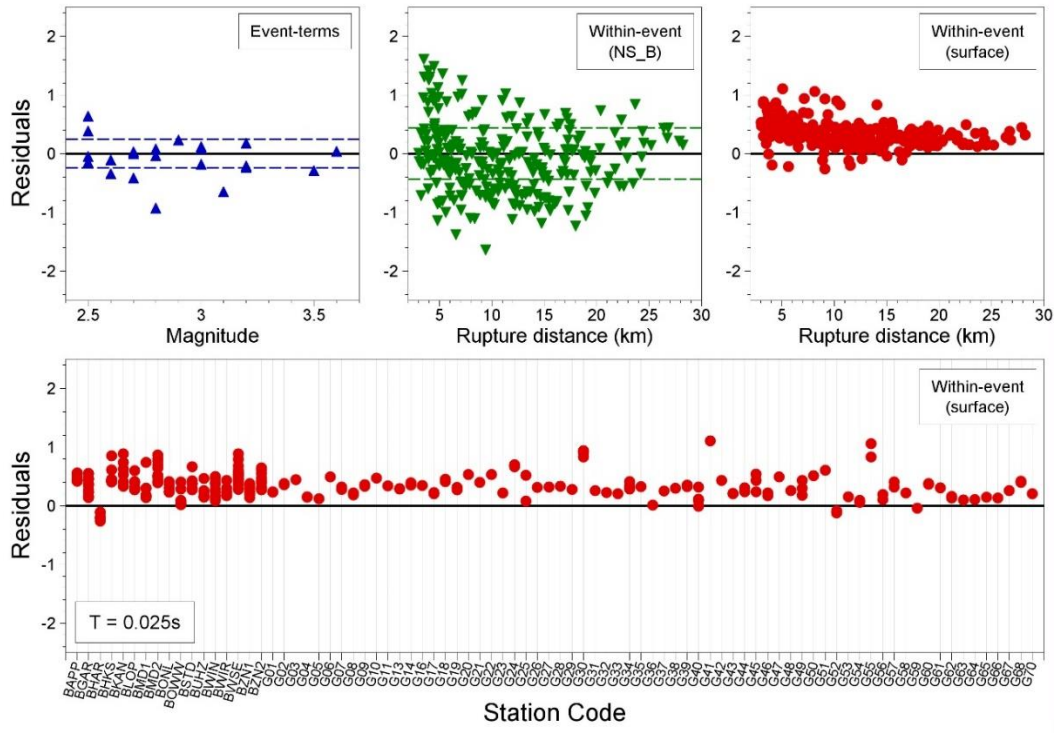

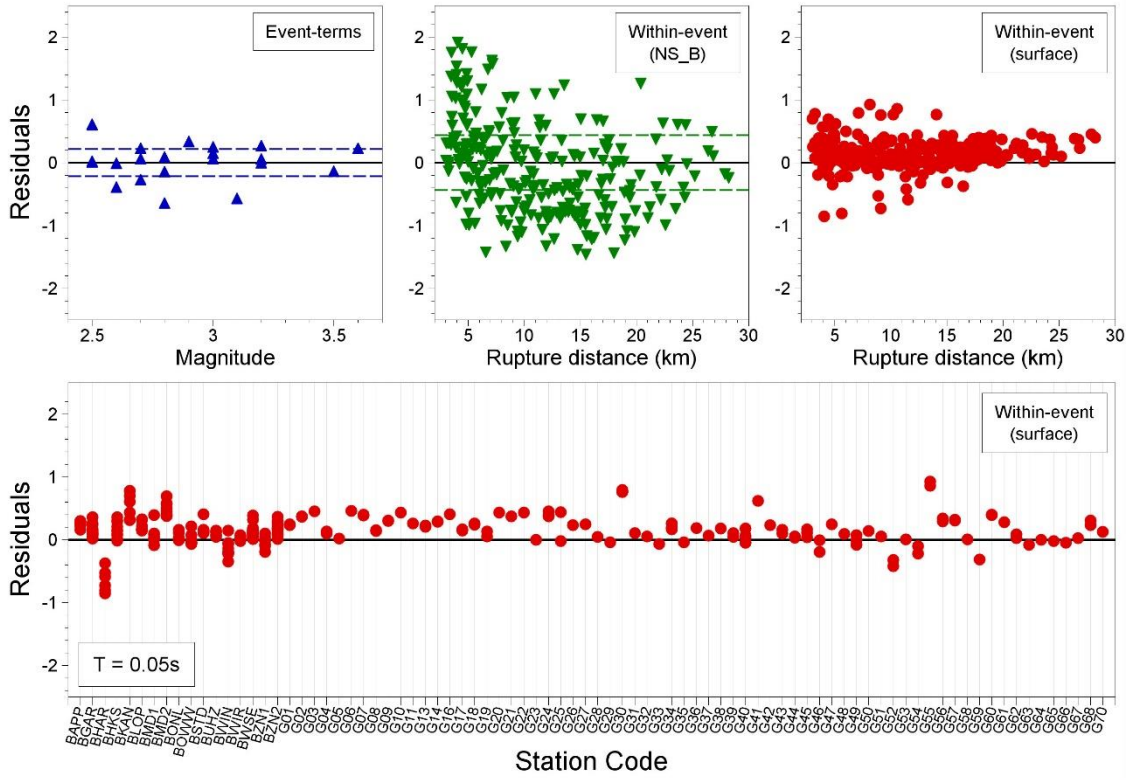
Event-terms
Within-event (NS_B)
Within-event (surface)
Residuals
Magnitude
Rupture distance (km)
Rupture distance (km)
Within-event (surface)
Residuals
T = 0.05s
Station Code

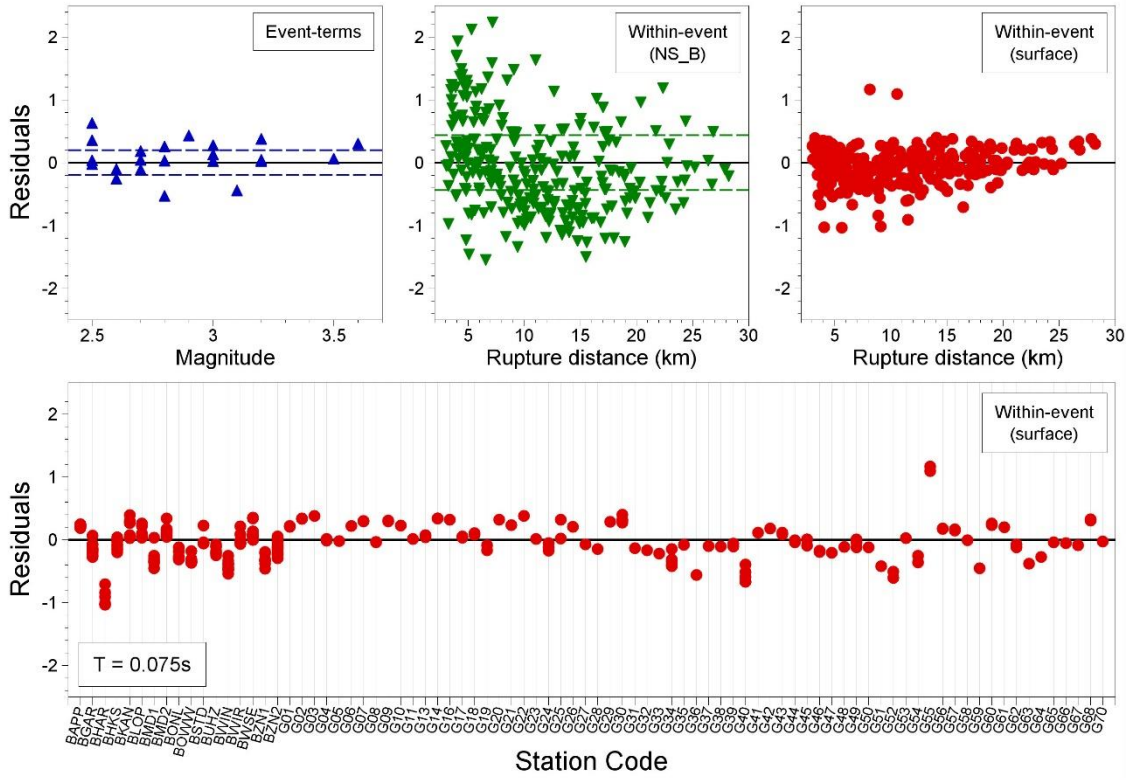
Event-terms
Within-event (NS_B)
Within-event (surface)
Residuals
Magnitude
Rupture distance (km)
Rupture distance (km)
Within-event (surface)
Residuals
T = 0.075s
Station Code

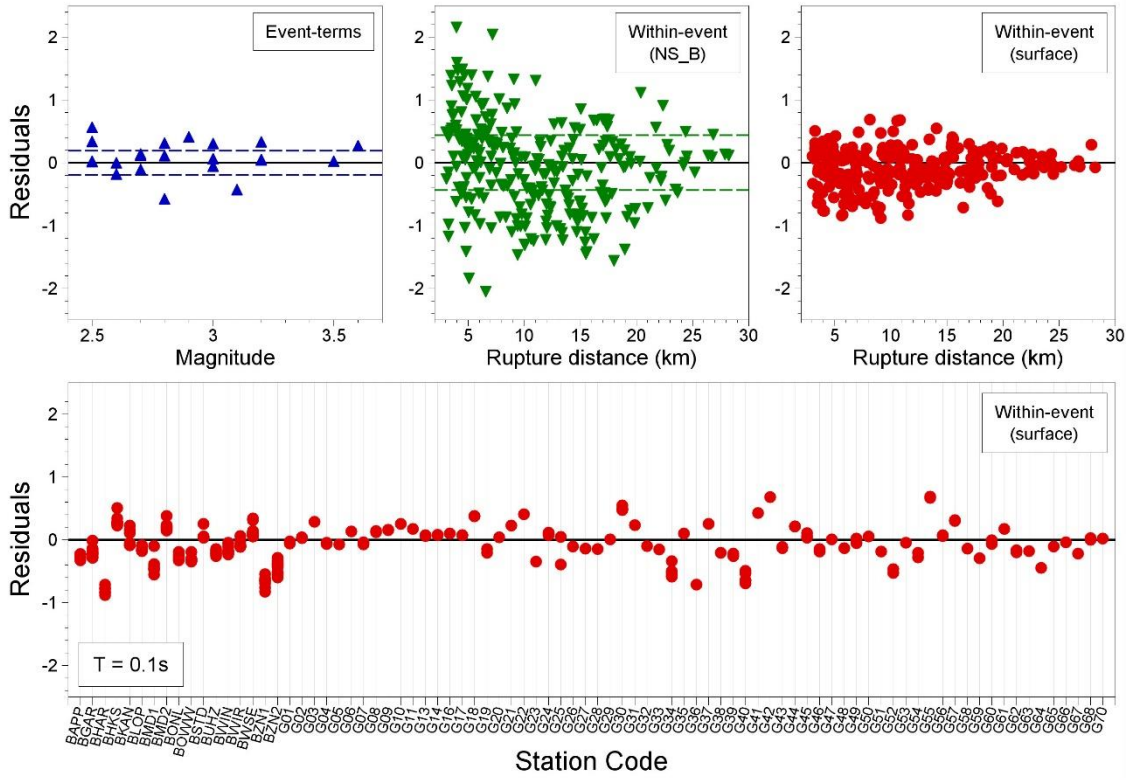
Event-terms
Within-event (NS_B)
Within-event (surface)
Residuals
Magnitude
Rupture distance (km)
Rupture distance (km)
Within-event (surface)
Residuals
T = 0.1s
Station Code

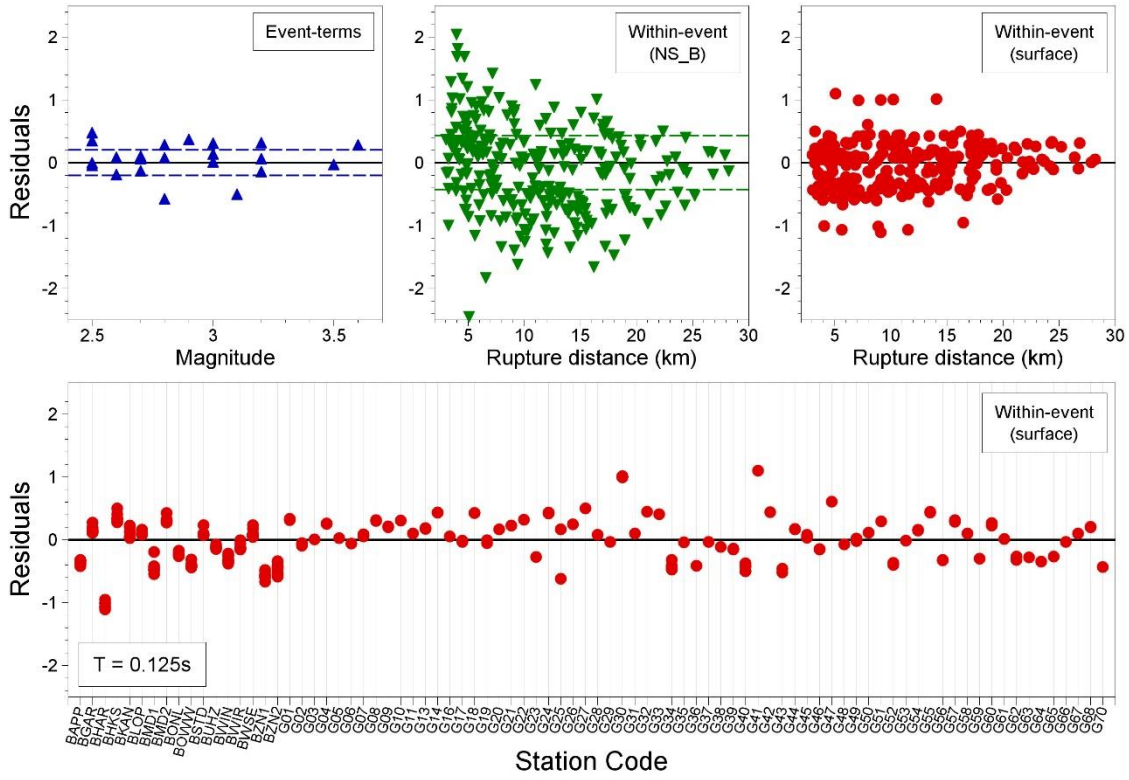
Event-terms
Within-event (NS_B)
Within-event (surface)
Residuals
Magnitude
Rupture distance (km)
Rupture distance (km)
Within-event (surface)
Residuals
T = 0.125s
Station Code

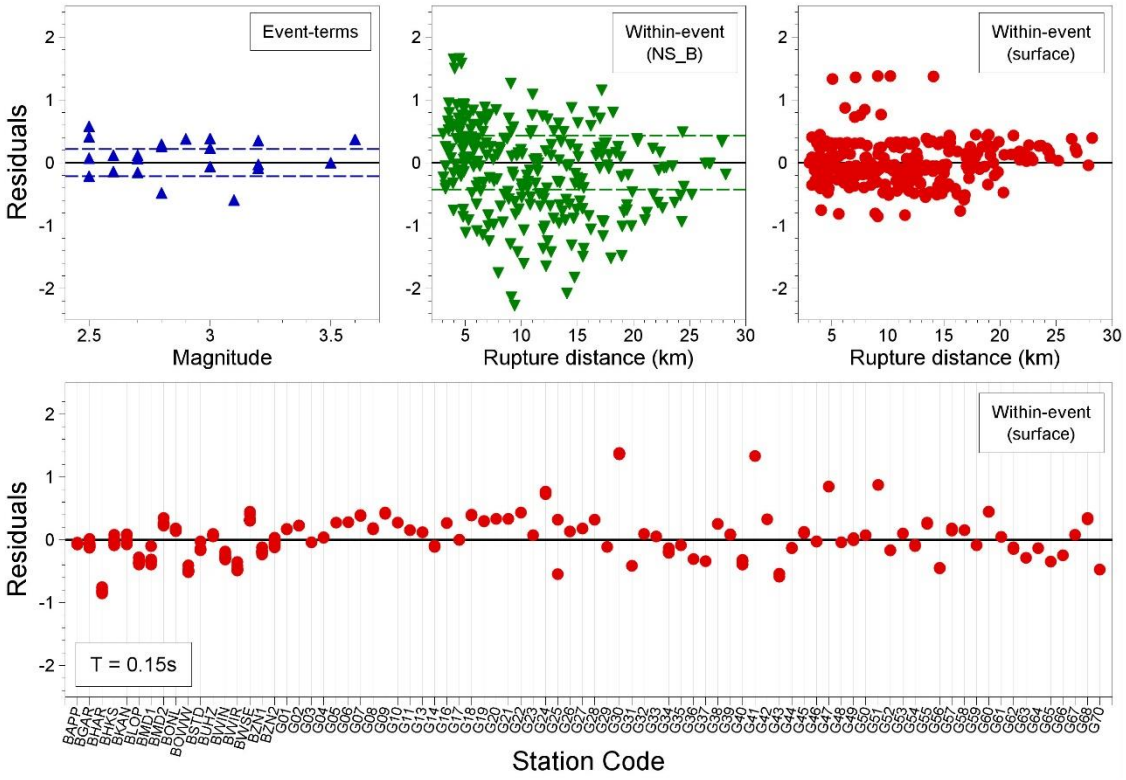
Event-terms
Within-event (NS_B)
Within-event (surface)
Residuals
Magnitude
Rupture distance (km)
Rupture distance (km)
Within-event (surface)
Residuals
T = 0.15s
Station Code

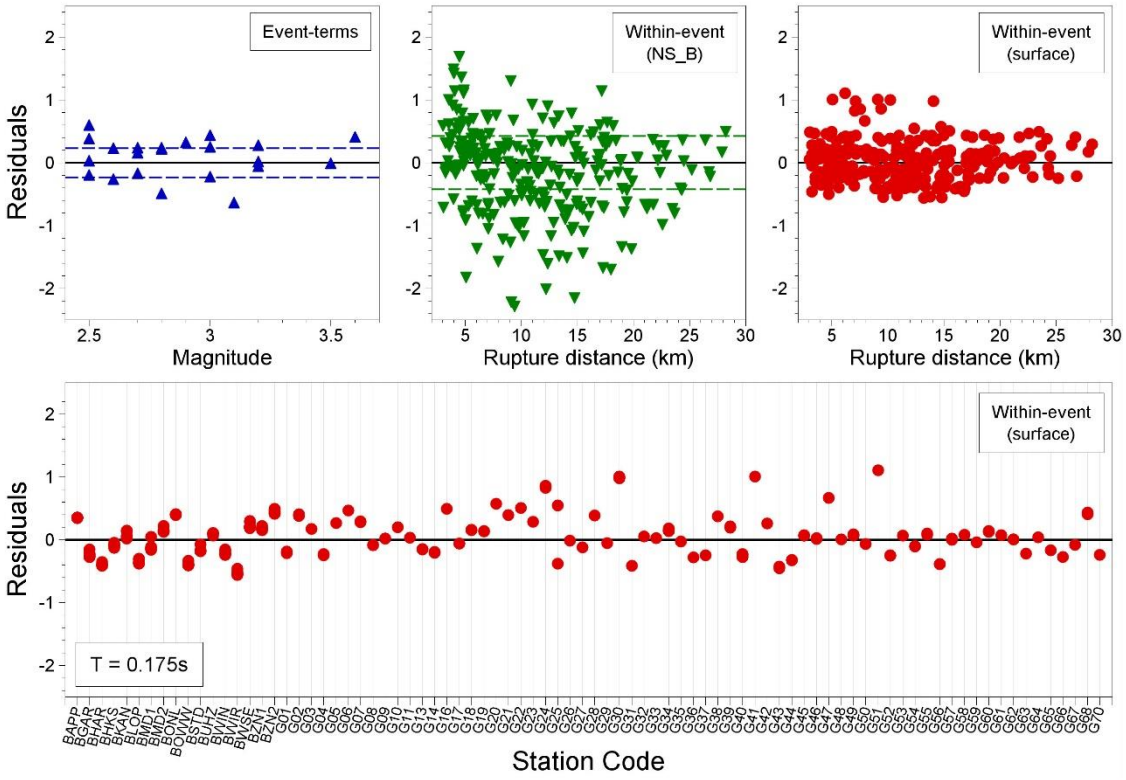
Event-terms
Within-event (NS_B)
Within-event (surface)
Residuals
Magnitude
Rupture distance (km)
Rupture distance (km)
Within-event (surface)
Residuals
T = 0.175s
Station Code

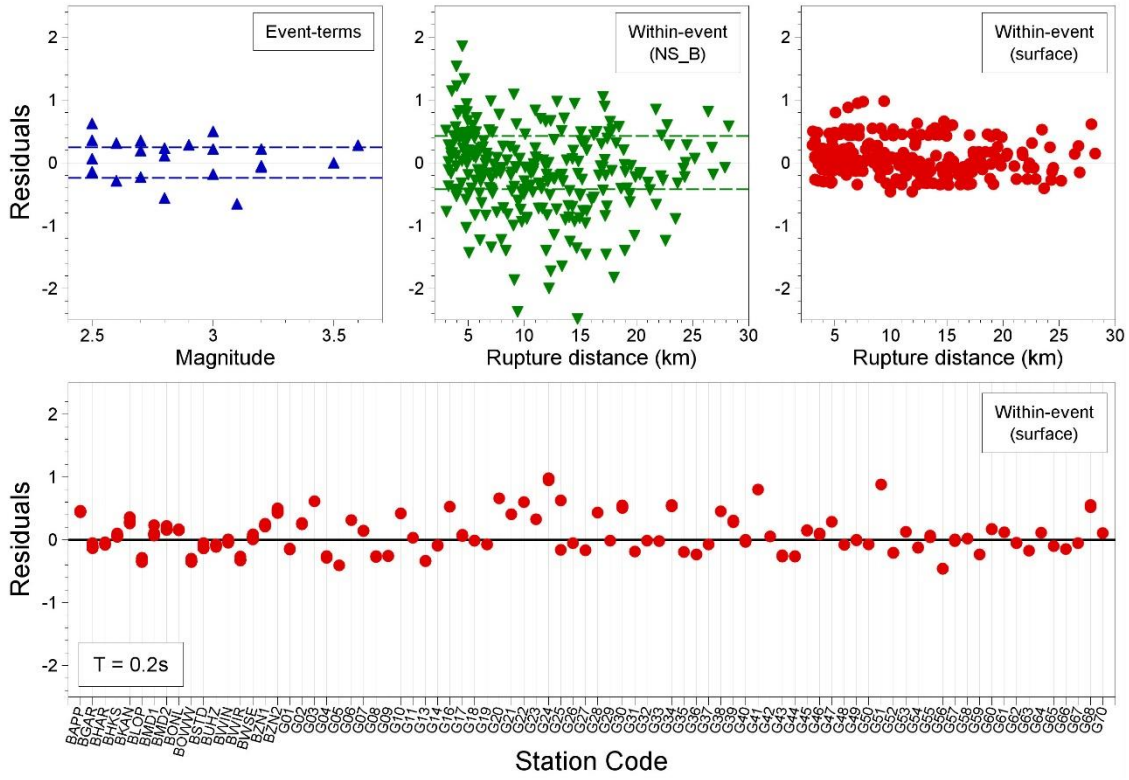
Event-terms
Within-event (NS_B)
Within-event (surface)
Residuals
Magnitude
Rupture distance (km)
Rupture distance (km)
Within-event (surface)
Residuals
T = 0.2s
Station Code

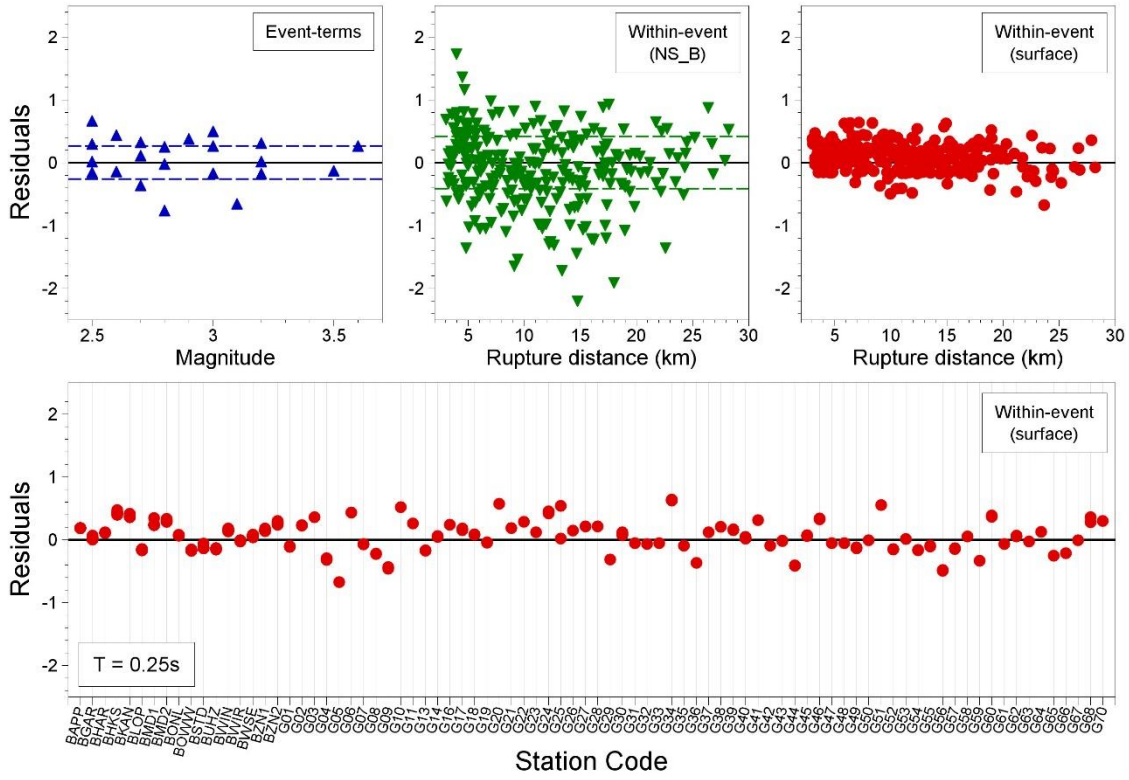
Event-terms
Within-event (NS_B)
Within-event (surface)
Residuals
Magnitude
Rupture distance (km)
Rupture distance (km)
Within-event (surface)
Residuals
T = 0.25s
Station Code

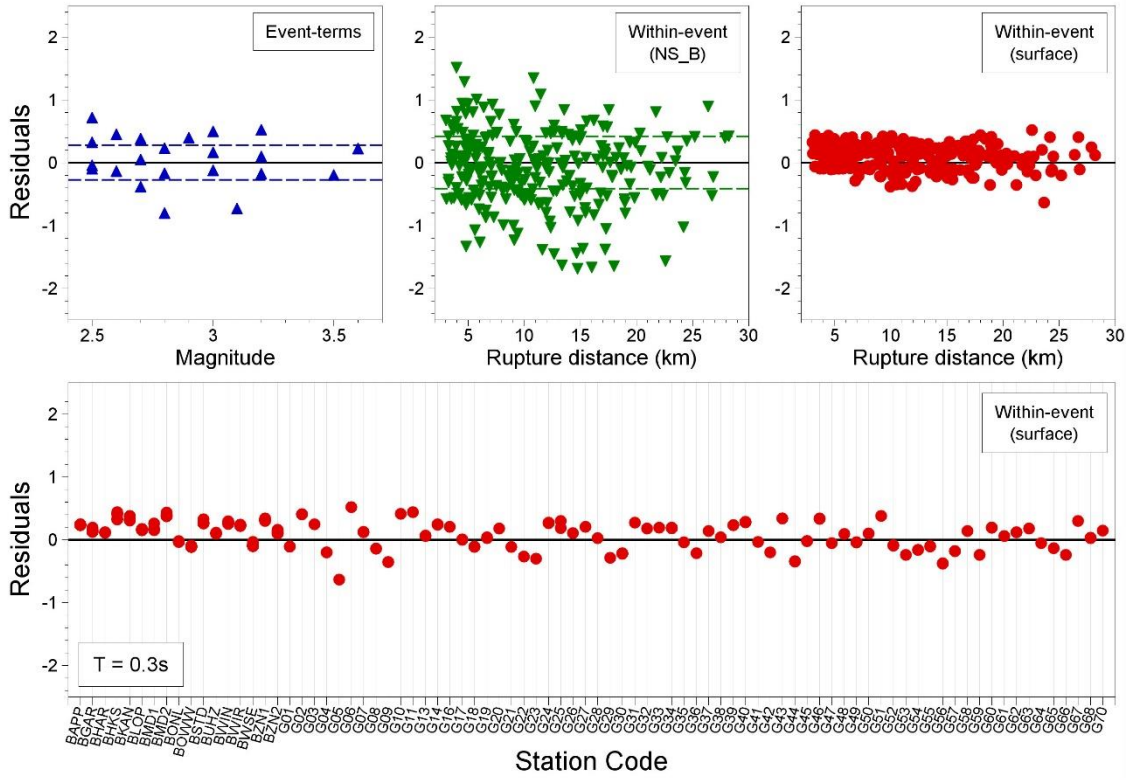
Event-terms
Within-event (NS_B)
Within-event (surface)
Residuals
Magnitude
Rupture distance (km)
Rupture distance (km)
Within-event (surface)
Residuals
T = 0.3s
Station Code

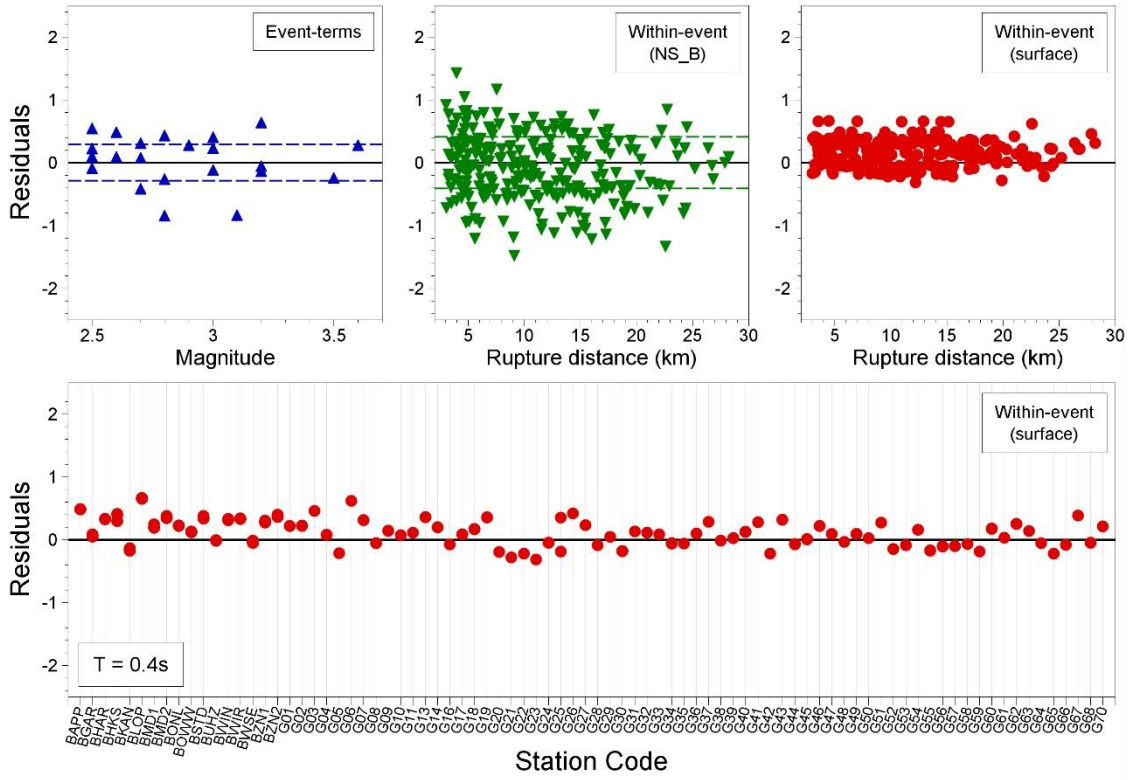
Event-terms
Within-event (NS_B)
Within-event (surface)
Residuals
Magnitude
Rupture distance (km)
Rupture distance (km)
Within-event (surface)
Residuals
T = 0.4s
Station Code

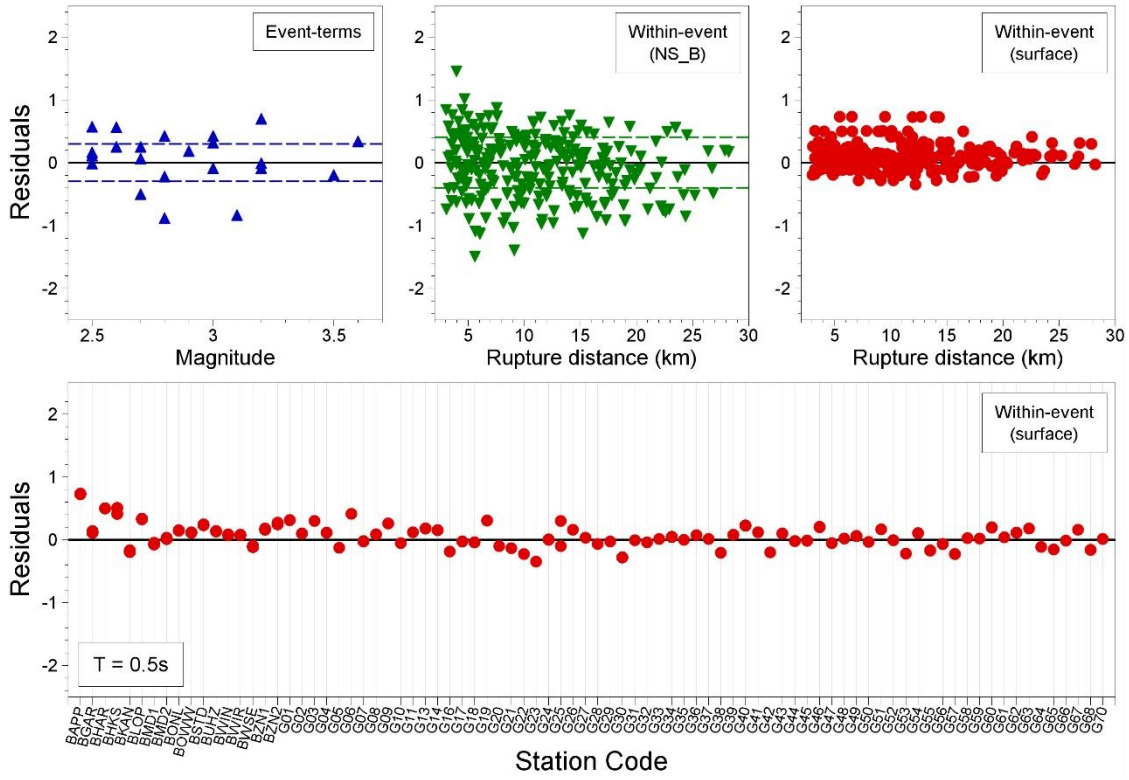
Event-terms
Within-event (NS_B)
Within-event (surface)
Residuals
Magnitude
Rupture distance (km)
Rupture distance (km)
Within-event (surface)
Residuals
T = 0.5s
Station Code

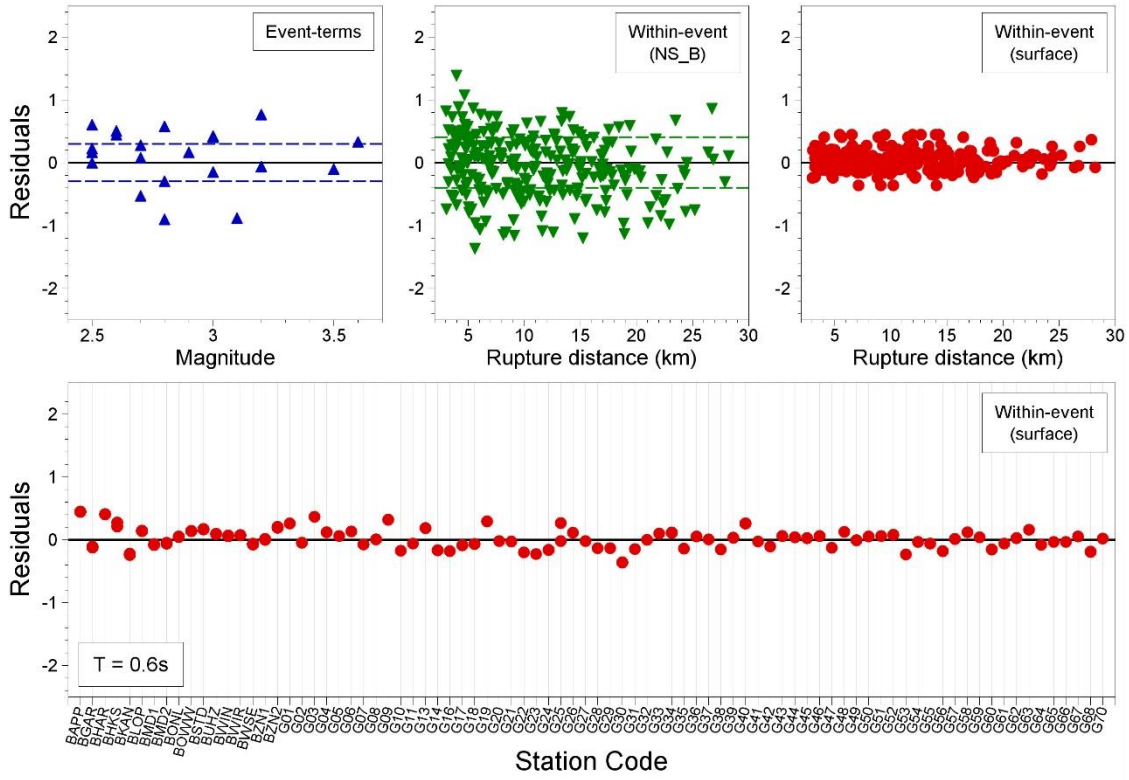
Event-terms
Within-event (NS_B)
Within-event (surface)
Residuals
Magnitude
Rupture distance (km)
Rupture distance (km)
Within-event (surface)
Residuals
T = 0.6s
Station Code

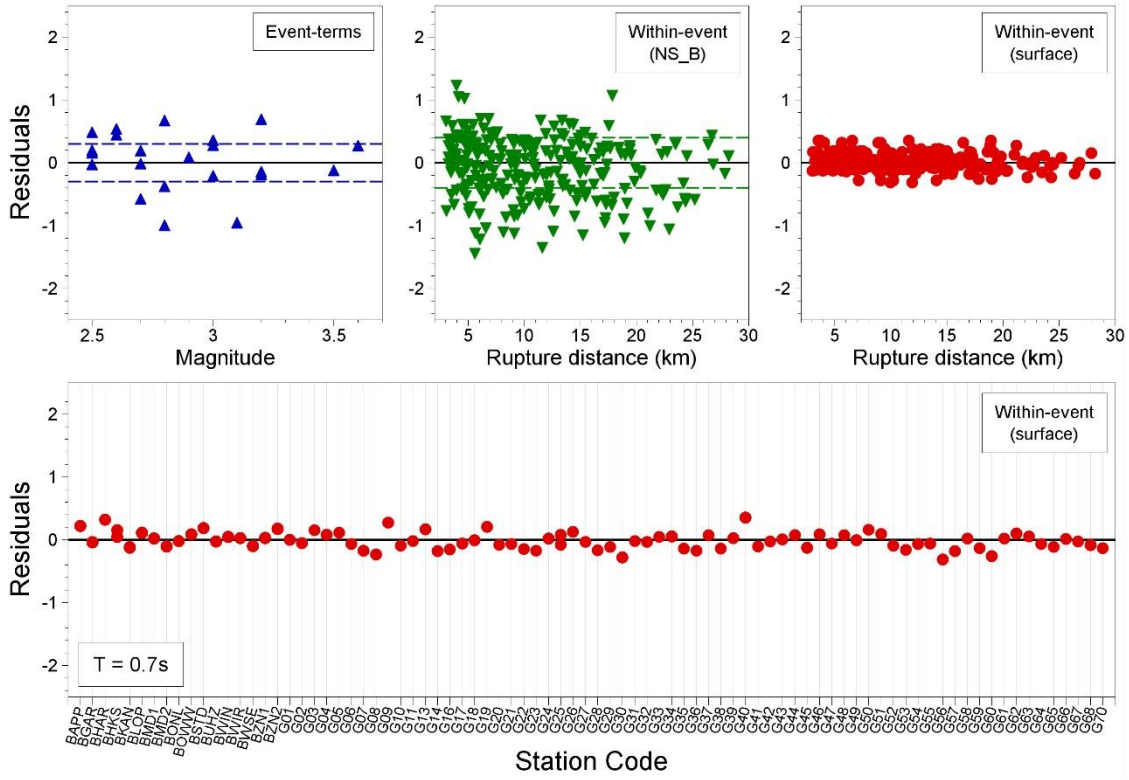
Event-terms
Within-event (NS_B)
Within-event (surface)
Residuals
Magnitude
Rupture distance (km)
Rupture distance (km)
Within-event (surface)
Residuals
T = 0.7s
Station Code

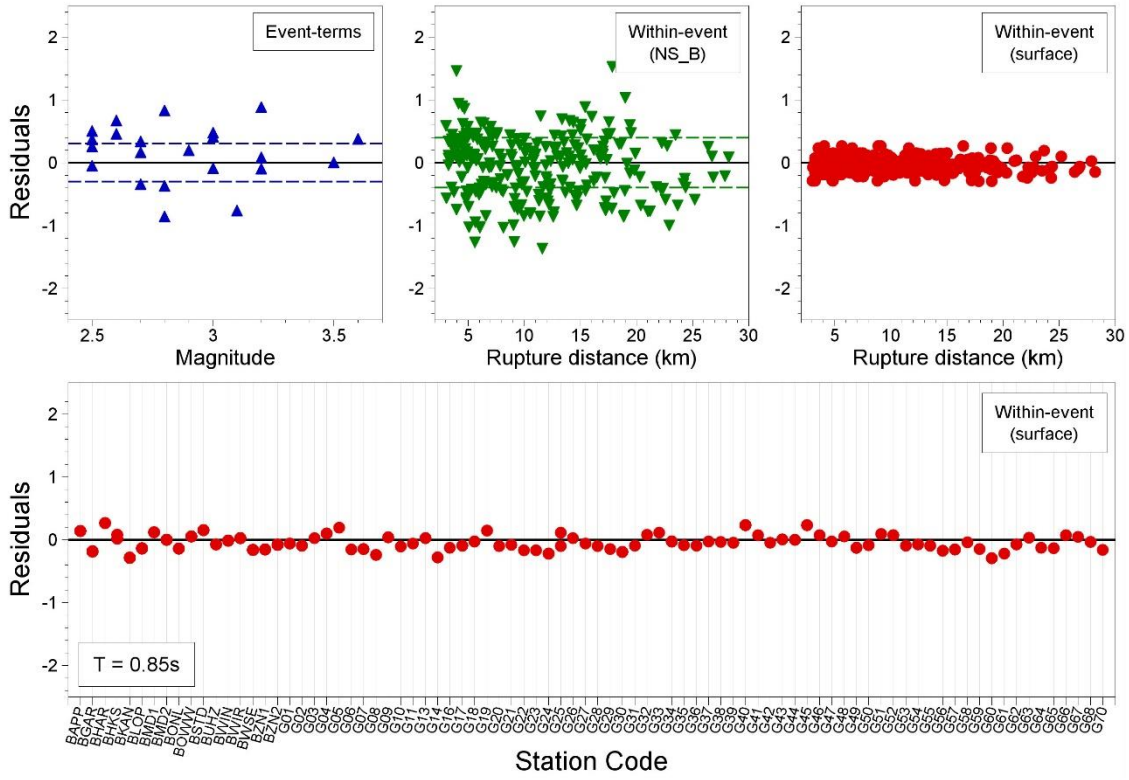
Event-terms
Within-event (NS_B)
Within-event (surface)
Residuals
Magnitude
Rupture distance (km)
Rupture distance (km)
Within-event (surface)
Residuals
T = 0.85s
Station Code

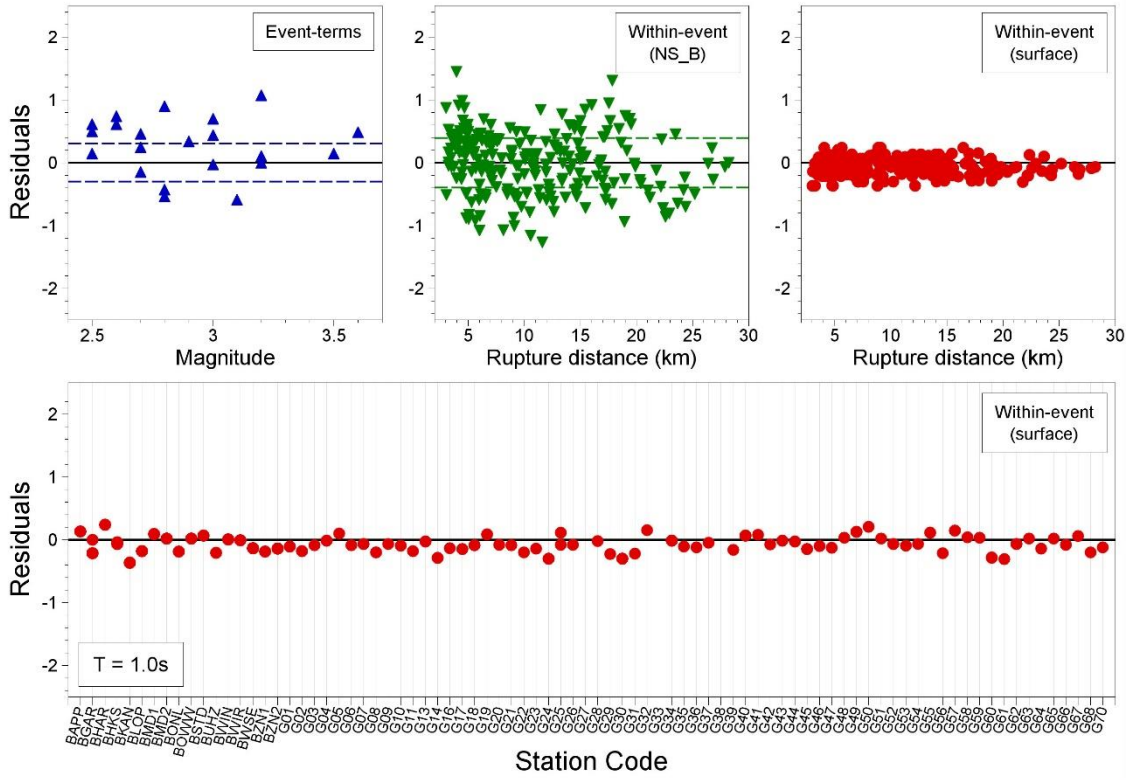
Event-terms
Within-event (NS_B)
Within-event (surface)
Residuals
Magnitude
Rupture distance (km)
Rupture distance (km)
Within-event (surface)
Residuals
T = 1.0s
Station Code

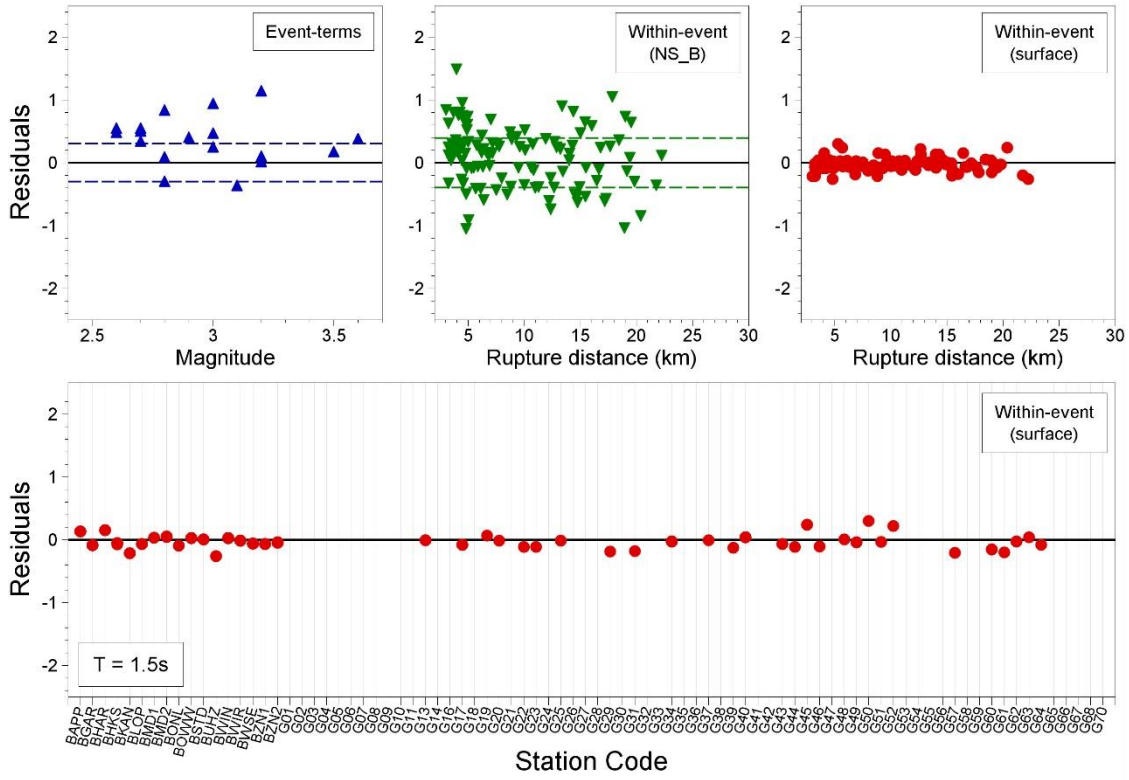
Event-terms
Within-event (NS_B)
Within-event (surface)
Residuals
Magnitude
Rupture distance (km)
Rupture distance (km)
Within-event (surface)
Residuals
T = 1.5s
Station Code

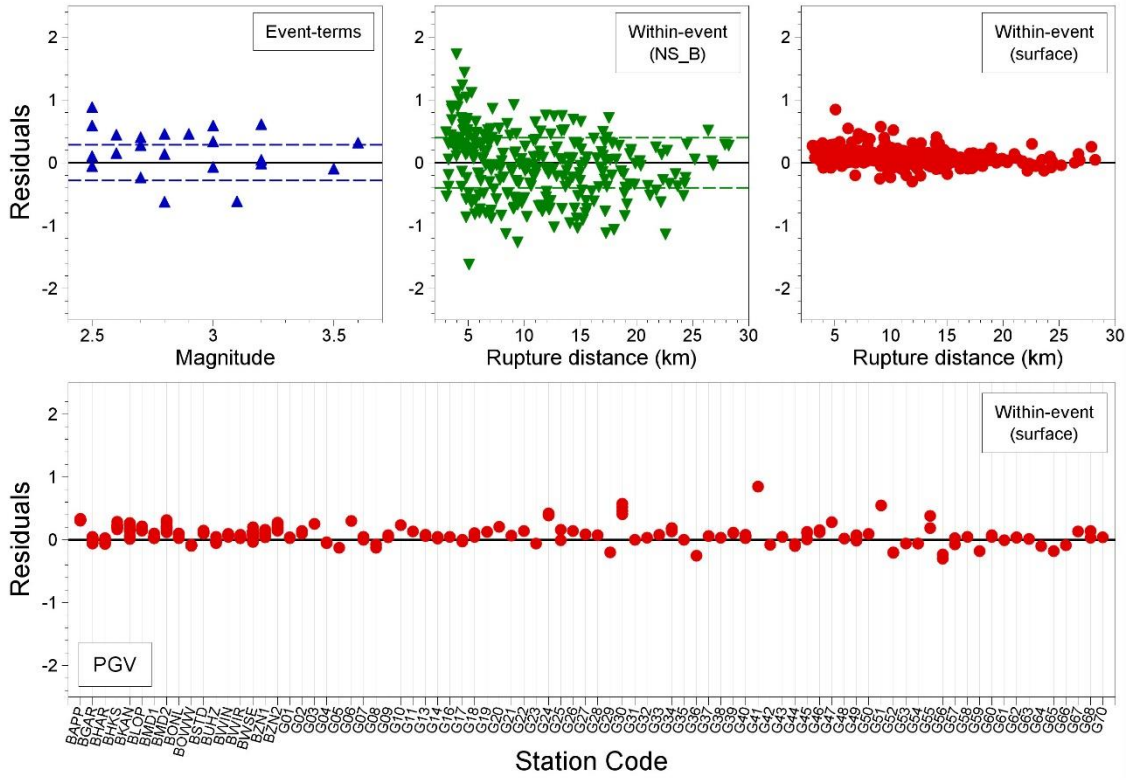
Event-terms
Within-event (NS_B)
Within-event (surface)
Residuals
Magnitude
Rupture distance (km)
Rupture distance (km)
Within-event (surface)
PGV
Residuals
Station Code

APPENDIX VII

Median Predictions of Motions at Surface

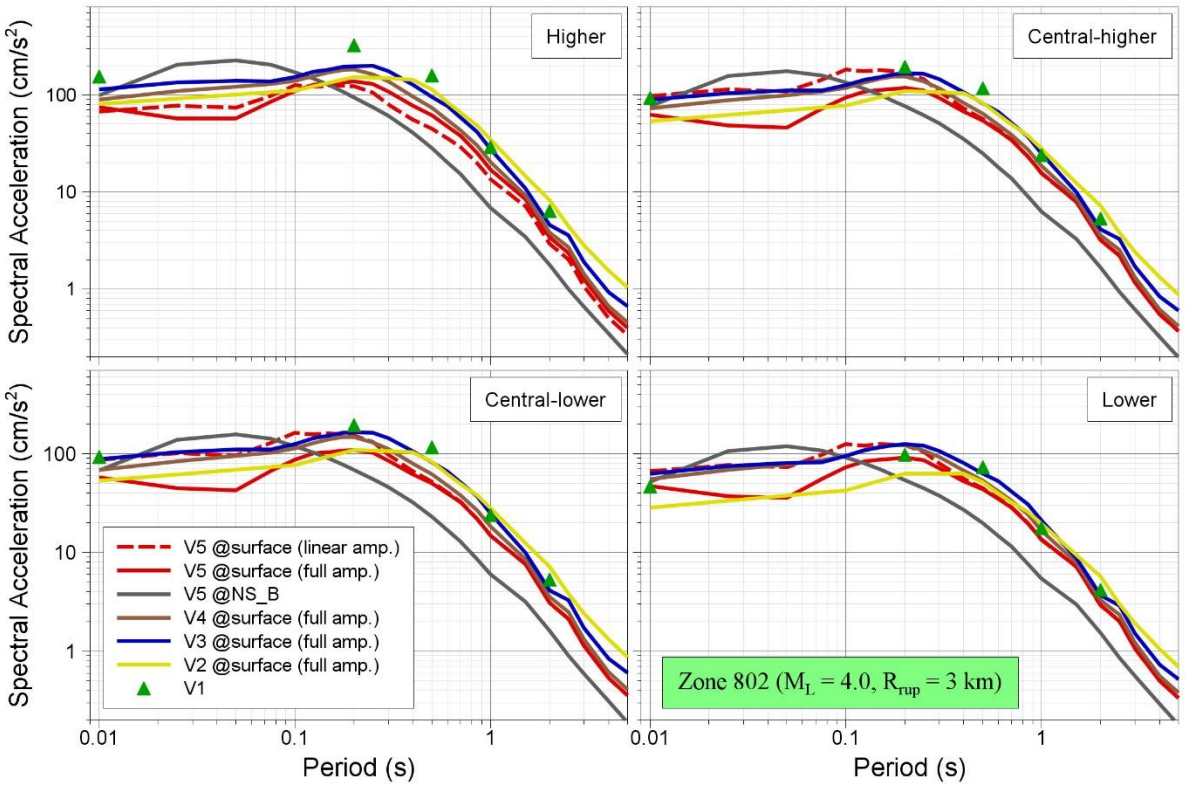

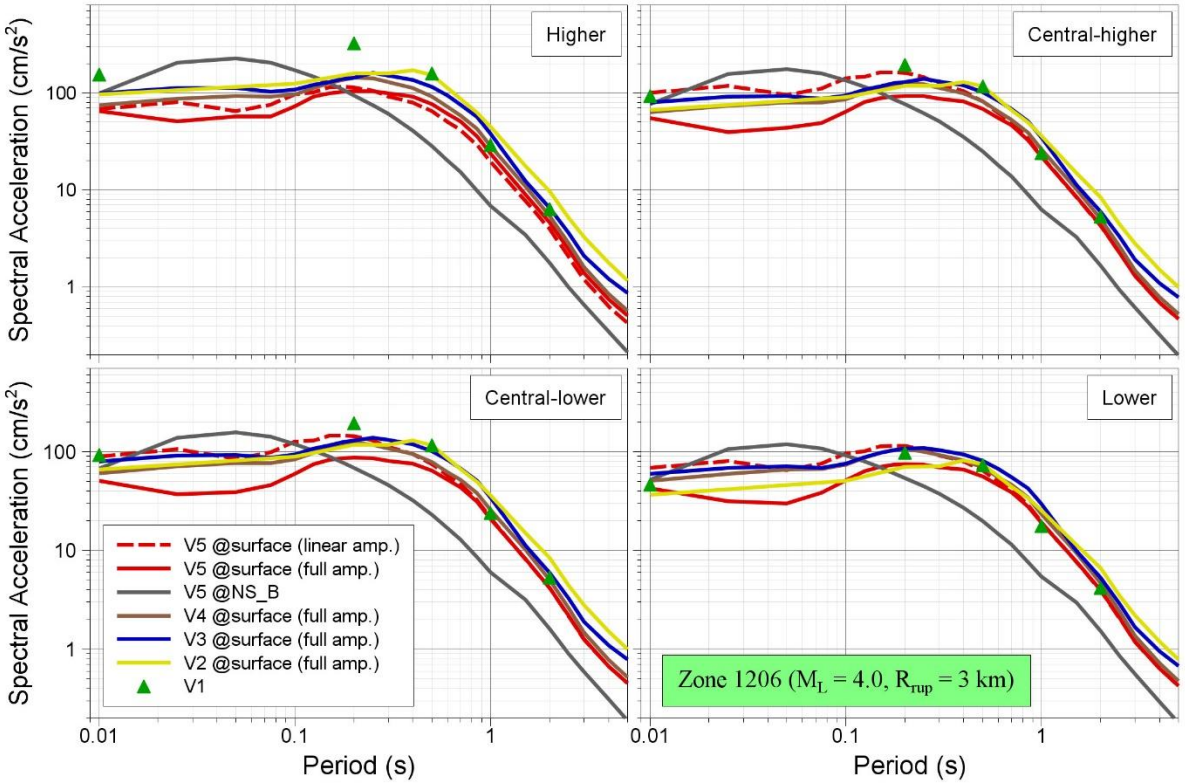
Higher
Central-higher
Central-lower
Lower
Spectral Acceleration (cm/s²)
Period (s)
V5 @surface (linear amp.)
V5 @surface (full amp.)
V5 @NS_B
V4 @surface (full amp.)
V3 @surface (full amp.)
V2 @surface (full amp.)
V1
Zone 1206 (M_L = 4.0, R_rup = 3 km)

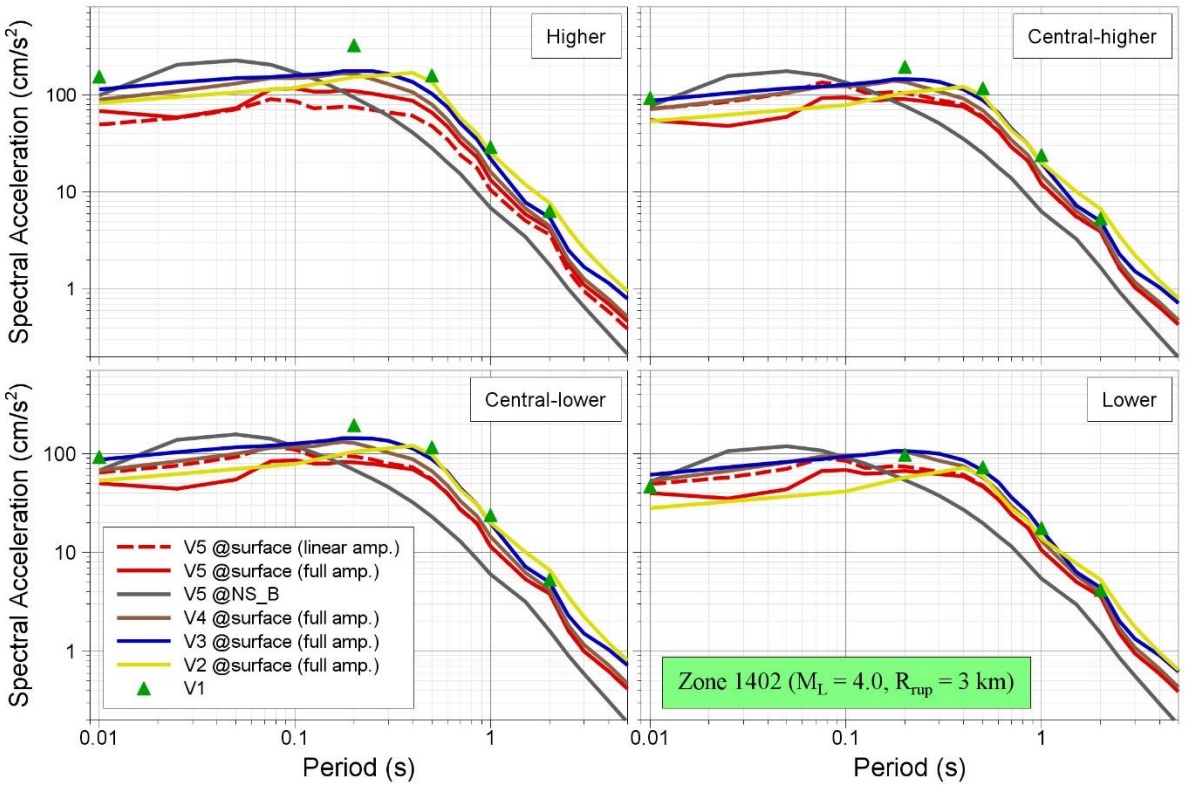
Higher
Central-higher
Central-lower
Lower
Spectral Acceleration (cm/s²)
Period (s)
V5 @surface (linear amp.)
V5 @surface (full amp.)
V5 @NS_B
V4 @surface (full amp.)
V3 @surface (full amp.)
V2 @surface (full amp.)
V1
Zone 1402 (M_L = 4.0, R_rup = 3 km)

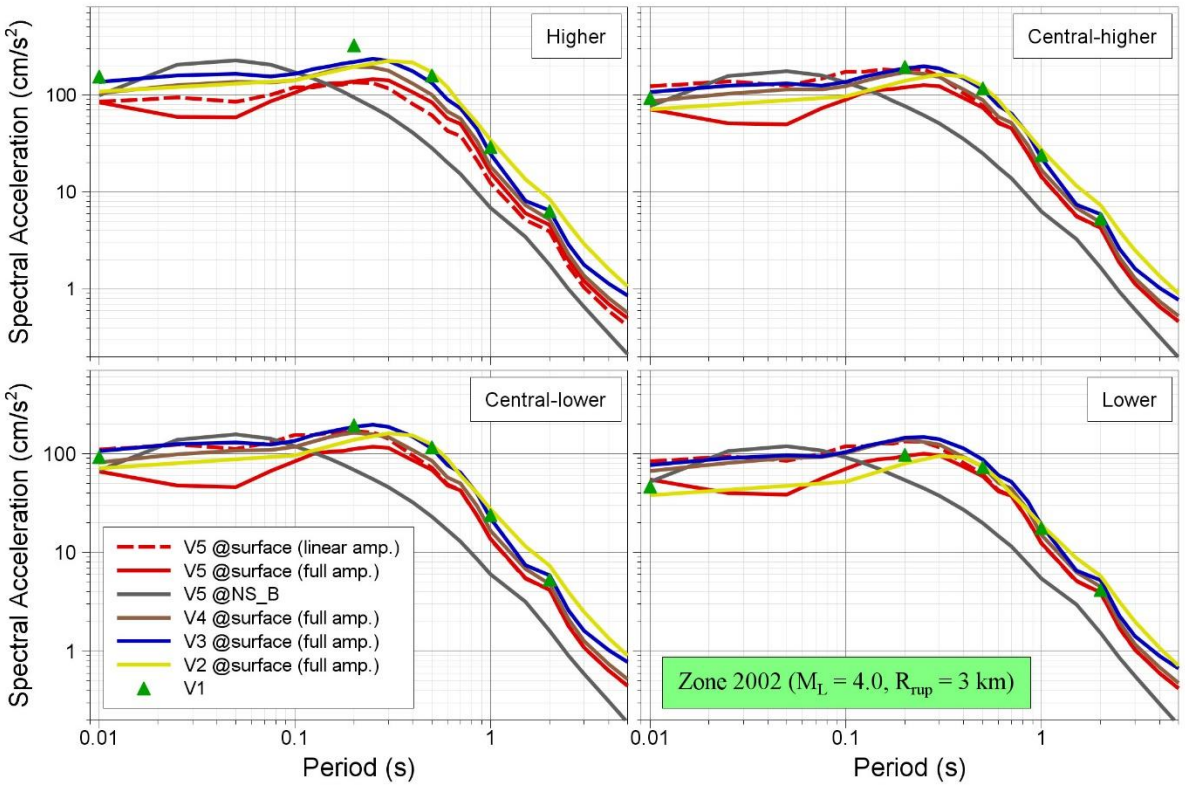
Higher
Central-higher
Central-lower
Lower
Spectral Acceleration (cm/s²)
Period (s)
V5 @surface (linear amp.)
V5 @surface (full amp.)
V5 @NS_B
V4 @surface (full amp.)
V3 @surface (full amp.)
V2 @surface (full amp.)
V1
Zone 2002 (M_L = 4.0, R_rup = 3 km)

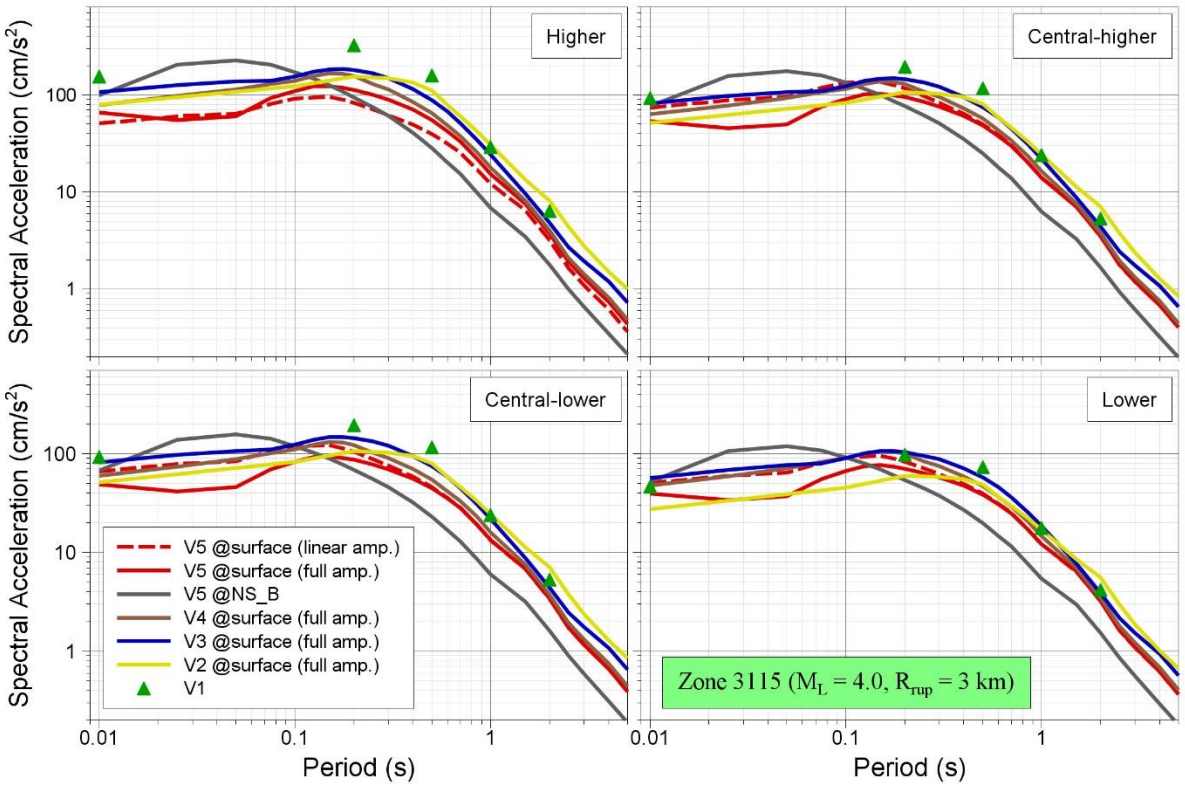
Higher
Central-higher
Central-lower
Lower
Spectral Acceleration (cm/s²)
Period (s)
V5 @surface (linear amp.)
V5 @surface (full amp.)
V5 @NS_B
V4 @surface (full amp.)
V3 @surface (full amp.)
V2 @surface (full amp.)
V1
Zone 3115 (M_L = 4.0, R_rup = 3 km)

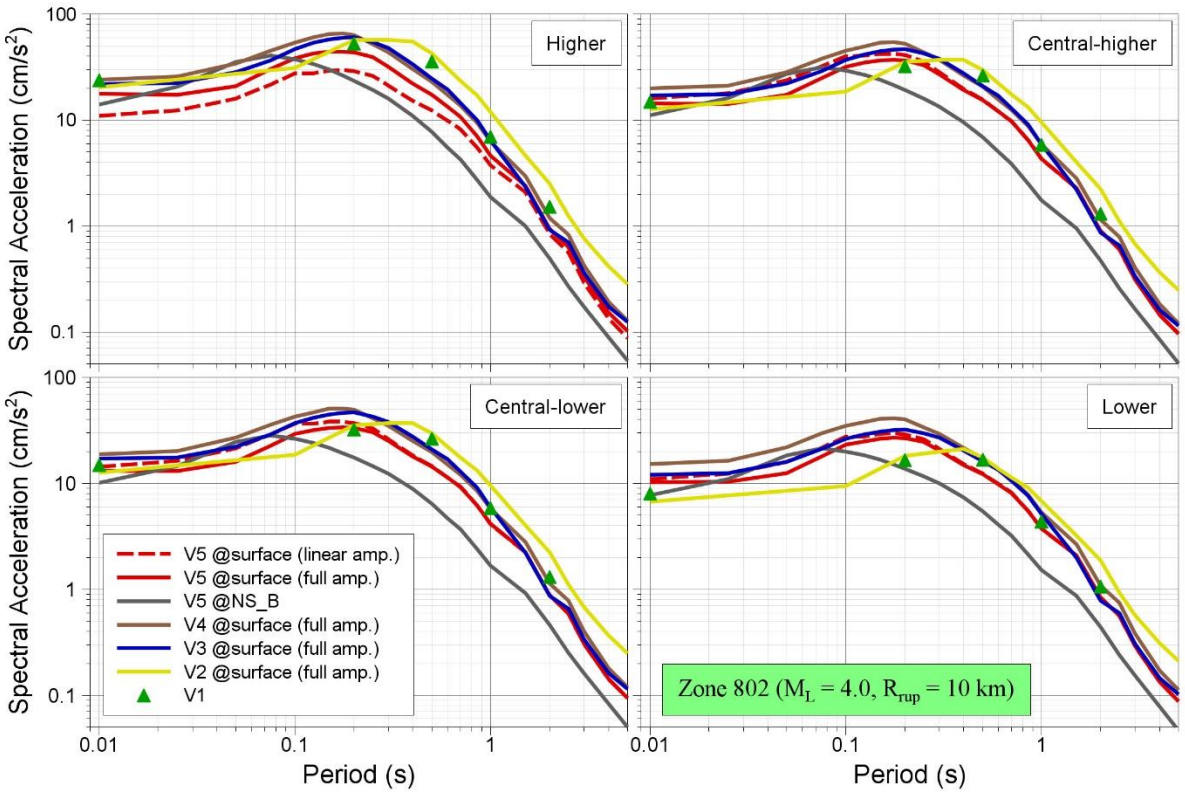
Higher
Central-higher
Central-lower
Lower
Spectral Acceleration (cm/s²)
Period (s)
V5 @surface (linear amp.)
V5 @surface (full amp.)
V5 @NS_B
V4 @surface (full amp.)
V3 @surface (full amp.)
V2 @surface (full amp.)
V1
Zone 802 (M_L = 4.0, R_rup = 10 km)

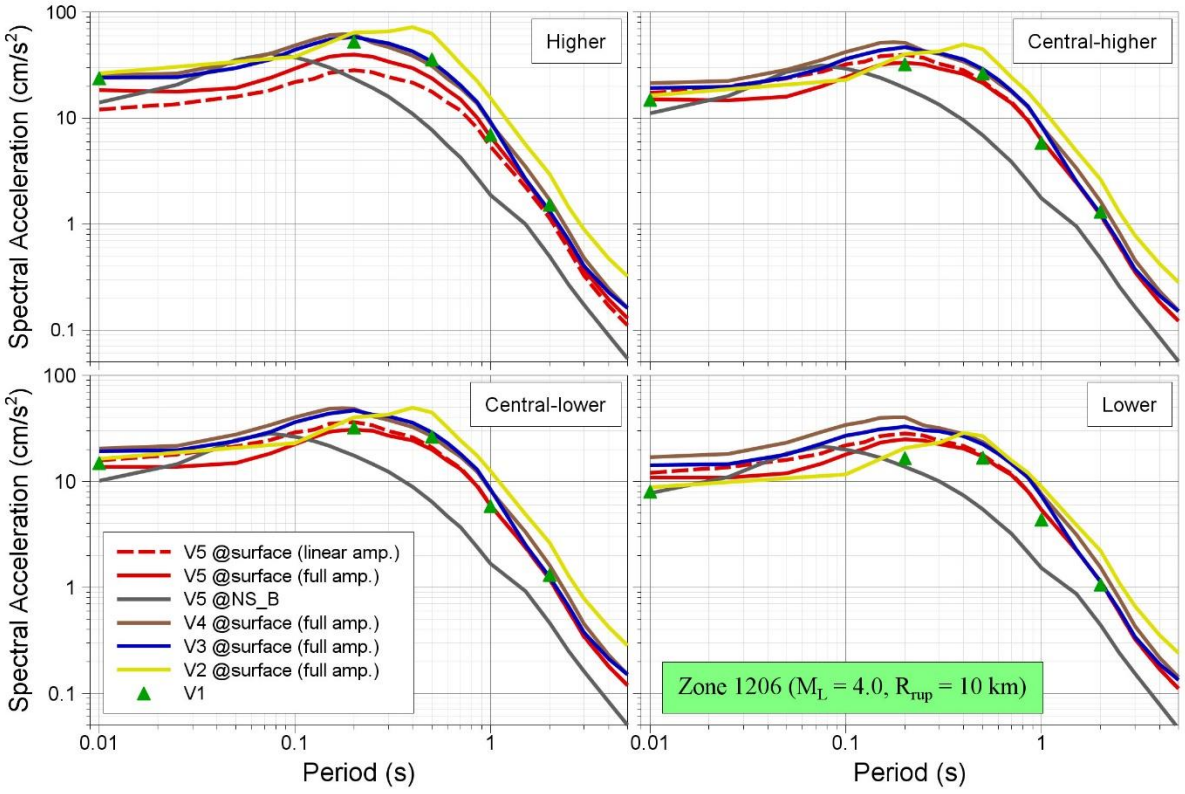
Higher
Central-higher
Central-lower
Lower
Spectral Acceleration (cm/s²)
Period (s)
V5 @surface (linear amp.)
V5 @surface (full amp.)
V5 @NS_B
V4 @surface (full amp.)
V3 @surface (full amp.)
V2 @surface (full amp.)
V1
Zone 1206 (M_L = 4.0, R_rup = 10 km)

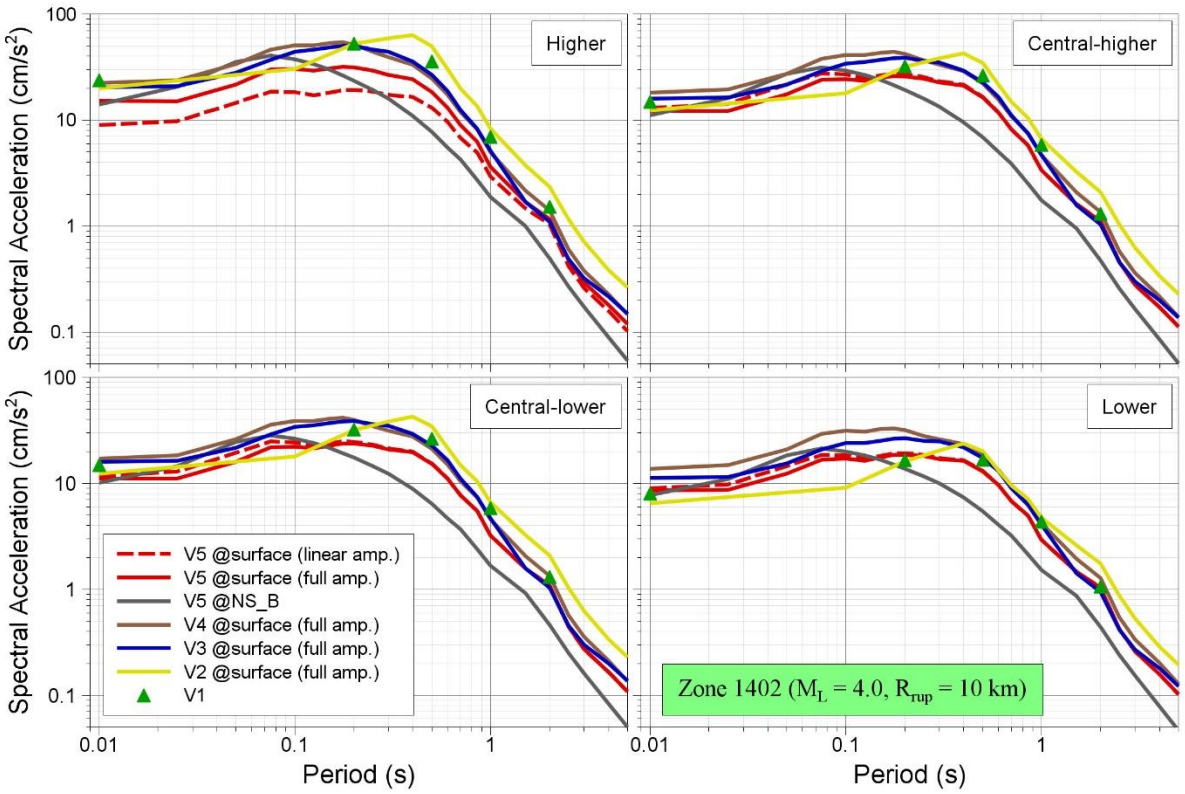
Higher
Central-higher
Central-lower
Lower
Spectral Acceleration (cm/s²)
Period (s)
V5 @surface (linear amp.)
V5 @surface (full amp.)
V5 @NS_B
V4 @surface (full amp.)
V3 @surface (full amp.)
V2 @surface (full amp.)
V1
Zone 1402 (M_L = 4.0, R_rup = 10 km)

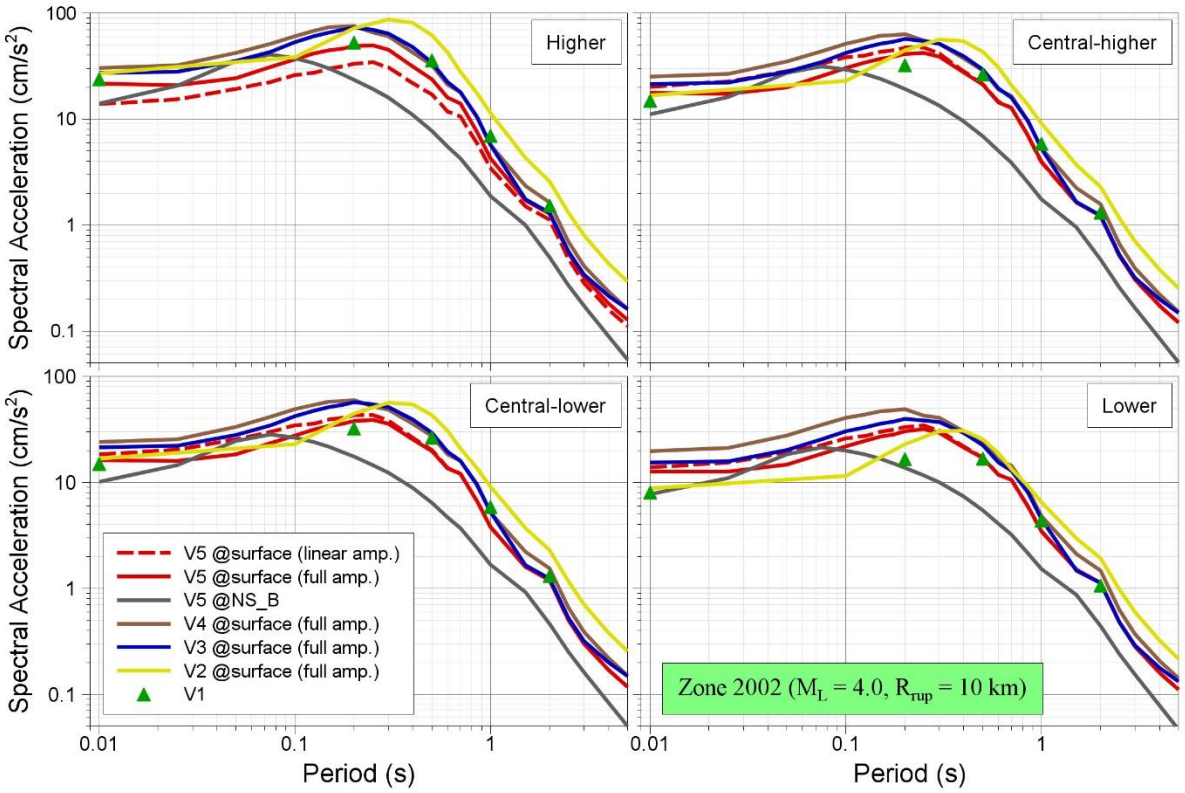
Higher
Central-higher
Central-lower
Lower
Spectral Acceleration (cm/s²)
Period (s)
V5 @surface (linear amp.)
V5 @surface (full amp.)
V5 @NS_B
V4 @surface (full amp.)
V3 @surface (full amp.)
V2 @surface (full amp.)
V1
Zone 2002 (M_L = 4.0, R_rup = 10 km)

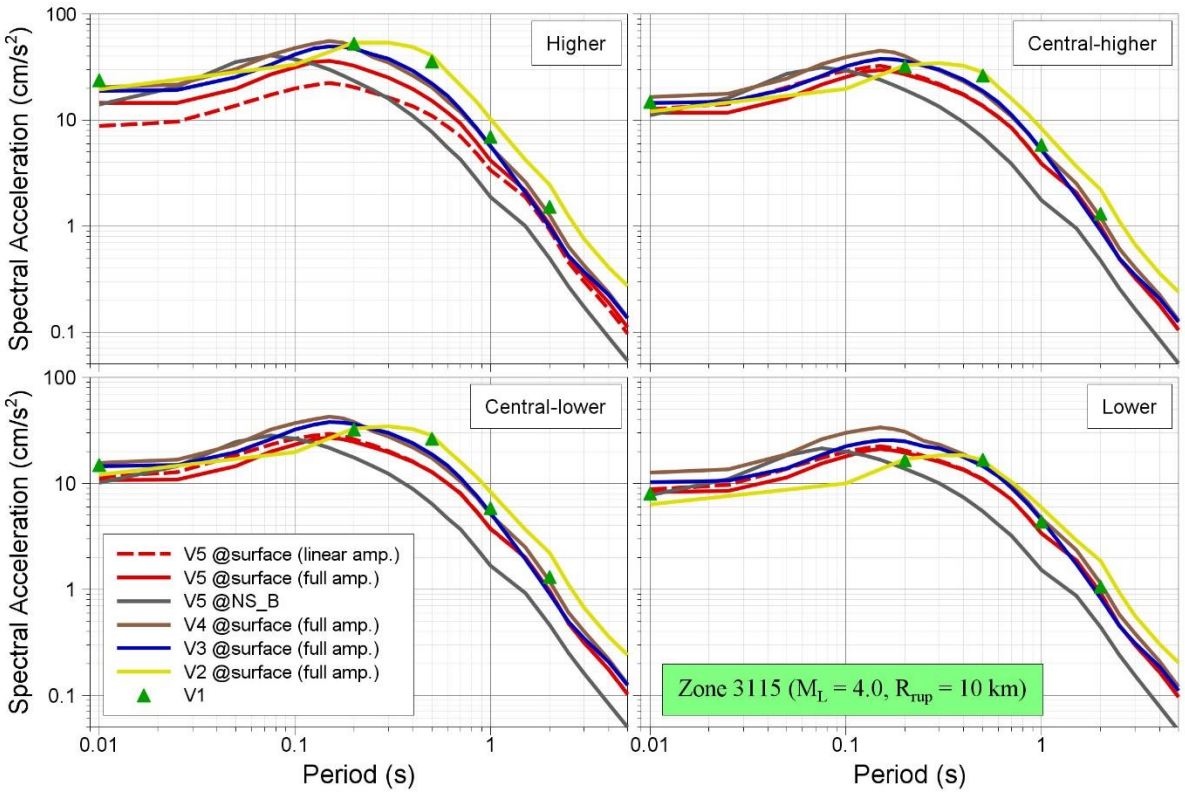
Higher
Central-higher
Central-lower
Lower
Spectral Acceleration (cm/s²)
Period (s)
V5 @surface (linear amp.)
V5 @surface (full amp.)
V5 @NS_B
V4 @surface (full amp.)
V3 @surface (full amp.)
V2 @surface (full amp.)
V1
Zone 3115 (M_L = 4.0, R_rup = 10 km)

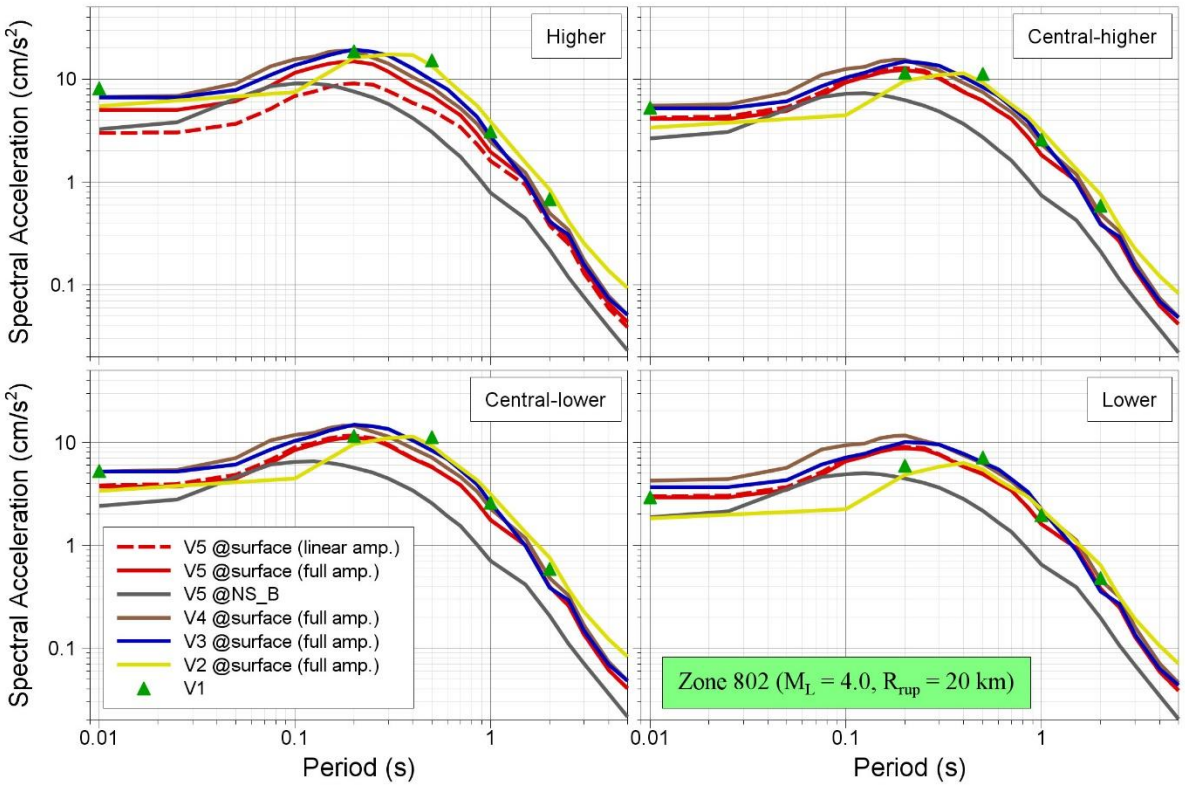
Higher
Central-higher
Central-lower
Lower
Spectral Acceleration (cm/s²)
Period (s)
V5 @surface (linear amp.)
V5 @surface (full amp.)
V5 @NS_B
V4 @surface (full amp.)
V3 @surface (full amp.)
V2 @surface (full amp.)
V1
Zone 802 (M_L = 4.0, R_rup = 20 km)

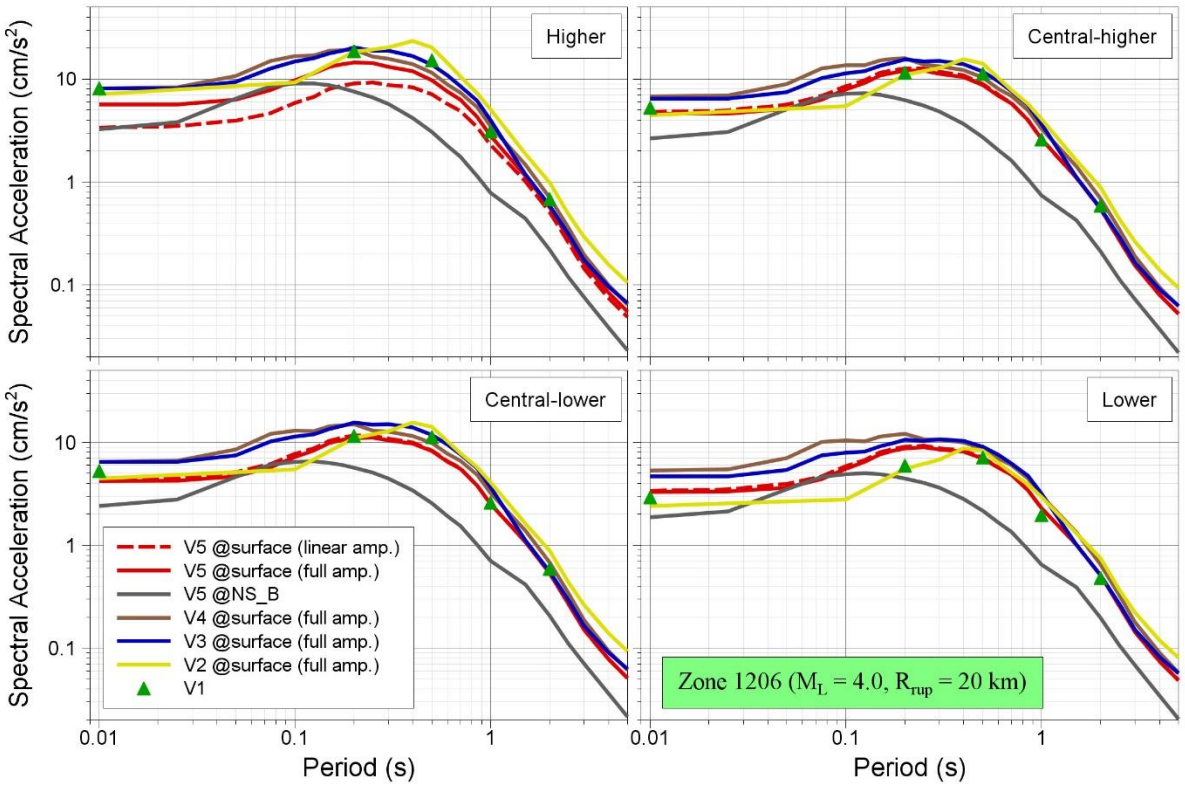
Higher
Central-higher
Central-lower
Lower
Spectral Acceleration (cm/s²)
Period (s)
V5 @surface (linear amp.)
V5 @surface (full amp.)
V5 @NS_B
V4 @surface (full amp.)
V3 @surface (full amp.)
V2 @surface (full amp.)
V1
Zone 1206 (M_L = 4.0, R_rup = 20 km)

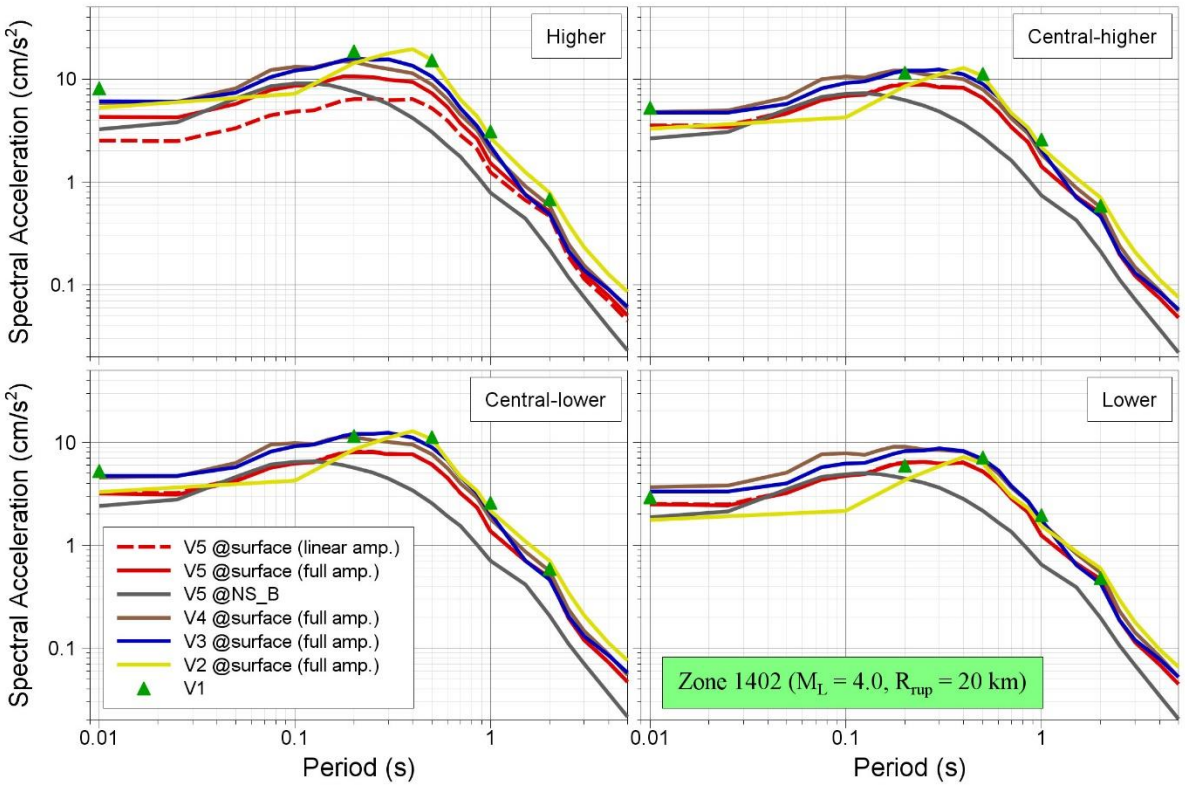
Higher
Central-higher
Central-lower
Lower
Spectral Acceleration (cm/s²)
Period (s)
V5 @surface (linear amp.)
V5 @surface (full amp.)
V5 @NS_B
V4 @surface (full amp.)
V3 @surface (full amp.)
V2 @surface (full amp.)
V1
Zone 1402 (M_L = 4.0, R_rup = 20 km)

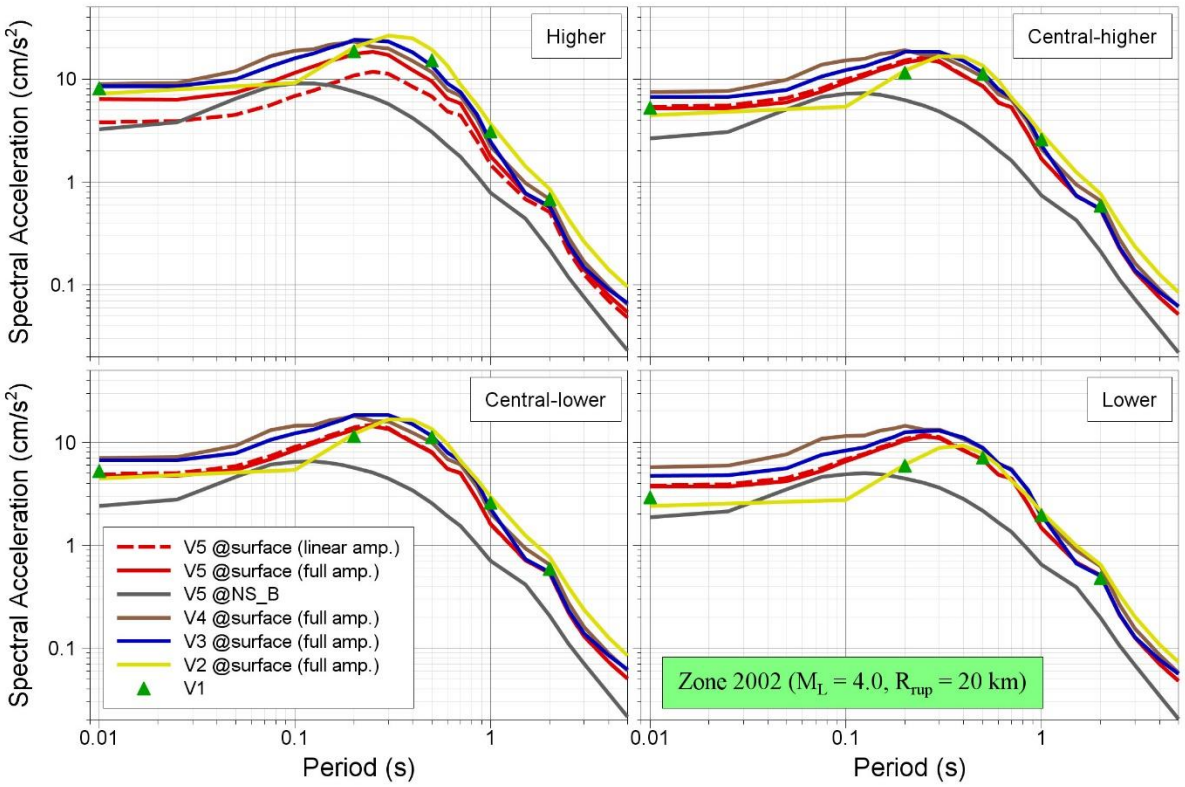
Higher
Central-higher
Central-lower
Lower
Spectral Acceleration (cm/s²)
Period (s)
V5 @surface (linear amp.)
V5 @surface (full amp.)
V5 @NS_B
V4 @surface (full amp.)
V3 @surface (full amp.)
V2 @surface (full amp.)
V1
Zone 2002 (M_L = 4.0, R_rup = 20 km)

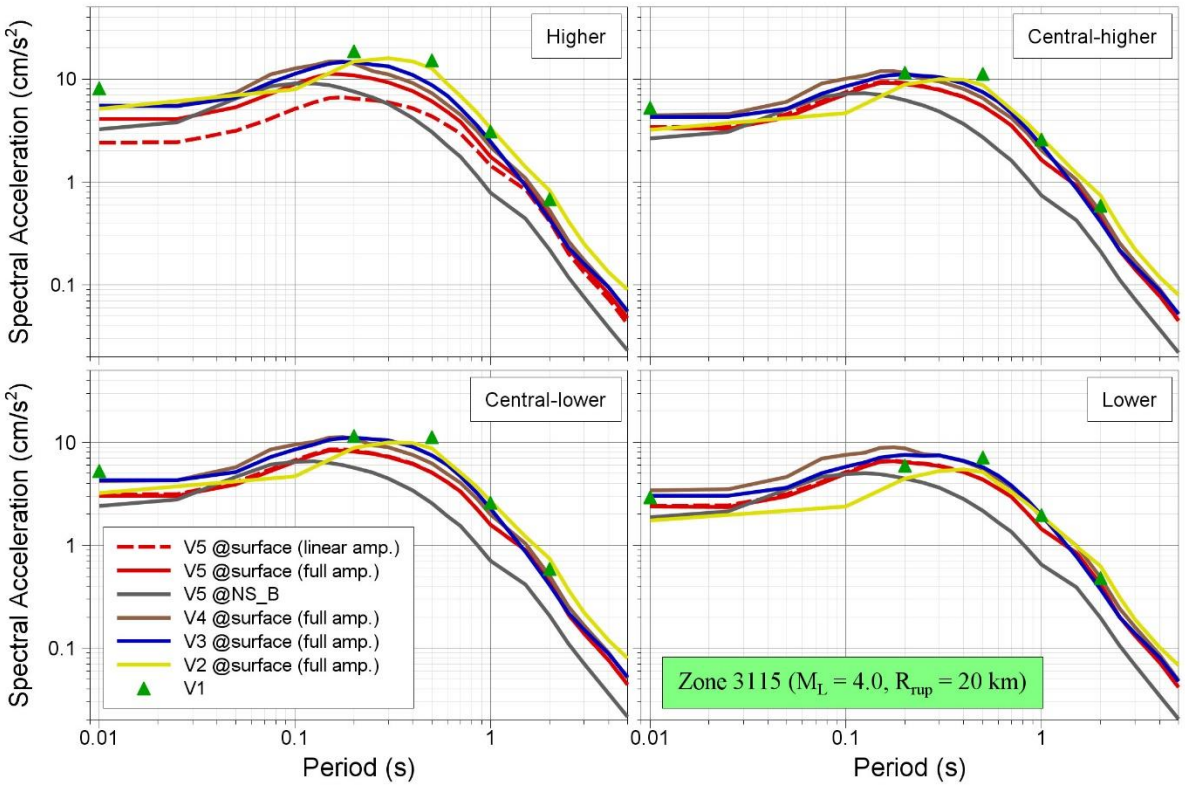
Higher
Central-higher
Central-lower
Lower
Spectral Acceleration (cm/s²)
Period (s)
V5 @surface (linear amp.)
V5 @surface (full amp.)
V5 @NS_B
V4 @surface (full amp.)
V3 @surface (full amp.)
V2 @surface (full amp.)
V1
Zone 3115 (M_L = 4.0, R_rup = 20 km)

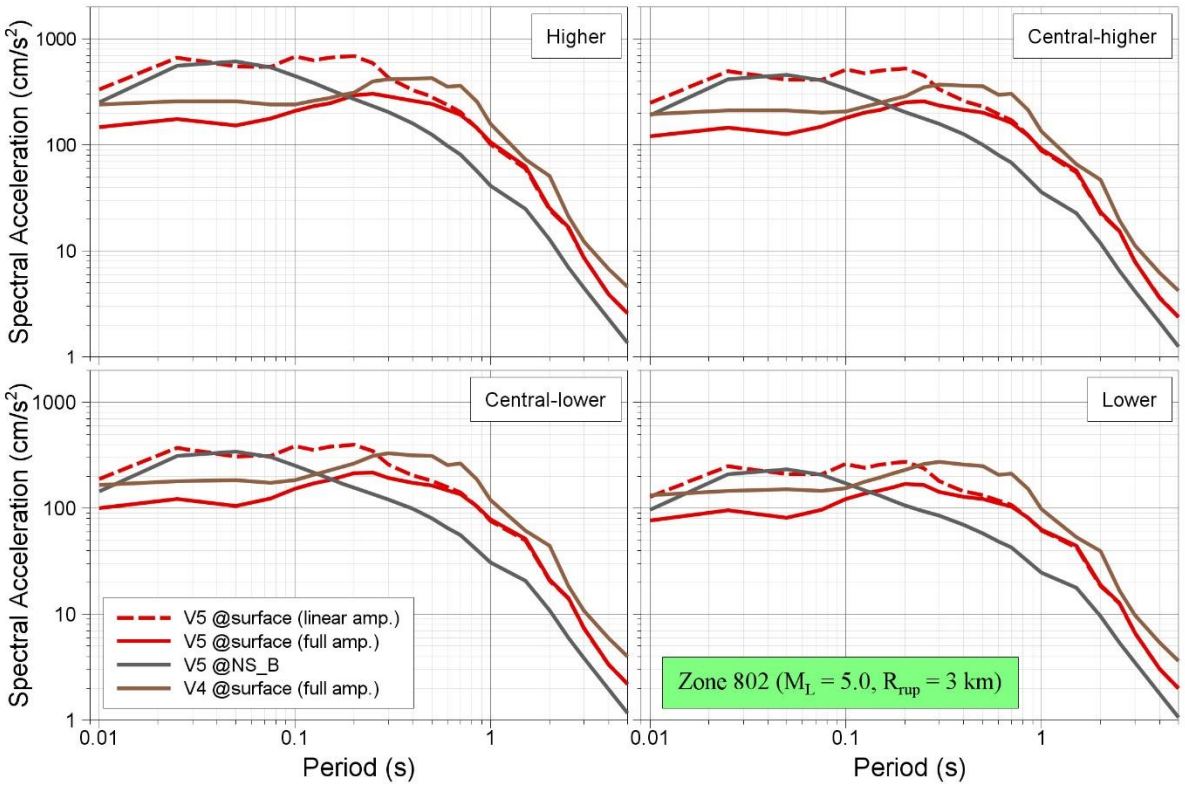
Higher
Central-higher
Central-lower
Lower
Spectral Acceleration (cm/s²)
Period (s)
V5 @surface (linear amp.)
V5 @surface (full amp.)
V5 @NS_B
V4 @surface (full amp.)
Zone 802 (M_L = 5.0, R_rup = 3 km)

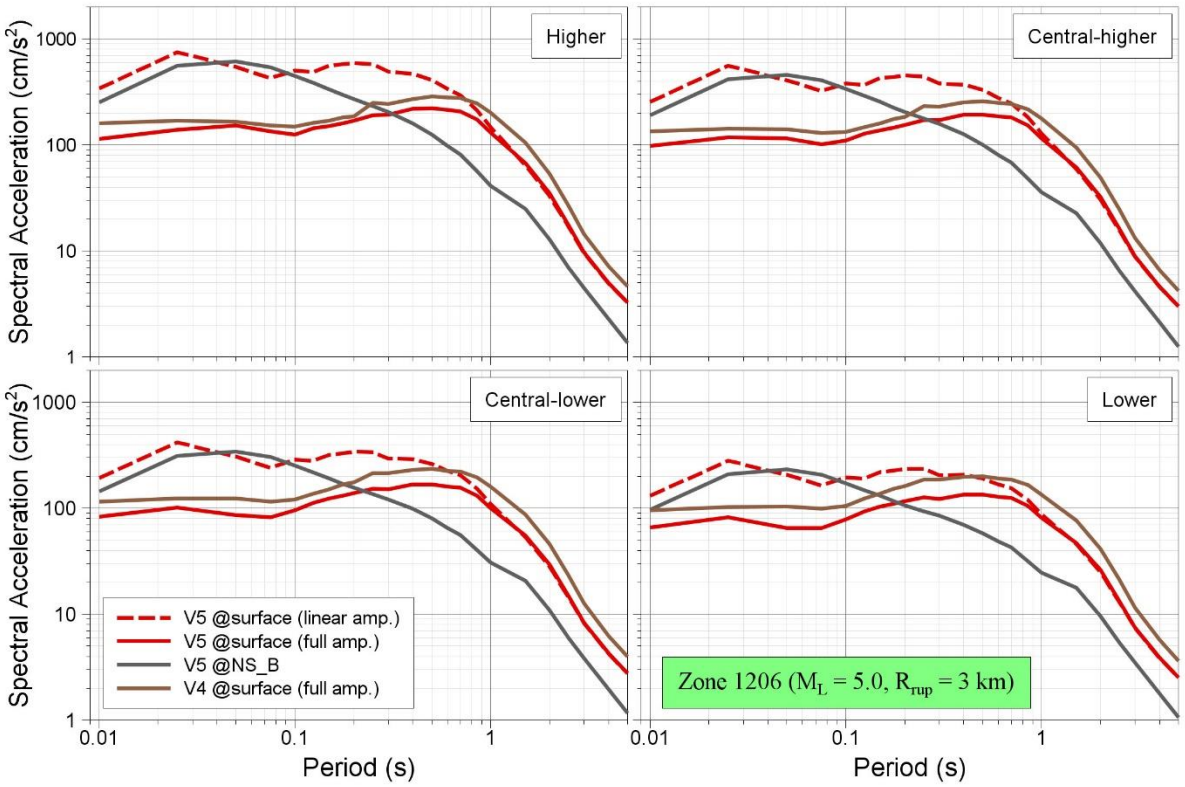
Higher
Central-higher
Central-lower
Lower
Spectral Acceleration (cm/s²)
Period (s)
V5 @surface (linear amp.)
V5 @surface (full amp.)
V5 @NS_B
V4 @surface (full amp.)
Zone 1206 (M_L = 5.0, R_rup = 3 km)

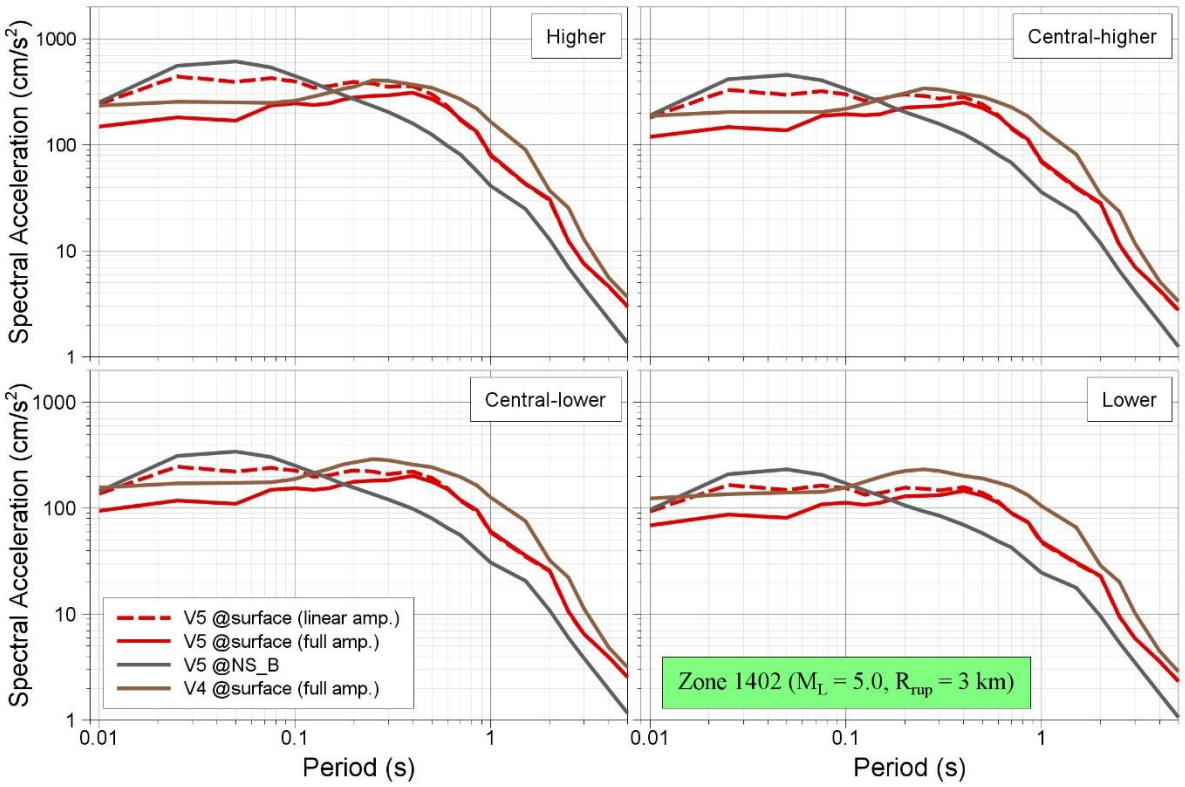
Higher
Central-higher
Central-lower
Lower
Spectral Acceleration (cm/s²)
1000
100
10
1
0.01
0.1
1
Period (s)
V5 @surface (linear amp.)
V5 @surface (full amp.)
V5 @NS_B
V4 @surface (full amp.)
Zone 1402 (M_L = 5.0, R_rup = 3 km)

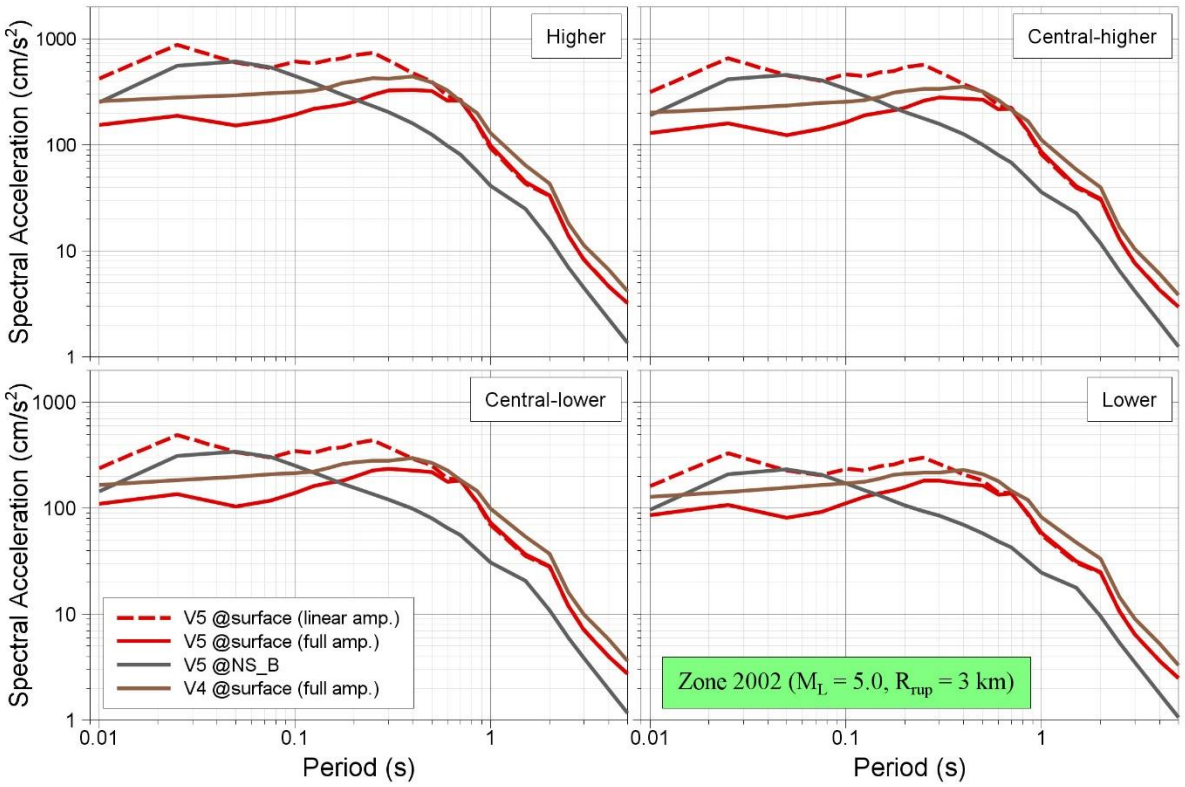
Higher
Central-higher
Central-lower
Lower
Spectral Acceleration (cm/s²)
1000
100
10
1
0.01
0.1
1
Period (s)
V5 @surface (linear amp.)
V5 @surface (full amp.)
V5 @NS_B
V4 @surface (full amp.)
Zone 2002 (M_L = 5.0, R_rup = 3 km)

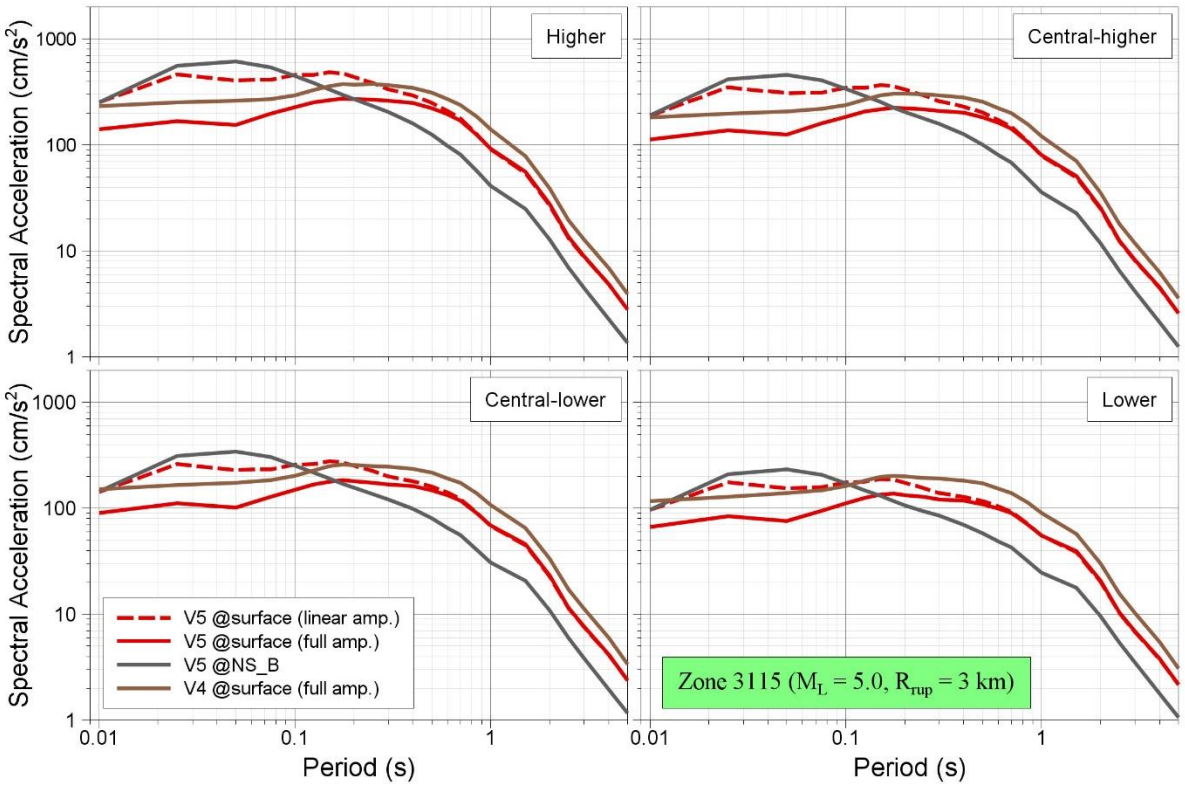
Higher
Central-higher
Central-lower
Lower
Spectral Acceleration (cm/s²)
Period (s)
V5 @surface (linear amp.)
V5 @surface (full amp.)
V5 @NS_B
V4 @surface (full amp.)
Zone 3115 (M_L = 5.0, R_rup = 3 km)

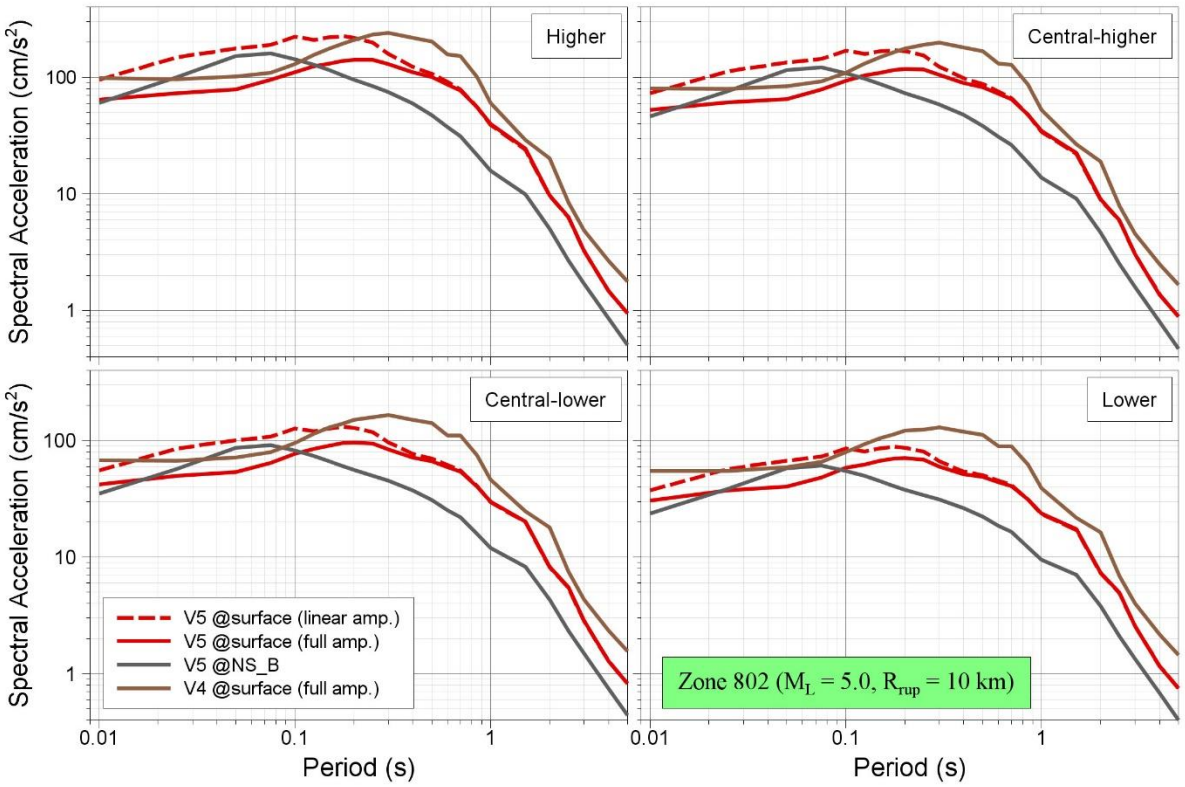
Higher
Central-higher
Central-lower
Lower
Spectral Acceleration (cm/s²)
Period (s)
V5 @surface (linear amp.)
V5 @surface (full amp.)
V5 @NS_B
V4 @surface (full amp.)
Zone 802 (M_L = 5.0, R_rup = 10 km)

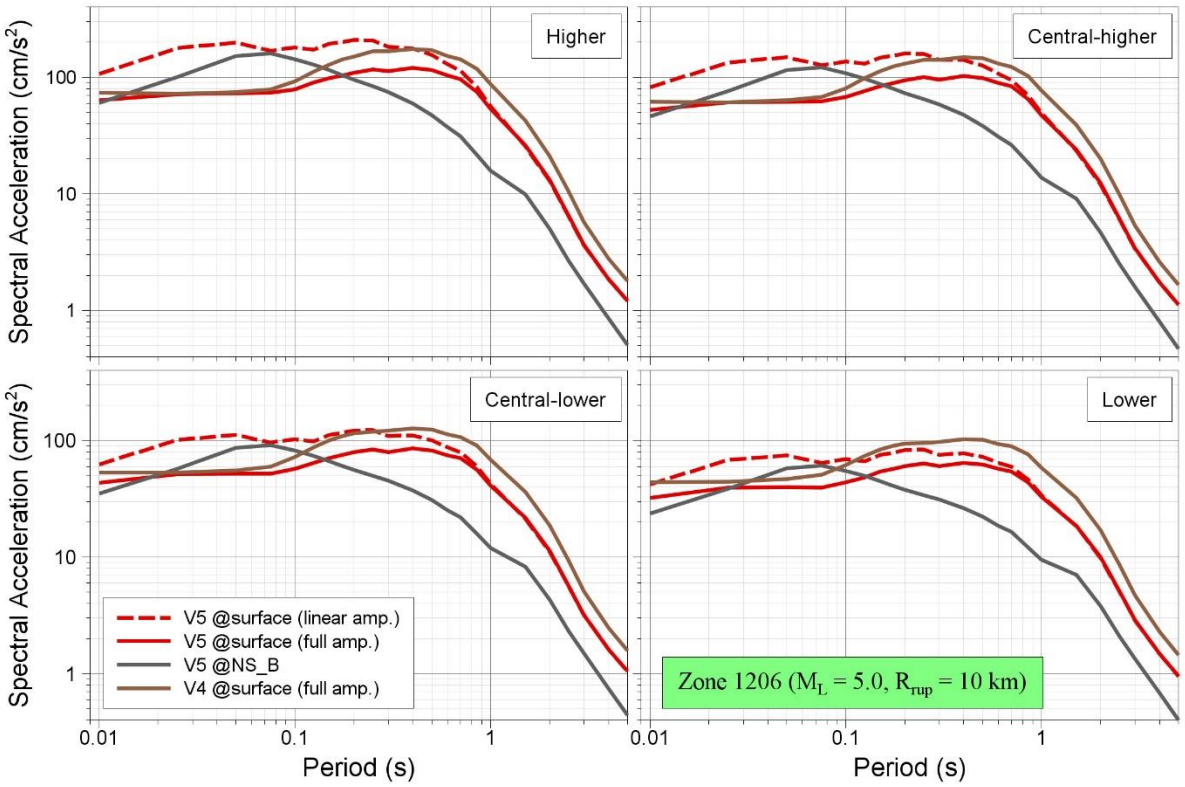
Higher
Central-higher
Central-lower
Lower
Spectral Acceleration (cm/s²)
100
10
1
0.01
0.1
1
Period (s)
V5 @surface (linear amp.)
V5 @surface (full amp.)
V5 @NS_B
V4 @surface (full amp.)
Zone 1206 (M_L = 5.0, R_rup = 10 km)

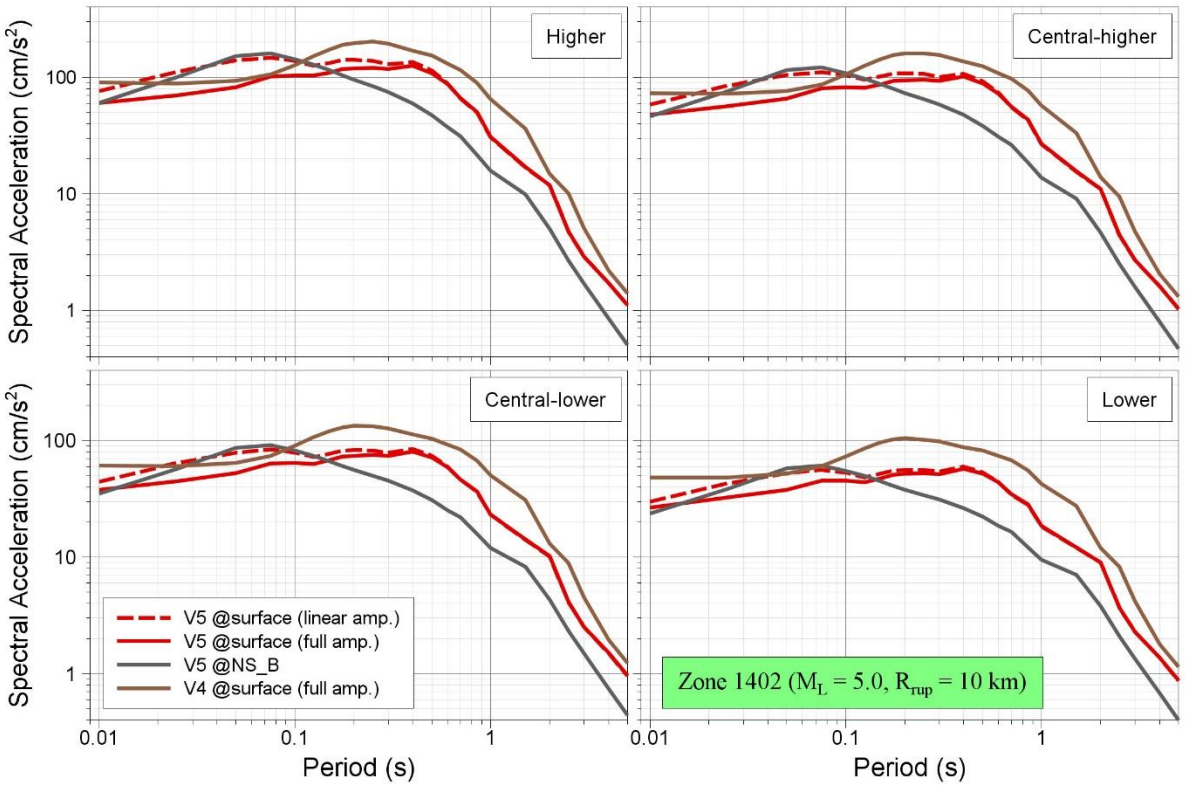
Higher
Central-higher
Central-lower
Lower
Spectral Acceleration (cm/s²)
100
10
1
0.01
0.1
1
Period (s)
V5 @surface (linear amp.)
V5 @surface (full amp.)
V5 @NS_B
V4 @surface (full amp.)
Zone 1402 (M_L = 5.0, R_rup = 10 km)

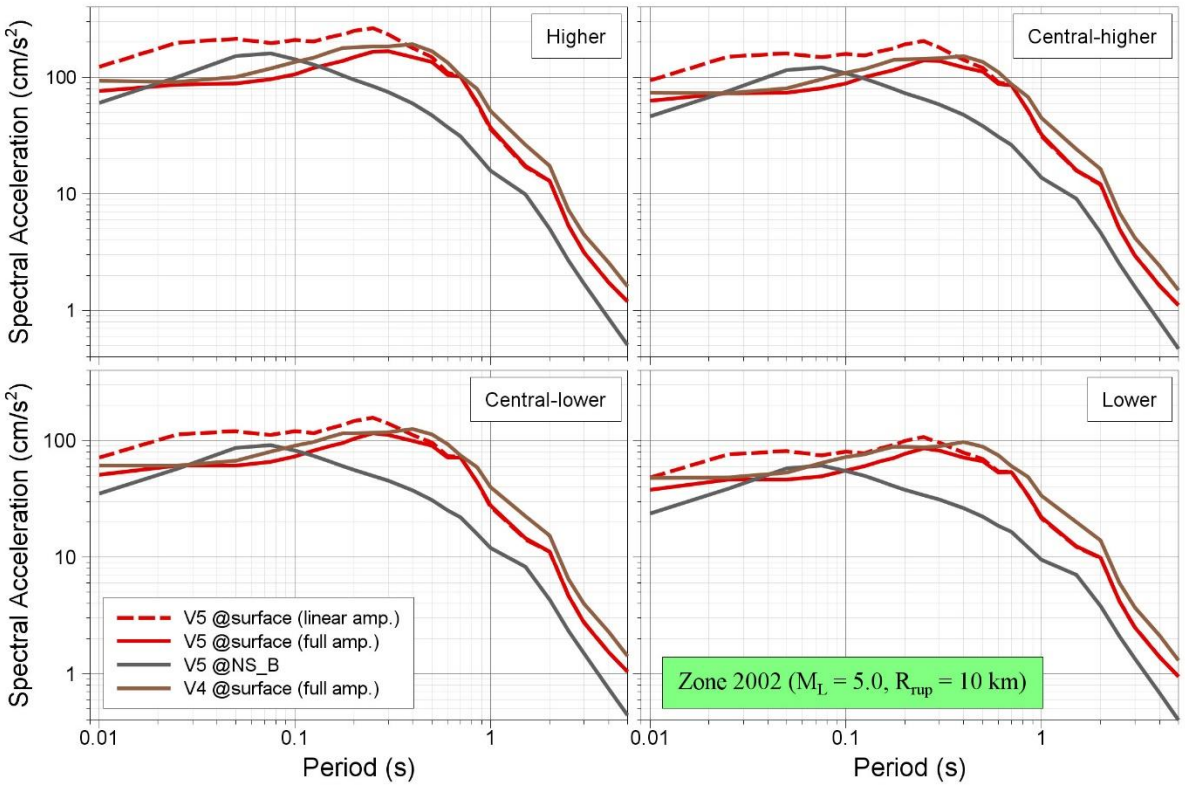
Higher
Central-higher
Central-lower
Lower
Spectral Acceleration (cm/s²)
100
10
1
0.01
0.1
1
Period (s)
V5 @surface (linear amp.)
V5 @surface (full amp.)
V5 @NS_B
V4 @surface (full amp.)
Zone 2002 (M_L = 5.0, R_rup = 10 km)

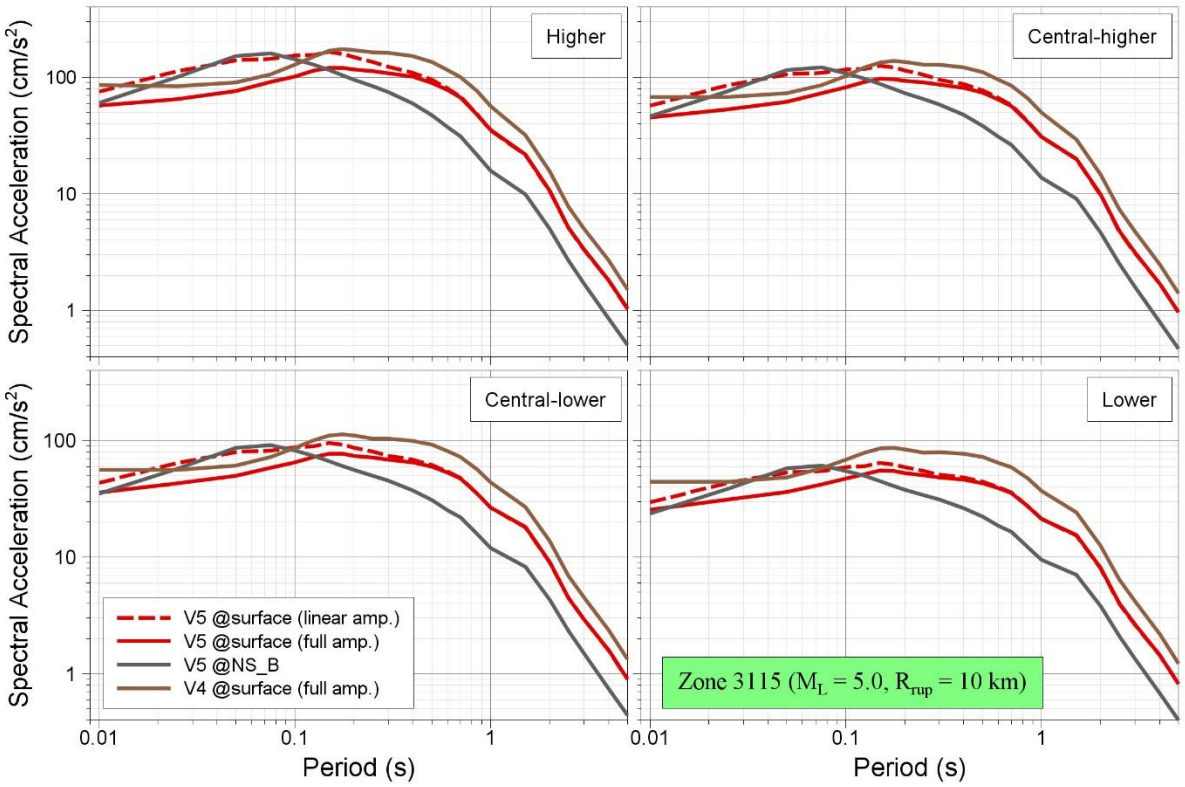
Higher
Central-higher
Central-lower
Lower
Spectral Acceleration (cm/s²)
100
10
1
0.01
0.1
1
Period (s)
V5 @surface (linear amp.)
V5 @surface (full amp.)
V5 @NS_B
V4 @surface (full amp.)
Zone 3115 (M_L = 5.0, R_rup = 10 km)

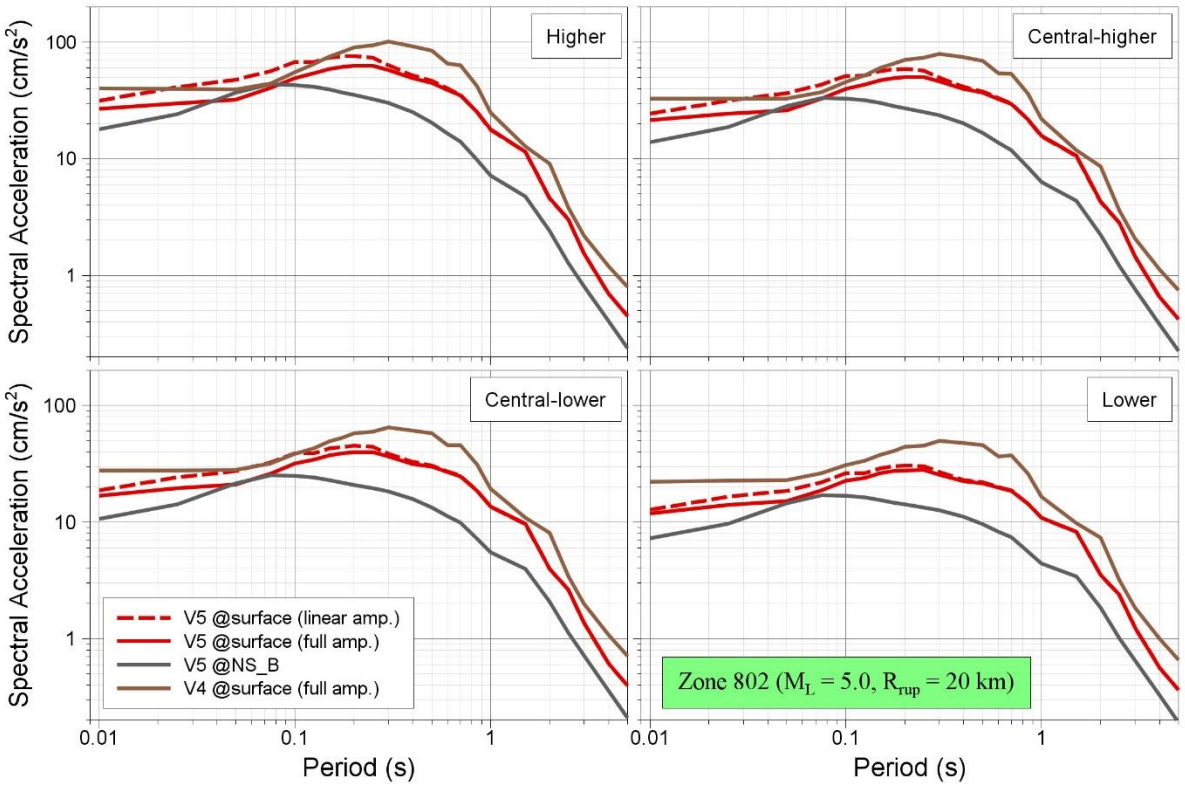
Higher
Central-higher
Central-lower
Lower
Spectral Acceleration (cm/s²)
Period (s)
V5 @surface (linear amp.)
V5 @surface (full amp.)
V5 @NS_B
V4 @surface (full amp.)
Zone 802 (M_L = 5.0, R_rup = 20 km)

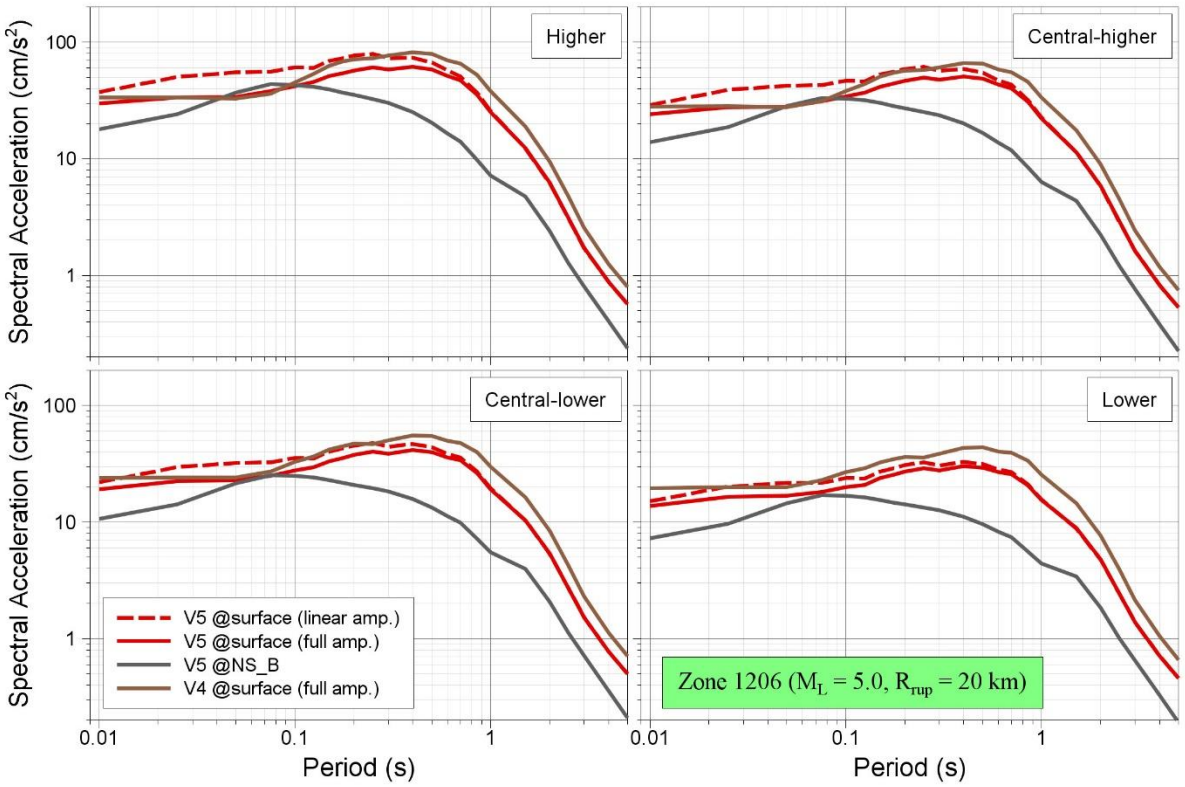
Higher
Central-higher
Central-lower
Lower
Spectral Acceleration (cm/s²)
Period (s)
V5 @surface (linear amp.)
V5 @surface (full amp.)
V5 @NS_B
V4 @surface (full amp.)
Zone 1206 (M_L = 5.0, R_rup = 20 km)

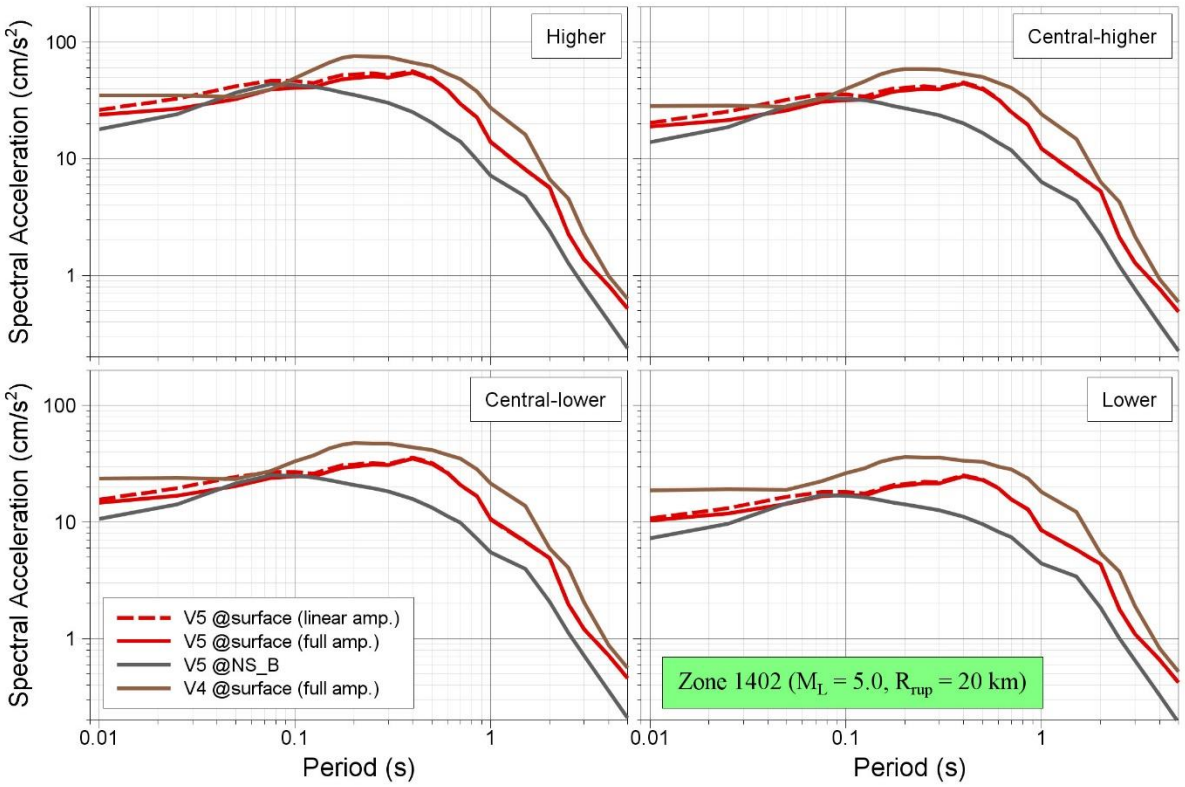
Higher
Central-higher
Central-lower
Lower
Spectral Acceleration (cm/s²)
100
10
1
0.01
0.1
1
Period (s)
V5 @surface (linear amp.)
V5 @surface (full amp.)
V5 @NS_B
V4 @surface (full amp.)
Zone 1402 (M_L = 5.0, R_rup = 20 km)

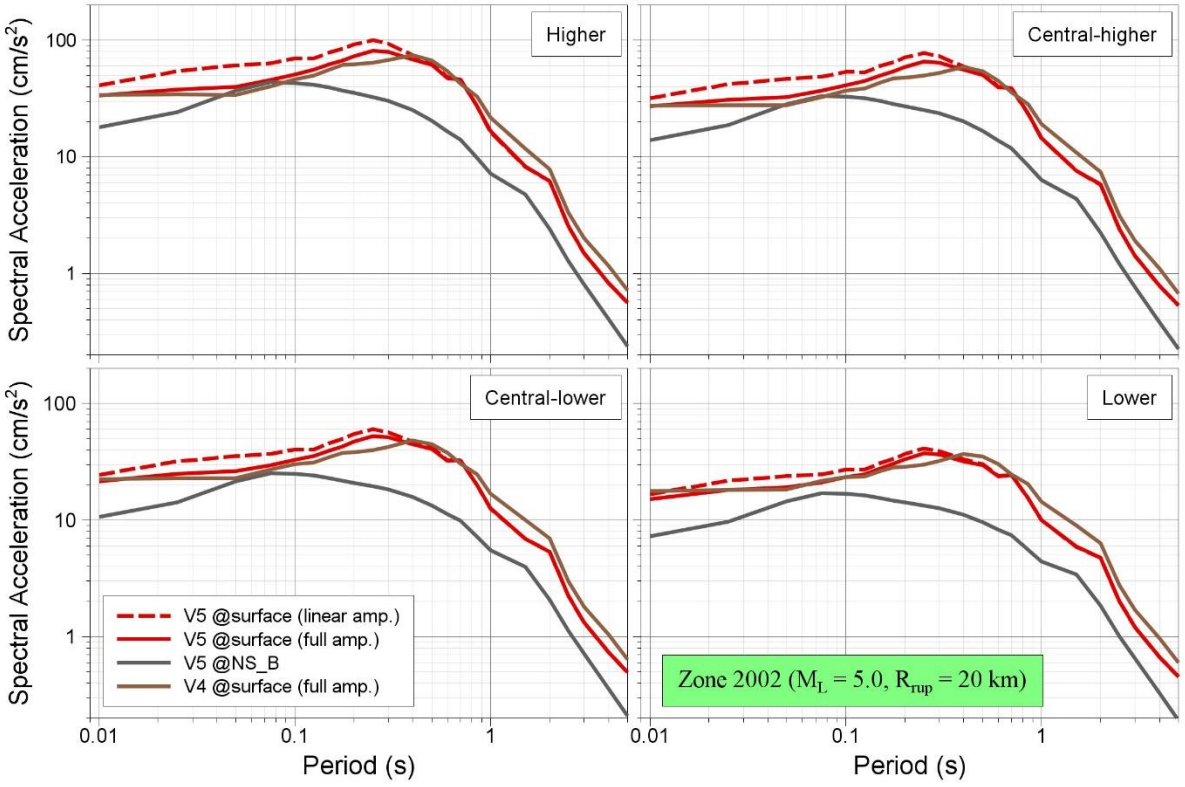
Higher
Central-higher
Central-lower
Lower
Spectral Acceleration (cm/s²)
100
10
1
0.01
0.1
1
Period (s)
V5 @surface (linear amp.)
V5 @surface (full amp.)
V5 @NS_B
V4 @surface (full amp.)
Zone 2002 (M_L = 5.0, R_rup = 20 km)

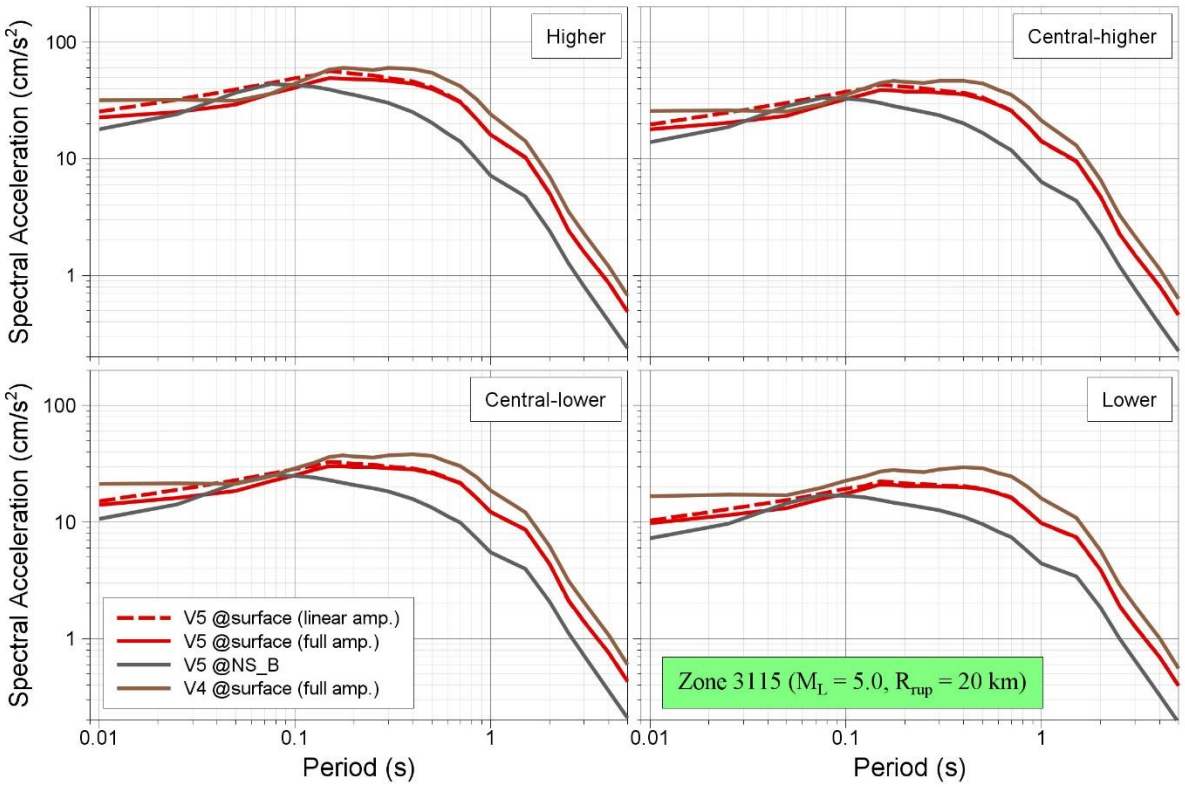
Higher
Central-higher
Central-lower
Lower
Spectral Acceleration (cm/s²)
Period (s)
V5 @surface (linear amp.)
V5 @surface (full amp.)
V5 @NS_B
V4 @surface (full amp.)
Zone 3115 (M_L = 5.0, R_rup = 20 km)

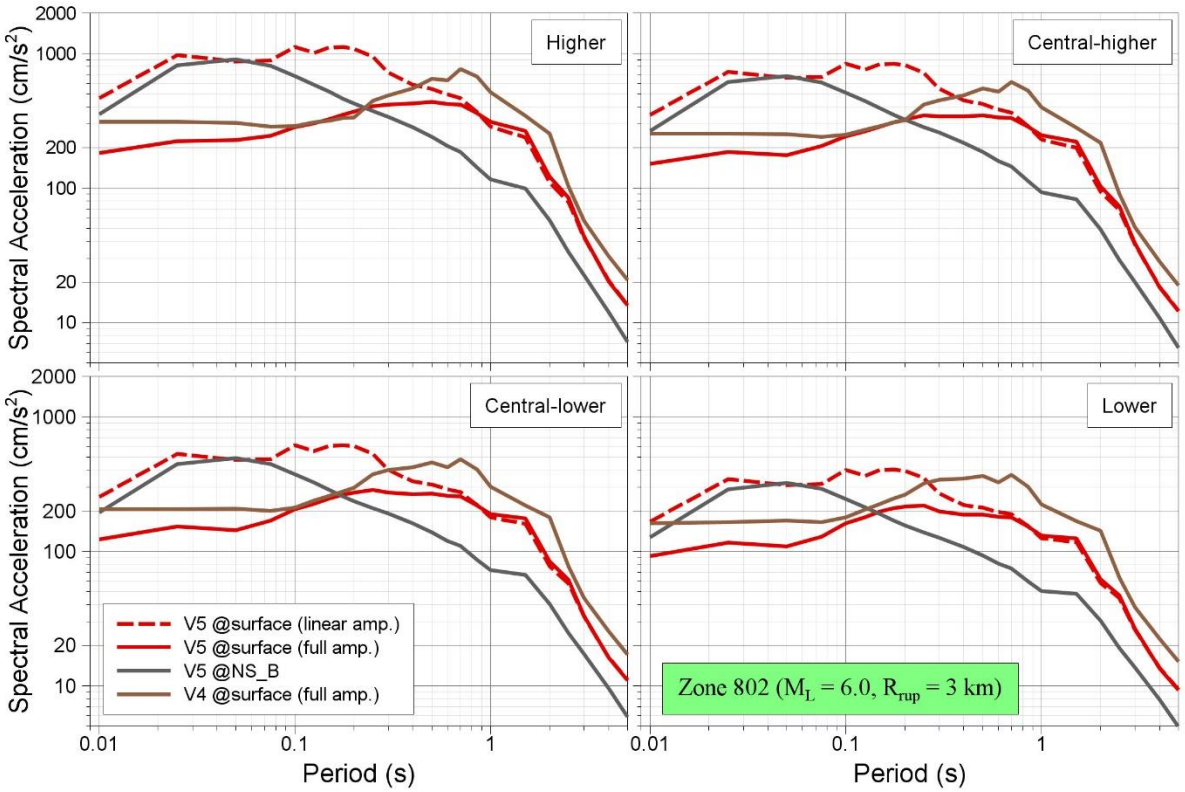
Higher
Central-higher
Central-lower
Lower
Spectral Acceleration (cm/s²)
Period (s)
V5 @surface (linear amp.)
V5 @surface (full amp.)
V5 @NS_B
V4 @surface (full amp.)
Zone 802 (M_L = 6.0, R_rup = 3 km)

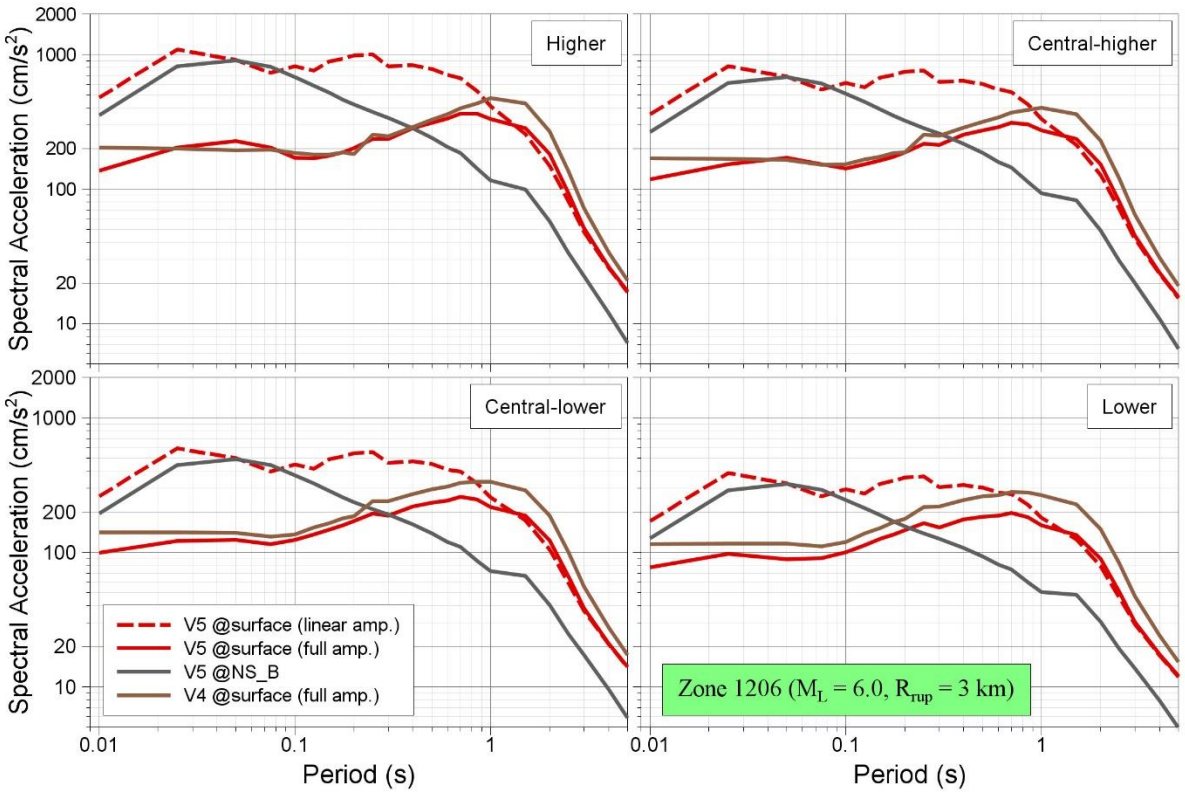
Higher
Central-higher
Central-lower
Lower
Spectral Acceleration (cm/s²)
2000
1000
200
100
20
10
0.01
0.1
1
Period (s)
V5 @surface (linear amp.)
V5 @surface (full amp.)
V5 @NS_B
V4 @surface (full amp.)
Zone 1206 (M_L = 6.0, R_rup = 3 km)

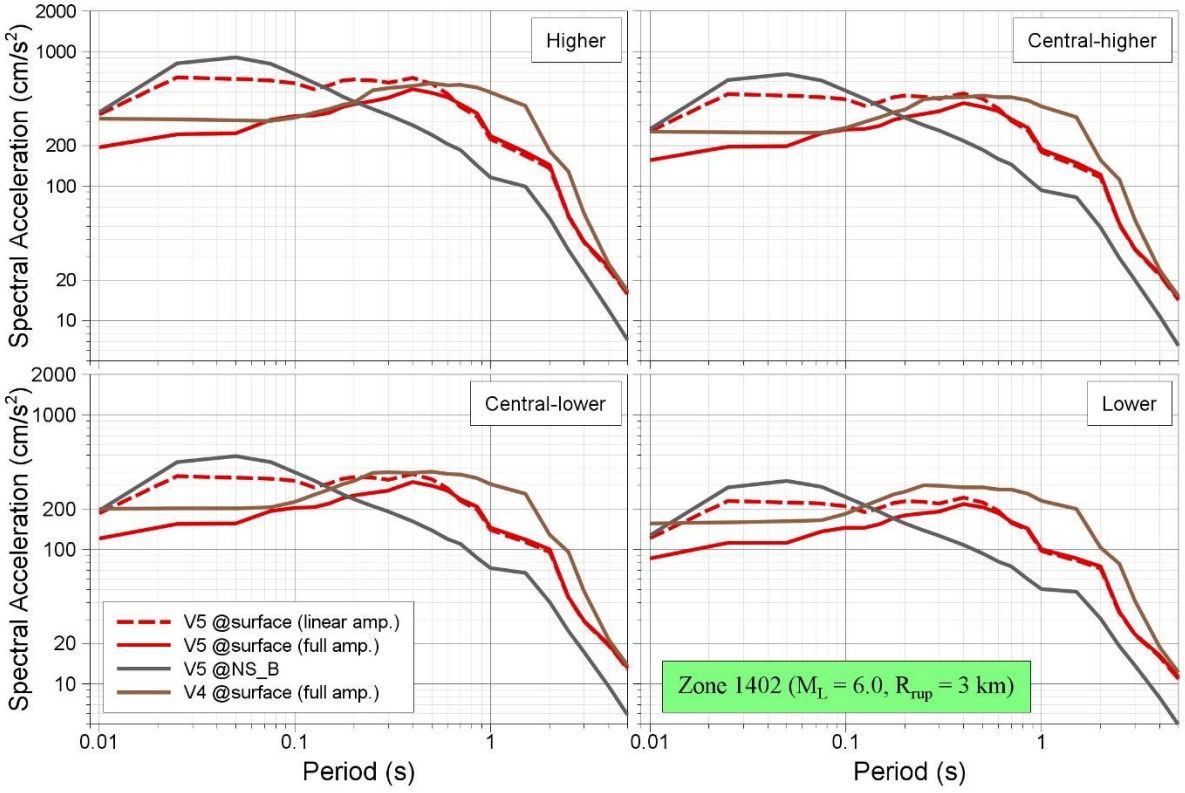
Higher
Central-higher
Central-lower
Lower
Spectral Acceleration (cm/s²)
2000
1000
200
100
20
10
0.01
0.1
1
Period (s)
V5 @surface (linear amp.)
V5 @surface (full amp.)
V5 @NS_B
V4 @surface (full amp.)
Zone 1402 (M_L = 6.0, R_rup = 3 km)

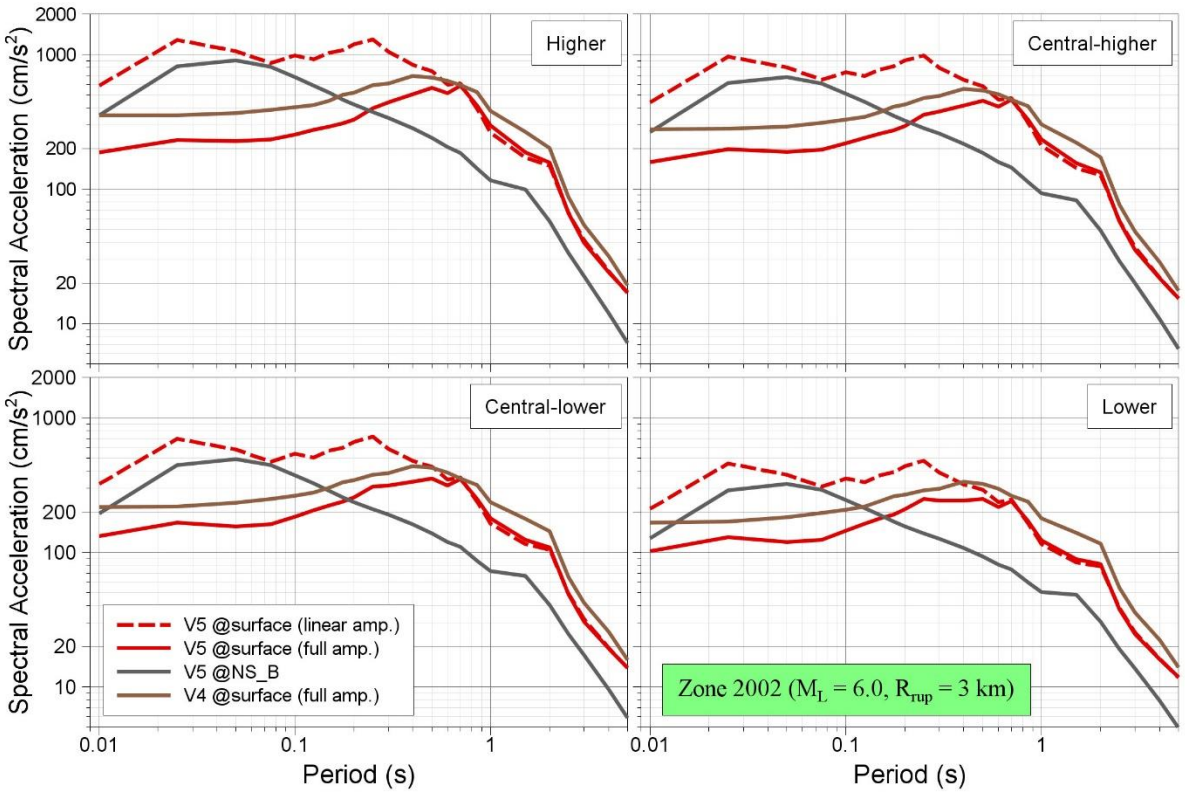
Higher
Central-higher
Central-lower
Lower
Spectral Acceleration (cm/s²)
2000
1000
200
100
20
10
0.01
0.1
1
Period (s)
V5 @surface (linear amp.)
V5 @surface (full amp.)
V5 @NS_B
V4 @surface (full amp.)
Zone 2002 (M_L = 6.0, R_rup = 3 km)

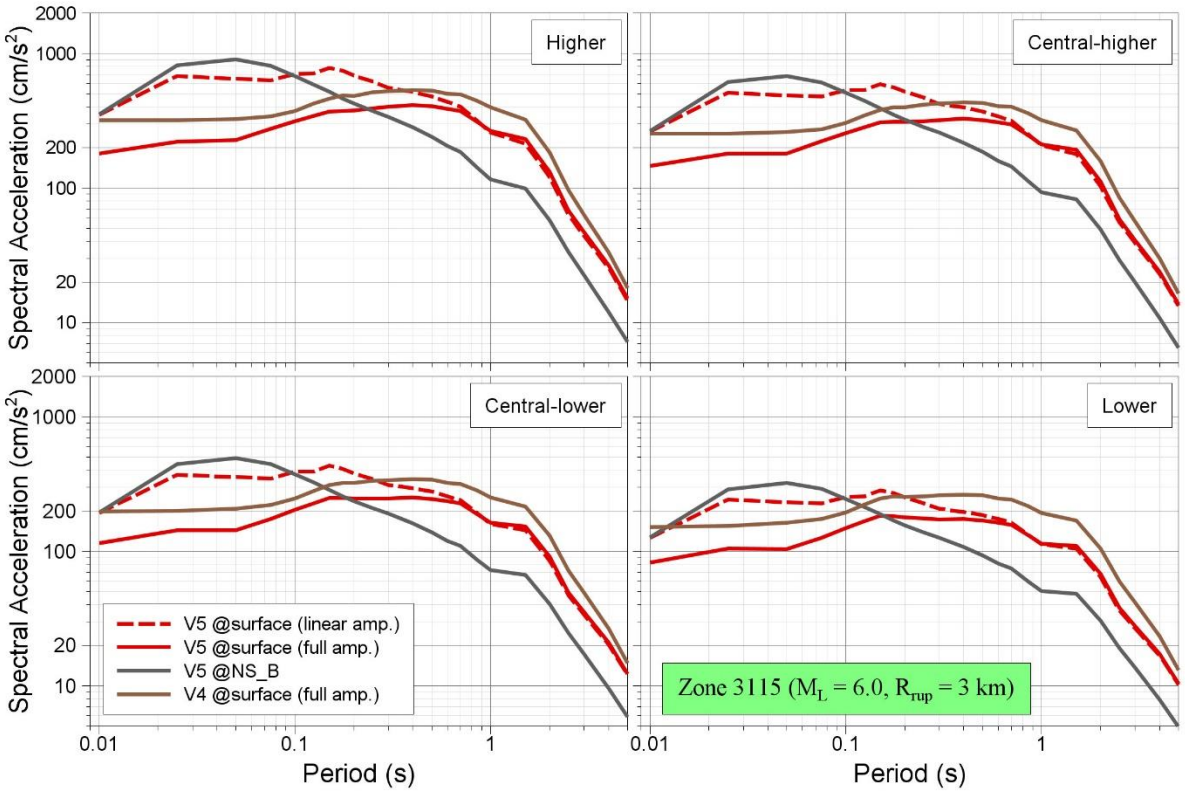
Higher
Central-higher
Central-lower
Lower
Spectral Acceleration (cm/s²)
2000
1000
200
100
20
10
0.01
0.1
1
Period (s)
V5 @surface (linear amp.)
V5 @surface (full amp.)
V5 @NS_B
V4 @surface (full amp.)
Zone 3115 (M_L = 6.0, R_rup = 3 km)

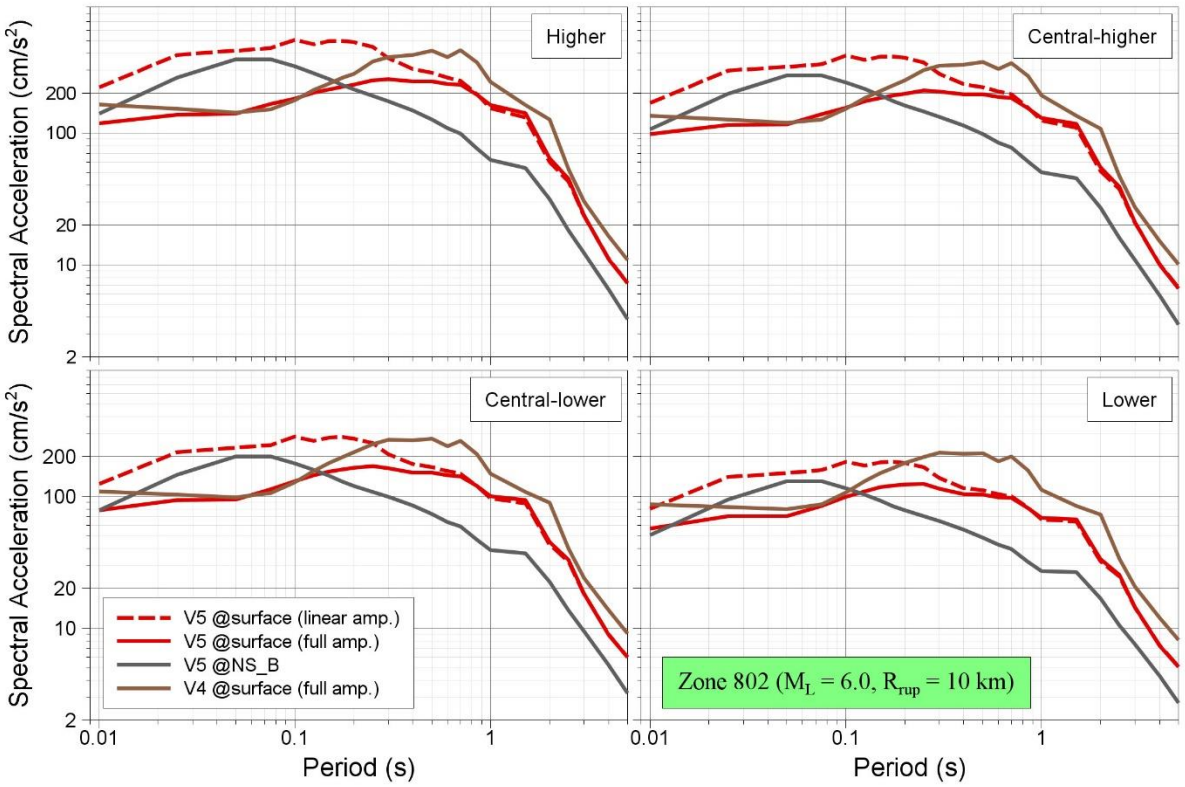
Higher
Central-higher
Central-lower
Lower
Spectral Acceleration (cm/s²)
Period (s)
V5 @surface (linear amp.)
V5 @surface (full amp.)
V5 @NS_B
V4 @surface (full amp.)
Zone 802 (M_L = 6.0, R_rup = 10 km)

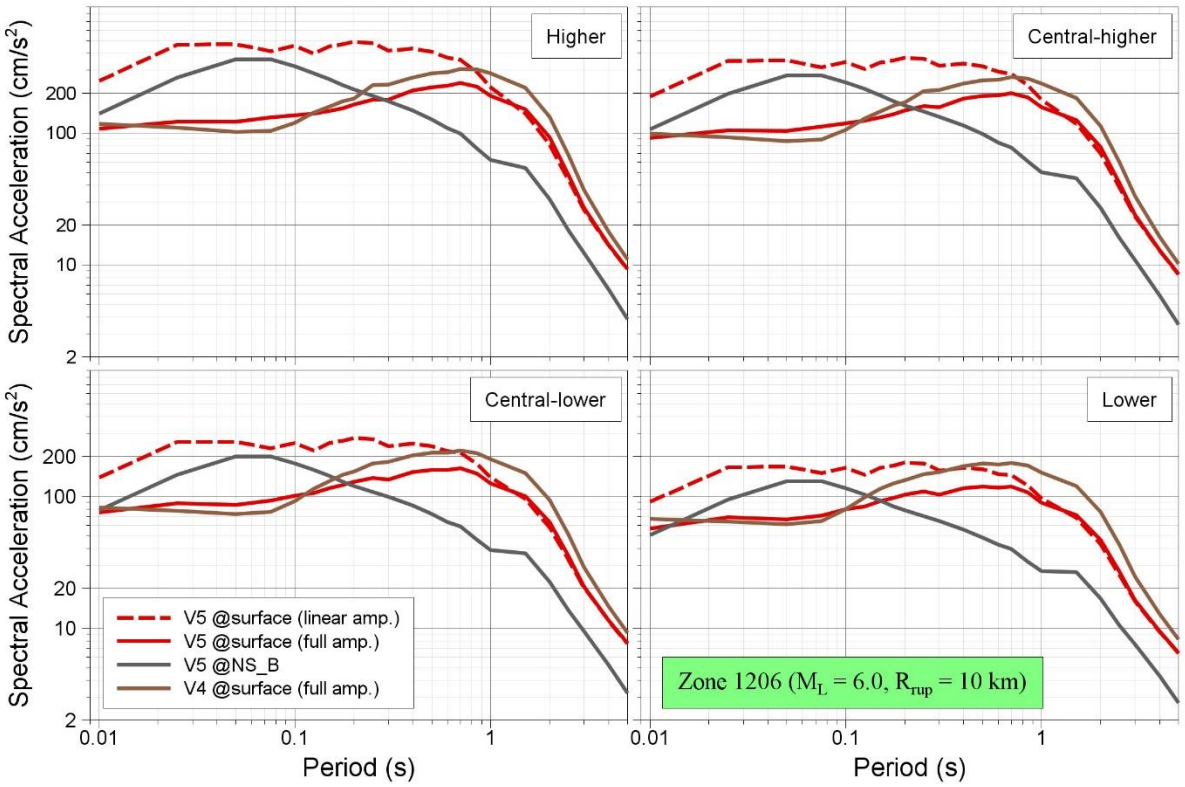
Higher
Central-higher
Central-lower
Lower
Spectral Acceleration (cm/s²)
Period (s)
V5 @surface (linear amp.)
V5 @surface (full amp.)
V5 @NS_B
V4 @surface (full amp.)
Zone 1206 (M_L = 6.0, R_rup = 10 km)

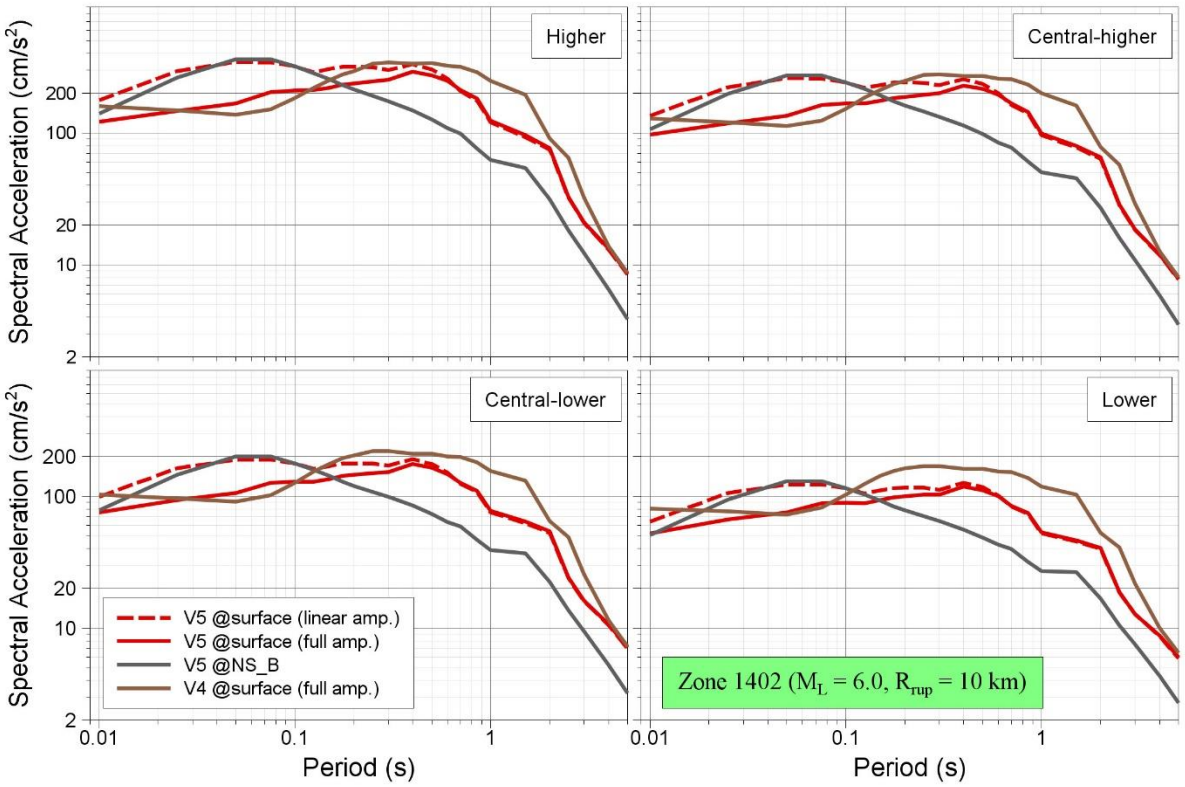
Higher
Central-higher
Central-lower
Lower
Spectral Acceleration (cm/s²)
Period (s)
V5 @surface (linear amp.)
V5 @surface (full amp.)
V5 @NS_B
V4 @surface (full amp.)
Zone 1402 (M_L = 6.0, R_rup = 10 km)

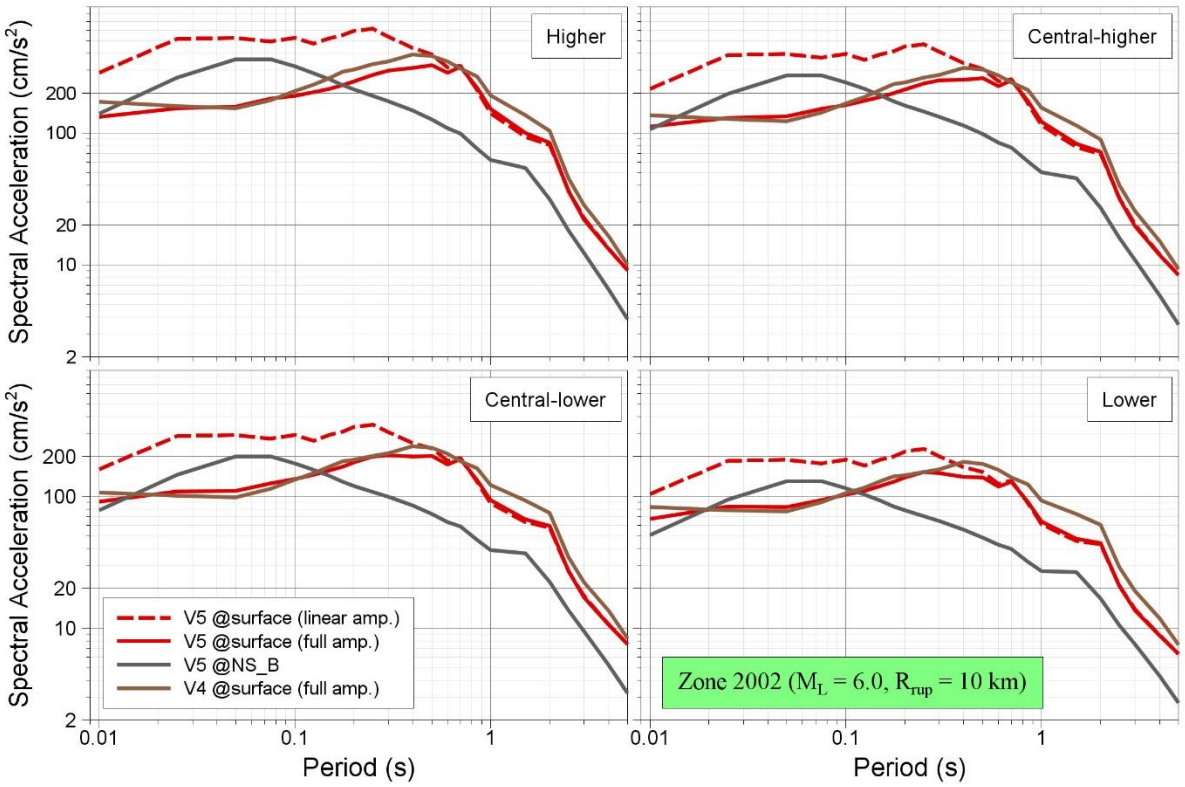
Higher
Central-higher
Central-lower
Lower
Spectral Acceleration (cm/s²)
Period (s)
V5 @surface (linear amp.)
V5 @surface (full amp.)
V5 @NS_B
V4 @surface (full amp.)
Zone 2002 (M_L = 6.0, R_rup = 10 km)

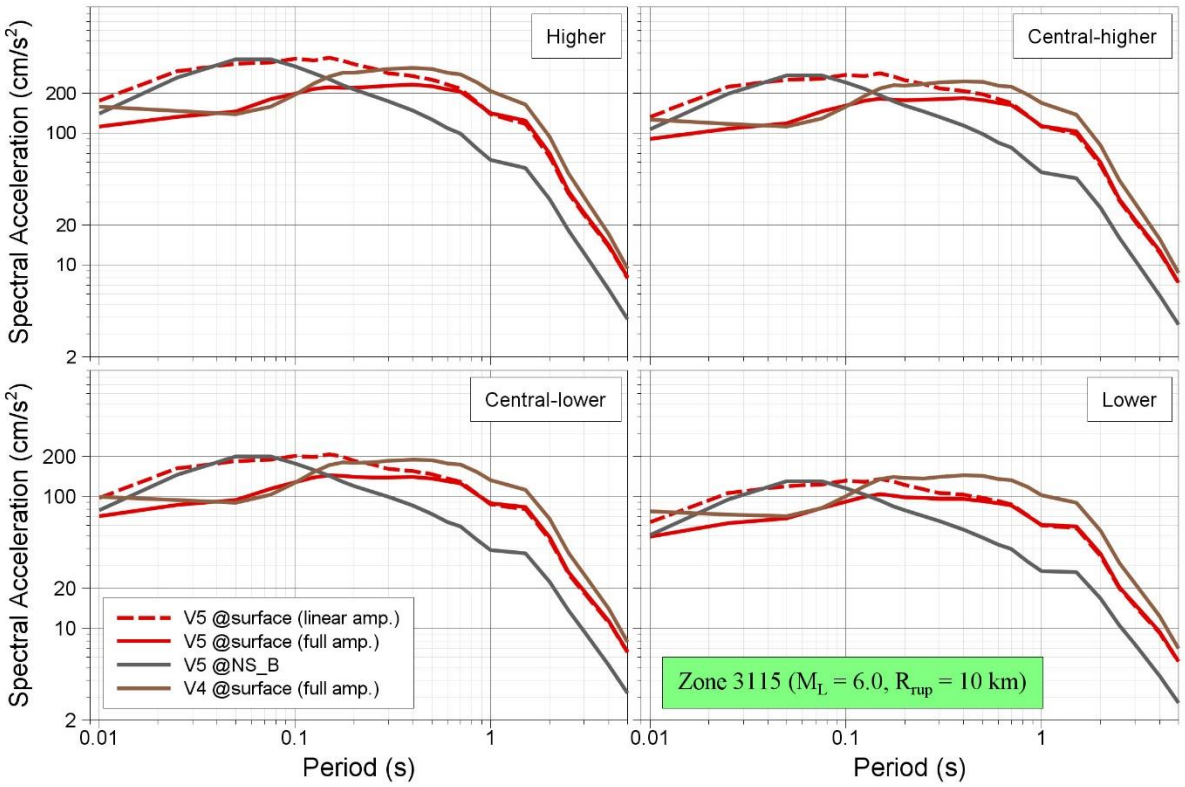
Higher
Central-higher
Central-lower
Lower
Spectral Acceleration (cm/s²)
Period (s)
V5 @surface (linear amp.)
V5 @surface (full amp.)
V5 @NS_B
V4 @surface (full amp.)
Zone 3115 (M_L = 6.0, R_rup = 10 km)

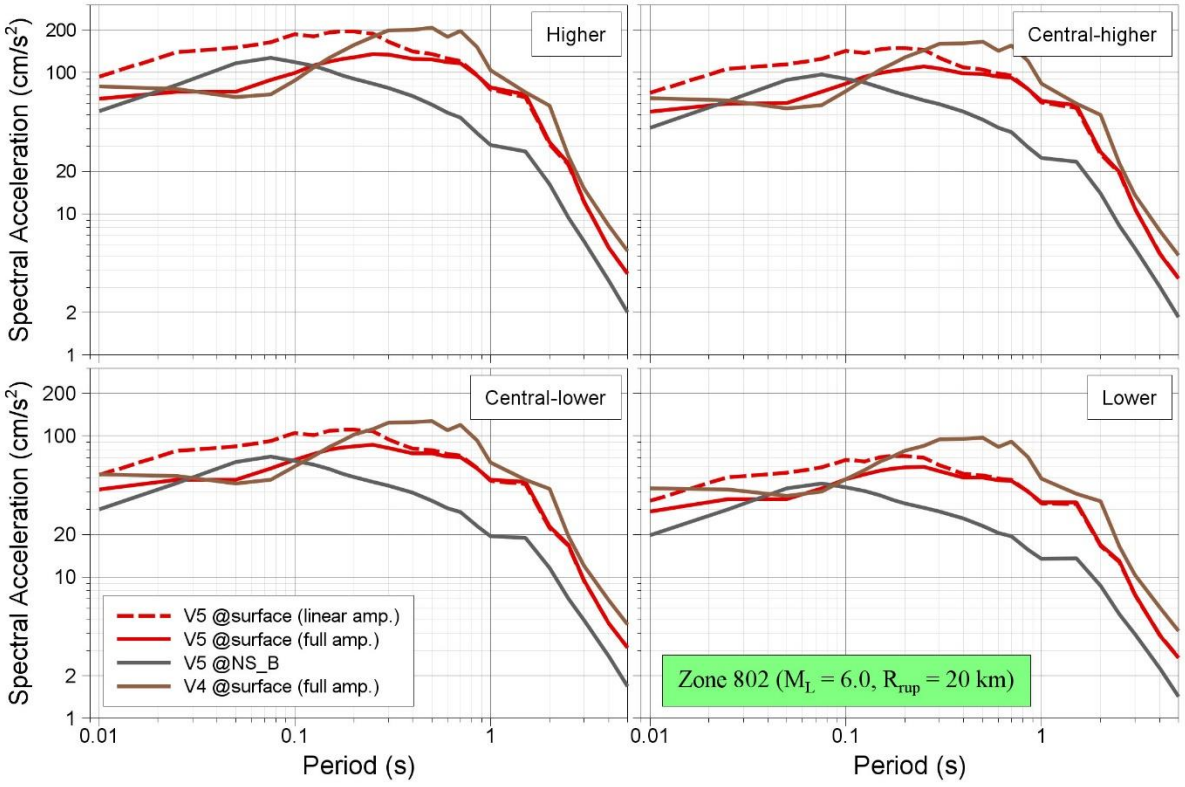
Higher
Central-higher
Central-lower
Lower
Spectral Acceleration (cm/s²)
Period (s)
V5 @surface (linear amp.)
V5 @surface (full amp.)
V5 @NS_B
V4 @surface (full amp.)
Zone 802 (M_L = 6.0, R_rup = 20 km)

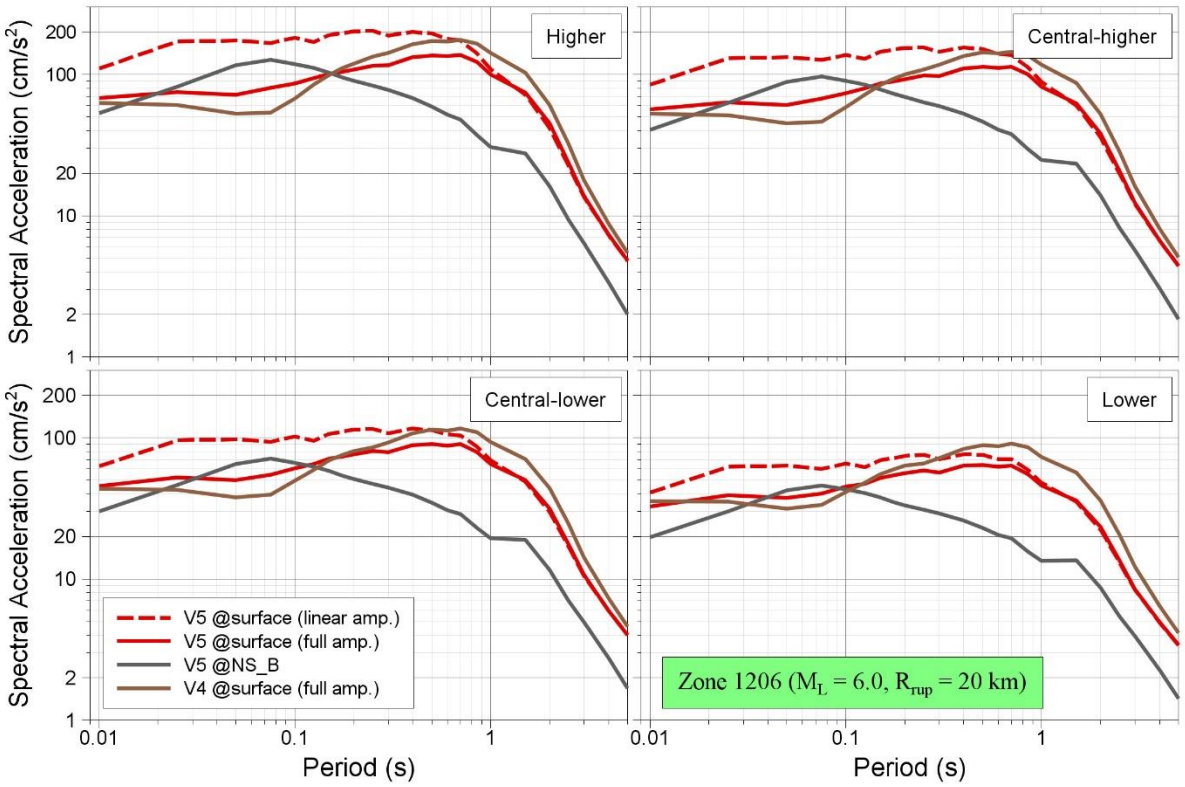
Higher
Central-higher
Central-lower
Lower
Spectral Acceleration (cm/s²)
Period (s)
V5 @surface (linear amp.)
V5 @surface (full amp.)
V5 @NS_B
V4 @surface (full amp.)
Zone 1206 (M_L = 6.0, R_rup = 20 km)

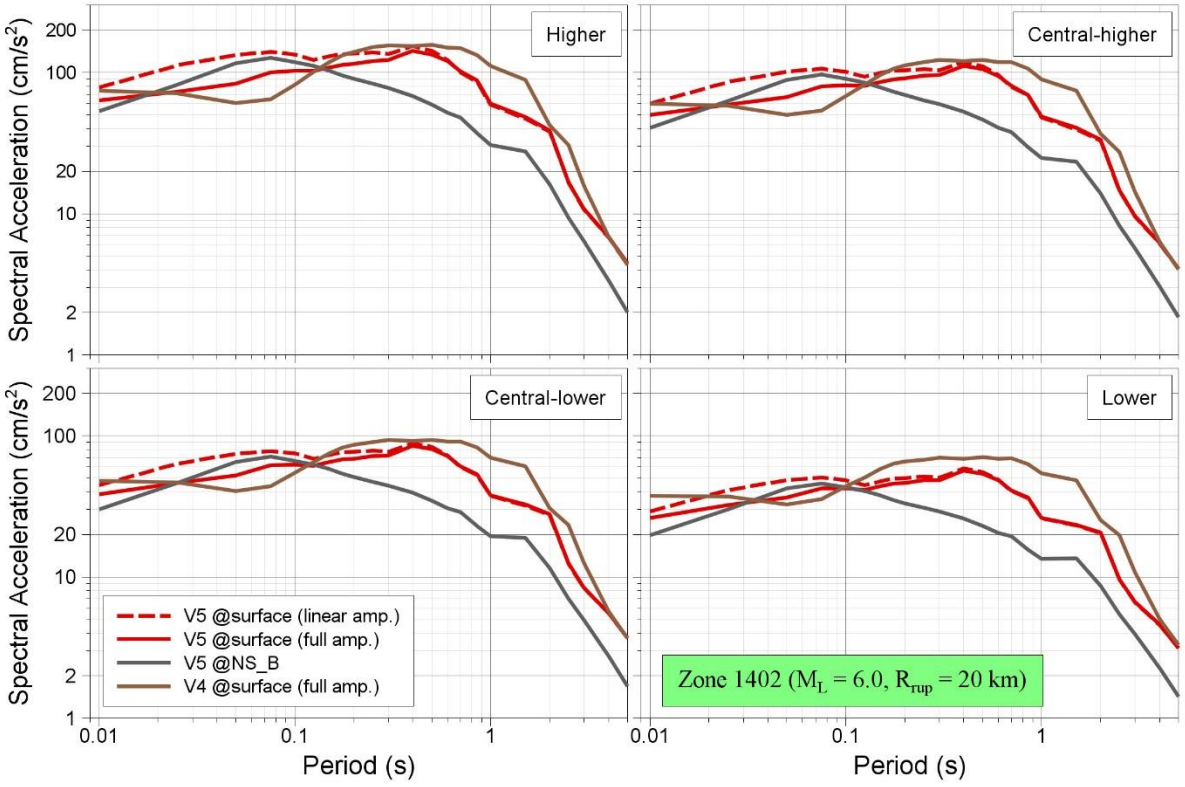
Higher
Central-higher
Central-lower
Lower
Spectral Acceleration (cm/s²)
Period (s)
V5 @surface (linear amp.)
V5 @surface (full amp.)
V5 @NS_B
V4 @surface (full amp.)
Zone 1402 (M_L = 6.0, R_rup = 20 km)

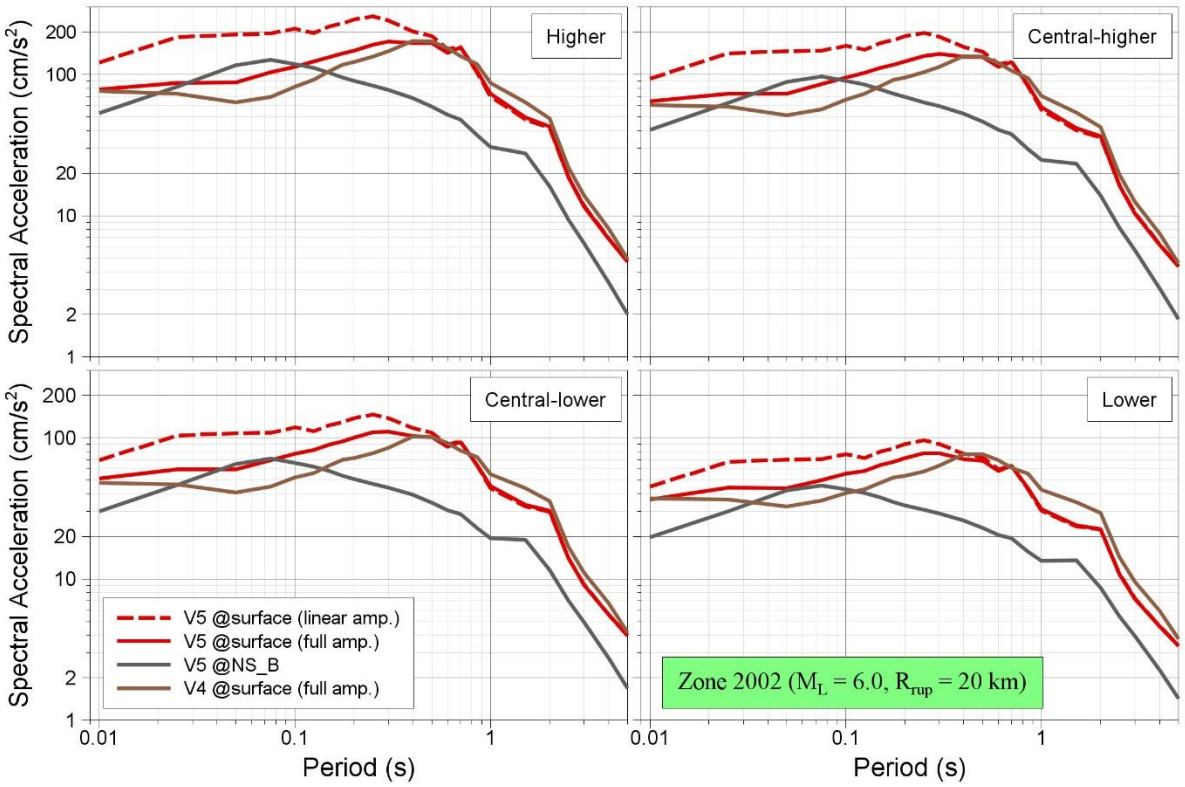
Higher
Central-higher
Central-lower
Lower
Spectral Acceleration (cm/s²)
Period (s)
V5 @surface (linear amp.)
V5 @surface (full amp.)
V5 @NS_B
V4 @surface (full amp.)
Zone 2002 (M_L = 6.0, R_rup = 20 km)

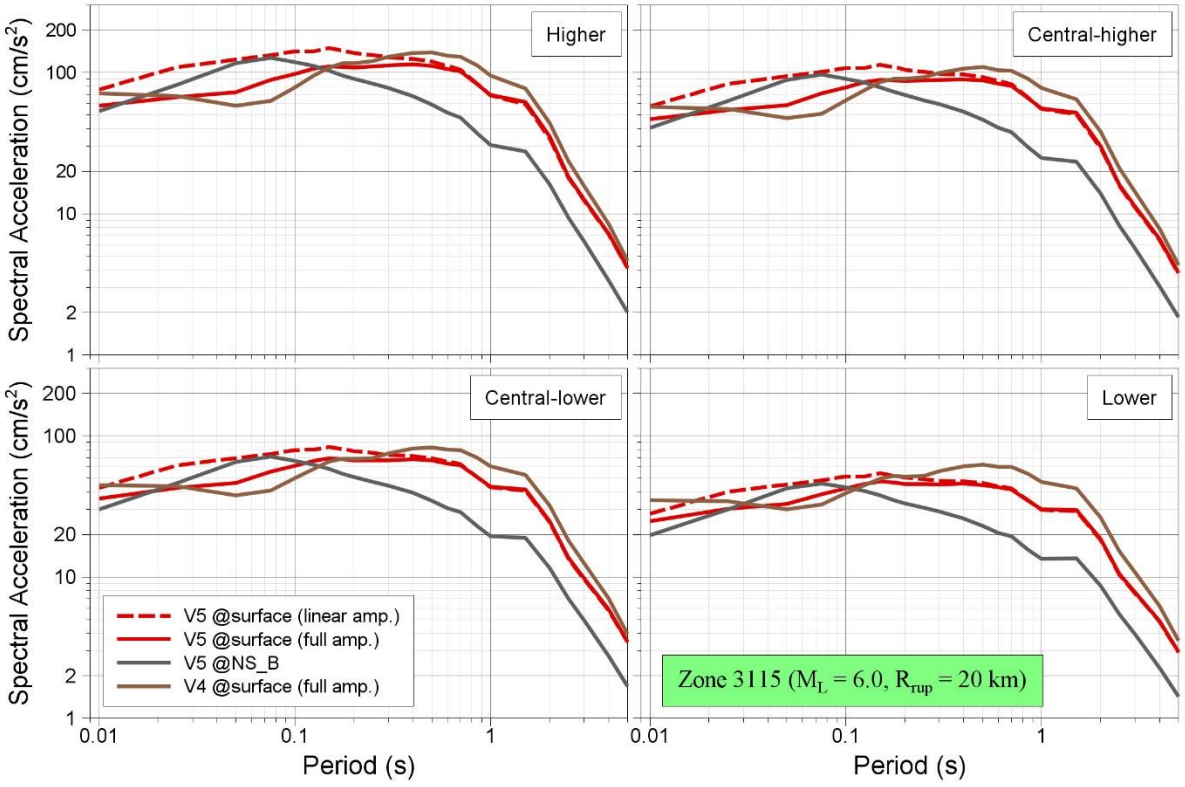
Higher
Central-higher
Central-lower
Lower
Spectral Acceleration (cm/s²)
Period (s)
V5 @surface (linear amp.)
V5 @surface (full amp.)
V5 @NS_B
V4 @surface (full amp.)
Zone 3115 (M_L = 6.0, R_rup = 20 km)